

**COMBUSTION OF NATURAL GAS WITH
ENTRAINED DIESEL IN A HEAVY-DUTY
COMPRESSION-IGNITION ENGINE**

by

CHRISTOPHER A. LAFORET

BASc., University of Windsor, 2005

A THESIS SUBMITTED IN PARTIAL FULFILLMENT OF THE
REQUIREMENTS FOR THE DEGREE OF

MASTER OF APPLIED SCIENCE

in

THE FACULTY OF GRADUATE STUDIES

(Mechanical Engineering)

THE UNIVERSITY OF BRITISH COLUMBIA

(Vancouver)

December 2009

© Christopher A. Laforet, 2009

ABSTRACT

High-pressure direct-injection of natural gas for use in compression-ignition engines has been found to reduce emissions without sacrificing performance relative to pure diesel operation. In the present work, prototype ‘co-injectors’ which inject a diesel and natural gas mixture from a single injector were tested in a heavy-duty, 6-cylinder Cummins ISX engine with 5 cylinders disabled. One prototype (‘B’) was tested under low-speed, low-load conditions, to determine the effects of fuel flows and in-cylinder conditions on the combustion characteristics of co-injection. Co-injector B, and a second prototype (Co-injector CS: A variation of Co-injector B which mixes the fuels differently) were tested at three engine modes using two injections per cycle to determine the effect of the duration of the first injection on emissions and combustion characteristics. The performance of the co-injectors was compared to Westport Innovation’s High Pressure Direct Injection (HPDI) J36 injector to determine if co-injection can produce comparable emissions.

Single injection tests carried out with Co-injector B at 800 RPM over a range of diesel flows, gas flows, injection pressures, and cylinder temperatures & pressures were used to generate response surfaces for knock intensity, ignition delay, and combustion efficiency. It was found that diesel flow and the cylinder pressure at the time of injection had the largest effect of knock intensity and ignition delay, and that the knock/ignition delay relationship in co-injection is inverse.

The double injection tests showed that the difference in diesel distributions within the gas plenums of CS and B results in more diesel being injected during the first injection in CS compared to B, which supports previous results. It was found that short first pulses resulted in the lowest emissions for both co-injectors, and that with low first gas pulse widths the performance of the co-injectors is comparable to that of Westport’s HPDI-J36 injector.

TABLE OF CONTENTS

ABSTRACT	ii
TABLE OF CONTENTS	iii
LIST OF TABLES.....	v
LIST OF FIGURES.....	vi
NOMENCLATURE	ix
ACKNOWLEDGEMENTS	xii
CHAPTER 1 - INTRODUCTION	1
1.1. NATURAL GAS AS A FUEL IN COMPRESSION-IGNITION (CI) ENGINES	1
1.2. HIGH PRESSURE DIRECT INJECTION (HPDI) OF NATURAL GAS	4
1.3. DUAL FUEL INJECTORS	6
1.3.1. J36 High Pressure Direct Injection (HPDI) Injector.....	6
1.3.2. Co-Injectors	7
1.4. THESIS STRUCTURE AND OBJECTIVES.....	16
CHAPTER 2 - EQUIPMENT.....	19
2.1. SINGLE CYLINDER RESEARCH ENGINE (SCRE).....	19
2.2. GASEOUS EMISSIONS MEASUREMENT	22
2.3. PARTICULATE MATTER (PM) EMISSIONS MEASUREMENT.....	25
2.4. INJECTOR CONTROL.....	27
2.5. BIAS CONTROL	28
CHAPTER 3 - METHODS OF ANALYSIS	30
3.1. RESPONSE SURFACES.....	30
3.1.1. Response Surface Error Analysis (See Meyers et al., 2002).....	31
3.2. INDICATED MEAN EFFECTIVE PRESSURE AND MECHANICAL EFFICIENCY	34
3.3. HEAT RELEASE RATE AND INTEGRATED HEAT RELEASE (HRR AND IHR).....	35
3.4. CYLINDER TEMPERATURE AT THE TIME OF INJECTION	36
3.5. COMBUSTION EFFICIENCY (η_{COMB}).....	38
3.6. IGNITION DELAY.....	39
3.7. KNOCK INTENSITY	40
CHAPTER 4 - SINGLE INJECTION TESTING RESULTS	45
4.1. TEST MATRICES AND DATA PRESENTATION	45

4.2. SAMPLE PRESSURE TRACES AND INTEGRATED HEAT RELEASES (IHRS)	48
4.3. RESPONSE SURFACES.....	50
4.3.1. <i>Response Surface Coefficients, Statistics and Residual Plots</i>	50
4.3.2. <i>Knock Intensity, Ignition Delay, Combustion Efficiency, and NO_x</i>	56
4.3.3. <i>Knock/Ignition Delay Relationship in Co-injector B</i>	64
4.3.4. <i>Suggested Region of Injector Operation</i>	68
4.3.5. <i>Effect of Injection Pressure</i>	71
4.4. KNOCK INTENSITY AND IGNITION DELAY POWER LAW DATA FITS	76
4.5. SUMMARY	78
4.5.1. <i>Effect of Fuel Flows</i>	78
4.5.2. <i>Effect of Cylinder Pressure and Temperature at the Time of Injection</i>	79
4.5.3. <i>Effect of Injection Pressure</i>	80
4.5.4. <i>Knock Intensity/Ignition Delay Tradeoff</i>	81
4.5.5. <i>Optimal Size of Pilot Injection</i>	82
CHAPTER 5 - DOUBLE INJECTION TESTING RESULTS.....	83
5.1. DOUBLE INJECTION TEST DESCRIPTION.....	83
5.2. HEAT RELEASE, EMISSIONS, KNOCK INTENSITY, AND IGNITION DELAY	85
5.3. FUEL CONSUMPTION AND COMBUSTION STABILITY	102
CHAPTER 6 - CONCLUSIONS AND RECOMMENDATIONS.....	107
6.1. CONCLUSIONS.....	107
6.2. RECOMMENDATIONS	111
REFERENCES	114
APPENDIX A - REPEATABILITY POINT GASEOUS EMISSIONS PLOTS.....	120
APPENDIX B - BIAS CONTROL EQUATIONS AND FLOW RESTRICTOR DETAILS.....	123
APPENDIX C - CYCLIC VARIATION	127
APPENDIX D - MODIFIED KNOCK INTENSITY RESPONSE SURFACE	132
APPENDIX E - DOUBLE INJECTION HEAT RELEASE RATE CURVES	134
APPENDIX F - GAS FLOWS FROM IVC EXPERIMENTS.....	186
APPENDIX G - RAW DATA INFORMATION	188

LIST OF TABLES

Table 1-1 – EPA and Euro Emissions Standards for Heavy Duty Diesel Engines (nmHC: Non-Methane Hydrocarbons) [Dieselnet, 2009].....	2
Table 2-1 – Engine Geometry	19
Table 2-2 – Test Cell Components [From Brown, 2008]	20
Table 2-3 – Controlled Engine Parameters.....	22
Table 2-4 – Repeatability Point for Co-Injector B	24
Table 2-5 – Average and Standard Deviation of Gaseous Emissions for Co-Injector B Repeatability Points	24
Table 4-1 – Single Injection Test Matrices.....	45
Table 4-2 – Single Injection Response Surface Coefficients, R^2 , and Standard Error Values	50
Table 4-3 – Single Injection Response Surface Variable Transformation Values.....	51
Table 4-4 – Gas Pulse Width Required to Provide Either 12.5 mg/inj or 25 mg/inj (Number in Parentheses) of CNG as a Function of Cylinder Pressure at Injection and Gas Supply Pressure.	57
Table 5-1 – Test Matrix for Double Injection Tests with Co-Injector B and CS.....	84
Table 5-2 – Cylinder Pressures and Estimated Gas Flows during the Second Injections (for 0.8ms GPW at Low Load and 1.4ms GPW at High Load).....	89

LIST OF FIGURES

Figure 1-1 – High Pressure Direct Injection (HPDI) Injector [From Brown, 2008].....	5
Figure 1-2 – Westport’s J36 Injector (Simplified Representation).....	7
Figure 1-3 – Co-Injector B (Simplified Representation).....	9
Figure 1-4 – Visualization of the J36 Diesel Injection (Left) and Co-Injector B Injection (Right) [From Birger <i>et al.</i> , 2009].....	10
Figure 1-5 – Low Load Hydrocarbon Emissions (Left) and High Load PM Emissions (Right) Comparison between Co-Injector A (I2I) and J36	11
Figure 1-6 – Hydrocarbon, CO, and NO _x Emissions vs. Volume Ratio (Left) and Mass Ratio (Right) [From McTaggart-Cowan (2006)]	12
Figure 1-7 – Heat Release Rate Plots of Co-Injector A (Top) and B (Bottom) for Different Diesel Flows [From Brown, 2008]	13
Figure 1-8 – Co-injector CS (Simplified Representation).....	14
Figure 1-9 – Hypothesized Diesel Distributions in Co-Injector B (Left) and CS (Right) Injections.....	15
Figure 2-1 – Single Cylinder Research Engine (SCRE).....	19
Figure 2-2 – Test Cell Layout [From Brown, 2008].....	20
Figure 2-3 – Test Engine Schematic.....	21
Figure 2-4 – Particulate Measurement System Schematic	25
Figure 2-5 – TEOM and Filter PM Mass Correlation (mass in mg).....	26
Figure 2-6 – Injector Command Diagram	27
Figure 2-7 – Fuel Control Module (FCM) Flow Diagram.....	29
Figure 3-1 – Response Surface Standard Error Map Example	33
Figure 3-2 – Response Surface Confidence Intervals.....	34
Figure 3-3 – Heat Release Rate and Integrated Heat Release Examples.....	36
Figure 3-4 – Logarithmic Plot of a Pressure-Volume Trace.....	37
Figure 3-5 – Pressure Trace Illustrating Knock.....	41
Figure 3-6 – Maximum HRR and IHR vs. Knock Intensity (Co-injector B Single Injection Tests).....	42
Figure 3-7 – Filtered and Unfiltered FFT of a Pressure Trace with High Knock [From Brown, 2008].....	44
Figure 4-1 – Pressure Traces and IHRs for Selected Single Injection Test Points	49
Figure 4-2 – Knock Intensity Residual Plots for 21 MPa (left) and 28 MPa (right) Injection Pressure	52
Figure 4-3 – Ignition Delay Residual Plots for 21 MPa (left) and 28 MPa (right) Injection Pressure.....	52
Figure 4-4 – Combustion Efficiency Residual Plots for 21 MPa (left) and 28 MPa (right) Injection Pressures	52
Figure 4-5 – Knock Intensity Normal Plots.....	53
Figure 4-6 – Ignition Delay Normal Plots	54
Figure 4-7 – Combustion Efficiency Normal Plots	54

Figure 4-8 – Normal Plot of Residuals from the Original (Left) and Transformed (Right) Response Surfaces	55
Figure 4-9 – Knock Intensity (bar) Contours (21 MPa Injection Pressure).....	56
Figure 4-10 – Fuel Density Distributions of Gaseous Fuel Jets [From Bruneaux, 2002].....	58
Figure 4-11 – Ignition Delay (ms) Contours (21 MPa Injection Pressure).....	60
Figure 4-12 – Combustion Efficiency Contours (21 MPa Injection Pressure)	62
Figure 4-13 – Knock Intensity vs. NO _x	64
Figure 4-14 – Knock Intensity, Ignition Delay, and Combustion Efficiency Contour Comparison (21 MPa Inj. Press.)	65
Figure 4-15 – Knock Intensity-Ignition Delay Tradeoff Data Stratified by CNG Flow	67
Figure 4-16 – Limits of Operation of Co-Injector B for Single Injection, Low Load, Low Speed	69
Figure 4-17 – Knock Intensity, Ignition Delay, and Combustion Efficiency Comparison for 21 and 28 MPa Gas Injection Pressure.....	72
Figure 4-18 – Operating Region Comparison for 21 and 28 MPa Gas Injection Pressure	75
Figure 4-19 – Measured and Predicted Knock Intensity and Ignition Delay vs. Calculated Knock Intensity and Ignition Delay.....	77
Figure 5-1 – Heat Release Rate Plot of Co-Injectors B (15mg/inj Diesel) and CS (11.5mg/inj Diesel) at the Repeatability Point.....	85
Figure 5-2 – Integrated Heat Releases of Co-Injectors at 1100 RPM, 6 bar GIMEP, 0% EGR (Top) and 30% EGR (Bottom).....	86
Figure 5-3 – Integrated Heat Releases of Co-Injectors at 1100 RPM, 13 bar GIMEP, 0% EGR (Top) and 30% EGR (Bottom).....	87
Figure 5-4 – Integrated Heat Releases of Co-Injectors at 1400 RPM, 13 bar GIMEP, 0% EGR (Top) and 30% EGR (Bottom).....	88
Figure 5-5 – 2 nd GPW vs. 1 st GPW for 0% EGR (Top) and 30% EGR (bottom)	90
Figure 5-6 – Injector CH ₄ Emissions with 0% EGR (Left) and 30% EGR (Right).....	94
Figure 5-7 – Injector tHC Emissions with 0% EGR (Left) and 30% EGR (Right)	95
Figure 5-8 – Injector CO Emissions with 0% EGR (Left) and 30% EGR (Right)	96
Figure 5-9 – Injector NO _x Emissions with 0% EGR (Left) and 30% EGR (Right).....	97
Figure 5-10 – Injector PM Emissions with 0% EGR (Left) and 30% EGR (Right).....	98
Figure 5-11 – Injector Ignition Delay with 0% EGR (Left) and 30% EGR (Right)	99
Figure 5-12 – Injector Knock Intensity with 0% EGR (Left) and 30% EGR (Right).....	100
Figure 5-13 – Injector GISFC (Diesel Equivalent) with 0% EGR (Left) and 30% EGR (Right).....	104
Figure 5-14 – Injector COV GIMEP with 0% EGR (Left) and 30% EGR (Right)	105
Figure 5-15 – Injector COV of Max. Cylinder Pressure with 0% EGR (Left) and 30% EGR (Right).....	106
Figure A-1 – Co-Injector CO Emissions from Repeatability Point.....	120
Figure A-2 – Co-Injector CO ₂ Emissions from Repeatability Point.....	120

Figure A-3 – Co-Injector O ₂ Emissions from Repeatability Point	121
Figure A-4 – Co-Injector CH ₄ Emissions from Repeatability Point.....	121
Figure A-5 – Co-Injector tHC Emissions from Repeatability Point.....	122
Figure A-6 – Co-Injector NO _x Emissions from Repeatability Point	122
Figure B-1 – Effect of Valve Position on Bias	125
Figure C-1 – Examples of Strong (Right) and Poor (Left) Correlation First Return Maps	127
Figure C-2 – Graphical Representation of the Symbol Sequence Statistic Calculation	129
Figure C-3 – Example of a Shannon Entropy Plot	130
Figure D-1 – Effect of Removing Low Gas Flow/High Cylinder Pressure Points from 21 MPa Knock Intensity Response Surface	132
Figure F-1 – Gas Flow vs. Cylinder Pressure for Co-Injector B	186
Figure F-2 – Gas Flow vs. Cylinder Pressure for Co-Injector CS	187
Figure G-1 – Chapter 4 Data Storage Structure.....	188

NOMENCLATURE

2GPW:	2 nd Gas Pulse Width
2GSOI:	2 nd Gas Start of Injection
2PSEP:	2 nd Pulse Separation (Time Between Pulses)
ATDC:	After Top Dead Centre
BDC:	Bottom Dead Centre
B:	Cylinder Bore
BMEP:	Brake Mean Effective Pressure
BP:	Back Pressure
BSFC:	Brake Specific Fuel Consumption
BTDC:	Before Top Dead Centre
c:	Speed of Sound
C:	Carbon
CA:	Crank angle
CA50:	Crank Angle at which the Integrated Heat Release Reaches 50% of its Maximum
CERC:	Clean Energy Research Centre
CH ₄ :	Methane
CHK:	Check Valve
CI:	Compression-ignition
CNG:	Compressed Natural Gas
CO:	Carbon Monoxide
CO ₂ :	Carbon Dioxide
CO _{2,LR} :	Low Range Carbon Dioxide
COV:	Coefficient of Variation
C _p :	Specific Heat
CR:	Compression Ratio
DAQ:	Data Acquisition
Df:	Degrees of Freedom
DI:	Diesel

DLR: Dome Loaded Regulator
 EGR: Exhaust Gas Recirculation
 EQR: Equivalence Ratio
 f: Frequency
 FID: Flame Ionization Detector
 FPGA: Field-Programmable Gate-Array
 GIKWh: Gross Indicated Kilowatt Hour
 GHG: Greenhouse Gas
 GIMEP: Gross Indicated Mean Effective Pressure
 GPW: Gas Pulse Width
 GSOI: Gas Start of Injection
 HC: Hydrocarbon
 HPDI: High-Pressure Direct-Injection
 HRR: Heat Release Rate
 IHR: Integrated Heat Release
 I2I: Co-Injector A
 INT: Intake
 INJ: Injection
 IVC: Injector Visualization Chamber
 k: Needle Valve Discharge Coefficient
 kWh: Kilowatt Hour
 LR: Low Range
 M: Molar Mass
 MAT: Manifold Air Temperature
 n: Polytropic Exponent
 N: (Revolutions per Second)/2
 NDIR: Non-dispersive infrared
 NG: Natural Gas
 NO: Nitrogen Monoxide
 NO_x: Oxides of Nitrogen
 O₂: Oxygen

P:	Pressure
PDR:	Primary Dilution Ratio
PM:	Particulate Matter
PSEP:	Pulse Separation (Time Between Pulses)
Q:	Flow Rate
R:	Gas Constant
R^2 :	Pearson Correlation Coefficient
s:	Standard Error
SCRE:	Single Cylinder Research Engine
SI:	Spark-ignited
SOC:	Start of Combustion
t_{id} :	Ignition Delay
T:	Temperature
TDC:	Top dead centre
tHC:	Total Unburned Hydrocarbons
TEOM:	Tapered Element Oscillating Microbalance
UBC:	University of British Columbia
uHC:	Unburned Hydrocarbons
V:	Volume
V_a :	Volume Flowrate of Air
V_s :	Swept Volume
x:	Response Surface Input Variable
X:	Residual Mass Fraction
Y:	EGR Mass Fraction or Response Variable
α :	Geometric Constant
β :	Response Surface Coefficient
η_v :	Volumetric Efficiency
η_{comb} :	Combustion Efficiency

ACKNOWLEDGEMENTS

I would first like to acknowledge my supervisor, Dr. Steven Rogak, for providing me with the opportunity to complete my research at UBC. His expertise and guidance throughout my time at UBC was invaluable and I have great appreciation for his contributions to my work. I feel that I have become a better engineer over the last two years, and this is in large part due to his help. Thank you.

I would next like to thank Scott Brown, who not only provided great advice regarding the direction of my research, but trained me to use my experimental equipment. Together with Bob Parry, they were instrumental in keeping the research engine running during my stay at UBC. Without their diligence and expertise, data collection may have taken years, rather than months. Koyo Inoshi from Westport Innovations was also a great help by repairing the prototype injectors which did not always function as expected. Experimental work can be a frustrating experience, but I was fortunate enough to have an excellent team around me.

Thank you to my fellow researchers in CERC for the laughs and the help, I wish you the best of luck. Also, thanks to Nick Birger for finishing and running the IVC, and Wu Ning, who also ran the engine and did much troubleshooting.

Thanks to Westport, in particular Dr. Hill and Dr. Munshi for their support of the SCRE and the co-injector project, and to NSERC and Auto 21 for the financial support.

Finally, I would like to thank my family, to whom I credit my existence. To Mom, Dad, Amy, and Casey, I owe the most gratitude for your unconditional support over the years. Thank you.

CHAPTER 1 - INTRODUCTION

1.1. *NATURAL GAS AS A FUEL IN COMPRESSION-IGNITION (CI) ENGINES*

Natural gas, which consists primarily of methane, is a promising fuel for use in compression-ignition engines. With concern growing regarding availability and cost of petroleum fuels and the threat of climate change, there is mounting pressure to increase fuel efficiency and decrease engine-out emissions. Diesel emissions typically consist of carbon dioxide, oxides of nitrogen (a mix of NO and NO₂, normally grouped as NO_x), carbon monoxide (CO), unburned hydrocarbons (uHC), and particulate matter (PM). The unburned hydrocarbons and carbon monoxide come from the incomplete combustion of the fuel and lubricating oil. Secondary reactions in the atmosphere involving NO_x and uHC result in ground-level ozone. While ozone in the upper atmosphere is desirable because it filters the sun's ultraviolet light, ground-level ozone has been found to irritate the respiratory system, reduce lung function, aggravate asthma [AIRNow, 2009] and contribute to global warming. NO_x can react with ammonia and moisture in the atmosphere to form very small particles which can penetrate the lungs causing respiratory problems [US EPA, 2009]. Particulate matter is a mixture of small particles and liquid droplets. Of most concern are particulates 1 micron in diameter or less [US EPA, 2009] because it is those particles which are most likely to make their way into the lungs and can enter into the bloodstream, resulting in lung and/or heart disease. Fine PM particles are also responsible for reduced visibility (haze) in cities and even national parks [US EPA, 2009]. Typically, engine particulate diameters range from 0.01 to 0.40 microns. Carbon monoxide is a toxic gas which can block the delivery of oxygen to the brain and vital organs, causing illness and even death. Carbon dioxide is a product of complete combustion and is therefore a byproduct of burning carbon-based fuels. It is a greenhouse gas (GHG) and can be reduced by increasing the fuel efficiency of the engine, reducing the amount of carbon in the fuel, or having fewer vehicles on the road. Methane has the lowest carbon to hydrogen ratio of all the hydrocarbons, meaning that it generates the least amount of carbon dioxide for a given amount of power of any carbon-

based fuel.

Engine-out diesel emissions can be controlled with exhaust aftertreatment systems such as traps PM and catalysts. Oxidation catalysts are typically used to turn CO, non-methane hydrocarbons and soluble organic fraction of the PM (heavy hydrocarbons condensed on the particles) into CO₂ and water. Particulate traps are used to filter out the solid particulates from the exhaust. The three-way catalysts typically used on SI engines are able to reduce NO_x, however they function optimally at stoichiometric conditions. Due to the lean conditions found in diesel engine operation, NO_x can only be catalyzed with efficiencies between 10-20% using an oxidation catalyst [NETT, 2009]. The most common way to reduce NO_x in diesel engines is to use exhaust gas recirculation (EGR). This involves mixing a fraction of the exhaust gases with the intake charge. Since most NO_x is formed as a result of high peak combustion temperatures [Heywood, 1988], the mostly inert exhaust gases tend to lower the peak temperatures, reducing the amount of NO_x generated (at the expense of higher PM – the well known PM-NO_x tradeoff [Heywood, 1998]). Selective catalytic reduction (SCR) is another technique used to reduce engine-out NO_x. For this method, ammonia or urea is added to the exhaust gas which is then passed through a ceramic catalyst. The NO_x is reduced to water and nitrogen, and, if urea is used, CO₂ is also a byproduct of the process. As emissions standards get tighter (see Table 1-1), lean NO_x traps and scrubbers may be required to reduce NO_x emissions further.

	Year	Test	HC	nmHC	NO_x	CO	PM
EPA (g/bhp-hr)	2010	Transient FTP	--	0.14	0.12	--	0.01
EURO (g/kWhr)	2013	ESC & ELR	0.13	--	0.4	1.5	0.01
EURO (g/kWhr)	2013	ETC	0.16	--	0.4	4	0.01

Table 1-1 – EPA and Euro Emissions Standards for Heavy Duty Diesel Engines (nmHC: Non-Methane Hydrocarbons) [Dieselnet, 2009]

When used as a replacement for diesel in compression-ignition engines, high pressure direct-injection of natural gas engines have also been shown to meet current U.S. EPA and CARB particulate and NO_x requirements (with some exhaust after treatment) [Westport Innovations, 2009a]. Also, since natural gas does not contain any aromatics, toxic emissions are much lower compared to pure diesel engines [Mustafi *et al.*, 2008]. However, since the warming effect of a molecule of methane is significantly worse than a carbon dioxide molecule, methane emissions in a natural gas are of critical importance and require lean burn catalytic converters which add to the cost of the engine.

In compression-ignition engines, the fuel/air mixture ignites when the piston is near top-dead-center and the temperature and pressure are sufficiently high. The cetane number is a measure of a fuel's ease of self ignition (the higher the cetane number, the better the self ignition properties of the fuel [Stone, 1999]). Natural gas has a relatively low cetane number which gives it very long and variable ignition delay times [Huang, 2004]. Therefore, the low cetane number of natural gas makes it a poor candidate for a CI engine fuel on its own. Thus, in natural gas-fueled CI engines, a small amount of 'pilot' diesel fuel is used along with the natural gas to promote ignition. The pilot (typically diesel) easily ignites in the cylinder and the energy released from the diesel ignition is sufficient to cause the natural gas to burn. Engines which use gaseous fuels with a diesel pilot are typically called 'Dual Fuel' engines.

Most dual fuel engines being researched use a configuration in which the gaseous fuel is premixed outside the cylinder with the air [Alla, 2000; Karim, 1992; Li, 2000; Kubesh, 1992; Song, 1987]. The fuel/air mixture is then inducted into the cylinder, where diesel is injected near TDC, as in a conventional CI engine. There are some drawbacks to this approach. First, premixing the gaseous fuel with the air results in a lower volumetric efficiency which can be expressed as [Stone, 1998]:

$$\eta_v = \frac{V_a}{V_s N}$$

Where V_a is the mass of inhaled air per cylinder per cycle, V_s is the swept volume, and N is one half the revolutions per second (for a four stroke engine). When methane is premixed with the air, about 10% of the air is displaced by the gas [Chiodi *et al.*, 2006], and thus the volumetric efficiency is reduced because the volume of air inducted into the cylinder is reduced.

Another problem with premixed air and natural gas is that high unburned hydrocarbon emissions (particularly methane) can result from natural gas being evenly distributed throughout the cylinder. For instance, if there is intake and exhaust valve overlap, some of the natural gas may short circuit directly to the exhaust [Miao *et al.*, 2005]. Also, at low load, where the gas/air fuel ratio is low, the turbulent flame propagation is suppressed, resulting in very high hydrocarbon emissions relative to pure diesel operation [Mustafi *et al.*, 2008]. Flame extinction from heat transfer to the cylinder walls can also lead to increased emissions since the gas near the walls may not burn or burn incompletely. Finally, the gas/air mixture is forced into crevice volumes during the compression stroke, some of which remains unburned, resulting in higher hydrocarbon (in this case methane) emissions [Mustafi *et al.*, 2008]. These penalties are eliminated if the gaseous fuel is injected directly into the cylinder. This alternative is discussed next in the next section.

1.2. HIGH PRESSURE DIRECT INJECTION (HPDI) OF NATURAL GAS

Westport Innovations has developed an injector which is capable of directly injecting both diesel and natural gas from a single injector, which is shown in Figure 1-1.

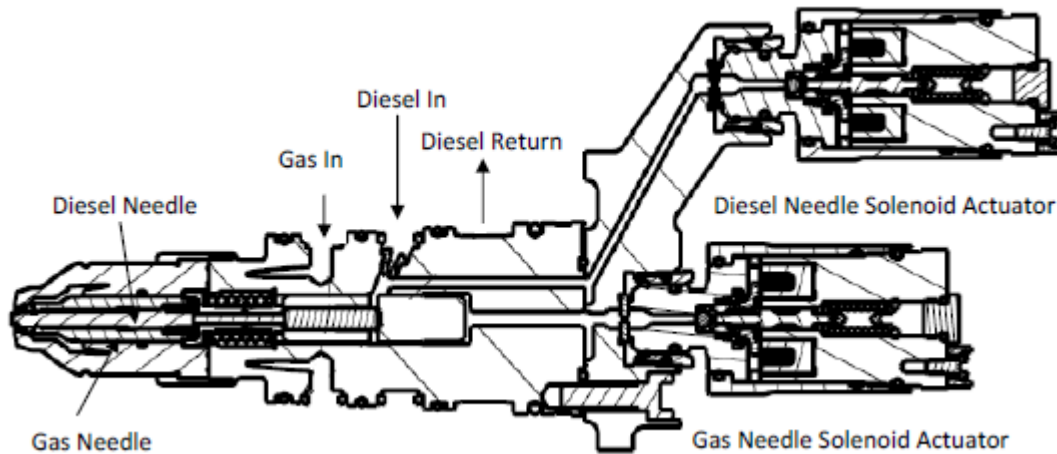


Figure 1-1 – High Pressure Direct Injection (HPDI) Injector [From Brown, 2008]

This injector is essentially two injectors packaged together. The HPDI injector (J36) first injects diesel into the combustion chamber, followed shortly by an injection of natural gas. Details regarding J36 model of the HPDI injector can be found in chapter 1.3.1. Direct injection of the natural gas results in a lower end gas fuel concentration compared to premixed engines and makes it impossible for the fuel to flow directly into the exhaust port since the fuel is injected after all valves have closed. This helps lower unburned hydrocarbon emissions and specific fuel consumption [Miao *et al.*, 2005]. Unfortunately, this option is more expensive than the premixed system. The HPDI injector is more complex than a typical diesel or gas injector, and direct injection means that the gas must be compressed to very high pressures (19-30 MPa). More detailed examinations of Westport's J36 can be found in the following references: Harrington *et al.* (2002), Hodgins *et al.* (1996), McTaggart-Cowan *et al.* (2003).

A new type of injector was proposed which uses only a single needle/actuator to inject both the natural gas and the diesel via 'Co-injection'. These 'Co-injectors' would mix the diesel and natural gas together within the injector and subsequently inject that mixture into the cylinder. The first prototype co-injectors (Co-injectors A and B – see section 1.3.2) are modified versions of Westport's J36. They still use two needle/actuator assemblies, but instead of injecting the diesel into the chamber, the diesel is injected into

the gas plenum within the injector (see Figure 1-3) after which the mixture is injected into the cylinder. The latest generation of co-injector (Co-injectors CS – see section 1.3.2), which are still modified versions of the J36, replace the diesel needle/actuator assembly with a simple flow restrictor (see Figure 1-8). In this injector, the diesel flows continuously into the natural gas plenum and the gas/diesel mixture is injected into the cylinder in the same way as with previous co-injectors. If co-injection can be shown to be as reliable and clean, or better, than the J36, then co-injectors could cut the cost of Westport's HPDI system significantly by replacing the double needle/actuator injector with a simpler single needle/actuator. Removing half the injector also has the advantage of reducing its size. Currently, the J36 is used in heavy duty truck applications with large engines. A smaller injector may allow Westport to fit its HPDI system into a much smaller package, opening up the light duty or even passenger car market to their natural gas direct injection system for compression-ignition engines.

1.3. DUAL FUEL INJECTORS

Much work has been done in the area of dual-fuel, compression-ignition engines. Many studies have been conducted using a gas (e.g natural gas, hydrogen, biogas, etc.) as the primary source of energy and diesel as an ignition promoter [Alla, 2000; Karim, 1992; Li, 2000; Kubesh, 1992; Song, 1987; Duc *et al.*, 2007; Akansu *et al.*, 2004]. In these engines, the gaseous fuel and air are mixed outside the cylinder, usually in the intake manifold. These dual-fuel engines require the ignition promoter due to the poor self-ignition properties of the gaseous fuels. The diesel is injected into the gas/air mixture inside the cylinder, where it readily self-ignites near TDC in the compression stroke, releasing enough energy to ignite the primary gaseous fuel.

1.3.1. J36 High Pressure Direct Injection (HPDI) Injector

Westport innovations has developed an injector which takes advantage of the emission and fuel properties of dual fuel engines without sacrificing volumetric efficiency by injecting both the gas and the diesel from a single injector directly into the cylinder. The

volumetric efficiency of the engine is not sacrificed because the gas is injected after the intake valve is closed and thus no air is displaced. A simplified schematic of Westport's injector (named J36) is given in Figure 1-2 below.

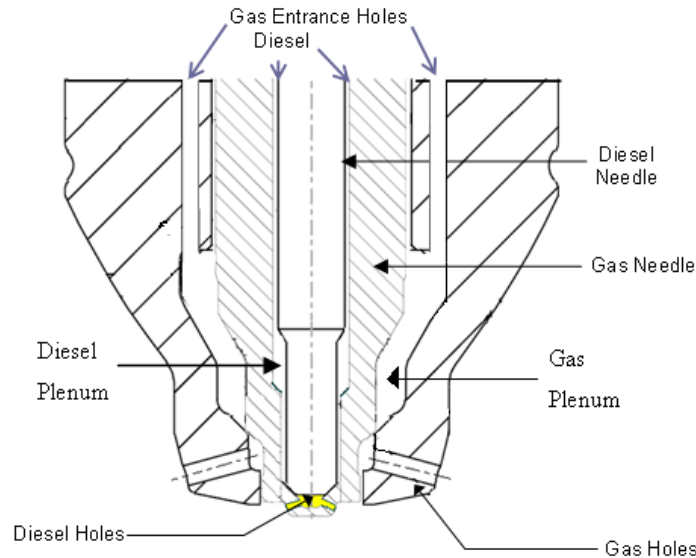


Figure 1-2 – Westport's J36 Injector (Simplified Representation)

As can be seen in Figure 1-2, the J36 is essentially two concentric injectors packaged in a single unit. Diesel flows from the diesel feed into the diesel plenum within the gas needle. The gas (in the current study, natural gas) flows to the gas plenum inside the injector body via the gas feed. Two injections are required to run the J36. First the diesel pulse is commanded (Pilot Pulse), which actuates the diesel needle, injecting the diesel into the cylinder. A sort time later (typically around 1ms), the main gas pulse is commanded which lifts the gas needle, injecting the natural gas into the cylinder.

1.3.2. Co-Injectors

Prototype 'co-injectors' have been built by modifying several parts of the J36 model HPDI injector. In co-injection, the diesel fuel is mixed with the gaseous fuel and this mixture is directly injected into the cylinder. The diesel acts as an ignition promoter for the gaseous fuel, which is the primary energy carrier. Co-injection has been described in patents by Yang (2002) and Denso Corporation (2005), but there is no information

regarding the operation or performance of these injectors. The most detailed work found on co-injection done outside the UBC research group is found in Miyake *et al.* (1985). In this paper, the first method (Type I) of co-injection described has the diesel fuel injected into the gas upstream of the injector, and then the fuel mixture is sent to the injector for direct injection into the cylinder. In the second method (Type II), the diesel is injected into the gas inside the injector, near the base of the needle. This form of co-injection is similar to the way in which Co-injector B functions (see below). It was found that for Type I injection, the pilot diesel fuel had to account for 40% of the total calorific value, but was able to operate the engine stably. It was found that with Type II injection, the diesel fuel needed only to account for 7 or 8% of the total calorific value of the fuel. It was also found when compared to pure diesel operation, their co-injection (it is unclear which type) had lower thermal efficiency by noting that the combustion duration was longer. The heat release rate plots for co-injection (again, it is unclear which type) had a lot of oscillation for the entire duration of combustion, however knock intensity (see section 3.7) was not discussed in the paper.

For the current work, two basic types of prototypes were constructed. The first type still uses separate needles for diesel and gas injection. The difference from the original J36 is that the diesel is injected into the gas reservoir instead of directly into the combustion chamber. Figure 1-3 shows this prototype which is called 'Co-injector B'.

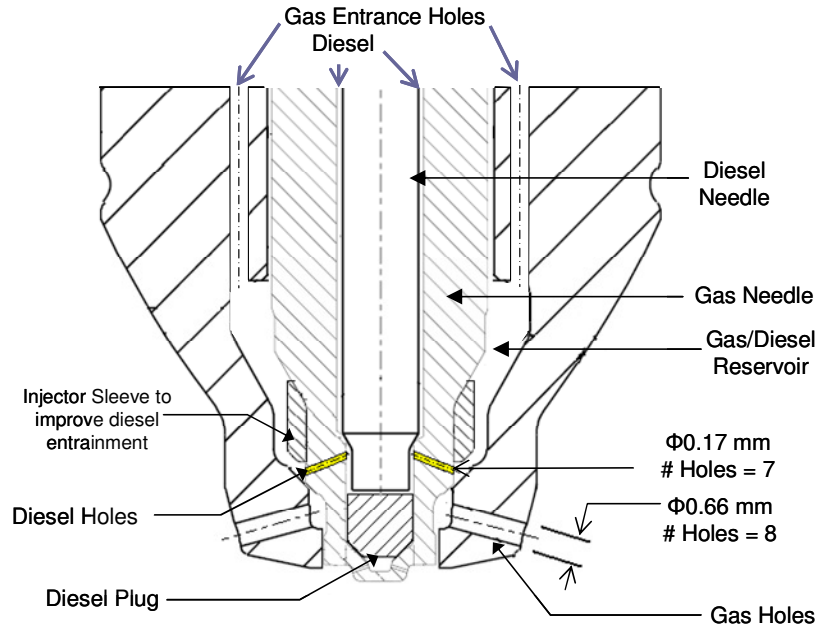


Figure 1-3 – Co-Injector B (Simplified Representation)

As is shown in Figure 1-3, the diesel holes from the J36 have been plugged and new holes have been made higher in the gas needle such that the diesel is injected into the gas reservoir rather than directly into the combustion chamber. The flow rate of the diesel is determined by the duration of the diesel injection as well as the differential pressure between the diesel and gas (bias pressure). The sleeve shown in Figure 1-3 is a modification made as a result of previous testing with a similar co-injector. The original prototype (called Co-injector A) had no sleeve. Figure 1-4 shows a Co-injector B injection (right) and the diesel injection from a J36 (left) in UBC's injector visualization chamber. Note how the diesel spray in Co-injector B is much wider and more dispersed than in the J36. This is because the diesel in Co-injector B is being injected with some gas, which assists in the atomization of the spray.

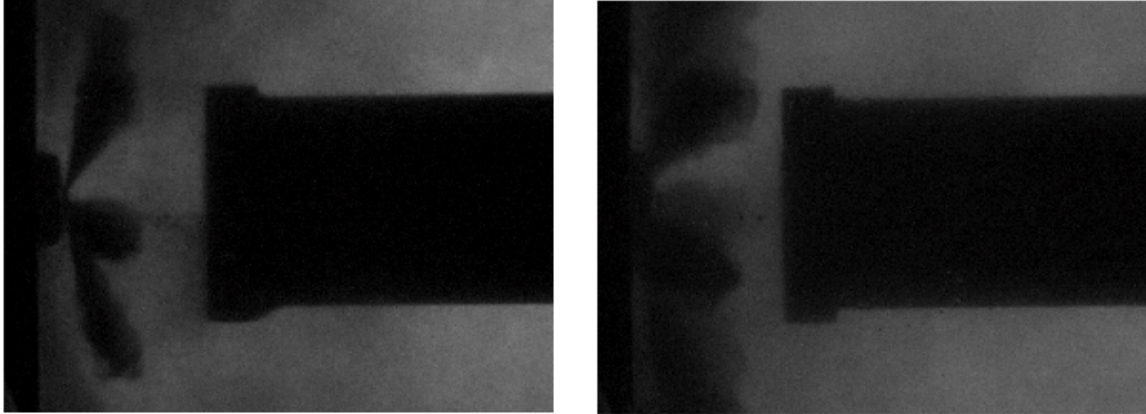


Figure 1-4 – Visualization of the J36 Diesel Injection (Left) and Co-Injector B Injection (Right)
[From Birger *et al.*, 2009]

Testing by Jones (2005b) suggested that due to high peak pressure, heat release rates, and NO_x , two gas injections were required for satisfactory operation of the co-injector. It was also found that with single injection, there was significant combustion noise when high diesel flow rates were injected. Thus, a double injection strategy was developed. Ideally, a short first injection (pilot gas injection) would contain mostly diesel and act as the ignition source for a longer second injection which would have very little diesel and thus be mostly gas.

Further testing by Jones (2006) compared Co-injector A with the J36 at conditions of mid speed/low load, mid speed/high load and high speed/high load. For high load cases the unburned hydrocarbons, CO and NO_x were found to be similar, while the co-injector had lower particulate emissions and fuel consumption (Figure 1-5 (Right) - Note 'I2I' is Co-injector A, and 'Pilot' refers to the diesel injection mass). At low loads, it was found that the unburned hydrocarbon emissions and CO were much higher for Co-injector A (Figure 1-5 (Left) – Note 'I2I' is Co-injector A).

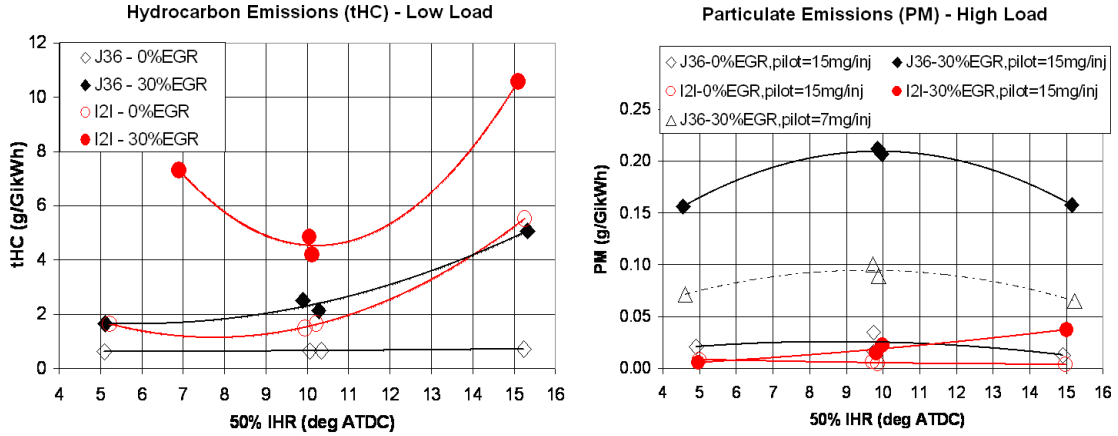
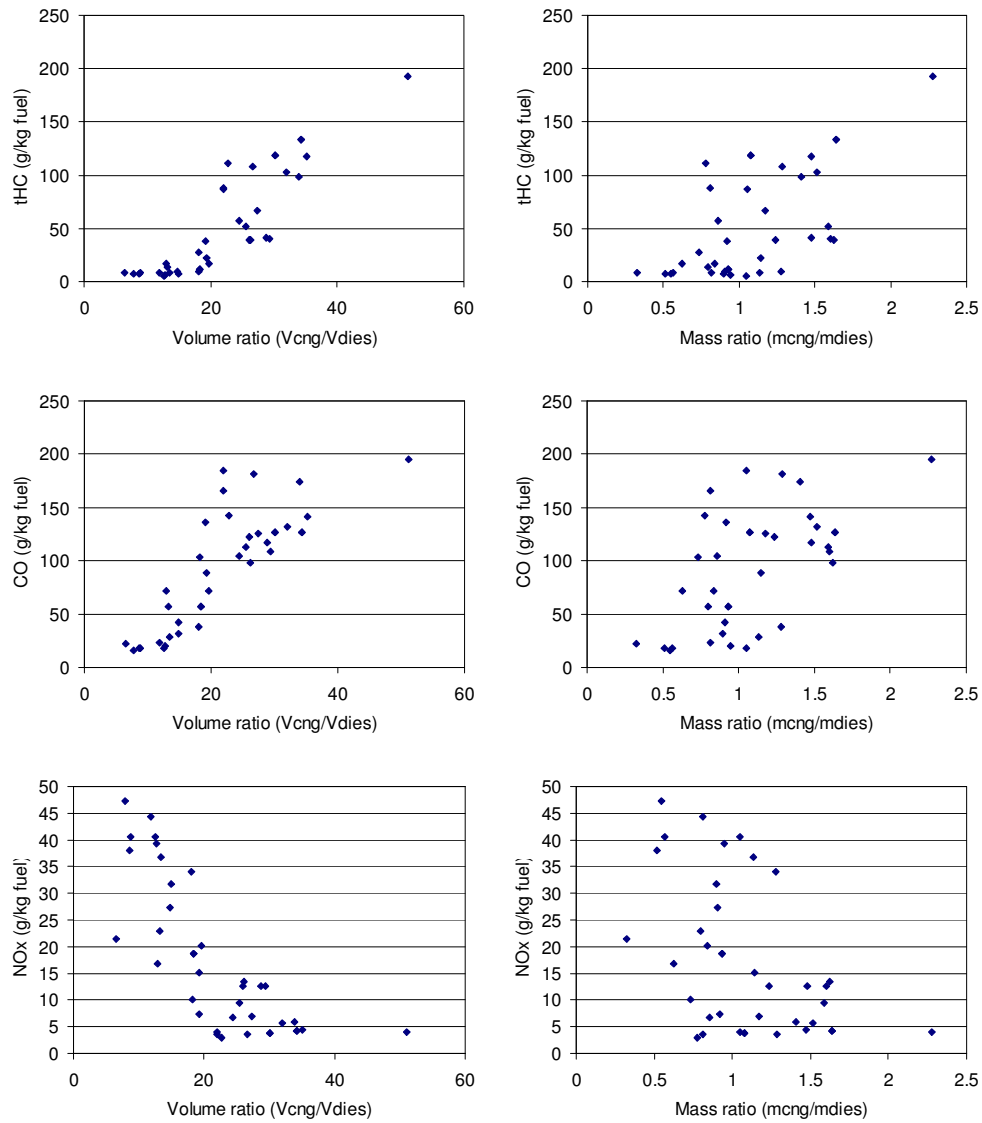


Figure 1-5 – Low Load Hydrocarbon Emissions (Left) and High Load PM Emissions (Right) Comparison between Co-Injector A (I2I) and J36

Single injection tests were performed by McTaggart-Cowan (2006) on Co-injector A which examined the stability of the injector at low loads. It was found that increasing the diesel flow rate substantially reduced the coefficient of variation (COV) of the gross indicated mean effective pressure (GIMEP). It was also shown that the volume ratio of natural gas to diesel correlated better with COV GIMEP, tHC, CO and NO_x than the mass ratio shown in Figure 1-6 below.



**Figure 1-6 – Hydrocarbon, CO, and NO_x Emissions vs. Volume Ratio (Left) and Mass Ratio (Right)
[From McTaggart-Cowan (2006)]**

Brown (2008) examined the interactions between the first and second pulses in double injection operation of the co-injectors A and B. Co-injector A double injection tests suggested that there was a significant amount of diesel present in the second (main) injection. The consequence of this was that there was little or no ignition from the first pulse resulting in wasted diesel and potentially poorer combustion. It was thought that adding an annular sleeve around the gas needle could accomplish two things:

1. A reduction in the gas reservoir volume to help constrain the diesel to the bottom of the reservoir near the injection holes so that more diesel would be injected in the first injection.
2. Increase the gas velocity by degreasing flow area. This would help remove diesel which may be lining the walls of the plenum. It would also aid in the atomization of the diesel during injection.

Brown (2008) found that the sleeve did improve the operation of the injector and Co-injector B became the benchmark co-injector. Figure 1-7 shows heat release rate (see section 3.3) plots for Co-injectors A and B. Note the stronger pilot event (between -5 and 5 degrees ATDC) for Co-injector B, which is attributed to increased diesel in the pilot pulse (see section 2.4 for injector control details).

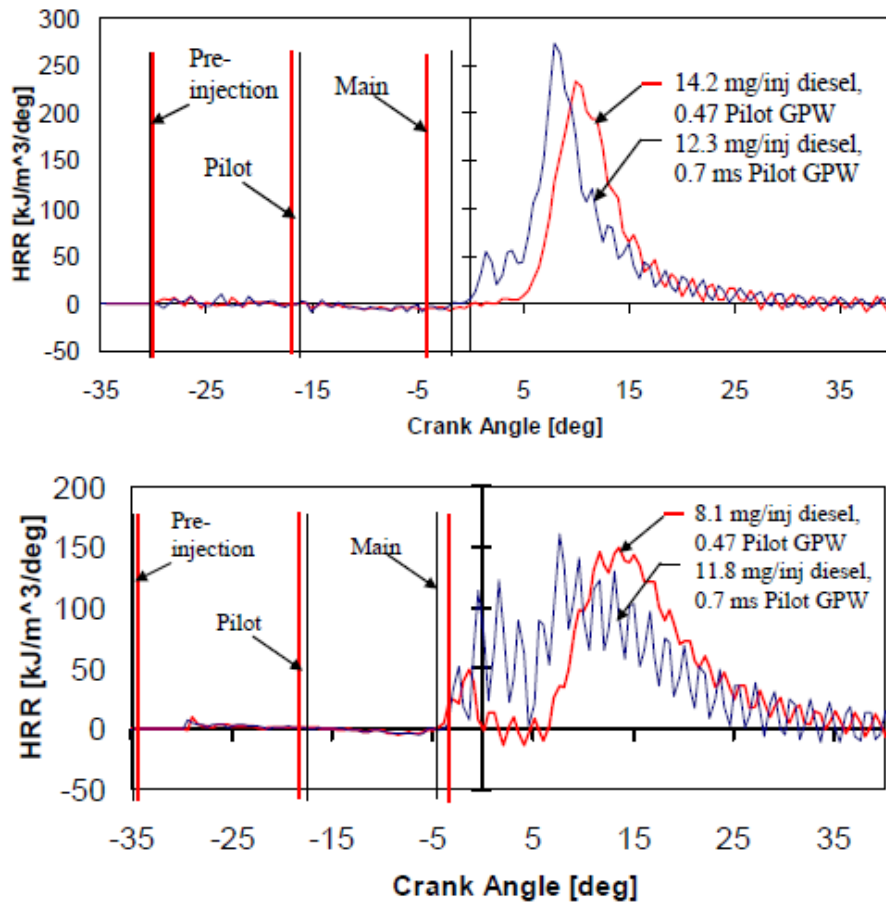


Figure 1-7 – Heat Release Rate Plots of Co-Injector A (Top) and B (Bottom) for Different Diesel Flows [From Brown, 2008]

Brown, as well as McTaggart-Cowan (2006) and Jones (2006) found that gas flow from the injectors for a given pulse width increased as cylinder pressures increased. It was initially thought that the increased pressure caused the gas needle to lift sooner, but tests done in UBC's injector visualization chamber (Birger *et al.*, 2009) showed no change in needle opening time with cylinder pressure. Brown also found that fuel specific emissions of CO and CH₄ were reduced by increasing the diesel flow rate or shortening the gas pulse width (see Section 2.4 for an explanation of the injector controls), which is attributed to the gas preventing the diesel from forming an ignitable mixture.

The next type of co-injector developed replaced the diesel needle with a flow restrictor. In this prototype, the diesel is not injected into the gas reservoir, but rather it flows (leaks) continuously into the reservoir at a rate determined by the bias pressure and the size of the flow restrictor. Pictured in Figure 1-8 below is Co-injector CS, which is one variation of this type of co-injector.

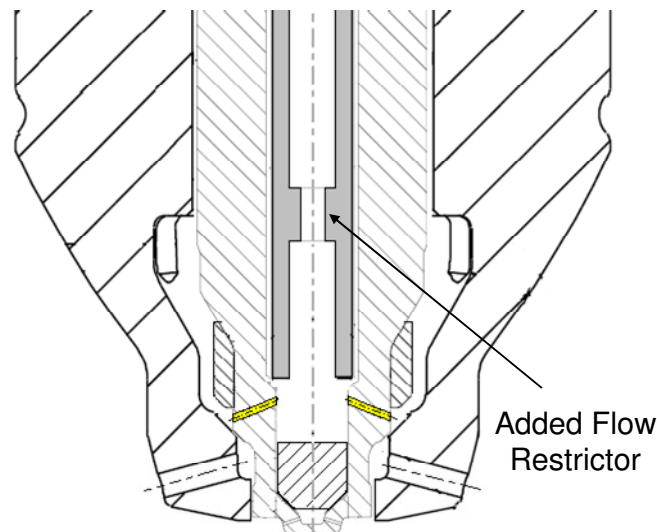


Figure 1-8 – Co-injector CS (Simplified Representation)

It is this type of injector which is the ultimate goal of the co-injector development. With a simple flow restrictor in place of an expensive diesel needle/actuator setup, costs can be reduced. It is expected that with the flow restrictor in CS, the diesel distribution within the gas during injection will be quite different. Since the majority of the diesel

pressure drop occurs across the flow restrictor in CS, the diesel will likely be more segregated from the gas, pooling near the bottom of the injector such that when injected, instead of being evenly distributed throughout the gas (which is the current assumption regarding the distribution for Co-injector B), the diesel will be concentrated more on the outer edges of the spray (see an example in Figure 1-9. Currently, the CS spray has not been visualized in the IVC, and therefore, the diesel distribution in the CS spray is not directly known, but Figure 1-9 shows one possible spray structure). This is expected to make CS more efficient regarding the burning of diesel since, in CS, more diesel is in contact with the air, making it easier to form an ignitable mixture.

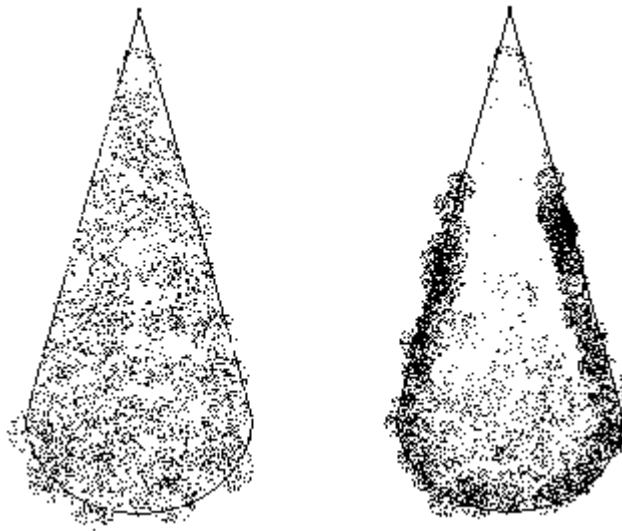


Figure 1-9 – Hypothesized Diesel Distributions in Co-Injector B (Left) and CS (Right) Injections

The flow restrictor in Co-injector CS was sized such that the target range for diesel flow could be achieved with bias pressures between 0.6 and 3.5 MPa. Details regarding flow restrictor calculations can be found in Appendix B. Note that, in Co-injector CS, B as well as the HPDI, there is also a small amount of leakage of diesel into the gas via a match fit within the injector. This leakage rate was measured by Nick Birger for Co-injector B and the HPDI to be 17mg/s with a 2.5 MPa bias (typical bias for B) and around 7mg/s for a 1.2 MPa bias (typical bias used for CS). The measured diesel flows represent the total flows, which include the match fit leakage.

Relative to the other co-injectors, CS is new and the work presented here represents some of the first testing done with it. Brown (2009) has done some tests comparing the co-injectors with the J36, and found that unlike Co-injector B, the diesel distribution between the two pulses in a double pulse test does not appear to be affected by the size of the second gas pulse (tests were only run for one engine condition – low speed, low load).

1.4. THESIS STRUCTURE AND OBJECTIVES

This thesis is divided into 6 chapters plus references and appendices. Chapter 1 provides the introductory material on natural gas engines, and the new co-injection concept. Chapter 2 provides an overview of the equipment used in the research, much of which is the same as that found in Brown (2008). The test engine and emissions analyzers will be described in detail. Chapter 3 outlines the methods of analysis used in processing the raw engine data.

The results of the current work are split into two parts. The first part (Chapter 4) is a continuation of the work started [Brown, 2008] on Co-injector B. Previous work has looked at the interactions between gas injection pulses during multiple injection operation in which a short primary gas pulse ideally containing mostly diesel is used to ignite the fuel from the longer second pulse, which is mostly gas. The aim of the work presented in chapter 4 was to simulate the first gas injection by running single injection tests at low load and low speed. The diesel and CNG flows, cylinder pressure and temperature at the time of injection, and injection pressure were varied over a range of conditions and response surfaces were generated to examine the knock intensity (see section 3.7), ignition delay, and combustion efficiency (see section 3.5) of Co-injector B.

For chapter 5, Co-injector B as well as a new prototype co-injector (CS) were run in a series of double pulse tests similar to the Series VIII tests found in Brown, (2008). Each injector was run at three engine modes (1100 RPM low load, 1100 RPM high load, 1400 RPM high load) with and without exhaust gas recirculation (EGR). For each engine

mode and EGR level, three different first gas pulse widths (GPW) were tested (0.5ms, 0.7ms, and 0.9ms).

Previous work on co-injection has yielded the following results regarding co-injector operation and combustion:

- It is best to run 'B-Type' co-injectors with two injections per cycle. The first injection is meant to contain mostly diesel and the heat release from the initial injection acts as the ignition source for the second, main injection which should ideally be mostly gas. It was found that running with two injections per cycle resulted in more stable combustion and less combustion noise compared to single injection operation.
- In practice, when running with 2 injections, it was found that the presence of the second injection reduces the amount of diesel which gets injected during the first injection. The amount of diesel 'scavenged' by the second injection was reduced by adding a sleeve (Co-injector B) around the gas needle. The sleeve is thought to increase the gas velocity by decreasing the gas plenum flow area and keep the diesel near the bottom of the gas plenum, so that more of it is cleared out during the first injection.
- Adding the sleeve increased the amount of combustion noise for a given diesel flow compared to the sleeveless injector (Co-injector A). However, the sleeve did increase the amount of diesel injected in the first pulse, which allowed for lower diesel flows to be used. Running with less diesel reduced the combustion noise to that of the sleeveless injector, and Co-injector B became the benchmark co-injector.
- It was also found that the hydrocarbon and CO emissions, as well as the ignition delay correlated more strongly with the diesel/CNG volume ratio than the mass ratio. The volume ratio calculation was done using the peak cylinder pressure and ambient temperature

The tests carried out in chapters 4 and 5 of the current work were done to further the understanding of co-injection combustion with the following specific objectives:

- Determine, within the load and speed range tested, whether the co-injectors can match the performance of the HPDI injector in terms of low hydrocarbon, CO, NO_x, and PM emissions.
- Compare results from Co-injectors B and CS to determine how different gas diesel mixing strategies (high velocity injection of the diesel vs. slow continuous leakage of the diesel into the gas plenum) affect the emissions and combustion characteristics of co-injection.
- Examine, for the load and speed range tested, how the first gas pulse width (GPW) in the double injection tests affects the emissions and combustion characteristics of B and CS. This will provide guidance regarding optimal GPW settings for use in future co-injector testing.
- Determine the effect of fuel flows, in-cylinder conditions, and injection pressure on knock intensity, ignition delay, and combustion efficiency of Co-injector B for low load, low speed, single injection conditions.

CHAPTER 2 - EQUIPMENT

2.1. SINGLE CYLINDER RESEARCH ENGINE (SCRE)

A modified six cylinder, 4-stroke, 400 hp Cummins ISX engine was used for all tests. The original 6-cylinder engine was modified by deactivating 5 cylinders to run on a single cylinder. The pistons in the deactivated cylinders have holes drilled in them to minimize losses. Details regarding engine geometry are given in Table 2-1.

Displacement (L)	2.5
Compression Ratio	17:1
Bore (mm)	137
Stroke (mm)	169
Connecting Rod (mm)	262

Table 2-1 – Engine Geometry

A GE eddy-current dynamometer is used to control the speed of the engine and a 30 kW electric motor is used to provide additional torque to overcome any frictional losses and inertia of the deactivated cylinders. A picture of the engine, as well as the layouts of the test cell and control room are shown below in Figure 2-1, Figure 2-2, and Table 2-2. A schematic of the engine and air flow systems is shown in Figure 2-3.



Figure 2-1 – Single Cylinder Research Engine (SCRE)

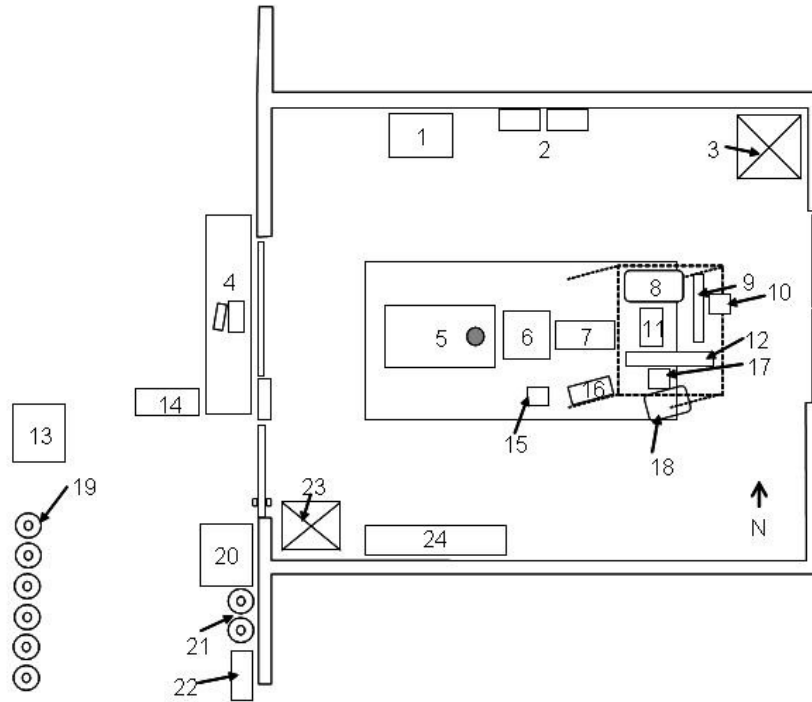


Figure 2-2 – Test Cell Layout [From Brown, 2008]

1	Cooling Tower	13	AVL Emissions Bench
2	Power Switches for charge air heater and drive motor	14	Control Panel
3	Cell Intake Air Duct	15	Signal Multiplexer
4	DAQ/Control Computer	16	Temperature/Voltage Wiring Tree
5	Single Cylinder Research Engine	17	Charge Air Heater
6	Dynamometer	18	Intake Surge Tank
7	Electric drive motor	19	Emissions Bench Calibration Gases
8	Exhaust Surge Tank	20	PM Dilution/Measuring System
9	EGR Cooler	21	PM Dilution Bottles
10	Back Pressure Valve	22	Vacuum Pump/Particulate Filters
11	High Pressure Diesel Pump	23	Cell Exhaust Air Duct
12	EGR Valve	24	Fuel Conditioning Module

Table 2-2 – Test Cell Components [From Brown, 2008]

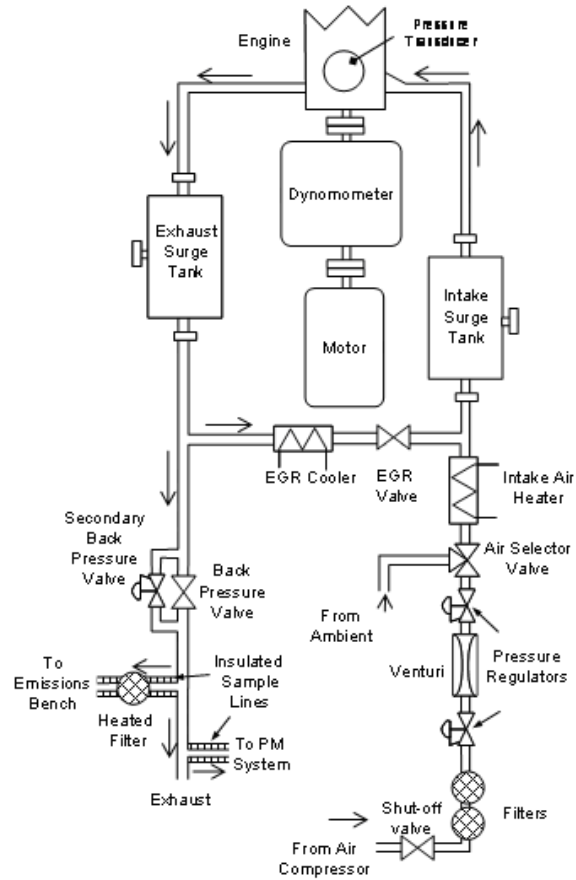


Figure 2-3 – Test Engine Schematic

The following engine parameters can be controlled either manually using valves and potentiometers on the control panel or via automatic control through the control computer which runs a custom designed Labview control program. Note that the gas pressure is controlled by the diesel pressure via a dome-loaded pressure regulator. Details of the fuel control are given in section 2.5.

<i>Parameter</i>	<i>Control</i>
Intake Pressure	Labview
Intake Temperature	Control Panel Pot.
EGR Fraction	Labview
Injection Timing	Labview
Diesel Pressure	Pressure Regulator
Bias Pressure (Diesel Press. – Gas Press.)	Needle Valves
Exhaust Backpressure	Control Panel Pot./Labview
Fuel Flows	Labview
Oil Temperature	Thermostat
Diesel Temperature	Cooling water through HEX (Hand Valve)
EGR Temperature	Cooling water through HEX (Hand Valve)
Electric Motor Torque	Control Panel Pot.
Dynamometer Torque	Control Panel Pot.

Table 2-3 – Controlled Engine Parameters

A screw-type compressor supplies high-pressure natural gas. Gas pressure is held at a pressure slightly below the diesel pressure using a dome-loaded regulator. A coriolis mass-flow meter is used on the gas supply. Diesel flow is supplied by a conventional Bosch diesel fuel pump; pressure is set with a back-pressure regulator. Most of the diesel flow is used for injector actuation and returned at low pressure to the small diesel supply tank. This tank sits on an electronic balance, from which the net mass of diesel injected into the engine can be inferred. Further details regarding the test cell setup can be found in Brown (2008).

Natural gas in Vancouver, Canada contains approximately 96% methane with 2% higher hydrocarbons and 2% $N_2 + CO_2$. The diesel was road-grade low-sulphur (<15 mg/kg) which met CAN/CGSB-3.520 standards. The cetane number of the diesel ranges from 41 to 45.

2.2. GASEOUS EMISSIONS MEASUREMENT

Gaseous emissions from the engine are taken just downstream of the exhaust surge tank, passed through a heated filter, and sent to the AVL CEB-NA emissions bench in the

control room. The emissions bench measures total unburned hydrocarbons (uHC), CO₂, O₂, CH₄, CO, and NO_x. CH₄, uHC, and NO_x are measured wet while the other emissions are measured dry (i.e. the water in the emission stream is removed).

A flame ionizing detector (FID), which uses a hydrogen flame inside and electric field to ionize organic hydrocarbons, measures the current produced by the ionization to determine the amount of carbon present. Separate FIDs are used to measure the uHC and CH₄ concentrations through the use of a thermochemical catalyst which converts all non-methane hydrocarbons to CO₂ and water.

When NO is burned with ozone, light is generated with wavelengths between 600 and 1200 nm. Using a chemiluminescent detector, the light intensity from this burning is measured, which is proportional to the amount of NO_x burned.

Oxygen is measured using the principle that oxygen becomes magnetic when exposed to a magnetic field. A dumbbell-shaped container containing oxygen-free gas is exposed to a non-uniform magnetic field, which causes the oxygen to gather to one side of the dumbbell. The resulting high pressure on one side of the dumbbell causes the container to rotate. The voltage needed to keep the dumbbell stationary is thus proportional to the amount of oxygen present.

CO and CO₂ are measured using non-dispersive-infrared absorption. A light emitter emits known wavelengths of light which go through the sample gas. CO and CO₂ absorb specific wavelengths of light. The unabsorbed light is then absorbed by constant pressure reference gases which change volume proportional to the amount of light absorbed. Thus the amount of light absorbed by the CO and CO₂ (which is proportional to their concentrations) can be calculated knowing the amount of light emitted and the volume change of the constant pressure reference gases.

The zero and span points of each analyzer were checked at the beginning and end of each testing day to verify that the sensors were properly calibrated throughout the testing period. The zero point is checked by running pure nitrogen through each analyzer and verifying that it gives a zero reading. The span is checked by flowing gases of known concentrations through each analyzer and verifying that the analyzer is measuring the correct value.

Another method used to check the emissions measurements (as well as other parameters), was running a repeatability point at the beginning of each test day. The repeatability point is a specific engine condition used to check how repeatable the engine and measurement systems are from day to day. Table 2-4 below shows the repeatability point for Co-injector B.

<i>Engine Speed</i>	1200 rpm
<i>EQR</i>	0.4
<i>Air Flow</i>	144 kg/hr
<i>Diesel Flow</i>	15 mg/inj
<i>Bias</i>	2.5 MPa

Table 2-4 – Repeatability Point for Co-Injector B

Table 2-5 below shows the average and standard deviations of the gaseous emissions measurements collected from the repeatability points run with Co-injector B over the span of a year. Plots of the emissions measurements from the repeatability point can be found in Appendix A.

	Average	Std. Deviation	No. of Points
<i>CO (ppm)</i>	381.1	111.6	19
<i>CO₂ (%)</i>	4.8	0.1	19
<i>NO_x (ppm)</i>	707.3	54.2	13
<i>O₂ (%)</i>	12.7	0.3	19
<i>CH₄ (ppm)</i>	181.0	37.2	19
<i>uHC (ppm, Methane Eq.)</i>	302.5	57.3	19

Table 2-5 – Average and Standard Deviation of Gaseous Emissions for Co-Injector B Repeatability Points

2.3. PARTICULATE MATTER (PM) EMISSIONS MEASUREMENT

A schematic of the system used for PM measurement is shown in Figure 2-4.

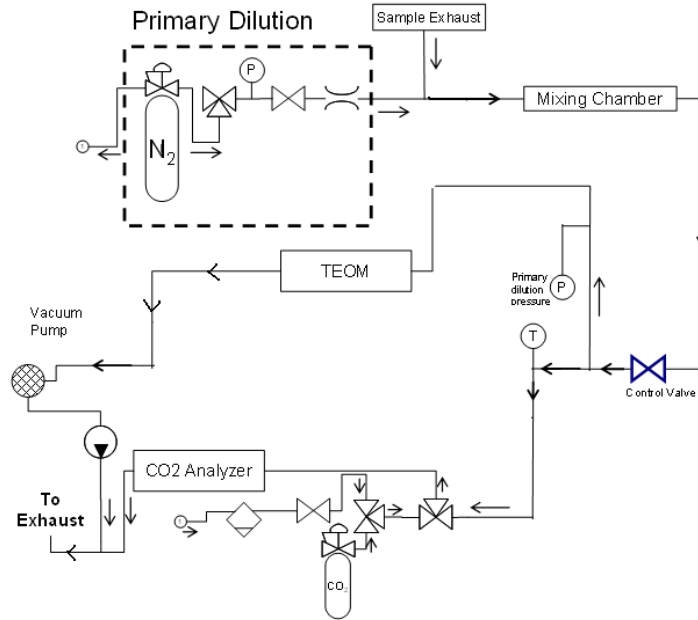


Figure 2-4 – Particulate Measurement System Schematic

In this system, a sample of the engine exhaust is diluted and cooled with nitrogen. This diluted mixture then flows through a residence tube and is sent to the sampling system which consists of a low range CO₂ analyzer and an R&P Series 1150 tapered element oscillating microbalance (TEOM). Using a tapered element with a small filter connected to the end, the TEOM measures total particulate mass. The tapered element is cantilevered and oscillates at its natural frequency. This natural frequency can be measured and is proportional to the mass accumulated on the filter. The low range CO₂ analyzer along with the CO₂ concentration in the raw exhaust measured by the AVL emissions bench is used to calculate the dilution ratio (PDR) as follows (concentrations are measured in %):

$$PDR = \frac{[CO_{2, wet}] - 0.03}{[CO_{2, LR, Dry}] \left(1 - \frac{[H_2O]}{([CO_{2, dry}] - 0.03) / ([CO_{2, LR, dry}] - 0.03)} \right) - 0.03} \quad (1)$$

Effectively this formula finds the ratio of the CO₂ in the raw exhaust and the CO₂ in the diluted exhaust, taking care of the amount of CO₂ in the atmosphere (0.03%*) and the effect of water. The dilution ratio was set to be between 10:1 and 12:1 for the current tests [Brown, 2008b; Jones, 2004].

The line to the TEOM is heated such that the inlet temperature of the TEOM is kept between 55 and 58°C which is the temperature range which has been found to give the TEOM mass the best correlation. Before testing with the TEOM began, baseline tests were run with exhaust samples collected with the TEOM as well as on filters which were weighed using a microbalance at UBC in order to validate the TEOM measurements. The correlation between the TEOM and filter sample measurements is given in Figure 2-5.

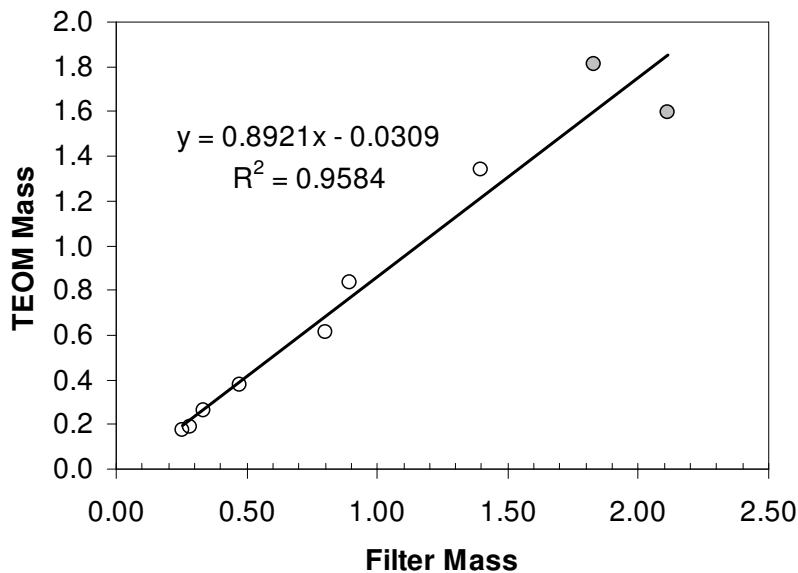


Figure 2-5 – TEOM and Filter PM Mass Correlation (mass in mg)

* The current atmospheric concentration of CO₂ in the atmosphere is closer to 0.04%, which changes the calculation of the PDR by about 0.3%, which did not affect the PM calculation

2.4. INJECTOR CONTROL

The injectors are controlled using a Labview program which sends injection signals to a Westport injector driver box, which sends the required current signals to the injector. Injection timings are specified in crank angle degrees, while injection durations are given in milliseconds. The injectors have separate diesel needle and gas needle actuators and separate signals are sent to each actuator. Figure 2-6 shows the injector commands and the units in which they are specified by the Labview program.

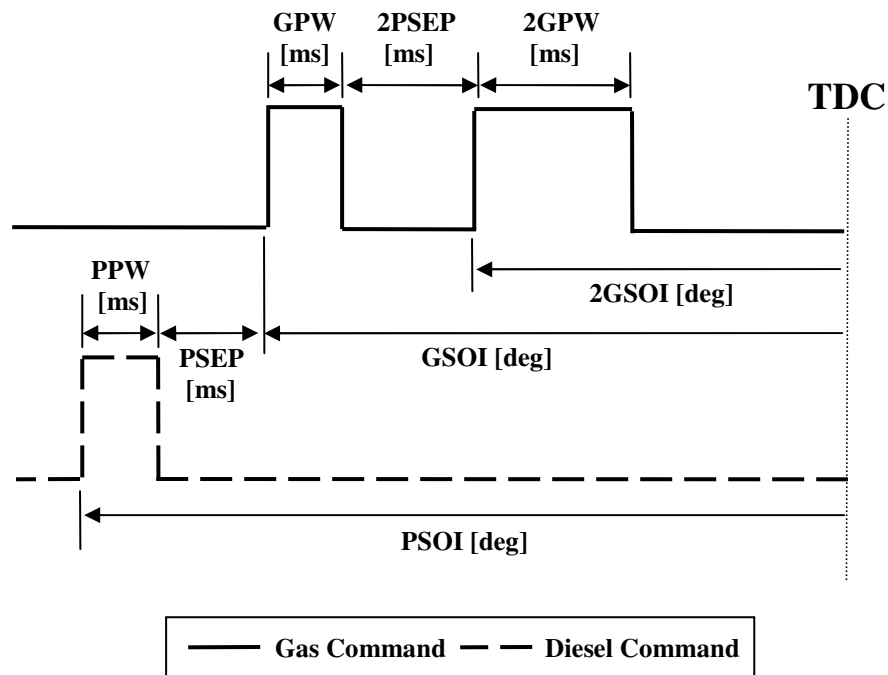


Figure 2-6 – Injector Command Diagram

The diesel injection is called the ‘Pilot’ injection. The pilot start of injection (PSOI) is the number of degrees after TDC to begin the diesel injection (this value is typically negative such that injection is commanded BTDC). The pilot pulse width (PPW) specifies the duration of the diesel injection in ms. The pulse separation (PSEP) specifies, in ms, the time between the end of the pilot injection and the beginning of the first gas injection. Note that for Co-injector CS, the pilot commands are not used because there is no diesel needle (see 1.3.2). GSOI and GPW similarly refer to the start of the

first gas injection (in degrees ATDC) and first gas pulse width (in ms), while 2GSOI and 2GPW refer to the start of injection and pulse width for the second gas injection. 2PSEP is the time in ms between the end of the first gas pulse and the start of the second gas pulse. The J36 normally runs with only one gas injection (i.e. 2GPW=0), but the co-injectors use two gas injections. As can be seen, the PSEP and 2PSEP commands are superfluous if GSOI and 2GSOI are specified. The Labview program allows the user to choose between specifying the start of injections or the pulse separations. Since most test matrices are run with specified pulse separations rather than the crank angles of injection, this is a time-saving option.

2.5. BIAS CONTROL

The Fuel Control Module (FCM) is the system used to control the fuel flows to the injector. Due to the nature of co-injection, the difference between diesel and natural gas injection pressures (called the 'Bias pressure') needs to be controlled precisely. This is accomplished by setting the pressure of the natural gas using the diesel pressure via a dome loaded regulator (DLR). The DLR has a preload spring inside it which determines the minimum pressure difference between the control and exit pressures. The control (diesel) pressure to the DLR is determined based on the setting of three needle valves in the system, which is shown in Figure 2-7 below.

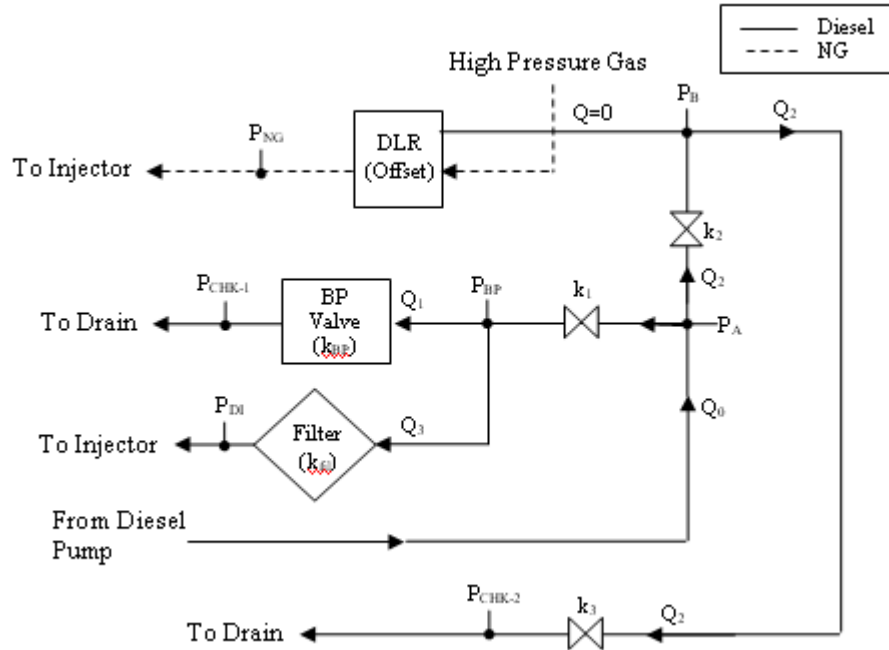


Figure 2-7 – Fuel Control Module (FCM) Flow Diagram

The bias pressure is the difference $P_{DI}-P_{NG}$. The control pressure to the DLR is P_B . Note that at junction B, the line which goes to the DLR has no flow. P_{CHK-1} and P_{CHK-2} are the pressures set by check valves used on the diesel drain line. Equations governing the flows and pressures in the system can be found in Appendix B.

CHAPTER 3 - METHODS OF ANALYSIS

This chapter outlines the various data analysis techniques used in the current research as well as the combustion parameters used to make injector comparisons.

3.1. RESPONSE SURFACES

Response surfaces were used to graphically show trends and characteristics of Co-injector B. A response surface is essentially a linear regression with multiple variables (15 in this case). Matlab code was written to perform the regressions. The response surfaces generated were quadratic and they take the form:

$$\hat{Y}(\bar{x}) = \beta_0 + x_1\beta_1 + x_2\beta_2 + x_3\beta_3 + x_4\beta_4 + x_1^2\beta_5 + x_1x_2\beta_6 + x_1x_3\beta_7 + x_1x_4\beta_8 + x_2^2\beta_9 + x_2x_3\beta_{10} + x_2x_4\beta_{11} + x_3^2\beta_{12} + x_3x_4\beta_{13} + x_4^2\beta_{14} \quad (2)$$

Where β_{0-14} are the coefficients which are solved to fit the surface to the data, x_1 is the intake temperature, x_2 is the intake pressure, x_3 is the CNG flow rate and x_4 is the diesel flow rate. Thus, for each output variable (ex: knock intensity), a unique response surface is generated. Because of the large dataset collected in Chapter 4, it was decided that response surfaces would be beneficial in analyzing the trends and interactions between variables on combustion. The response surface is intended to compliment the raw data by making trends which may exist over broad ranges of the dataset more easily identified and explained. For instance, in the current work, it will be shown using response surface contour plots that the interactions between cylinder pressure, diesel flow, and CNG flow, have non-linear effects on ignition delay. Although the response surface is only an approximation to the raw data, proper analysis of the accompanying statistics gives reliable bounds for where its predictions are accurate. Generally, the greatest confidence (lowest error) is achieved at the center of the data space. As one moves outward from the center, the confidence in the predictions is reduced (this is discussed quantitatively in section 3.1.1) until, as one moves outside the region where data was collected, the prediction becomes much less reliable.

Model Notes and Assumptions

- It is assumed that the true surface is adequately approximated as a quadratic and the bias error (i.e. the error due to approximating the surface as a quadratic when the true surface may actually be a higher order polynomial) is small and negligible compared to the precision error, particularly in the vicinity of the collected data points.
- It is assumed that the variance of the sample residuals is an unbiased estimator of the population variance
- It should be noted that the input values (temperature, pressure, diesel flow, CNG flow) used to fit the surface are taken as true values (i.e. since, for example, the CNG flow for a data point is an average of CNG flow readings over a finite time, it is assumed that the variance in the measurement and the measurement error is negligible compared to the total error)

3.1.1. Response Surface Error Analysis (See Meyers et al., 2002)

Equation 2 can be rewritten in the form:

$$\hat{Y}(\mathbf{x}) = \mathbf{x}\mathbf{b} \quad (3)$$

Where $\mathbf{x} = [1 \quad x_1 \quad x_2 \quad \dots \quad x_4^2]$ is a point on the surface and $\mathbf{b} = \begin{bmatrix} \beta_0 \\ \vdots \\ \beta_{14} \end{bmatrix}$ are the model

coefficients. Next, \mathbf{X} is a matrix containing the values of \mathbf{x} for each of the 'i' data points

collected as follows: $\mathbf{X} = \begin{bmatrix} \mathbf{1} & x_{1,1} & \dots & x_{4,1}^2 \\ \mathbf{1} & x_{1,2} & \dots & x_{4,2}^2 \\ \vdots & \vdots & \ddots & \vdots \\ \mathbf{1} & x_{1,i} & \dots & x_{4,i}^2 \end{bmatrix}$

The covariance matrix of \mathbf{b} is given as:

$$Cov(\mathbf{b}) = \sigma^2 (\mathbf{X}'\mathbf{X})^{-1} \quad (4)$$

$Cov(\mathbf{b})$ is a symmetric matrix whose diagonal elements are the variance of each element of \mathbf{b} , and whose off diagonal elements are the covariance between the elements of \mathbf{b} . An

unbiased estimator (if the residuals are normally distributed with a zero mean) of σ can take the form of:

$$s = \sqrt{\frac{\sum (residual)^2}{df}} \quad (5)$$

Where df is the number of degrees of freedom (number of collected points minus the number of coefficients) and the residuals are the actual values minus the predicted values. As was stated in the model assumptions, the bias error is considered negligible and the total error for each data point will be taken as the precision error (or standard error defined below). The variance in the prediction of the response surface at a given point is given as:

$$VAR[\hat{Y}(\mathbf{x})] = VAR[\mathbf{x}\mathbf{b}] \quad (6)$$

The standard error at a point is found by taking the square root of the variance of the prediction, giving:

$$STD_ERR\{Y(\mathbf{x})\} = s\sqrt{\mathbf{x}(X'X)^{-1}\mathbf{x}'} \quad (7)$$

By calculating the standard error at every point on the map, error surfaces are generated, an example of which is shown in Figure 3-1 below (In this plot, two of the four independent variables are held constant, while the other two are varied along the vertical and horizontal axes. The small \mathbf{x} 's represent locations where data was actually collected).

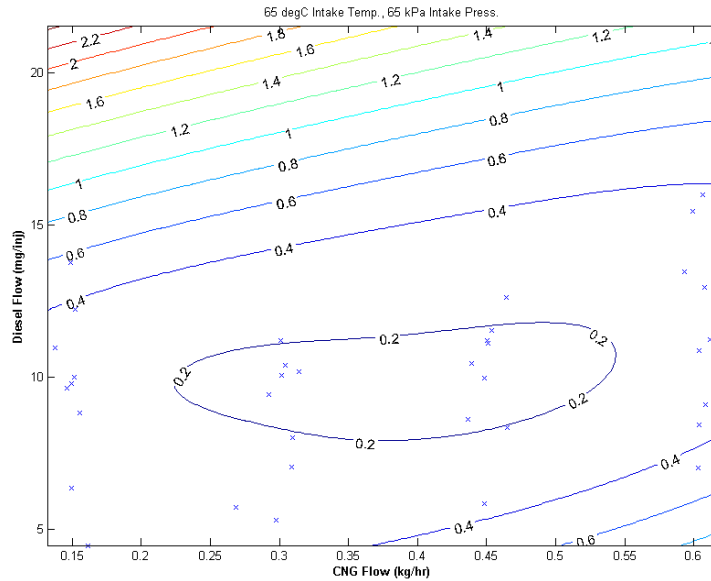


Figure 3-1 – Response Surface Standard Error Map Example

By adding and subtracting the error surface (multiplied by 1.96 to represent a 95% confidence interval) from the response surface, surfaces representing the upper and lower bounds of the 95% confidence interval on the mean are created. Then, for example, by plotting the 3 bar contour from the lower bound knock surface, it can be said that there is only a 5% chance that a mean knock value greater than 3 will be found on one side of the contour. The errors are low in the regions where the test points were collected as shown in Figure 3-2 (the dashed contours represent the 3 bar knock intensity limits).

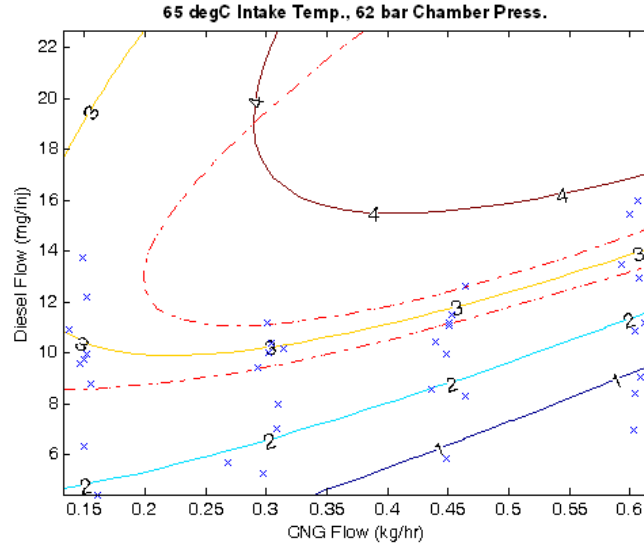


Figure 3-2 – Response Surface Confidence Intervals

3.2. INDICATED MEAN EFFECTIVE PRESSURE AND MECHANICAL EFFICIENCY

The indicated mean effective pressure is a measure of the indicated work output per unit of swept volume [Stone, 1999]. The net indicated work can be expressed as the cyclic integral of the pressure curve over all four strokes of the cycle [Heywood, 1988]:

$$W_i = \oint p dV \quad (8)$$

In the current work, only gross indicated mean effective pressure will be used (GIMEP). The GIMEP only takes into account the work delivered to the piston over the *compression and expansion* strokes (i.e. the pumping work is not included):

$$GIMEP = \frac{\int_{-180}^{180} p dV}{V_{swept}} \quad (9)$$

GIMEP has been used in all previous work done on the SCRE engine and is used along with equivalence ratio to specify the engine load at the various test points. Some limited data available which compared the GIMEP from tests conducted on the SCRE to brake mean effective pressure (BMEP – representative of the actual work output of the engine) of an ISX engine running on all six cylinders at the same conditions. Due to frictional

and heat losses, the BMEP is always lower than the IMEP, and therefore $\frac{BMEP}{IMEP}$ gives the mechanical efficiency of the engine. Mechanical efficiency was calculated to be ~0.7 at 1200 RPM, low load and ~0.9 at 1500 RPM, high load (it is suspected that the increase in efficiency is more due to load than speed since the increased load will increase the temperatures of the lubricating oils, which would reduce frictional losses). Unfortunately only a small amount of data was available which did not cover the speed/load conditions tested here. Nonetheless, it gives a rough approximation to mechanical efficiency for the conditions tested in the present work. In Chapter 5, the emissions are presented in grams normalized by gross indicated kilowatt hour (GIkWh) (which is a function of GIMEP, swept volume and engine speed). Therefore, to estimate how the emissions reported here translate to actual engine out emissions (i.e. g/kWh), one only needs to divide the low load (6 bar GIMEP) emissions by 0.7 and the high load (13 bar GIMEP) emissions by 0.9.

3.3. HEAT RELEASE RATE AND INTEGRATED HEAT RELEASE (HRR AND IHR)

The heat release rate is an approximation to the amount of energy released per crank angle degree due to the combustion. The apparent net heat release rate, which is defined as the difference between the apparent gross heat release rate and the heat transfer rate to the walls [Heywood, 1988] can be calculated using air-standard assumptions and the first law of thermodynamics with the following equation:

$$\frac{dQ_n}{d\theta} = \frac{\gamma}{\gamma-1} p \frac{dV}{dt} + \frac{1}{\gamma-1} V \frac{dp}{dt} \quad (10)$$

This is the heat release rate used in the current study. The pressure and volume in the cylinder are known quantities and the polytropic exponent (γ) is taken as 1.3 (Heywood (1998) recommends a value which reflects the air at the end of compression (1.3-1.34) and the burned gases (1.26-1.3)). The heat release rate plot is used to determine the start of combustion (see Section 3.6) and is useful in making comparisons between injectors

regarding rates of pressure rise and peak heat releases.

The integrated heat release is simply the integration of the heat release rate curve. Examples of unfiltered heat release rate and integrated heat release curves are given in Figure 3-3 below.

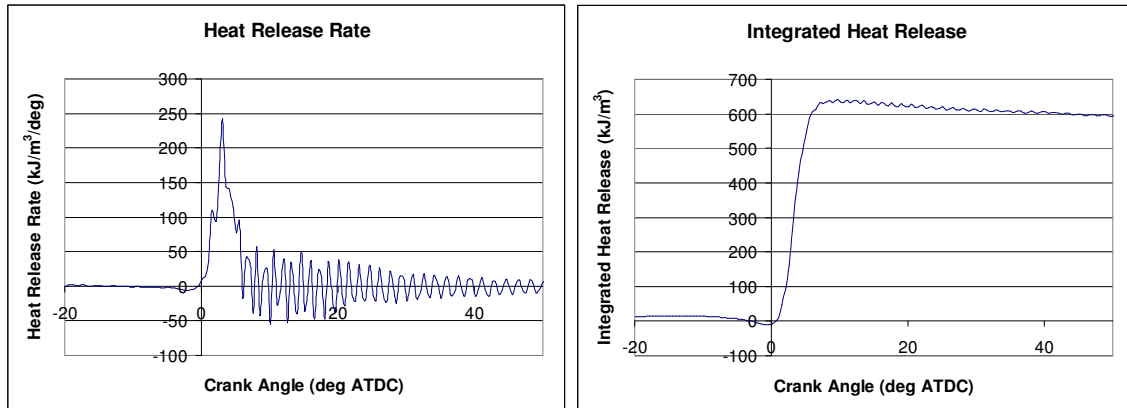


Figure 3-3 – Heat Release Rate and Integrated Heat Release Examples

3.4. CYLINDER TEMPERATURE AT THE TIME OF INJECTION

Different cylinder temperatures result from different intake temperatures, backpressures, and injection timings. The cylinder temperature at injection is calculated by assuming polytropic compression and ideal gas conditions, which gives the following relationship [Cengel, 2002]:

$$T_{@inj} = T_{@BDC} \left(\frac{V_{@BDC}}{V_{@inj}} \right)^{n-1} \quad (11)$$

Both volumes are known from the engine geometry and the time of injection. Due to the presence of residuals in the chamber at BDC, the temperature at bottom dead centre must be calculated using an energy balance as follows:

$$T_{@BDC} = \frac{X \cdot C_{p,resid} T_{exhaust} + (1-X)C_{p,air} T_{intake}}{(C_{p,exhaust} - C_{p,air})X + C_{p,air}} \quad (12)$$

The temperature at BDC is the temperature of a mixture of air at the intake temperature and residual gases at the exhaust gas temperature. X is the residual mass fraction in the cylinder, which is a function of the backpressure. Mixing is assumed to take place at constant pressure.

The polytropic compression of the charge gives rise to the equation below [Cengel, 2002] which makes it possible to calculate the value of n :

$$PV^n = C \quad (13)$$

Where C is a constant. Taking the logarithm of both sides and rearranging gives:

$$\log(P) = C - n \log(V) \quad (14)$$

Therefore, the required value of n is the negative value of the slope of the compression stroke on the logarithmic form of the pressure-volume curve. An example of such a curve is given in Figure 3-4 below (Note: the full compression stroke (lower line) is not fully shown on this plot).

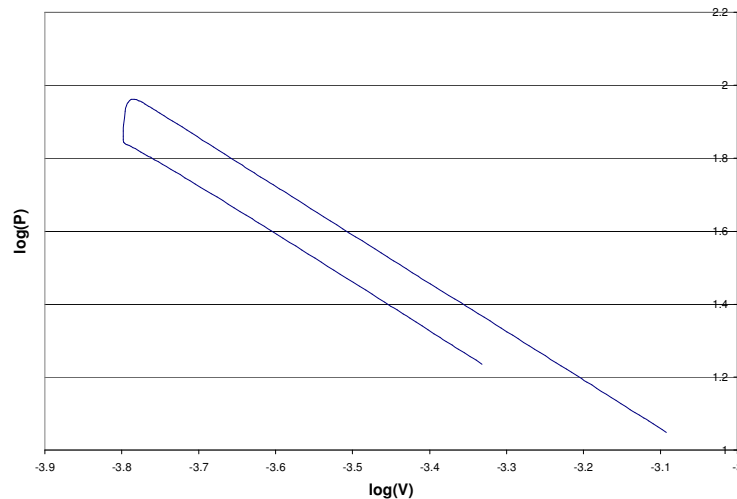


Figure 3-4 – Logarithmic Plot of a Pressure-Volume Trace

Thus, using the above approach, the cylinder temperature at the time of injection can be approximated for any (non-EGR) condition. If EGR is used, the temperature is calculated with a slightly different equation:

$$T_{@BDC} = \frac{X \cdot C_{p,resid} T_{exhaust} + Y \cdot C_{p,EGR} T_{EGR} + (1 - X - Y) C_{p,air} T_{int}}{X \cdot C_{p,exhaust} + Y \cdot C_{p,EGR} + (1 - X - Y) C_{p,air}} \quad (15)$$

Where, Y and T_{EGR} are the mass fraction and temperature of the EGR. X is the non-EGR residual mass fraction.

Note that heat transfer to the cylinder walls during compression has been neglected and therefore the calculated temperatures represent maximums, where the actual temperatures in the cylinder would be lower.

3.5. COMBUSTION EFFICIENCY (η_{COMB})

Emissions are not a major focus of the single injection testing discussed in Chapter 4, since they are discussed in more detail Chapter 5 as well as previous work [McTaggart-Cowan *et al.*, 2009; Brown, 2008]. Also, the single injection tests are meant to simulate the first pulse of a double pulse injection, and therefore the emissions are not necessarily very meaningful since in practice unburned hydrocarbons from the first pulse may get burned after the injection of the second pulse (The very low loads at which the engine runs during these tests are also unrealistic in terms of normal engine operation). However, for the single injection tests, it is useful to see the emissions trends to help understand the effects of various parameters on the combustion. Also, during single injection testing, the NO_x analyzer was malfunctioning for most of the single injection tests and therefore NO_x data is not available. Therefore, a parameter called combustion efficiency (η_{comb}) will be defined as the amount of carbon injected which is completely oxidized. This was calculated by estimating the total moles of carbon injected and the

total mols of carbon measured by the emissions bench as tHC (total unburned hydrocarbons, whose mass is calculated on a methane basis) and CO. The amount of carbon is calculated as:

$$Carbon = \frac{m}{M} \left(\frac{mol_{carbon}}{mol_{molecule}} \right) \quad (15)$$

Where m is the mass of the emission or fuel flow per injection and M is the molar mass of the substance in question (methane for tHC and CNG flow, $C_{12}H_{23}$ for diesel). The combustion efficiency is then defined as:

$$\eta_{comb} = 1 - \frac{C_{tHC} + C_{CO}}{C_{CNG,in} + C_{Diesel,in}} \quad (16)$$

Thus, combustion efficiency can be used as a measure of how much of the injected fuel is being completely oxidized.

3.6. IGNITION DELAY

Ignition delay in a compression-ignition engine is typically defined as the time between the start of fuel injection and the start of combustion [Heywood, 1998]. The ignition delay period can be decomposed into three parts:

- *Mechanical Delay:* This is the time between the command of injection and the actual injector needle opening. The mechanical delay can be found experimentally using an injector visualization chamber.
- *Physical Delay:* This is the time needed for the fuel to evaporate and mix with surrounding air in order to form an ignitable mixture
- *Chemical Delay:* This is the time needed for the chemical reactions to progress to the point where there is a sufficient amount of energy released to raise the temperature and pressure in the combustion chamber.

Note that the physical and chemical delay periods tend to overlap. This is because

chemical reactions begin before the entire quantity of fuel injected has been fully mixed with the air.

The start of combustion in this study was found in a similar way as in Brown (2008), by calculating the slope of the line between two points on the HRR curve (either 25 and 10 $\text{kJ/m}^3/\text{deg}$ or 10 and 5.5 $\text{kJ/m}^3/\text{deg}$, depending on the magnitude of the heat release) and finding the intercept of that line with the x-axis (0 $\text{kJ/m}^3/\text{deg}$ line). This intercept is taken as the crank angle at which the start of combustion occurs. Note that the start of combustion for each point was verified manually by visually checking an overlay of the heat release rate plots and calculated start of combustion. For a few points, the calculated start of combustion was found to be incorrect and was changed based on the heat release rate plots.

Correlations for ignition delay in dual-fuel engines were found to be different from diesel engines due to the reduced oxygen concentration as a result of the gaseous fuel and the change in the polytropic index of compression [Prakash *et al.*, 1999]. Co-injection, however, does not suffer from those differences due to the fact that the gaseous fuel is directly injected near TDC.

3.7. KNOCK INTENSITY

Knock in conventional compression-ignition engines is the result of rapid energy release from a large amount of premixed fuel burning at the time of ignition ('diesel knock'). The large energy release results in a fast local pressure rise which creates a shock wave in the chamber. The shock wave and its reflection off the chamber walls is what causes the pressure fluctuations [Heywood, 1988] seen in the pressure trace in Figure 3-5 below which is henceforth referred to as knock.

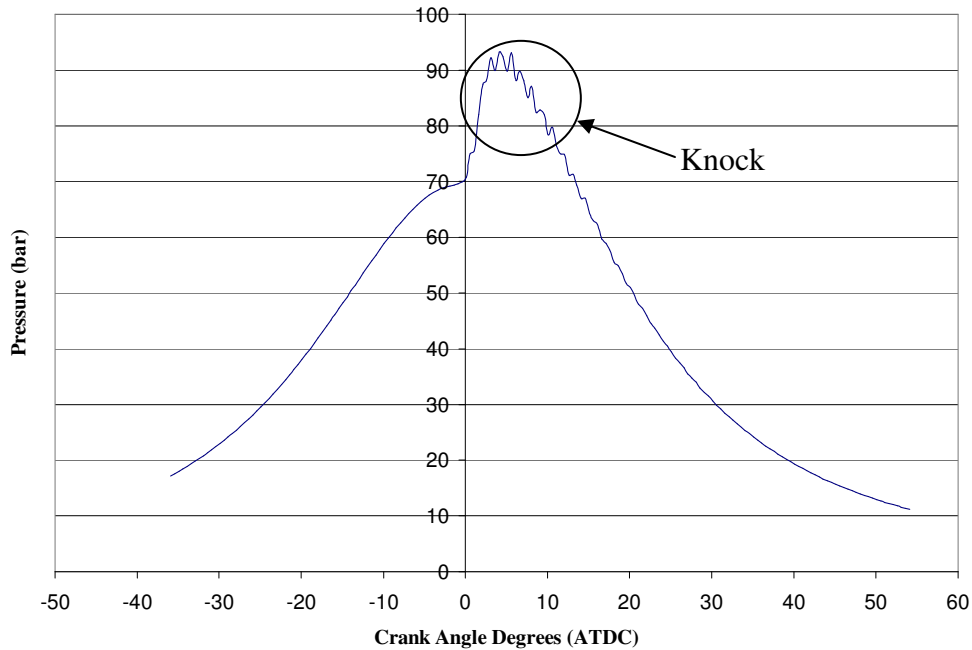


Figure 3-5 – Pressure Trace Illustrating Knock

In a spark ignition engine, knock is normally the result of spontaneous ignition of the end gases. As the flame moves outward from the spark, the gases upstream of the flame front are compressed and heated by the combustion products [Stone, 1999]. When combined with the compression of the piston and hotspots on the chamber walls, the fuel far from the spark can spontaneously ignite in these extreme conditions, causing similar fluctuations to the ones shown above. This type of knock is also found in fumigated dual-fuel compression-ignition engines, where the gaseous fuel is premixed with the air outside the cylinder and subsequently ignited by a small amount of diesel in the cylinder. Since there is an almost homogeneous mixture of gas in the cylinder, it is possible for the fuel near the chamber walls to spontaneously ignite as in spark ignition engines for the same reasons given above, as well as the fact that natural gas has a long burning rate [Nwafor, 2002]. In the current co-injection configuration, end gas autoignition is likely not a concern since the fuel is direct injected and thus the natural gas is more concentrated and the flame therefore does not need to travel as far to burn the gas before it can autoignite. Nonetheless, for co-injection, significant knock appears to be present as a result of the large amount of fuel which ignites immediately after the ignition delay

period. This type of knock has also been reported in dual fuel engines, but in those cases, knock overall has been found to decrease with increased pilot fuel and decreased gaseous fuel proportions [Nwafor, 2003; Selim, 2004] (which is opposite to what is found with co-injection. This is most likely due to end gas self-ignition being reduced with increased pilot and decreased gaseous fuel in dual-fuel engines). Kubesh (1992) showed that the longer ignition delays caused by the presence of the gaseous fuel lead to higher rates of pressure rise at the start of combustion, leading to diesel knock (again, it will be shown that with co-injection, increased gaseous fuel fraction reduces the knock intensity). So while knock intensity is affected by load in a dual fuel engine, in co-injection load does not have much of an effect, but it is the peak rate of heat release near the start of combustion which is the main factor. Figure 3-6 shows data from single injection tests for Co-injector B plotting maximum heat release rate and maximum integrated heat release (indicative of load) versus knock intensity.

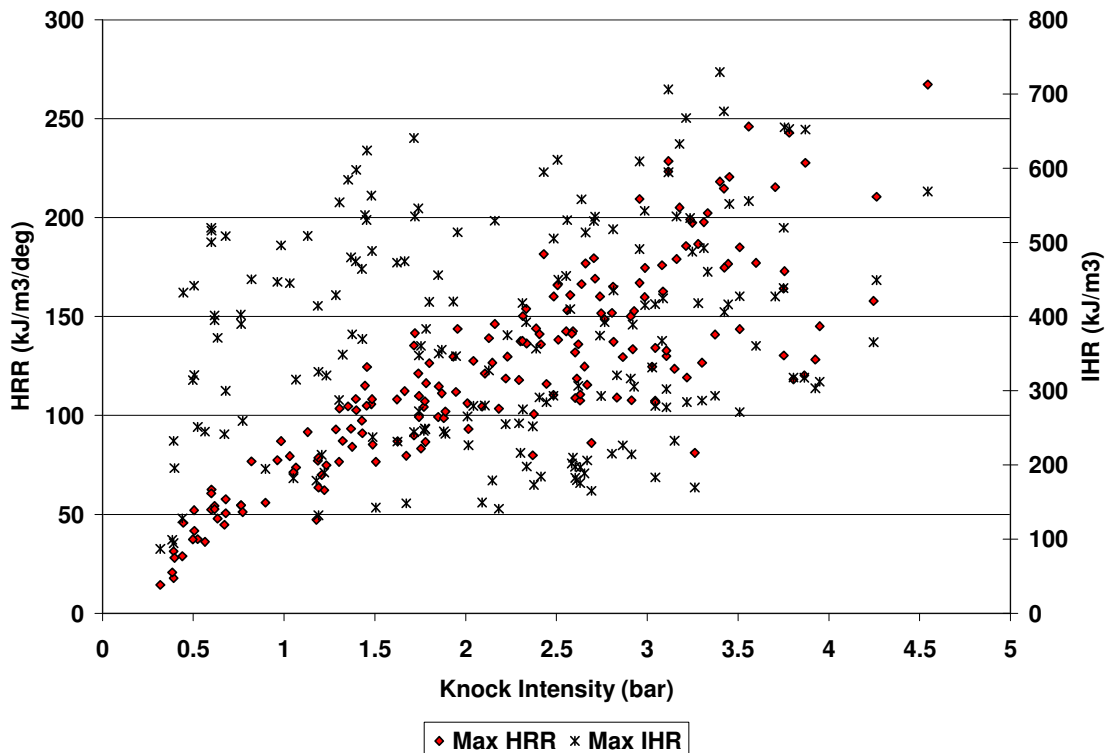


Figure 3-6 – Maximum HRR and IHR vs. Knock Intensity (Co-injector B Single Injection Tests)

Note that the correlation between HRR and knock intensity (knock intensity values and HRR values are 300 cycle-averaged, therefore, some spread in the correlation is should be expected) is quite strong, while there is virtually no correlation between knock intensity and the maximum IHR. Heat release rate figures in Appendix E may suggest that, for low knock intensities (<1.75 bar) the oscillations in the heat release rate do not originate from the start of the pilot combustion event. For knocking conditions above that, it is evident from the figures that the oscillations begin at the start of the pilot combustion event. For the low knocking cases, it is possible that the knock is the result of the pilot not releasing enough heat to burn the gas from the main injection smoothly. A low pilot heat release may result in longer gas (main injection) ignition delay, such that more gas is able to mix with air before the main combustion event begins, leading to more rapid combustion (i.e., much like conventional diesel knock).

The reason that knock at the time of ignition appears to be greater for co-injection compared to fumigated dual-fuel engines is likely that within a given volume containing the same amount of diesel, there is much more gas present in co-injection than in a fumigated engine. Also, since the gas is direct injected, no air is displaced and there is no oxygen depletion in the intake charge as a result (i.e. as the amount of gas is increased in a dual fuel engine, there is less oxygen available for combustion. In co-injection, increasing the gas does not affect the total oxygen concentration). As has been mentioned, the gas in a fumigated engine is distributed more or less homogeneously throughout the cylinder, while in co-injection the gas is concentrated in a dense jet. Therefore, with co-injection, the increased gas density in the vicinity of the diesel along with no decrease in oxygen concentration leads to a more rapid energy release at the beginning of combustion, resulting in higher knock intensities.

Knock can be damaging to engines by causing excessive vibrations which can damage components in the valve train, and piston rings leading to scoring of the cylinder walls. The shock waves caused by knock can also destroy the thermal boundary layers in the cylinder, which increases heat transfer which can lead to runaway knock, eventually

overheating and melting cylinder components [Stone, 1999].

Knock intensity has been quantified in the present work using a method proposed by Heywood (1998) who suggests that the pressure fluctuations occur at the first transverse mode acoustical frequency defined as [Ren *et al.*, 1999]:

$$f = \frac{c}{B} \alpha \quad (17)$$

Where c is the speed of sound of the gas in the cylinder, α is a geometric constant ($1.84/\pi$ [Brown, 2008]), and B is the cylinder diameter. Brown (2008) found that for the current configuration, the frequency should be around 3.7 kHz. An FFT of a pressure trace for high knock case of Co-injector B is shown in Figure 3-7 below.

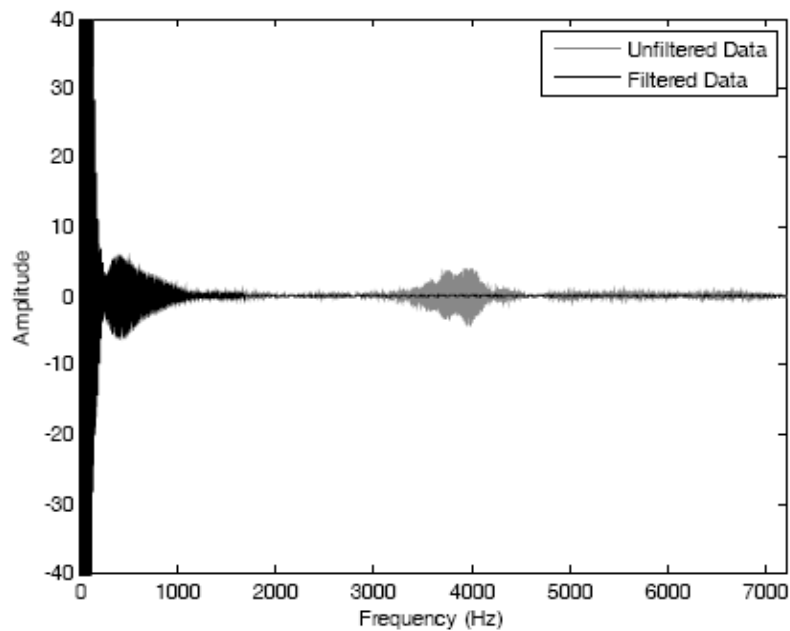


Figure 3-7 – Filtered and Unfiltered FFT of a Pressure Trace with High Knock [From Brown, 2008]

To calculate the knock intensity, the pressure signal is filtered above 3 kHz and then the filtered signal is subtracted from the unfiltered signal. The maximum difference in pressure is the knock intensity for that cycle. In the current work, the knock intensity at a given condition is the knock intensity averaged over 300 successive cycles.

CHAPTER 4 - SINGLE INJECTION TESTING RESULTS

4.1. TEST MATRICES AND DATA PRESENTATION

A full factorial test matrix varying the parameters shown in Table 4-1 below was applied to Co-injector B with gas injection pressures of 21 MPa and 28 MPa.

	Test Parameter	Values	Comments
21 MPa Gas Injection Pressure	Intake Valve Temp. (°C)	41, 65	
	Cylinder Pressure at Injection (bar)	37.5, 50, 62	The low-pressure case had an injection timing of 18.5° BTDC, while the other pressure cases had a timing of 8.25° BTDC
	CNG Flow (mg/inj)	25, 18.8, 12.5, 6.3	
	Diesel Flow (mg/inj)	High, Medium, Low	Flow ranges from 4.5 to 22.7 mg/inj
28 MPa Gas Injection Pressure	Cylinder Pressure at Injection (bar)	37.5, 62	The low pressure tests were done with an intake valve temperature of 41°C and an injection timing of 18.5° BTDC. The high pressure tests had an intake temperature of 65°C and an injection timing of 8.25° BTDC
	CNG Flow (mg/inj)	25, 18.8, 12.5, 6.3	
	Diesel Flow (mg/inj)	High, Medium, Low	Flow ranges from 8.4 to 26.3 mg/inj

Table 4-1 – Single Injection Test Matrices

Parameters held constant are as follows:

- Engine speed was 800 RPM
- Bias pressure was held at 2.5 MPa

- Coolant temperature was 80°C
- Oil temperature was 87°C
- PSEP held at 1.0ms
- Exhaust back pressure was 20 kPa above the intake pressure

Recall that, for the response surfaces, x_1 is the intake temperature, x_2 is the cylinder pressure, x_3 is the CNG flow, and x_4 is the diesel flow. The tests were performed in an order which allowed the most efficient use of the engine and were thus not completely randomized. Repetitions were never collected back to back and rarely collected on the same day.

Note that a smaller set of testing was done with a gas injection pressure of 28 MPa. The smaller set of tests (each with three repetitions) were used to create response surface of a slightly different form than that given in Section 3.1 since only linear pressure and temperature effects can be accounted for with this matrix (three distinct points are required to make quadratic fits). The 28 MPa response surfaces take the form (note only 13 coefficients are needed compared to the original 15 shown in Eq. 2 because the quadratic temperature and pressure terms have been dropped):

$$\hat{Y}(\bar{x}) = \beta_0 + x_1\beta_1 + x_2\beta_2 + x_3\beta_3 + x_4\beta_4 + x_1x_2\beta_5 + x_1x_3\beta_6 + x_1x_4\beta_7 + x_2x_3\beta_8 + x_2x_4\beta_9 + x_3^2\beta_{10} + x_3x_4\beta_{11} + x_4^2\beta_{12} \quad (18)$$

The matrix was reduced due to time constraints, but the reduced matrix still allows for a comparison between the two injection pressures in order to estimate the effect that injection pressure has on combustion.

The high, low and medium diesel flows were chosen based on the knock and misfire limits of the research engine. First the temperature, pressure and CNG flow parameters would be set and the diesel flow was set such that the engine was running stably without any knock. Then, the diesel flow was increased by increasing the PPW (while adjusting

the GPW to keep the CNG flow constant) until engine knocking was clearly heard and observed on the oscilloscope. This was recorded as a case of 'High' diesel flow. Next the PPW was reduced (while adjusting GPW) until significant misfiring occurred (which was quantified as having total unburned hydrocarbon emissions of 650ppm or greater). This was recorded as a case of 'Low' diesel flow. For "Medium' diesel flow, the average PPW between the high and low cases was used.

In addition to the 21 MPa tests shown in Table 4-1, nine points (three test points and three repetitions of each) were collected at 53°C intake temperature, 56.5 bar cylinder pressure, 15.5mg/inj CNG flow and high, low and medium diesel flows. Therefore, the initial full factorial tests (with three repetitions each) plus the nine additional points give a total of 225 test points used to create the quadratic response surfaces for the 21 MPa tests described in Section 3.1.

The 21 MPa response surface plots are presented six at a time and they are stratified such that the top four plots are at the 8.25° BTDC injection timing, while the bottom two plots are at the 18.5° BTDC timing. Each pair of plots in a row has the same cylinder pressure at the time of injection. For the four 8.25° BTDC timing plots, both plots in the left column have a cylinder temperature of 540°C at the time of injection, while the plots in the right column have a temperature of 505°C. The cylinder temperature and pressures are labeled at the top of each plot.

In each individual plot, the intake valve temperature and cylinder pressure at injection is held constant, while the CNG flow and diesel flow are varied along the horizontal and vertical axes. The shaded areas represent regions of the surface where the standard error is greater than 1.35 times the standard deviation of the residuals ('s' – See section 3.1.1) which represents regions outside the boundaries of the test matrix. The 'x' markers on the plot represent combinations of CNG and diesel flows which were actually tested in that region.

Because of the reduced 28 MPa test matrix, the 28 MPa response surfaces are not presented separately, but rather chosen knock intensity, ignition delay and combustion efficiency contours are overlaid on the same plots to show the effect of injection pressure.

4.2. SAMPLE PRESSURE TRACES AND INTEGRATED HEAT RELEASES (IHRs)

Before looking at the response surfaces of the data, it is helpful to look at the actual combustion measurements in order to visualize what is happening during combustion. Figure 4-1 shows pressure traces with the knock intensity and ignition delay for each case indicated in the inset table. Although these plots do not cover the entire range of data collected, they give some insight into the effects of temperature, pressure and fuel flow rates on the combustion, which will be expanded on in later sections. In the top plot of Figure 4-1, the solid vertical line represents the command of injection for traces #1-5, and the dashed line is the command of injection for trace #6 (early injection case). Traces 1 and 2 are high and low diesel flow cases (other variables held nearly constant). Traces 3 and 4 show test points with high and low cylinder temperatures at the time of injection for the same injection timing (calculated from measured pressures and intake temperature). Finally, traces 5 and 6 show cases for different injection timings with similar fuelling rates. The relative knock intensities can be seen in the oscillations of the pressure traces, and the calculated values of knock and ignition delay are given. As can be seen, knock intensity is most increased with increasing diesel flow (compare Traces 1 and 2). Early timing, which results in lower cylinder pressure and temperature at injection decreases the knock intensity and increases the ignition delay. Cylinder temperature clearly has an effect on the rate of energy release (compare traces 3 and 4) likely by way of the chemical kinetics of the combustion reactions. While these traces are helpful in understanding some of the interactions, it is useful to look at the response surfaces which bring together all the data points.

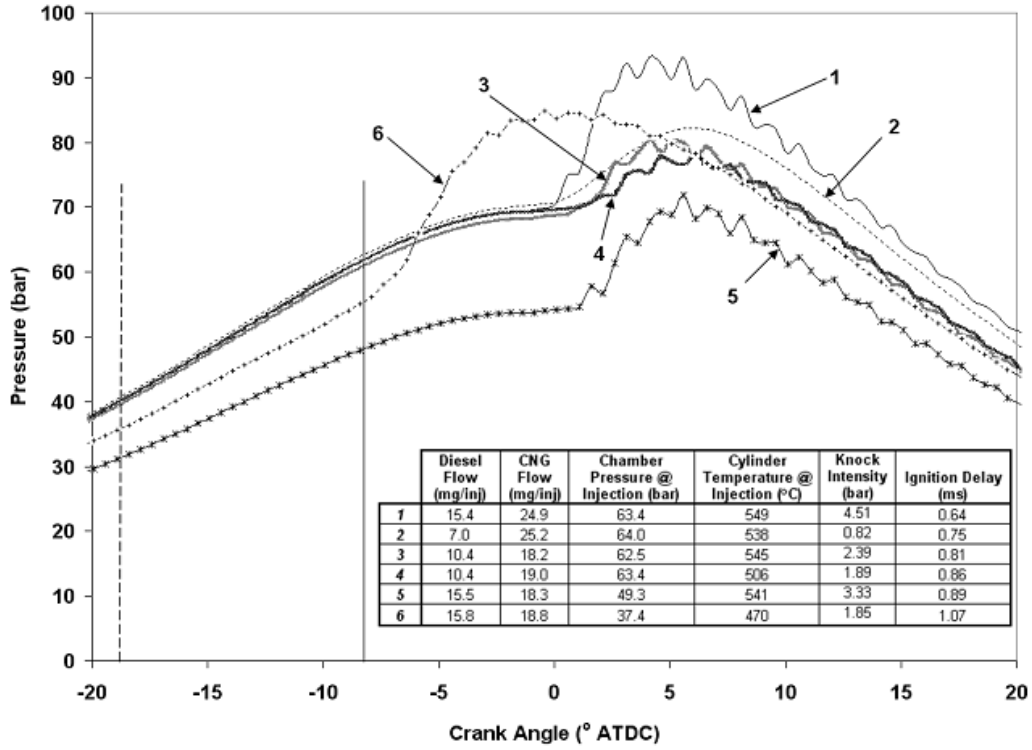


Figure 4-1 – Pressure Traces and IHRs for Selected Single Injection Test Points

4.3. RESPONSE SURFACES

4.3.1. Response Surface Coefficients, Statistics and Residual Plots

The response surfaces which will be presented in this chapter are multi-dimensional curve fits of the data which was collected from the SCRE. This section provides the statistical analysis of the response surfaces which justify their use and help determine the regions where the surfaces are most representative of the data. Table 4-2 below shows the coefficients, R^2 values, and 's' (standard error – see section 3.1.1) values for each response surface.

<i>Coefficients</i>	21 MPa Models			28 MPa Models		
	Knock Intensity	Ignition Delay	Comb. Efficiency	Knock Intensity	Ignition Delay	Comb. Efficiency
β_0	2.514	0.861	0.763	4.667	0.813	0.942
β_1	0.498	-0.093	0.168	1.84	0.366	0.010
β_2	1.059	-0.240	-0.032	0.948	-0.4967	0.027
β_3	-1.026	0.186	-0.095	-2.07	0.0374	-0.026
β_4	2.735	-0.185	0.232	4.843	0.0005	0.0539
β_5	-0.258	0.006	-0.069	-0.408	0.145	-0.075
β_6	-0.268	0.047	0.023	-0.899	-0.486	0.017
β_7	0.448	-0.018	0.070	0.086	0.534	-0.215
β_8	-0.609	0.026	-0.169	0.2154	0.225	0.064
β_9	0.299	0.106	0.100	2.046	-0.08	-0.044
β_{10}	0.441	-0.112	-0.018	0.177	0.09	0.014
β_{11}	-0.347	0.274	-0.025	-0.231	-0.598	0.289
β_{12}	-0.666	-0.020	0.052	0.364	0.411	-0.368
β_{13}	1.585	-0.155	0.123	-	-	-
β_{14}	-0.913	0.093	-0.169	-	-	-
Parameters						
R^2	0.76	0.92	0.86	0.96	0.94	0.96
S	0.50 (bar)	0.06 (ms)	0.035	0.23 (bar)	0.06 (ms)	0.023

Table 4-2 – Single Injection Response Surface Coefficients, R^2 , and Standard Error Values

Note that the coefficients shown here are used in equation 2 and 18 to construct the response surfaces. However, these coefficients are for x_1 , x_2 , x_3 , and x_4 values which have been transformed such that their values range between -1 and 1. This was done for each variable through the following equation:

$$x_n = \frac{2X_n - (X_{n,\max} + X_{n,\min})}{X_{n,\max} - X_{n,\min}} = aX_n + b \quad (19)$$

Where x_n is the normalized input variable, and X_n is the input in its natural units ($^{\circ}\text{C}$, kPa, mg/inj). The max and min values are the maximum and minimum temperatures, pressures, and fuel flows achieved during testing. The values for ‘a’ and ‘b’ are given below for each case.

	21 MPa		28 MPa	
	a	b	a	B
x_1	0.076	4.079	0.079	4.231
x_2	0.069	3.559	0.078	3.998
x_3	0.099	1.545	0.098	1.517
x_4	0.110	1.488	0.104	1.837

Table 4-3 – Single Injection Response Surface Variable Transformation Values

Therefore, when using the coefficients in Table 4-2 with raw, untransformed data, equation 2 becomes:

$$\hat{Y} = \beta_0 + (a_1X_1 + b_1)\beta_1 + (a_2X_2 + b_2)\beta_2 + \dots + (a_4X_4 + b_4)^2\beta_{14} \quad (20)$$

Note that the R^2 values, which represent the percent of the variation in the data which is accounted for by the model are all above 0.85 except for the knock intensity surface for the 21 MPa case. As will be discussed in section 4.3.2, this lower correlation is due to the low gas flow cases (6.3 mg/inj). The effect of removing some of these points from the knock intensity response surface calculation is discussed in Appendix D.

Next, the residual plots for the models are shown. The residual plot is simply the experimentally measured value at a point minus the predicted value ($r = Y - \hat{Y}$). The vertical axes on the right sides of the plots are the residuals in units of the parameter being examined (bar, ms, g/hr). The left side vertical axis is the residual normalized by the standard error (s). The horizontal axes are the values of the parameters predicted by

the surfaces at each point.

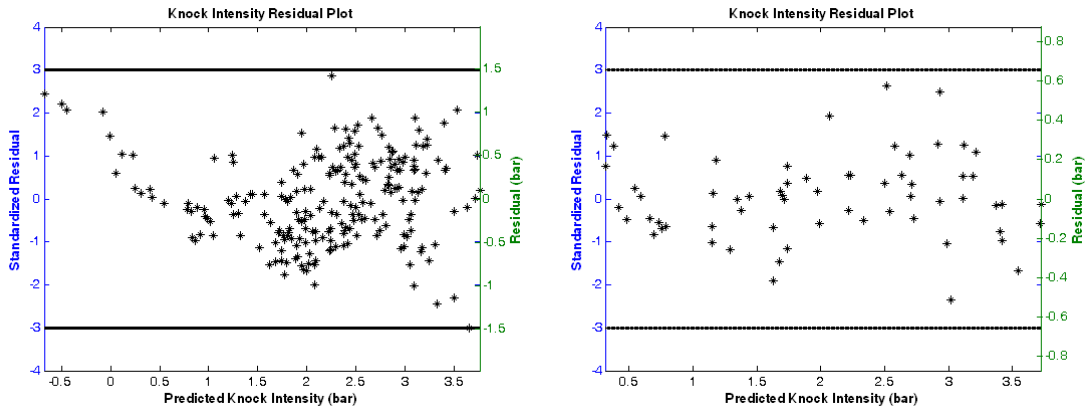


Figure 4-2 – Knock Intensity Residual Plots for 21 MPa (left) and 28 MPa (right) Injection Pressure

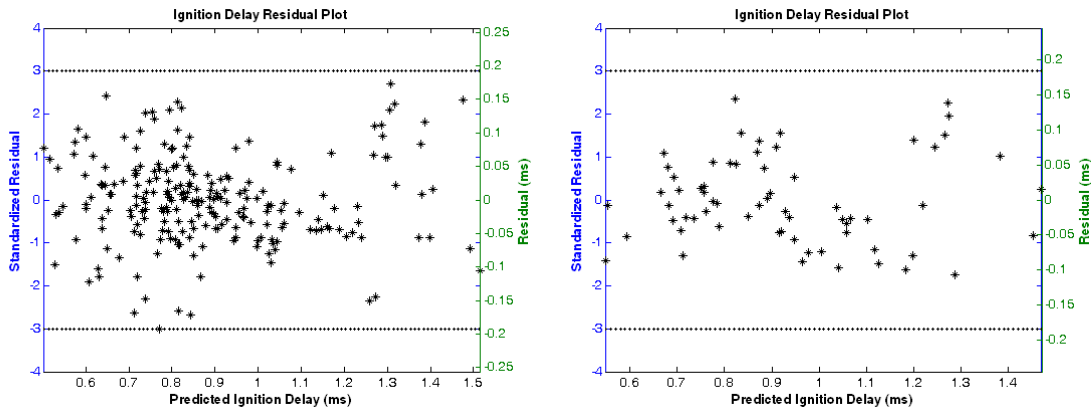


Figure 4-3 – Ignition Delay Residual Plots for 21 MPa (left) and 28 MPa (right) Injection Pressure

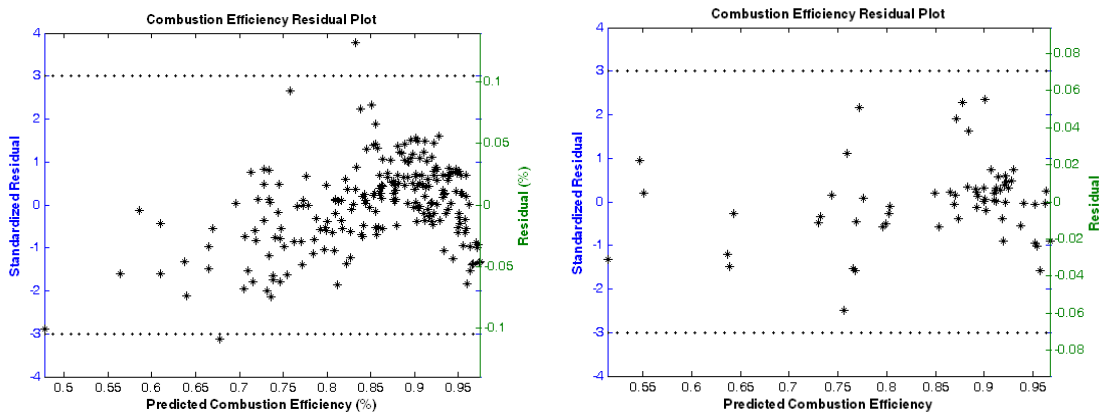


Figure 4-4 – Combustion Efficiency Residual Plots for 21 MPa (left) and 28 MPa (right) Injection Pressures

The residual plots should be scattered randomly about zero to satisfy the assumption of the value of ‘s’ being an unbiased estimator of the population variance. From the figures above, it appears that the knock intensity and combustion efficiency surfaces have a somewhat non-random distribution. This is likely due to the fact that there are not enough parameters in the model (i.e. the true surface is a higher order polynomial [Montgomery *et al.*, 2001]). For example, as can be seen in the knock residual plot, the when the surface approaches low values of knock intensity (<1bar), the shape of the surface no longer adequately approximates the true shape. To verify the degree of non-normality of the distributions, normal plots of the residuals are shown below. For data which are normally distributed, the points on these plots should lie along a straight line. Non-normality (which is likely the result of an insufficient number of model parameters used to predict the true surface shape) in the data introduces curvature to these plots [Engineering Statistics Handbook, 2009; Montgomery *et al.*, 2001].

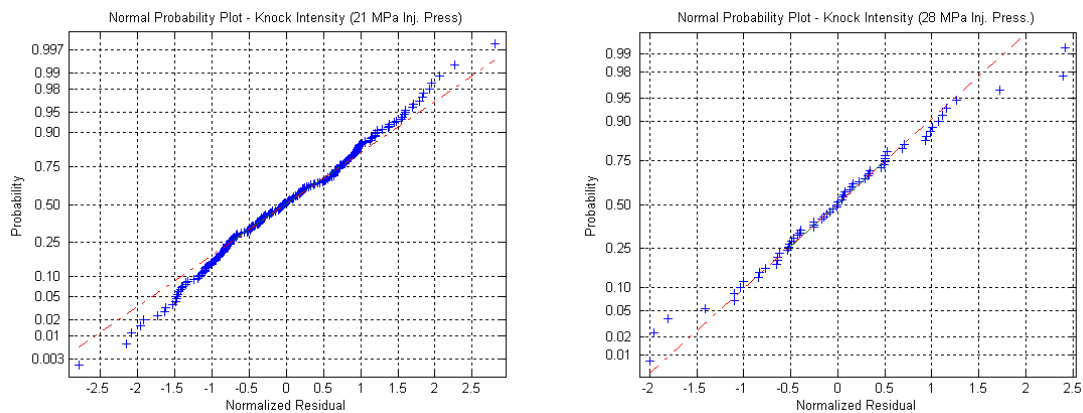


Figure 4-5 – Knock Intensity Normal Plots

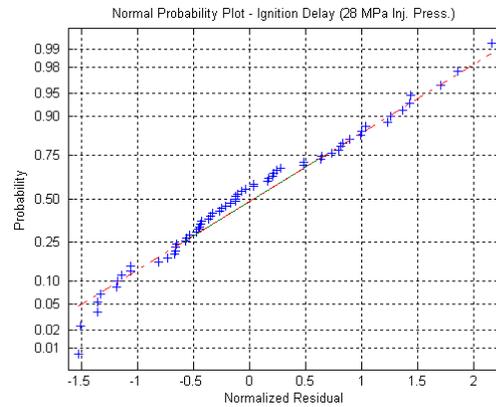
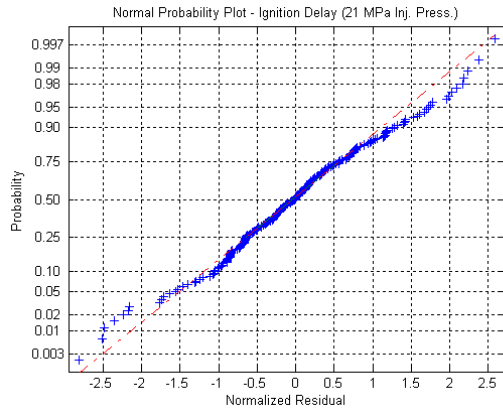


Figure 4-6 – Ignition Delay Normal Plots

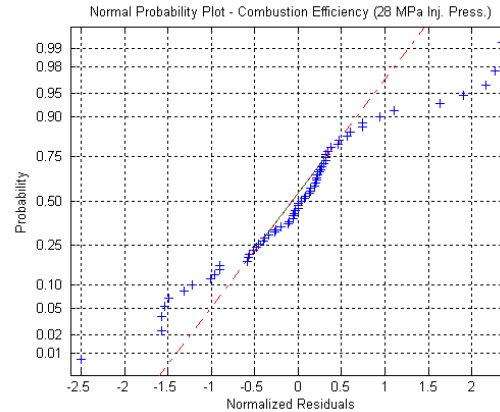
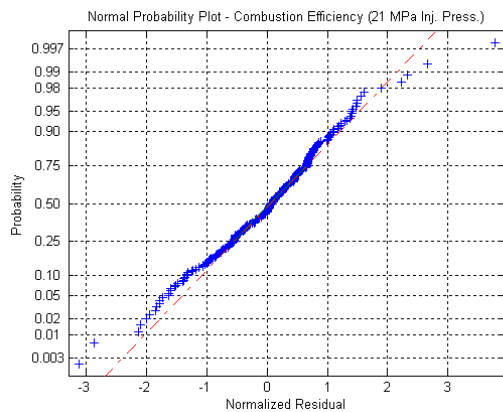


Figure 4-7 – Combustion Efficiency Normal Plots

These plots indicate that the residuals are not perfectly normally distributed because the data tends to break the linear trend at the tail ends, particularly for the combustion efficiency. Note however that the dashed line is a line added by the Matlab ‘normplot’ function which joins the first and third quartiles of the data and then extrapolates to the rest of the data. Thus, the line is not a least squares regression of the data (look, for example at the knock intensity plot for the 21 MPa injection pressure case. If the line were rotated slightly counter-clockwise, the data would appear to fit it more closely). These plots reinforce the fact that the models are most reliably used in the vicinity of the data collected and that at the edges of the test matrix the predictions become less reliable. The s-shapes (particularly the high injection pressure combustion efficiency case) suggest that the distribution may be double exponential rather than normal [Engineering Statistics

Handbook, 2009; Montgomery *et al.*, 2001]. The double exponential distribution is shaped like the normal distribution, but it declines more rapidly and has longer tails. This implies that a transformation of variables could improve the model accuracy. One variable transformation suggested by Meyers *et al.* (2002) in which the response surface for the natural logarithm of the response variable is generated such that the model takes the form:

$$\begin{aligned} \ln(\hat{y}) &= \beta_0 + x_1\beta_1 + x_2\beta_2 \dots \\ \hat{y} &= e^{(\beta_0 + x_1\beta_1 + x_2\beta_2 \dots)} \end{aligned} \quad (21)$$

This technique was used in an effort to improve the residuals of the knock intensity model, but no improvements could be made using logarithmic or power transformations. Appendix D shows an improvement to the knock intensity model via the removal of some key points from the calculation which are known to be poorly predicted by the response surface. The logarithmic transformation was also applied to the 28 MPa injection pressure combustion efficiency response surface, which shows significant curvature in the normal plot. The result of the transformation is shown in below.

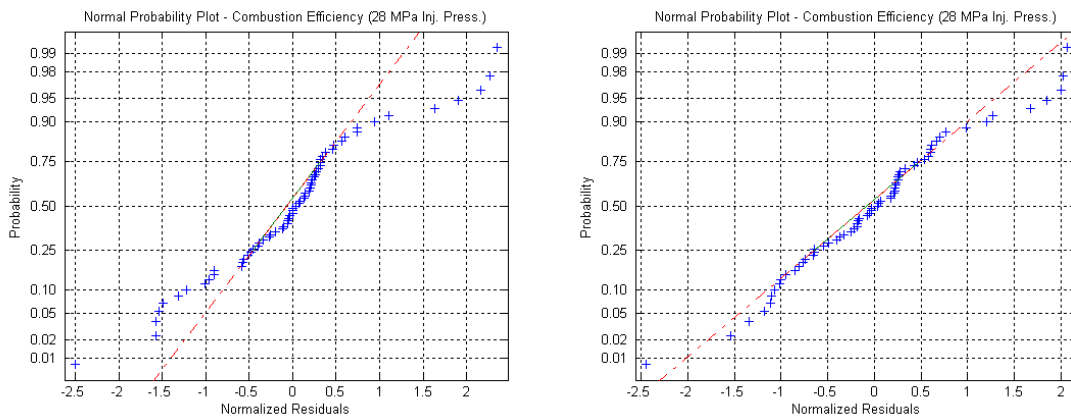


Figure 4-8 – Normal Plot of Residuals from the Original (Left) and Transformed (Right) Response Surfaces

The transformation took away some, but not all of the curvature in the probability plot. Other approaches raising the response variable to different powers was also tried, but gave no better results than the logarithmic transformation. Note that even after the transformation, the R^2 and s values were unchanged and the response surface in the areas of interest did not show any significant changes.

4.3.2. Knock Intensity, Ignition Delay, Combustion Efficiency, and NO_x

Figure 4-9 shows contours of constant knock intensity from projections of the knock intensity response surface (21 MPa injection pressure).

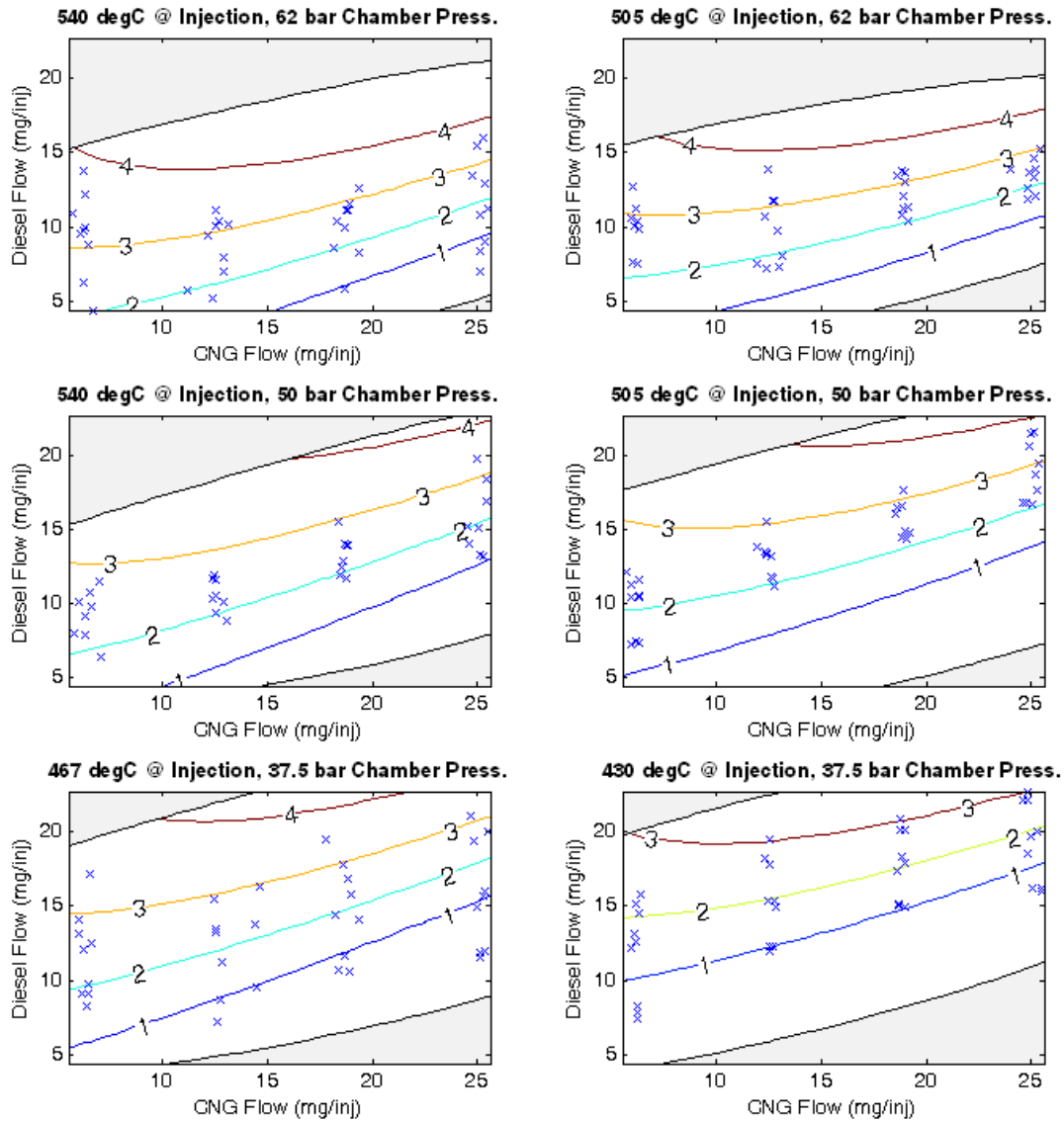


Figure 4-9 – Knock Intensity (bar) Contours (21 MPa Injection Pressure)

The response surface shows that as diesel fueling is increased, the knock intensity also increases. An increase in gas fueling decreases the knock intensity, but has a much

smaller effect than the diesel flow. These results are consistent with single injection tests done by McTaggart-Cowan (2006) and double injection tests done by Brown, 2008, where maximum diesel and minimum gas flows were limited by the onset of knock. Diesel essentially increases the effective cetane number of the diesel/gas mixture, and therefore, as the amount of diesel increases, the mixture becomes more reactive, releasing more energy more quickly at the start of combustion, which produces the knock (see section 3.7). The cylinder temperature at the time of injection has only a slight effect on knock intensity. Increased cylinder temperature tends to increase the knock intensity, if only by a small amount relative to the effect of diesel flow. The effect of cylinder pressure on knock intensity appears to be much more significant than temperature over the ranges tested. When looking at plots in the same row (i.e. constant cylinder pressure, different intake valve temperature), one sees a slight change in the position of the contours, whereas when one looks at, for instance the two plots in the upper left box (constant temperature, different cylinder pressures), one notices a much more pronounced shift in the contours. It has been found by Biger *et al.* (2009), that cylinder pressure and injection pressure have an effect on gas flow likely via the electro-mechanical dynamics of the injector. It was found that higher cylinder pressures resulted in higher gas flows for a given GPW. This means that for a given gas flow, the required GPW is lower at higher cylinder pressures (see Table 4-4) which means that most of the fuel is delivered to the cylinder sooner at higher cylinder pressures. This means that there is more time available for the fuel and air to mix, leading to greater energy release at the beginning of combustion.

	21 MPa Injection Pressure	28 MPa Injection Pressure
37.5 bar Cylinder Pressure @ Injection	0.73 (0.9)	0.62 (0.71)
62 bar Cylinder Pressure @ Injection	0.6 (0.74)	0.45 (0.65)

Table 4-4 – Gas Pulse Width Required to Provide Either 12.5 mg/inj or 25 mg/inj (Number in Parentheses) of CNG as a Function of Cylinder Pressure at Injection and Gas Supply Pressure.

However, as will be shown, ignition delay also is reduced with increased cylinder pressure, which means that some of the extra time acquired by injecting the fuel sooner is lost to a shorter delay period. Thus other factors may be causing the increased knock intensity at higher cylinder pressures. Bruneaux (2002) studied mixture formation in a gaseous methane jet under diesel-like conditions using Planar Laser Induced Fluorescence (PLIF) using nitrogen as the ambient gas. The images in Figure 4-10 below show the fuel concentration (color scale on the right of the image in kg/m^3) distribution in an averaged jet (averaged from 100 images) with different injection pressures and temperatures (P_i is the injection pressure and ρ_{ch} is the nitrogen density which correspond to pressures of 27 bar and 13 bar) at 1.25ms after injection.

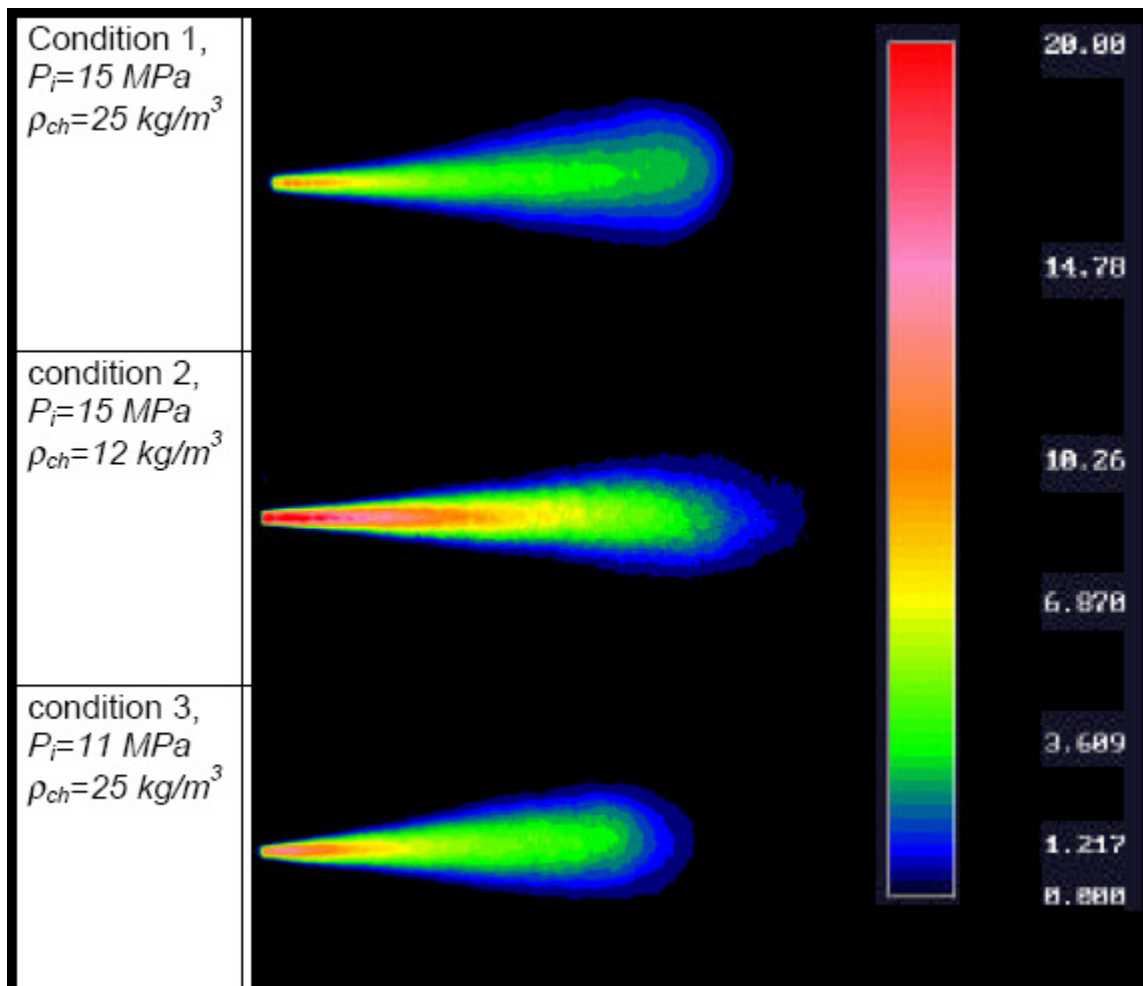


Figure 4-10 – Fuel Density Distributions of Gaseous Fuel Jets [From Bruneaux, 2002]

Although the conditions are not exactly the same as the ones in the SCRE (the pressures are higher for SCRE conditions), Figure 4-10 is useful in examining the pressure effects on the injected fuel (recall that it is assumed that the co-injector fuel is a fine diesel spray uniformly distributed in the gas). For instance, comparing conditions 1 and 2, where condition 1 has a higher ambient pressure at the same injection pressure. The fuel concentrations near the center of the jet at condition 2 are lower than in condition 1. This implies that more nitrogen (or air in the case of the co-injector jet) penetrates deeper into the jet at higher cylinder pressures. Since, in Co-injector B, the diesel is expected to be almost uniformly distributed throughout the jet, if the air penetrates deeper, then more diesel is likely to form an ignitable mixture by the time of ignition, resulting in a greater energy release and higher knock intensity. The cylinder temperature tends to increase knock intensity, likely due to increased reaction rates.

Figure 4-11 shows the ignition delay contours in the same manner as the knock intensity contours shown above. These contours are clearly different in form from the knock contours at higher pressures.

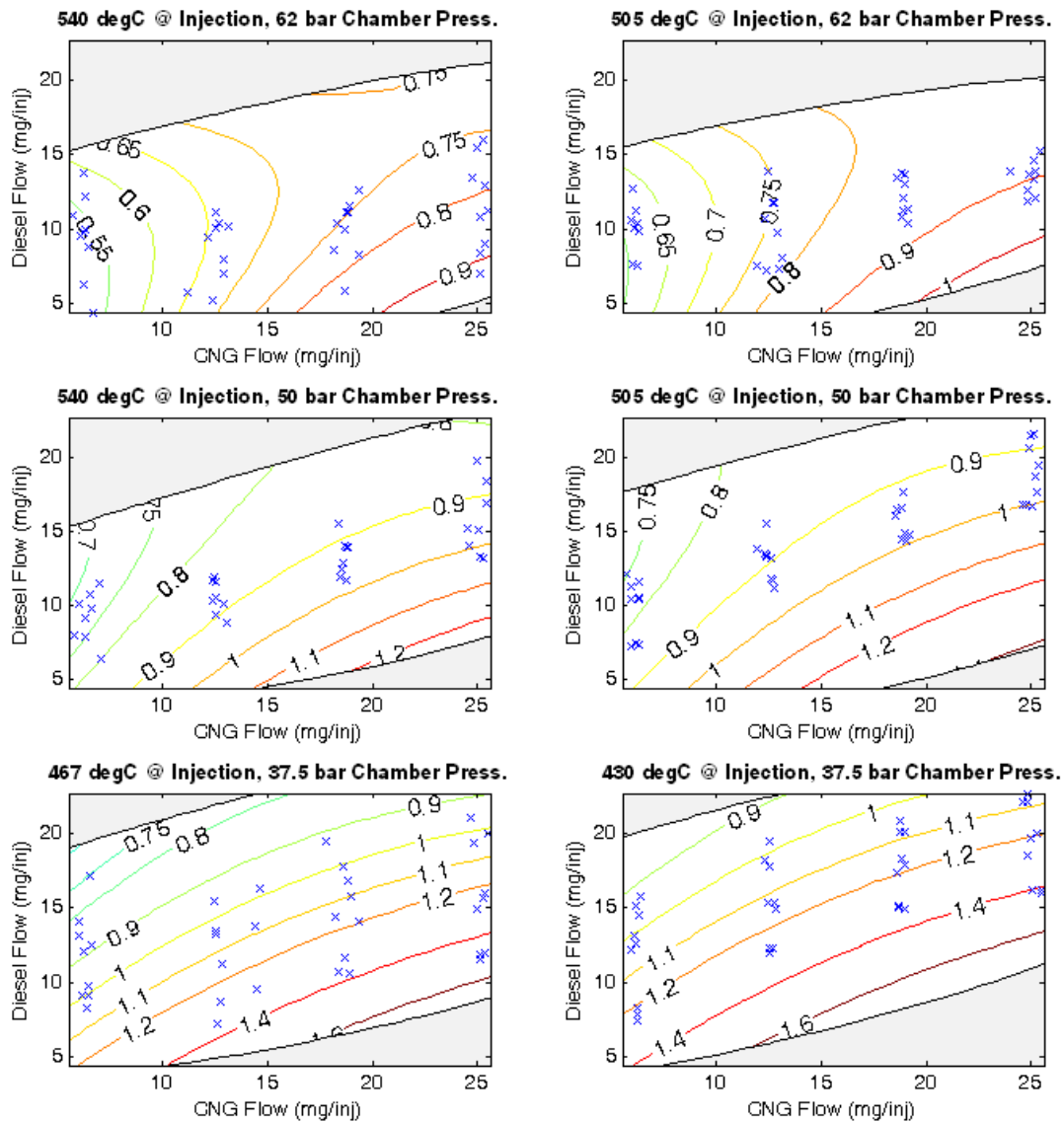


Figure 4-11 – Ignition Delay (ms) Contours (21 MPa Injection Pressure)

Increasing the temperature decreases the ignition delay, while increased pressure not only shortens the ignition delay time, but also changes the relationship between the fuel flows and the ignition delay. At low pressures, the delay clearly decreases as diesel fueling is increased and slightly increases with increased gas fueling. As the pressure is increased (see the top row), the effect of diesel on ignition delay becomes negligible. It should be

noted that the spacing between the contours at high pressure is 0.05 ms while at low pressure the spacing is 0.1 - 0.2 ms. Thus, as ignition delay is decreased, the changes in ignition delay as a result of different fuelling combinations are also decreased. This is because ignition delay typically has an exponential form and therefore as ignition delay is decreased, its rate of change is also decreased, which is the trend seen in Figure 4-11. The contours suggest that increased cylinder pressure reduces the ignition delay to a point where increasing the diesel can no longer speed up ignition. As was discussed with knock intensity, increasing cylinder pressure allows more fuel to be injected sooner for a given injection timing, resulting in a reduction in ignition delay. For longer ignition delays ($>0.75\text{ms}$), increasing diesel reduces the ignition delay time. Since the start of ignition is calculated by finding the point when a given amount of energy is released, the increased reactivity of the fuel mixture (i.e. the increase in possible ignition sites) as a result of a higher diesel concentration results in a more rapid energy release, reducing the ignition delay. Thus, it appears that increasing the cylinder pressure and temperature reduces the physical delay (mixture preparation time), while increasing the diesel/gas ratio reduces the chemical delay (chemical delay of the gas such that more diesel results in a greater heat release such that some gas can ignite sooner and contribute to the initial combustion event. The chemical delay of the diesel is not affected by the amount of diesel). Therefore at high cylinder pressures and temperatures, the physical delay is reduced to the scale of the chemical delay and the chemical delay approaches its minimum (i.e. the chemical delay of the diesel) which is seen in the top two plots of Figure 4-11 where the contours curve to become nearly independent of diesel flow (for a given gas flow).

The contours of combustion efficiency are shown in Figure 4-12. As would be expected, combustion efficiency increases with increased diesel mass, which follows from previous discussions where increasing the diesel mass has been described as increasing the effective cetane number of the mixture which would lower the emissions by producing more rapid, hotter combustion. Also, as would be expected, increased temperature (at constant pressure) at the time of injection leads to higher combustion efficiency due to

higher reaction rates and greater laminar burning speeds [Stone 1999].

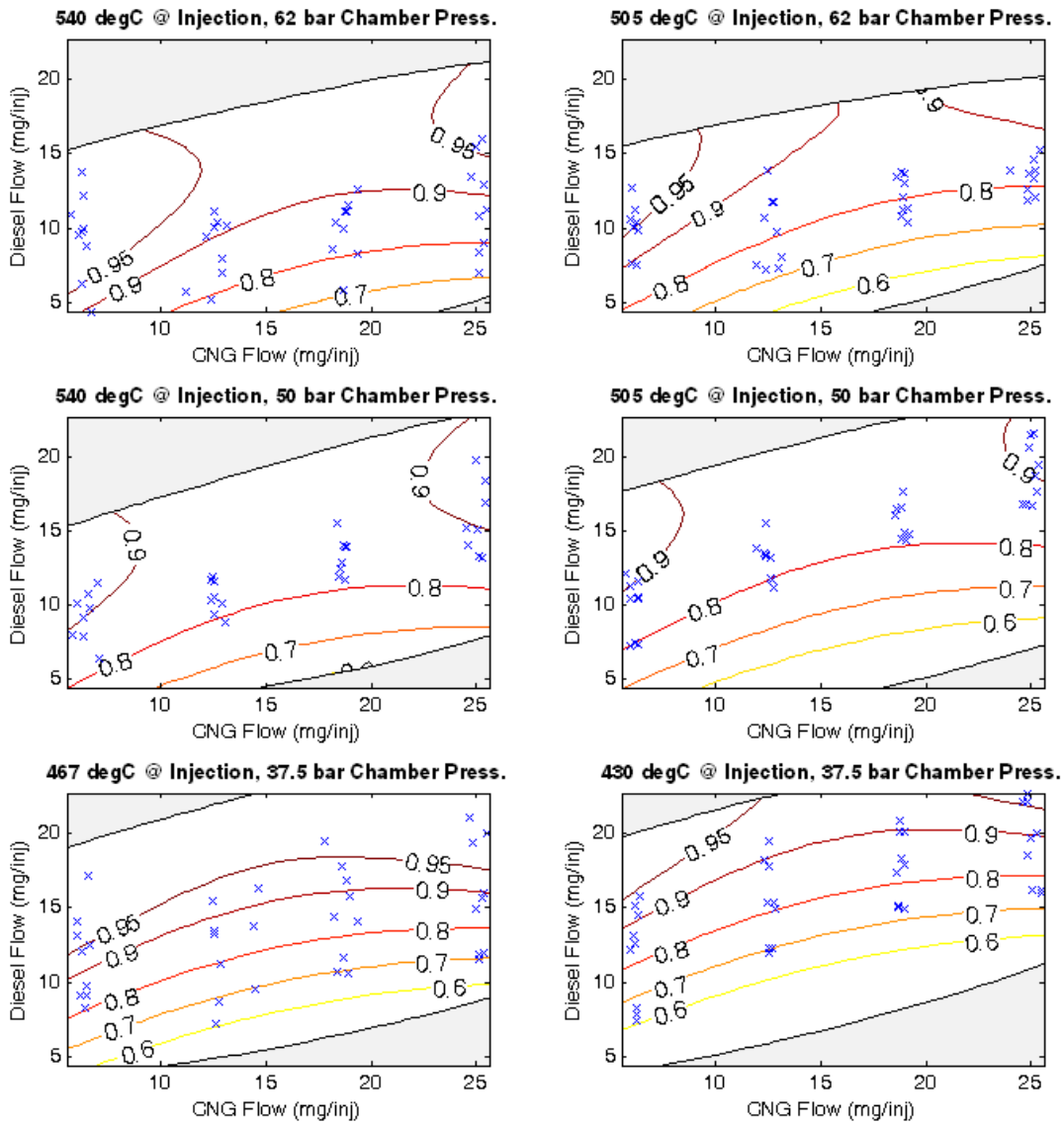


Figure 4-12 – Combustion Efficiency Contours (21 MPa Injection Pressure)

For low diesel flows, increased cylinder pressure has the effect of raising the combustion efficiency. At high diesel flows, however, the effect of pressure is less clear. The injection timing is likely a key factor in this case. For high diesel flow, the early timing conditions (bottom two plots) appear to have higher combustion efficiency than the two

center plots (later timing). When compared to the high pressure, later timing plots, the combustion efficiency looks comparable. Therefore, at high diesel flows, the combination of cylinder pressure at injection and timing are important for combustion efficiency. In general, for a given combustion timing, it appears that combustion efficiency is increased with increasing cylinder pressure. The effect of timing on the emissions of Co-injector B running in normal conditions can be found in Brown (2008). Emissions of Co-injector B will be further studied in Chapter 5.

Due to equipment failure, there was not enough NO_x data available for a full response surface model in the current tests, but some data is available and plotted versus knock intensity stratified by gas flow rate in Figure 4-13 below. McTaggart-Cowan (2006) related the CO, hydrocarbon and NO_x emissions to the volume ratio of the gas and diesel in Co-injector A. The volume ratio was found by treating the diesel as incompressible and treating the gas as ideal at ambient temperature and maximum cylinder pressure (which was admittedly not the best approximation to the gas volume). Despite the rough approximation, it was found that NO_x emissions were proportional to the diesel gas volume ratio. No knock data was processed for those tests.

As shown in Figure 4-13, knock and NO_x are positively correlated for all conditions (data was taken from all six combinations of cylinder temperature and pressure shown in Figure 4-9). NO_x emissions are generally the product of high local temperatures during combustion [Stone, 1999]. Thus, when knock intensity increases for a given gas flow, NO_x is also increased due to the rapid heat release.

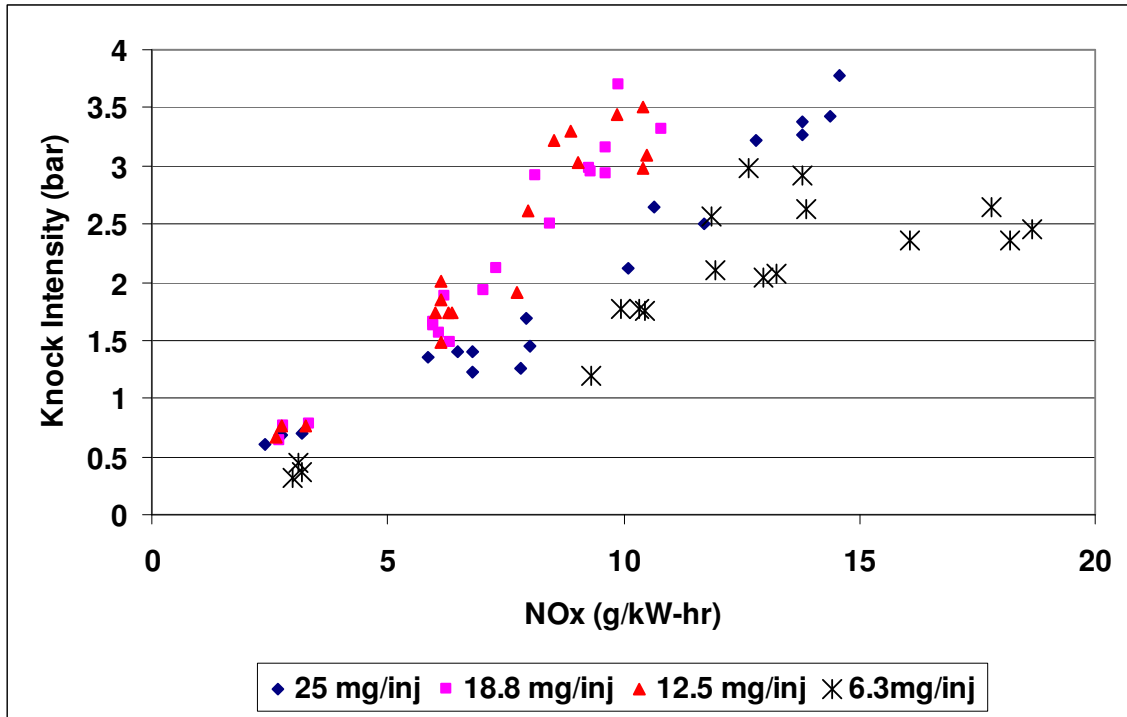


Figure 4-13 – Knock Intensity vs. NO_x

4.3.3. Knock/Ignition Delay Relationship in Co-injector B

In conventional diesel engines, the relationship between knock intensity and ignition delay is positive. As ignition delay increases, there is time for more of the diesel to form a combustible mixture, resulting in a greater energy release at ignition, which leads to higher knock. The same is true in spark ignition engines and dual-fuel engines where longer ignition delay gives less time for the flame front to propagate to the cylinder walls to burn up the end gas before the pressure and temperature cause it to autoignite (see section 3.7). As can be seen from the ignition delay and knock intensity contours, the ignition delay/knock intensity relationship for Co-injector B is inverse. This is more clearly seen in Figure 4-14.

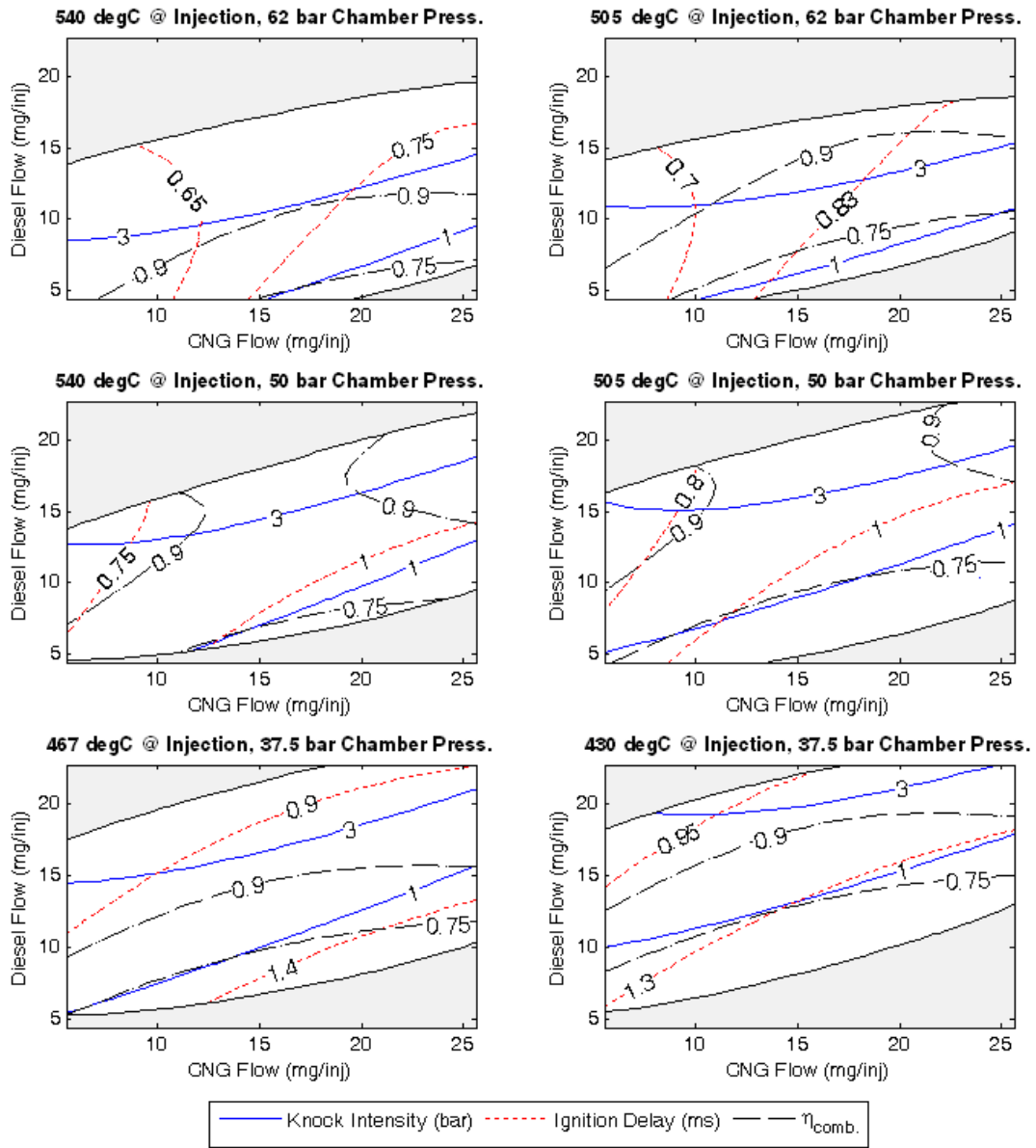


Figure 4-14 – Knock Intensity, Ignition Delay, and Combustion Efficiency Contour Comparison (21 MPa Inj. Press.)

At high CNG flow rates, the knock and ignition delay contours are nearly parallel, and inversely related. As one reduces the gas flow, the contours become skewed relative to each other until, at high cylinder pressure, the contours are almost perpendicular. This could indicate that when there is a large amount of gas present at a given cylinder pressure, not as much diesel is able to mix with the air in the chamber. Even at high

pressure, the ignition delay may be physically limited for high gas flows since the large amount of gas may inhibit the diesel/air mixing. Consider Figure 4-10 again. The figure shows the fuel density distribution, but in co-injection each volume of fuel is made up of CNG and diesel. Therefore, in a given region, the amount of diesel available for mixing is a function of both the fuel density in that location as well the diesel/gas ratio. Thus, for high CNG flows at the pressures and temperatures tested, adding diesel always lowers the physical delay by increasing the amount of diesel available for mixing. This also results in higher knock intensity because more diesel burning at ignition means that more gas will burn at ignition resulting in an increase in the rate of heat release.

A similar trend is found at low cylinder pressures with low CNG flows. In this case, rather than the physical delay being limited by the presence of large amounts of gas displacing the air, the delay is limited by how quickly the fuel is injected (and the knock intensity is reduced due to reduced air entrainment). Therefore, as pressure is increased, the physical delay is reduced by allowing the fuel to be injected sooner, to the point where the chemical delay becomes the dominant mechanism in ignition delay and the addition of more diesel no longer reduces it. Again, knock intensity will increase (up to a point, discussed below) at low CNG flows with increasing cylinder pressure due to the increased air entrainment into the fuel jet.

Figure 4-15 shows raw engine data of knock intensity vs. ignition delay at high and low cylinder pressure (please note that the injection timings are different for each plot, so the high pressure plot also has a higher cylinder temperature at ignition). The data has been stratified into series of gas flow rates to reinforce the validity of the response surface contour comparison.

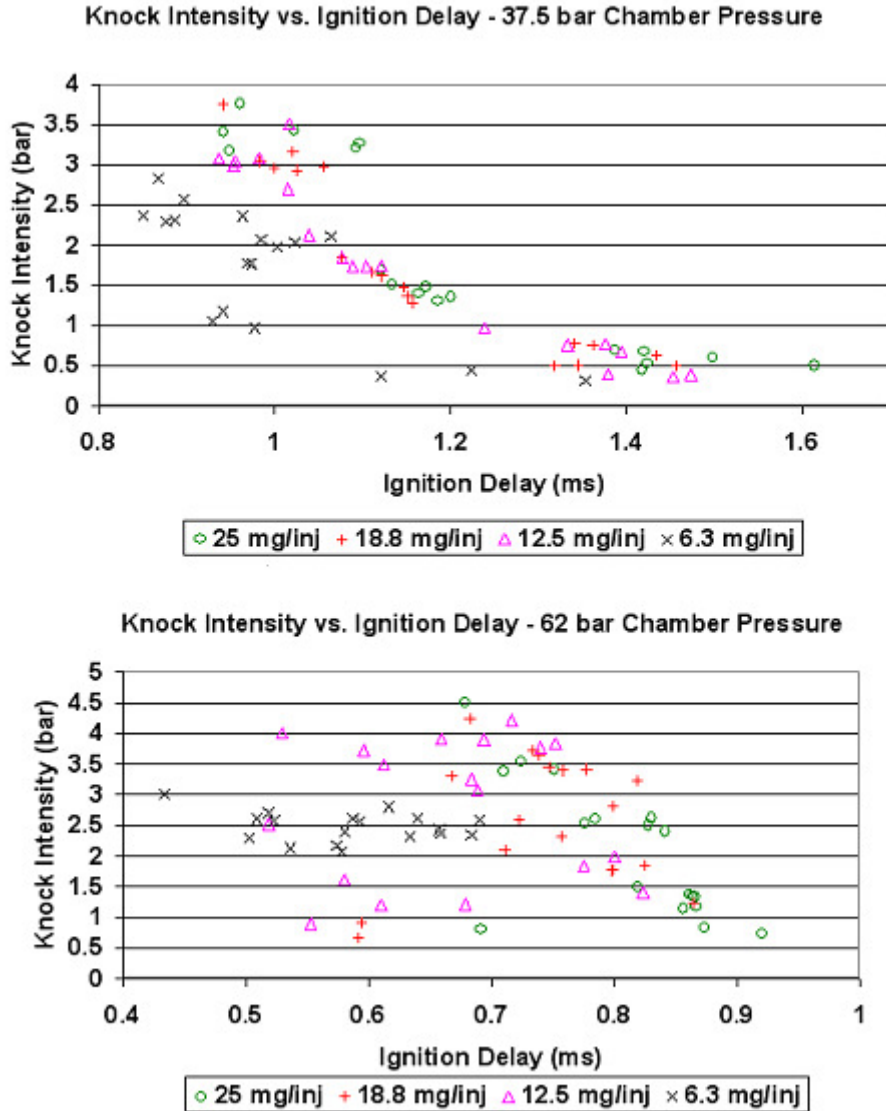


Figure 4-15 – Knock Intensity-Ignition Delay Tradeoff Data Stratified by CNG Flow

As can be seen in the preceding figures, the 25 mg/inj CNG flow shows a predominantly negative correlation between ignition delay and knock intensity for both cases. For the other three gas flow rates, the correlation is negative for the low pressure/temperature case, but then becomes much less correlated at high pressure/temperature with lower gas flows resulting in lower correlations. Another observation which can be made from Figure 4-15 is that the knock intensity does not vary by much for the 6.3 mg/inj CNG flow despite the fact that different amounts of diesel were injected. There is a much

greater dispersion in knock intensity for the case shown in Figure 4-9. The nearly constant value of knock intensity at high pressure/temperature suggests that the response surface does not adequately predict the knock intensity in this region. It could be that with such a low gas flow and ignition delay, there is not enough time for increased amounts of diesel to mix and combust, or perhaps the volume of the small amount of gas becomes so small that only low diesel flows are needed to burn most of it rapidly. At low cylinder pressure, the gas volume will be larger and thus increasing diesel again causes more of the gas to burn at ignition. Nonetheless, the response surface contours do not show this behavior and thus may not be reliable in the area with very low gas flow at high pressure/temperature. Appendix D explores how the surface changes when these 18 high pressure, low gas flow points are removed from the knock intensity response surface calculation.

4.3.4. *Suggested Region of Injector Operation*

Using some of the data presented above, it is possible to establish a region of ‘optimal’ operation by overlaying contours which represent possible limits of operation. In the following case, two limits of operation will be discussed and used to map out an operating region over the conditions tested (with 21 MPa injection pressure). The first limit of operation is knock intensity. As is discussed in Brown, 2008, a maximum knock intensity of 3 bar should not be exceeded over long durations in order to prevent engine damage. Thus, an upper limit on knock intensity of 3 bar will be used as the first limit. The second limit will be a combustion efficiency of 75%. This limit represents a condition where the engine is significantly misfiring and thus is not a desirable condition (As was discussed, while testing at a given gas flow, the diesel flow was lowered until hydrocarbon emissions reached 100 g/hr. At these conditions the engine was misfiring. The 75% combustion efficiency corresponds is representative of this lower diesel limit). Figure 4-16 shows the 95 % confidence (discussed below) 3 bar knock and 75% combustion efficiency contours plotted together

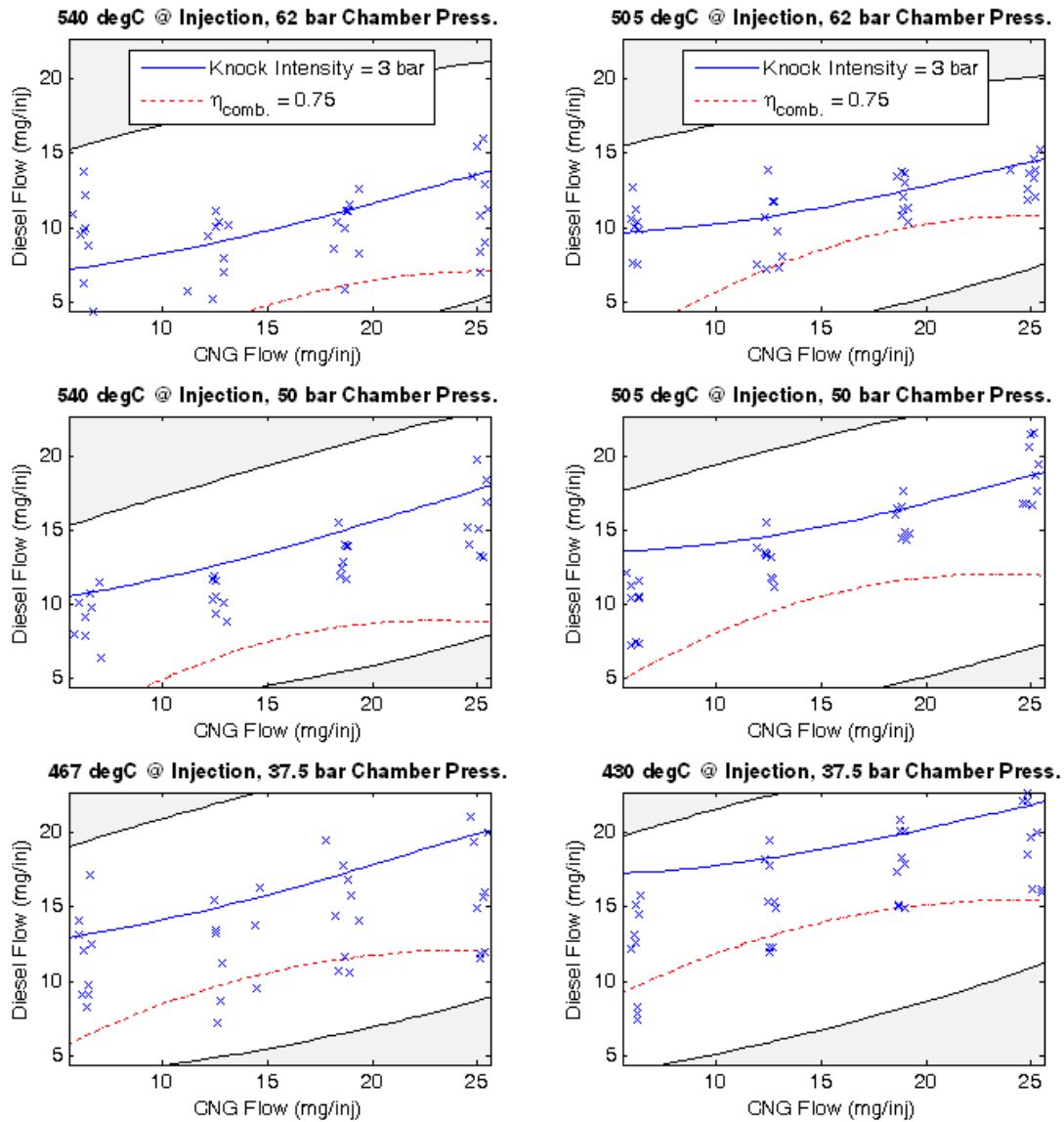


Figure 4-16 – Limits of Operation of Co-Injector B for Single Injection, Low Load, Low Speed

The 3 bar knock and 75% combustion efficiency contours were plotted with 95% confidence on the mean (See section 3.1.1 and Figure 3-2). This means that statistically, if a test was conducted multiple times at a diesel/CNG combination which lies on the solid 3 bar knock contour, there is a 95% chance that the *average* knock intensity of those tests will be at most 3 bar. As one moves further below the 3 bar contour, the knock

intensity with 95% confidence gets lower and lower (2.5 bar, 2 bar, 1.75 bar, etc.). Thus staying in the region below the solid 3 bar knock contour gives good statistical confidence that the knock intensity, on average, will be below 3 bar. The same is true for the dashed 75% efficiency contour and the region *above* it. As one moves above the dashed line, there is good statistical confidence that the efficiency in these regions is higher than 75%. Thus, the region between the solid 3 bar contour and dashed 75% efficiency contour is defined as a region of 'optimal operation' for the single injection, low load, low speed case. Of course, this region is only a guide, since a full analysis should include NO_x and PM emissions as well, but it is believed that the regions shown in Figure 4-16 give a good first approximation to the limits of operation (Note that PM emissions were not recorded during these tests and NO_x data is incomplete due to equipment failures during most of the tests).

Figure 4-16 gives some interesting insights into how the fuel flows may need to be changed based on the cylinder temperatures and pressures. First, it can be seen that raising the temperature in the cylinder widens the region (particularly at higher cylinder pressure). This is because increased temperature leads to higher combustion efficiency while having a much smaller effect on the knock intensity. This is particularly true at high pressure.

Increasing the pressure increases combustion efficiency, but increases knock to a greater degree. Thus, when the pressure is increased, the operating region is narrowed and the range of acceptable diesel flows for a given gas flow is greatly reduced. Also, at lower cylinder pressure, the range of allowable diesel flow is shifted up, such that both the maximum and minimum diesel flows for a given gas flow are higher at lower cylinder pressure.

Perhaps one of the most important conclusions which can be drawn from Figure 4-16 is that at high cylinder pressures, it is important to have high intake temperatures in order to keep as much flexibility in the fueling rates as possible. At low pressures, this is not such

a problem, but it is clearly a concern when looking at the top two plots, in which the operating range in the right plot is much more restricted than the range shown in the left plot. It should be noted, however, than in the context of a normal double pulse test, where the above behavior represents the output of the first, or ‘pilot’ pulse, the unburned hydrocarbons and CO could be consumed in the second pulse, meaning that the efficiency limit may not be as important as the knock limit.

4.3.5. Effect of Injection Pressure

It was mentioned at the beginning of the chapter that tests were also carried out at a higher injection pressure (see Table 4-1). Due to time constraints, only two combinations of intake pressure and temperature were tested: high pressure/temperature and low pressure/temperature. Note that, as in the case with the 21 MPa injection pressure tests, the low pressure/temperature conditions occur at an earlier timing. The diesel/gas bias for all tests is 2.5 MPa with a PSEP of 1.0 ms.

The plots (Figure 4-17) are arranged with high cylinder temperature and pressure cases on the right and low cylinder temperature/pressure cases on the left. Each row of plots corresponds to a specific response variable (knock intensity, ignition delay, and combustion efficiency). Contours for each injection pressure are overlaid, with two values of the response variable shown on each plot in order to examine how injection pressure affects the response variables. The fuel flow scales on all six plots are identical.

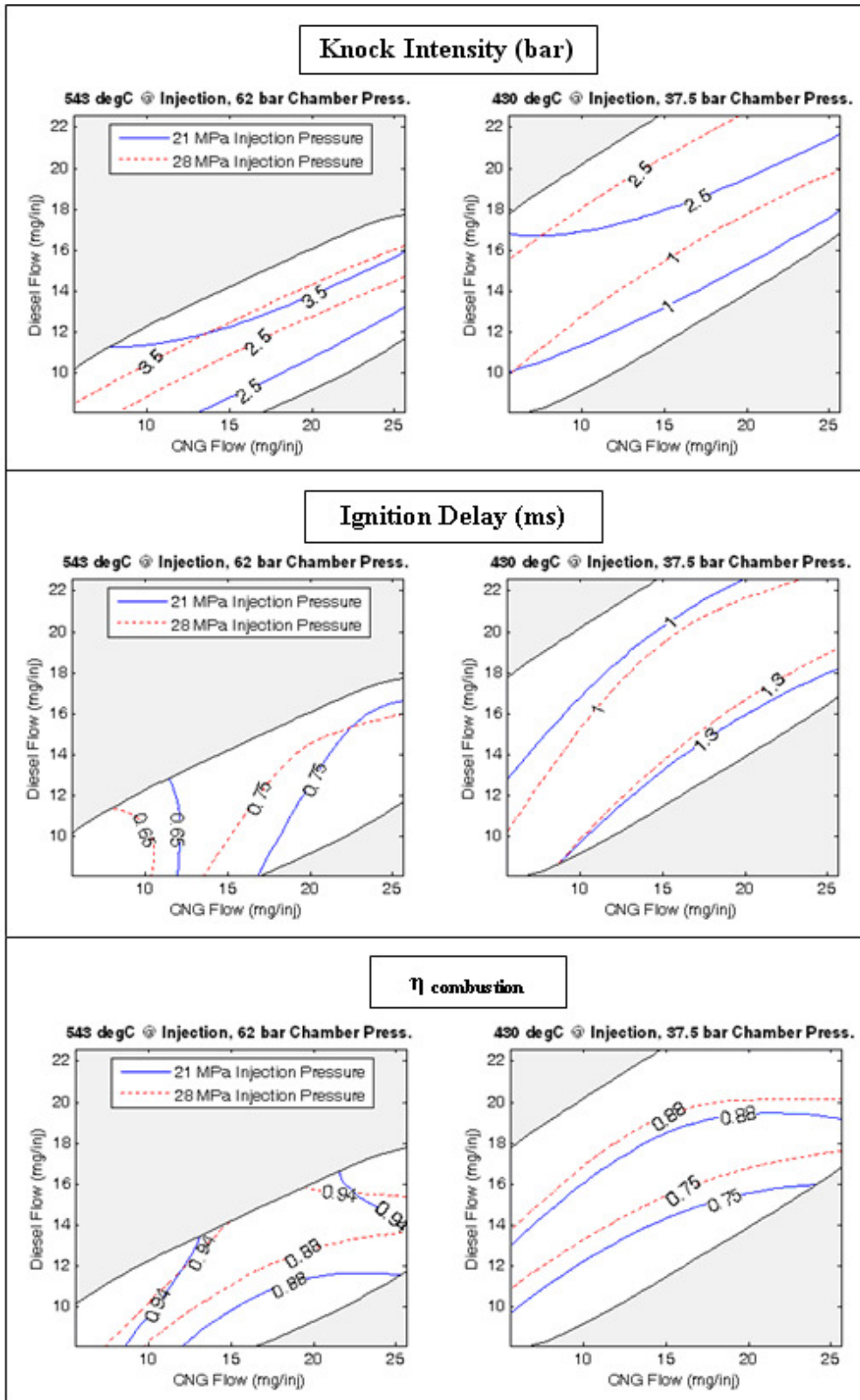


Figure 4-17 – Knock Intensity, Ignition Delay, and Combustion Efficiency Comparison for 21 and 28 MPa Gas Injection Pressure

From Figure 4-17, it is clear that the effect of injection pressure on knock intensity is greatest at high gas flows. At high gas flows, the knock intensity is decreased with increased injection pressure, and this increase is more significant for the low temperature/pressure case. Also, it appears that at high temperature and pressure, the knock gradient is increased with increased injection pressure. This is evidenced by the fact that the knock contours are closer together in the upper left plot. Thus (at higher injection pressures), although the knock intensity is lower at low diesel flows for high injection pressure, knock intensity increases faster with increasing diesel at high injection pressure and therefore high diesel flows produce comparable knock to the low injection pressure case. The gradient does not appear to be as affected for the low cylinder pressure/temperature case, however, the knock intensity is lower for those conditions, so it may be that the effect of injection pressure gets weaker at high knock intensities. The knock intensity also seems to converge for both injection pressures at low gas flow (Note from Figure 4-15 that the response surface predictions for low gas flow at the high cylinder temperature/pressure case are not valid, where knock becomes mostly independent of diesel flow). The reason for the decrease in knock intensity at high injection pressure is not clear. Figure 4-10 does not show large differences in the fuel concentrations for different injection pressures, however the difference in injection pressure is not as large in that case (4 MPa compared to 7 MPa for the current data). Also, in Figure 4-10, the fuel flow rate for the 11 MPa injection pressure case is lower compared to the high injection pressure (3 g/s compared to 4 g/s). Therefore, at the time shown, there is more fuel present in the high pressure jet than the low pressure jet, making it even more difficult to compare. Injector dynamics may be a factor since the GPWs at high injection pressures were much lower (see Table 4-4). The increased fuel density at the injector nozzle is known to have complex effects on the fuel jet structure and air entrainment characteristics [Ouellete *et al.*, 2000; Rubas *et al.*, 1998] (higher jet penetration could lead to wall impingement which can extinguish the flame [Stone, 1999]), leading to the lower knock intensity (and combustion efficiency) found at higher injection pressure), which are no doubt factors which play a role in the differences. It is also possible that since the ignition delay is the same as in the 21 MPa injection pressure

case, but the fuel is injected sooner (higher injection pressure results in increased flow rate and reduced mechanical delay), that there is overleaning of the fuel on the outer parts of the fuel jet, resulting in lower knock and reduced combustion efficiency.

Increasing the injection pressure still results in the same type of transition in the shape of the ignition delay curves. It is interesting that ignition delay is not decreased at higher injection pressures. As is the case with increased cylinder pressure, increased gas pressure reduces the gas pulse width required to deliver a given amount of fuel, as well as the mechanical delay, meaning the fuel will be injected sooner. It would therefore be expected that increased injection pressure would reduce ignition delay. But Figure 4-17 shows that the ignition delay changes very little or actually increases slightly at high cylinder pressures and temperatures. Knock intensity has been shown to be inversely correlated to ignition delay for this injector. Therefore, it is likely that the reduction in knock intensity at high injection pressure causes an increase in ignition delay which counters the expected decrease caused by the earlier gas injection, resulting in very little change in ignition delay.

The combustion efficiency seems to follow the same trend as the knock intensity, where combustion efficiency is reduced at higher injection pressures (however, this increase is quite small), except at high efficiencies, where the injection pressure effect seems to weaken.

Figure 4-18 shows a comparison of the operating region of the injector for the low speed, single injection condition discussed in section 4.3.4. At low cylinder pressure and temperature, increased injection pressure opens the operating region significantly at high gas flows by allowing much higher diesel flows to be used without the barrier of high knock intensity. As gas flow is reduced, the operating regions become less and less sensitive to injection pressure. At high cylinder temperature and pressure, the lower knock intensity resulting from higher injection pressure, slightly widens the operating range. It is again important to note that the low gas flow case at high cylinder pressure

and temperature is not well represented in these figures and in fact at low gas flow, the knock intensity is relatively constant at between 2 and 3 bar at the diesel flows tested. Thus, for the 21 MPa injection pressure case, the knock intensity contour should actually be much higher up at low gas flows than is shown since it is known from the raw data that knock intensity below 3 bar is achievable for the diesel flows tested in that region..

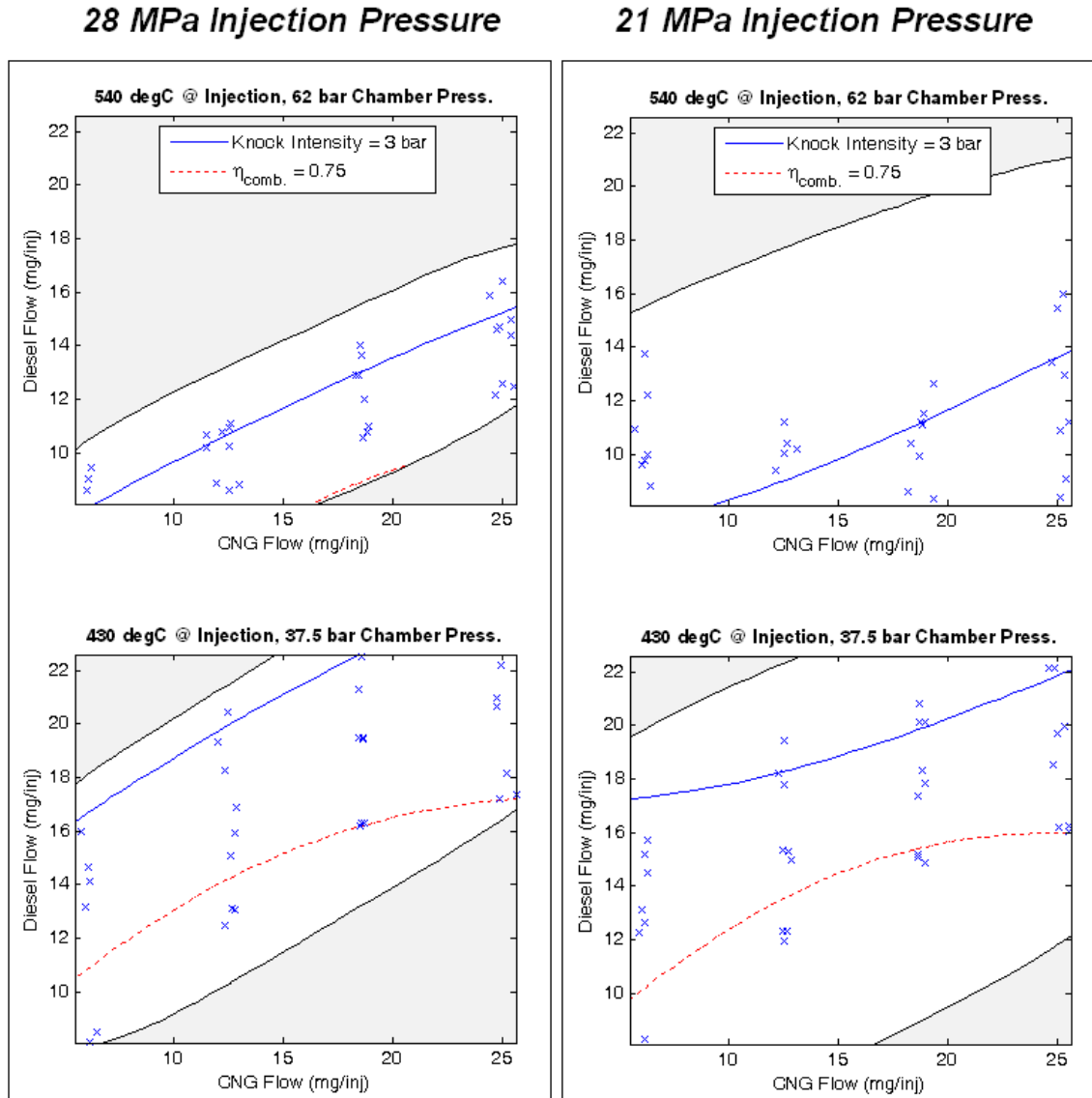


Figure 4-18 – Operating Region Comparison for 21 and 28 MPa Gas Injection Pressure

4.4. KNOCK INTENSITY AND IGNITION DELAY POWER LAW DATA FITS

Based on the results from the response surfaces for knock intensity and ignition delay presented in sections 4.3.2 and 4.3.5, an alternative method of analysis was used which assumed that measured variables are a power-law product of pressures, temperatures and fuel flows. The exponents were determined by optimizing the fit to the measurements (considering all possible exponent combinations between -2 and 2 at intervals of 0.1). The combination which gave the highest R^2 value was chosen. The following equations predict knock and ignition delay using the optimal product of powers of the measured variables as the independent variable (Note: masses are in kg, pressures are in bar and temperature is in °C):

$$Knock = 0.0003 \left(\frac{m_{diesel}^{1.2} P_{cyl} T_{cyl}^{1.1}}{m_{CNG}^{0.7} P_{inj}^{0.4}} \right) - 2.9722 \quad [\text{bar}] \quad (22)$$

$$t_{ign} = 5.4927 \times 10^{-7} \left(\frac{m_{CNG}^{0.7} P_{inj}^{0.1}}{m_{diesel}^{0.9} P_{cyl}^{1.8} T_{cyl}^{1.9}} \right) + 0.4414 \quad [\text{ms}] \quad (23)$$

This analysis leads to the same main conclusions as the response surface methodology. For example, T_{cyl} , P_{cyl} and m_{diesel} increase knock and decrease ignition delay significantly. Figure 4-19 shows the measured knock and ignition delays versus the values calculated from the above equations. The predictions from the response surfaces have also been plotted; both fitting methods have similar fitting quality, despite the different fitting form. This provides additional evidence that the interpretations of the response surface contours are not artifacts of the fitting function form.

Note that the power law fits for the knock intensity did not include the 6.3 mg/inj gas flow points when calculating the correlation (although the response surfaces discussed previously did). For these low gas flows, there was little correlation found with Eq. 22 and knock intensity at medium and high diesel flows (the low gas flow points are shown on the knock intensity plot as red triangles). It should be noted that the 28 MPa injection pressure data at low gas flow correlated much better to Eq. 22 than the 21 MPa data, but

the correlation was still weak. Ignition delay, however, correlated with all the conditions tested and all the data for ignition delay was used for that correlation.

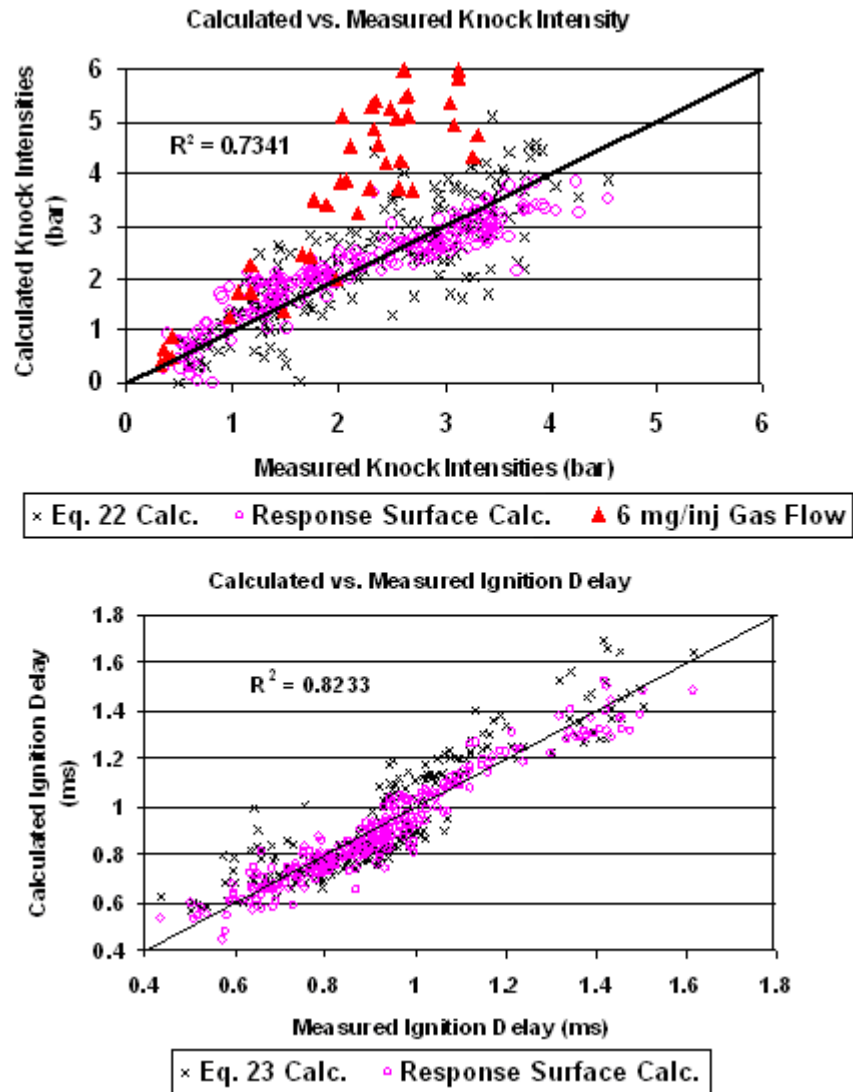


Figure 4-19 – Measured and Predicted Knock Intensity and Ignition Delay vs. Calculated Knock Intensity and Ignition Delay

4.5. SUMMARY

4.5.1. Effect of Fuel Flows

It is believed that the diesel acts as an ignition promoter for the natural gas (which has very poor self-ignition properties). Therefore, as the proportion of diesel relative to the gas increases, the diesel/gas mixture becomes more easily ignited, leading to greater energy release at the start of combustion. Since the gas and diesel are injected together, there is a large amount of gas in the vicinity of the diesel and therefore the more diesel that ignites at the end of the ignition delay, the more gas is likely to ignite as well, leading to much higher energy release at the start of combustion than is found in HPDI or dual fuel engines. This is reflected in the knock intensity, which was found to be primarily affected by diesel mass. Increasing diesel mass always leads to increased knock intensity. This effect is reduced at conditions with low gas flows (6.3mg/inj) and seems to disappear when the cylinder pressure at the time of injection is high (62 bar) and the gas flow is low (6.3mg/inj). Increasing the gas flow for constant diesel flow tends to lower the knock intensity, but the effect is much smaller than was found with the diesel flow. As gas flow increases relative to the diesel, the gas will dilute the diesel in the fuel mixture and displace more air in the vicinity of the diesel, resulting in less diesel igniting at the end of ignition delay and therefore, a lower knock intensity. At the highest cylinder pressure at the time of injection tested (62 bar), it was found that knock intensity was not affected by diesel flow. This is likely because the amount of gas injected is so low and concentrated that co-injection becomes closer to pure diesel combustion.

At the lower cylinder pressures tested (37.5-50 bar), ignition delay decreased with increasing diesel flow. Again, this is attributed to the ignition promotion characteristics that increased diesel gives to the fuel mixture. Ignition delay is essentially calculated by finding where the heat release rate curve crosses zero. Therefore, the more reactive the fuel mixture, the shorter will be the ignition delay period. It is not surprising, then, that as the gas flow is increased, the ignition delay is increased for the same reasons that knock intensity is decreased. At high cylinder pressure (62 bar), the contours start to

become more vertical as gas flow is decreased, indicating that ignition delay is becoming independent of diesel flow. For high gas flows, the trend is the same as with low cylinder pressure. This is believed to be a result of the fact that the ignition delay approaches its minimum at high cylinder pressure. For high gas flows, the delay is still long enough that increasing diesel flow results in a further decrease in ignition delay. As gas flow is decreased, the ignition delay becomes sufficiently short that increasing the diesel cannot make any further reductions (i.e. the ignition delay starts to become limited by the chemical delay of the diesel).

Combustion efficiency is increased with increasing diesel and slightly decreased with increasing gas flow for all pressures and temperatures tested. This follows from the above discussion where increasing the diesel flow relative to the gas results in a greater earlier heat release, which results in lower hydrocarbon and carbon monoxide emissions.

4.5.2. Effect of Cylinder Pressure and Temperature at the Time of Injection

Cylinder pressure was another important variable regarding knock intensity. For constant diesel and gas flows, increasing cylinder pressure increases the knock intensity. This is believed to be the result of increased air entrainment in the two-phase jet. At higher cylinder pressure, air is entrained deeper into the gas jet, providing greater mixing between the diesel and the oxygen, leading to a larger quantity of diesel which is ignitable at the end of the delay period and thus a greater energy release. At high cylinder pressure (62 bar) and low gas flow, the knock intensity becomes independent of diesel flow, which has been previously discussed as likely being caused by the small volume of gas and high diesel/gas ratio resulting in a pure diesel-like combustion. The cylinder temperature at the time of injection at constant pressure was also found to increase knock intensity. The increased temperature likely increases the speed of the chemical kinetics resulting in a slightly higher energy release at ignition.

Ignition delay was decreased with increasing cylinder pressure. Previous work done in the injector visualization chamber (IVC) at UBC, as well as an examination of the effect

of cylinder pressure on gas pulse width showed that when cylinder pressure is increased, the gas flow rate is higher. Therefore, at higher cylinder pressure, the gas is delivered sooner, which likely results in the reduced ignition delay. The improved air entrainment and higher oxygen concentration at higher pressure is another factor which likely lowers the ignition delay. As has been discussed, for the highest pressure tested (62 bar), the ignition delay appears to approach its minimum and it is unlikely that higher pressures would result in a further decrease in the ignition delay period. Increasing cylinder temperature (at constant pressure) has been found to reduce the ignition delay, likely as a result of increased reaction rates. The effect of temperature is much less than that of pressure since increased temperature lowers the oxygen concentration in the cylinder (higher temperature intake charge has a lower density) and does not result in higher gas flow rates, as is the case with increased pressure.

For low diesel flows (<10mg/inj), it was found that combustion efficiency increases with increased pressure. At higher diesel flows, the injection timing seems to play a role in the combustion efficiency. It was seen that at earlier timing with a lower cylinder pressure (37.5 bar), the combustion efficiency was slightly higher than conditions with higher cylinder pressure (50 bar) and later timing. It is clear, however, that for a given timing, combustion efficiency is reduced with increased pressure, for the same reasons cited for the increase in knock intensity. Increased cylinder temperature also results in higher combustion efficiency, which is to be expected due to the increased reaction rates and flame speeds associated with higher temperatures.

4.5.3. Effect of Injection Pressure

Except for low gas flows (6.3mg/inj) and high knock intensities (>3 bar) knock intensity is decreased at increased injection pressure. With 6.3mg/inj gas flows the knock intensities are comparable for both injection pressures tested. The reduction in knock intensity for most conditions is not completely clear, but may be caused by increased wall impingement as a result of higher injection momentum. The wall impingement may result in flame extinguishment resulting in lower energy releases.

Ignition delay was changed very little and even increased with injection pressure. Increased injection pressure was expected to decrease ignition delay since it results in higher fuel flow rates (as was the case with increased cylinder pressure). However, with co-injection, knock intensity was found to be inversely related to ignition delay except at low gas flows (6.3mg/inj). Therefore, it is likely that the decrease in knock intensity at higher injection pressure (which should increase ignition delay) is opposing the effect of increased fuel flow rate (which should reduce ignition delay) such that the ignition delay is unchanged or even slightly increased.

Combustion efficiency is lowered at higher injection pressure. Again, this may be attributed to the increased penetration of the fuel jet resulting in wall impingement and ultimately flame extinguishment which leads to higher emissions of CO and hydrocarbons.

4.5.4. Knock Intensity/Ignition Delay Tradeoff

It was found that with co-injection (with two needles), ignition delay and knock intensity are inversely related to one another. This is contrary to what is found in pure diesel and dual fuel engines. In those engines, increased ignition delay more premixed diesel at the time of combustion, resulting in higher knock intensity. Because the diesel is surrounded by concentrated amounts of gas in co-injection, the factors which tend to increase knock intensity also reduce ignition delay. For instance, in dual fuel engines, increasing the amount of gas in the intake charge tends to increase knock intensity and ignition delay. This is because increasing the amount of gas in those engines results in a lower oxygen concentration. Therefore, it takes longer for the diesel to form an ignitable mixture, lengthening the ignition delay. Also the richer premixed gas and air charge is more ignitable when the diesel ignites (also the richer end gases will be more prone to self ignition, resulting in end gas knock). Since the gas is directly injected with co-injection, there is no oxygen depletion. As more gas is added, the ignition delay increases because the fuel mixture becomes diluted by the gas making it more difficult for the diesel to mix

with air (Note that the gas in co-injection is much more concentrated than in a dual fuel engine). Less diesel is then likely to ignite at the start of combustion and the knock intensity will drop as a result. Therefore, it is important to note that even though co-injection and dual fuel engines work on similar principles, the specifics of the combustion process are quite different.

4.5.5. Optimal Size of Pilot Injection

It was found that low pulse widths should be optimal for co-injector operation. Ultimately, it is best to keep as low a gas/diesel ratio as possible in order to keep ignition delay low and combustion efficiency high. Regions of very low gas flow (6.3mg/inj) give the best performance with regards to low ignition delay, knock and high combustion efficiency. However, the pulse width should be increased as cylinder pressure decreases and the diesel flow should be increased with decreasing cylinder pressure in order to maintain these characteristics.

CHAPTER 5 - DOUBLE INJECTION TESTING RESULTS

5.1. *DOUBLE INJECTION TEST DESCRIPTION*

Brown (2008) previously investigated the effect of combustion timing on the performance of Co-injector B. Unlike the testing discussed in Chapter 4 - which involved only one injection per cycle, Brown's tests used two injections per cycle (See section 1.3.2). The tests were carried out at three different speed/load combinations: 1100 RPM/Low Load, 1100 RPM/High Load and 1400 RPM/High Load. For each engine mode, the combustion timing was varied such that the point of 50% integrated heat release occurred at 5, 10 and 15 degrees ATDC. The current tests are modeled after Brown's series VIII tests, with the difference being that instead of varying the combustion timing, the duration of first gas pulse width is varied. The tests were completed with 0% and 30% EGR as shown in Table 5-1 below. By running these tests on both injectors, a comparison can be made which will help clarify the effect of the flow restrictor on the diesel distribution within the injector. This work will also give valuable insight into the effect of the first pulse width on combustion. Previous work with the co-injectors used a first pulse width of 0.7ms almost exclusively for all operating conditions. These tests should provide guidance for future testing as to how the first pulse width should be changed under certain conditions for the best combustion performance. Finally, a comparison of these results with J36 data will be made to demonstrate whether or not co-injection can match the performance of the J36. Both Co-injector B and Co-injector CS were tested with 3 repetitions of each point except for some CS tests where equipment failure resulted in only 2 repetitions being possible (See Table 5-1). The tests were run in an order which allowed for the most efficient use of the engine and were thus not completely randomized. No points were repeated sequentially and whenever possible, repetitions were run on different days.

	<i>Engine Speed (RPM)</i>	<i>GIMEP (bar)</i>	<i>EQR</i>	<i>1st GPW (ms)</i>	<i>EGR (%)</i>	<i>B Repetitions</i>	<i>CS Repetitions</i>
1	1100	6	0.3	0.5	0	3	3
2	1100	6	0.3	0.7	0	3	3
3	1100	6	0.3	0.9	0	3	3
4	1100	13	0.55	0.5	0	3	3
5	1100	13	0.55	0.7	0	3	3
6	1100	13	0.55	0.9	0	3	3
7	1400	13	0.55	0.5	0	3	3
8	1400	13	0.55	0.7	0	3	2
9	1400	13	0.55	0.9	0	3	2
10	1100	6	0.3	0.5	30	3	3
11	1100	6	0.3	0.7	30	3	3
12	1100	6	0.3	0.9	30	3	3
13	1100	13	0.55	0.5	30	3	3
14	1100	13	0.55	0.7	30	3	3
15	1100	13	0.55	0.9	30	3	2
16	1400	13	0.55	0.5	30	3	2
17	1400	13	0.55	0.7	30	3	2
18	1400	13	0.55	0.9	30	3	2

Table 5-1 – Test Matrix for Double Injection Tests with Co-Injector B and CS

Other parameters are fixed as follows:

- CA50 is set to 10° ATDC
- Bias pressure for Co-injector B is 2.5 MPa with PPWs between 0.9 and 1.3ms for a diesel flow of ~15 mg/inj.
- Bias pressure for CS was between 0.7 and 1.2 MPa to achieve a diesel flow of ~11.5mg/inj
- Exhaust backpressure is 20 kPa above the intake pressure
- Coolant and oil temperatures set to 80°C and 100°C respectively
- Intake air is heated to 50°C measured at the intake valve
- Time between the end of the diesel and beginning of the first gas injection (PSEP) for Co-injector B was held at 1ms
- Time between the end of the first and beginning of the second gas injection (2PSEP) for both injectors was held at 1.5ms

It should be noted that Co-injector CS had to be run with a lower diesel flow than Co-injector B. While the target diesel flow for Co-injector B was 15mg/inj, the target diesel

flow for CS had to be lowered to 11.5mg/inj. This is because it was found that at the repeatability point (see section 2.2) the knock intensity was much too high when running CS with 15mg/inj diesel. Therefore, the diesel flow was reduced to 11.5mg/inj until the noise in the heat release rates at the repeatability point was similar to that of Co-injector B. Figure 5-1 shows HRR plots of Co-injectors B and CS at the repeatability point.

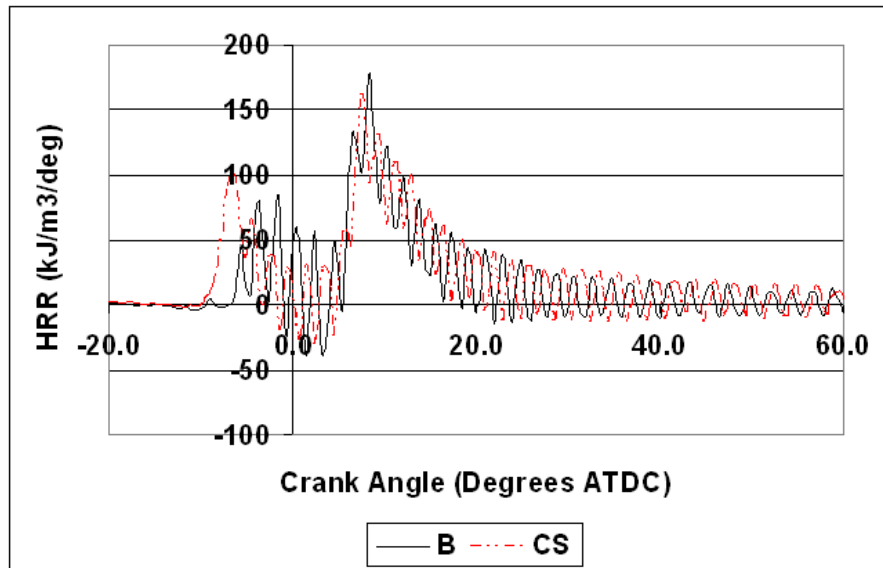


Figure 5-1 – Heat Release Rate Plot of Co-Injectors B (15mg/inj Diesel) and CS (11.5mg/inj Diesel) at the Repeatability Point

5.2. HEAT RELEASE, EMISSIONS, KNOCK INTENSITY, AND IGNITION DELAY

Figure 5-2 to Figure 5-4 show integrated heat release curves for Co-injectors B and CS at each engine mode, 1st GPW and EGR condition listed in Table 5-1. Each figure is an engine speed/load combination with the 0% EGR condition shown at the top, and the 30% EGR condition shown at the bottom. For every condition (except perhaps for 1400 RPM, 30% EGR) the heat release from the pilot injection is larger for CS than for Co-injector B (for equal GPW). Brown (2008) showed that for Co-injector B, the presence of second gas pulse had an effect on how much diesel was injected during the first pulse. He also showed that for Co-injector CS, the second gas pulse had no effect on the first gas pulse [Brown, 2009].

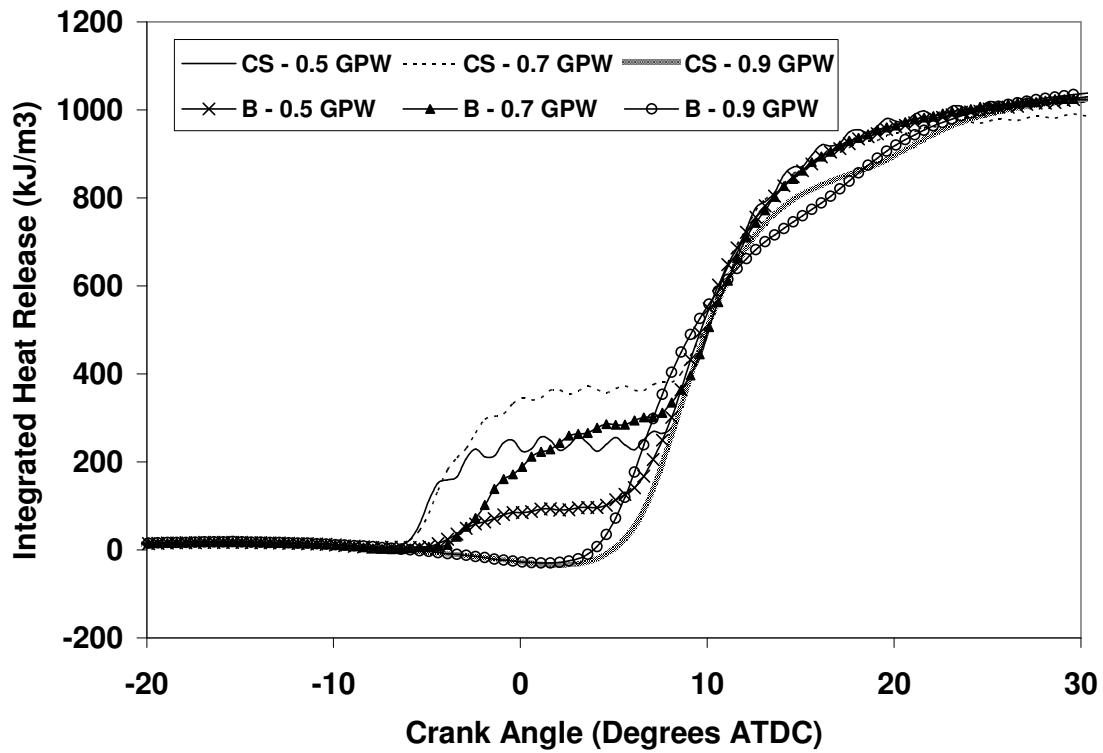
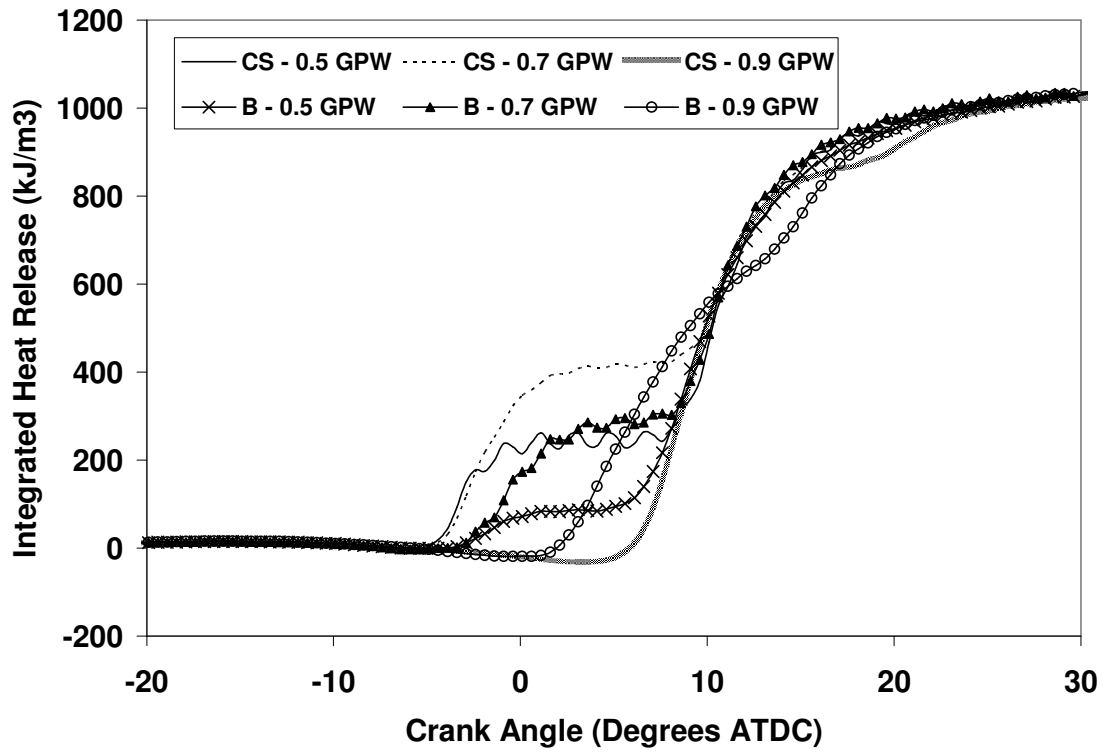


Figure 5-2 – Integrated Heat Releases of Co-Injectors at 1100 RPM, 6 bar GIMEP, 0% EGR (Top) and 30% EGR (Bottom)

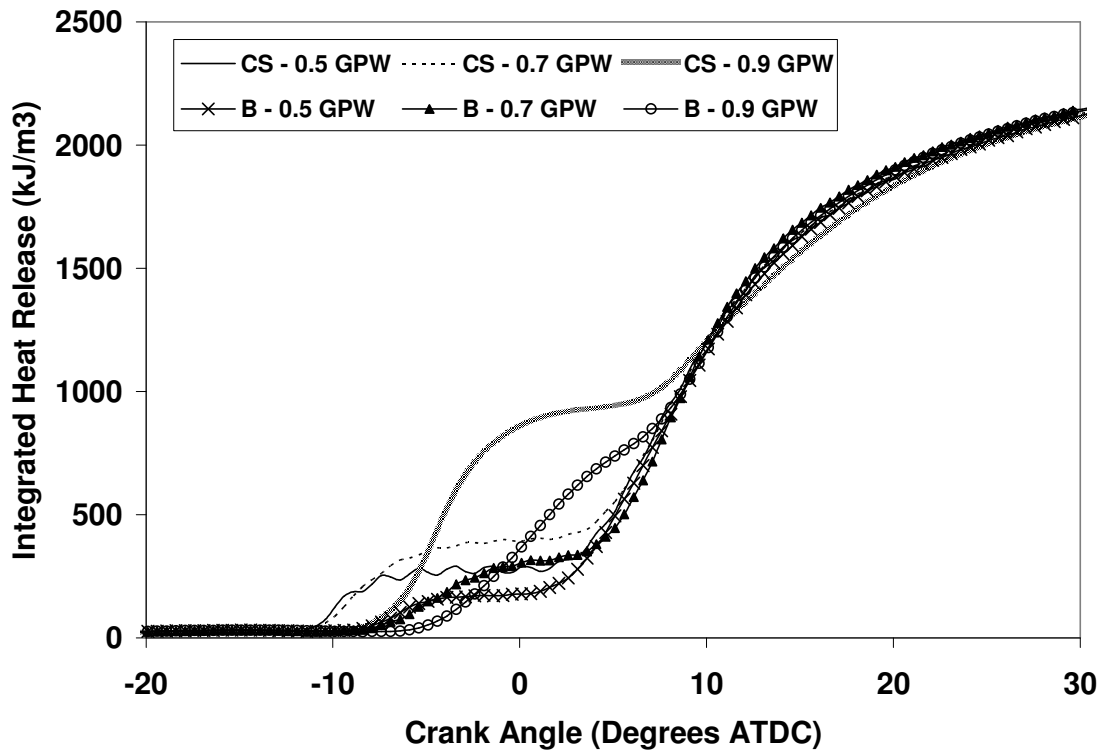
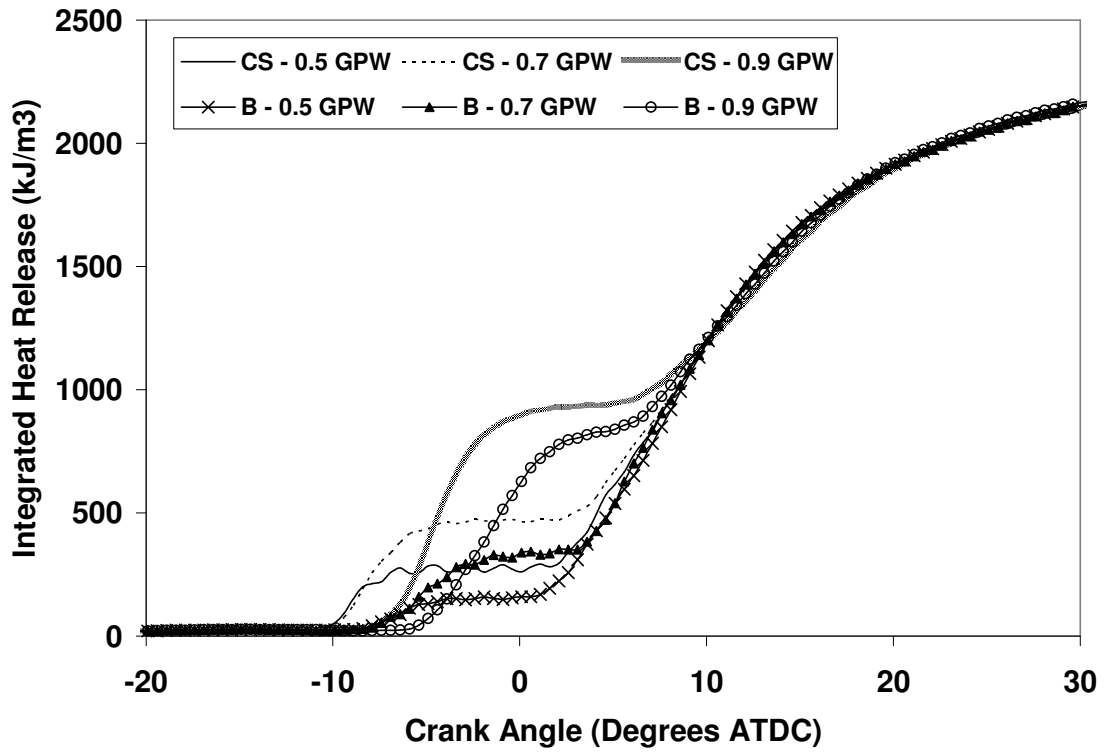


Figure 5-3 – Integrated Heat Releases of Co-Injectors at 1100 RPM, 13 bar GIMEP, 0% EGR (Top) and 30% EGR (Bottom)

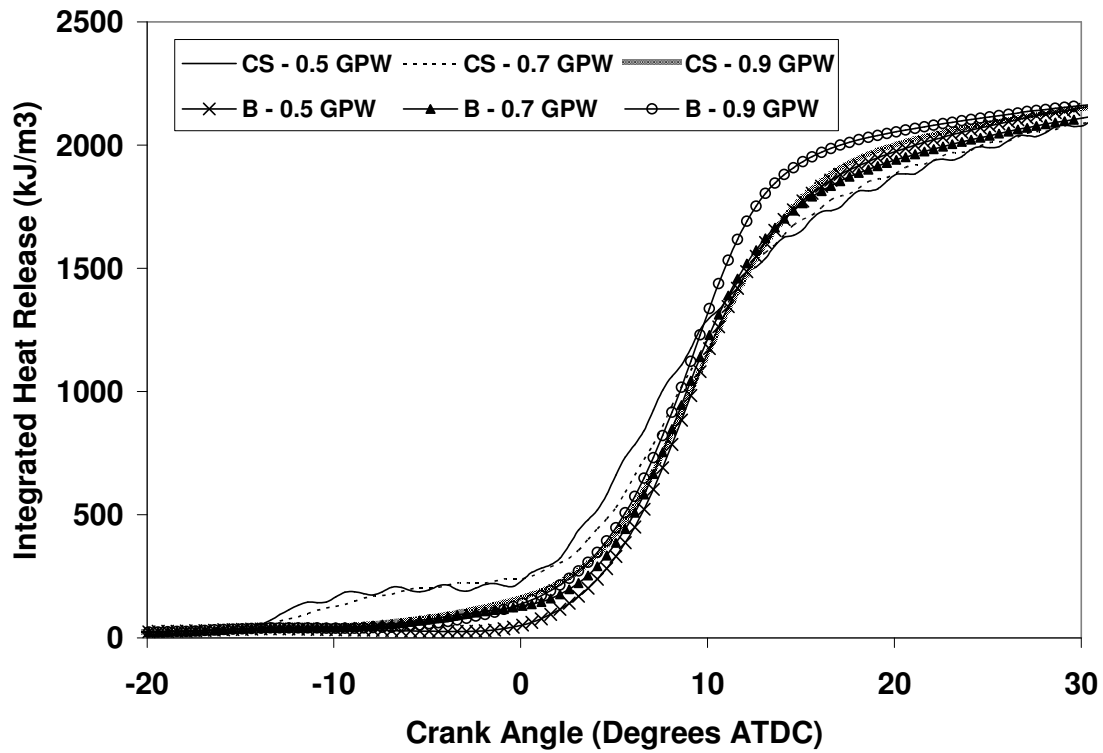
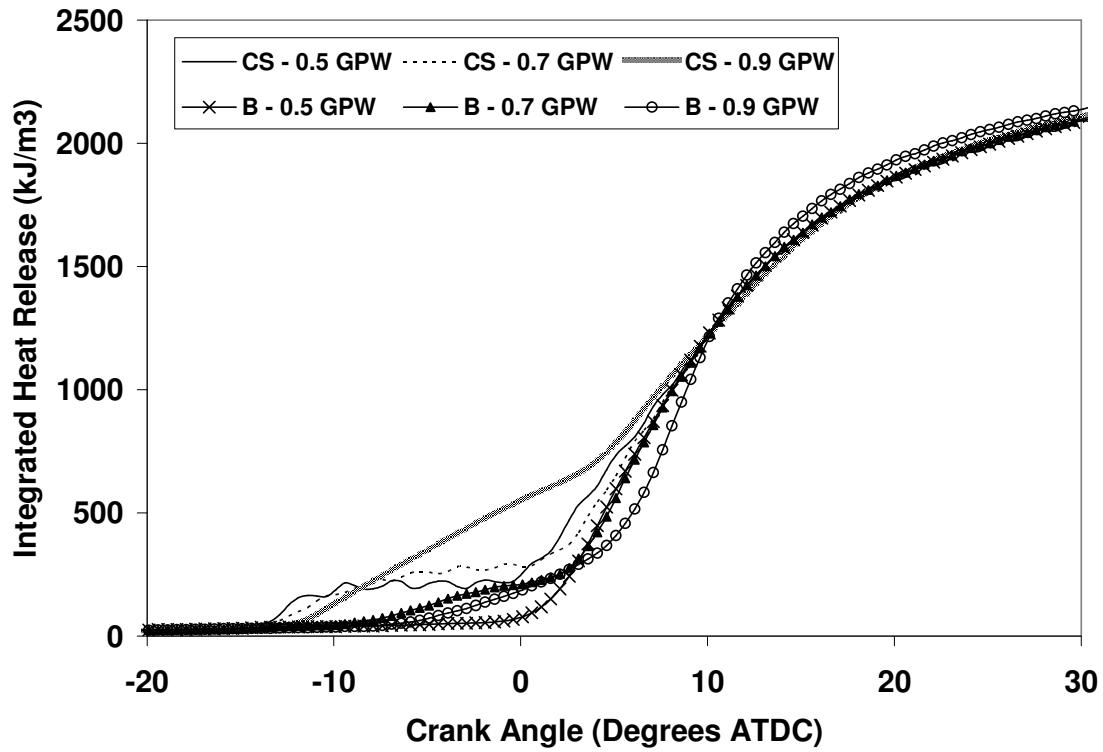


Figure 5-4 – Integrated Heat Releases of Co-Injectors at 1400 RPM, 13 bar GIMEP, 0% EGR (Top) and 30% EGR (Bottom)

Brown's results suggest that more diesel is present in the first gas injection for CS compared to B. More diesel present in the first gas pulse would suggest that less gas is injected during that pulse, and thus more gas must be injected during the second gas pulse for Co-injector CS relative to B. Table 5-2 shows an estimation of the gas flows in the 2nd gas pulses for B and CS. The gas flows are calculated based on IVC data given in Appendix F for pulse widths of 0.8 ms (representative of low load) and 1.4 ms (representative of high load) and average cylinder pressures at the time of injection from the engine tests. It should be noted that for the IVC data, CS was tested with ~15 mg/inj diesel and B had ~12 mg/inj (whereas in the engine tests, it is unknown how much diesel is present in the second pulse, but the amount of diesel is expected to be much less than those values, particularly with CS which has a *total* diesel flow of 11.5mg/inj).

		GPW1		GPW2		Cylinder Pressure (bar) (From Engine Data)		Est. Gas Flow (mg/inj) (From IVC Using Cylinder Pressure & GPW2)		Difference in Gas Flow of CS & B for GPW2
						CS	B	$m_{g,CS}$	$m_{g,B}$	$m_{g,CS} - m_{g,B}$
1100 RPM, Low Load	0% EGR	0.5	0.8	75	66	60	44	15		
		0.7	0.8	80	70	62	46	16		
		0.9	0.8	75	75	60	49	11		
	30% EGR	0.5	0.8	90	72	67	47	20		
		0.7	0.8	85	78	65	51	14		
		0.9	0.8	79	81	62	52	10		
1100 RPM, High Load	0% EGR	0.5	1.4	82	77	159	143	16		
		0.7	1.4	94	82	165	146	19		
		0.9	1.4	118	97	179	156	23		
	30% EGR	0.5	1.4	90	88	163	150	13		
		0.7	1.4	96	89	167	151	16		
		0.9	1.4	122	98	181	157	24		
1400 RPM, High Load	0% EGR	0.5	1.4	64	64	149	134	14		
		0.7	1.4	67	66	150	136	15		
		0.9	1.4	78	73	156	140	16		
	30% EGR	0.5	1.4	68	65	151	135	16		
		0.7	1.4	68	66	151	136	15		
		0.9	1.4	62	64	148	134	13		

Table 5-2 – Cylinder Pressures and Estimated Gas Flows during the Second Injections (for 0.8ms GPW at Low Load and 1.4ms GPW at High Load)

Table 5-2 shows that for equal gas pulse widths at the conditions tested, CS has a higher gas flow than B. Since the total gas flow for B and CS are about the same for a given load, this implies that there is less gas injected in the first gas pulse for CS:

$$\begin{aligned}
 m_{g,total} &= m_{g,GPW1} + m_{g,GPW2} \\
 m_{g,GPW2,CS} > m_{g,GPW2,B} &\Rightarrow \therefore m_{g,GPW1,CS} < m_{g,GPW1,B}
 \end{aligned}
 \tag{24}$$

Next, Figure 5-5 shows the 2nd GPW plotted against the 1st GPW for all the points tested for B and CS. Note that the 2nd GPW for CS is always equal or greater than that of B for equal load, speed and 1st GPW.

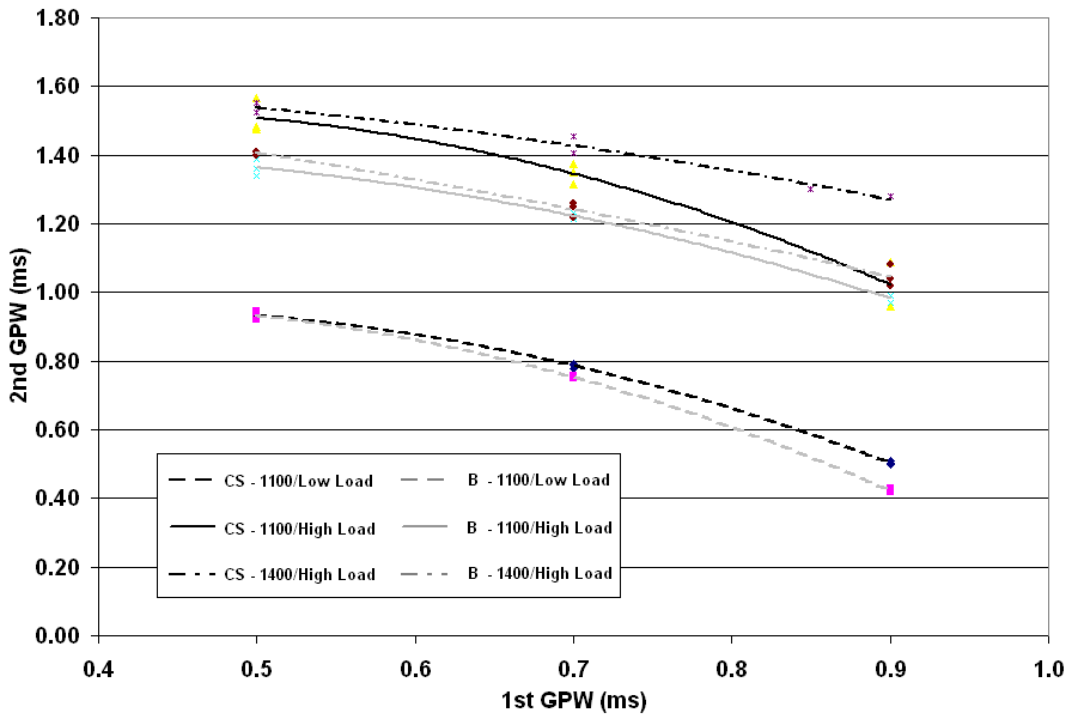
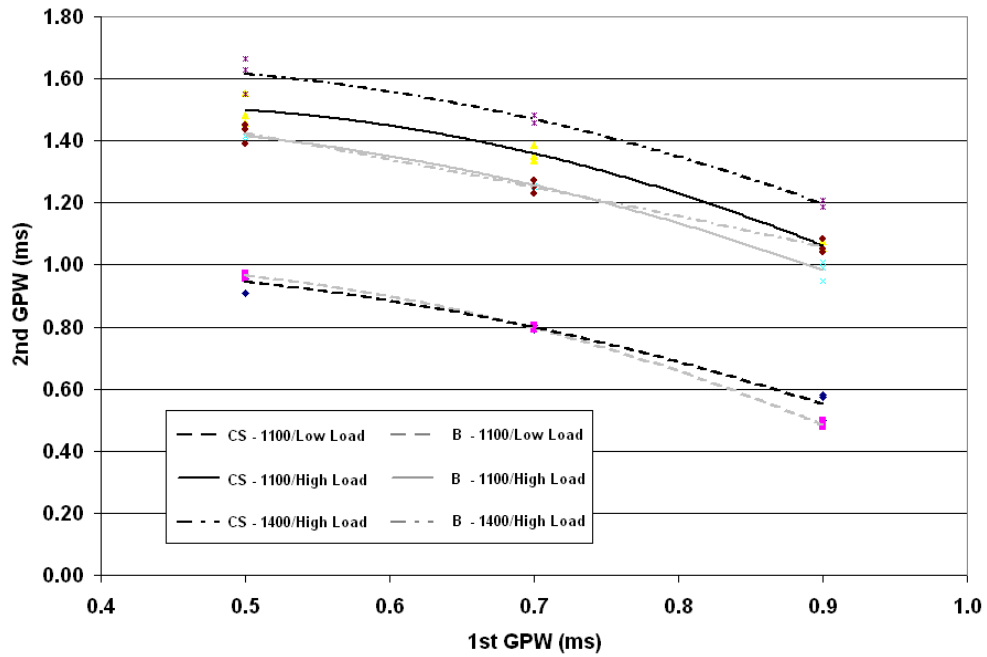


Figure 5-5 – 2nd GPW vs. 1st GPW for 0% EGR (Top) and 30% EGR (bottom)

Therefore, if less gas is being injected during the first pulse for Co-injector CS, it is likely that this is the result of more diesel being injected during that pulse compared to B. Another interesting feature of Figure 5-5 is that at high load, as speed increases, the 2nd GPW of CS also increases while that of B remains constant. Reasons for the change in GPW with speed in CS are currently unclear. It is also probable that injector to injector variability plays a role in the behaviors discussed above. It should be emphasized, however, that tests run in UBC's injector visualization chamber showed that both injectors have the same mechanical delay (the time between the command of injection and when fuel is first seen coming out of the injector).

Another reason the pilot combustion event is likely stronger in CS than B is the distribution of the diesel within the fuel jet. The pilot events shown in the IHR plots seem to support the distributions postulated in Figure 1-9. In CS, because the diesel leaks into the plenum and likely pools mostly at the bottom, the diesel may be more concentrated at the edge of the spray at injection, which makes it more readily exposed to the air for mixing. The diesel in Co-injector B's fuel spray is more evenly distributed within the plume of gas, making it more difficult for the diesel to mix with air (the diesel in the center of the plume may not mix as quickly with the air due to the surrounding natural gas - see Chapter 4) relative to CS.

Figure 5-2 to Figure 5-4 indicate that Co-injector CS operating with a 1st gas pulse width of 0.5 ms provides the most consistent pilot combustion event over all modes because this is the only case where the integrated heat release of the pilot event is nearly constant over all modes and EGR levels (210-250 kJ/m³). The 0.7 pulse width is similar, but drops off more at high speed. The 0.9ms GPW pilot event is also strong at low speed, but appears to have the strongest pilot event at 1100 RPM, high load (Figure 5-3). This makes sense, since at low load, the 0.9 ms 1st gas pulse is injecting most of the fuel, making it more like a single injection event, where the timing is delayed so far to achieve the CA50, that combustion doesn't begin until 4 or 5 degrees ATDC (Figure 5-2) during the expansion stroke. At higher load, the 0.9ms event accounts for only about half of the

fuel delivery and thus the timing is advanced and combustion again begins BTDC, giving higher temperature and pressure and therefore better combustion. EGR does not appear to have a significant effect on the pilot events for CS, except for the 0.9ms GPW at high speed where EGR drastically increases the ignition delay. For this condition, the timing had to be advanced (timing had to be advanced for most EGR cases) to achieve the CA50 (back to $\sim 37^\circ$ BTDC). With the lower temperatures caused by the early timing, as well as EGR, the ignition delay for this case was greatly increased, resulting in the loss of the distinct pilot event.

The 0.5ms GPW for Co-injector B also maintains its IHR at low speed ($\sim 100\text{kJ/m}^3$) but at high speed, the pilot event disappears (see the increase in ignition delay in Figure 5-11). This is likely an artifact of the very little diesel which is present in the pilot event for Co-injector B at such a low GPW. Less diesel has been found to make the gas/diesel mixture less reactive (see section 4.3). It has also been shown [Brown, 2008] that for Co-injector B, the presence of a second gas pulse affects the amount of diesel present in the first gas pulse. Therefore, with such a small first gas pulse at high load, it is likely that the amount of diesel present in the pilot event is low. Since low diesel means the mixture is less reactive, it is likely that at high speed, the combustion in the pilot event is too slow to show up on the IHR curve. This does not mean that the overall combustion is bad for this case. Figure 5-6 to Figure 5-10 show that the emissions are lowest (with the exception of NO_x) at this GPW for this condition for Co-injector B and thus the overall combustion must be quite good. For both injectors, particularly at low load, the hydrocarbon emissions are by far the lowest at 0.5ms GPW. This makes sense since the ignition delays are also lowest at low GPWs, so, for instance, the pilot pulse is fully injected and has begun burning before the second injection has even begun (e.g. for 1100 RPM, low load, 0.5 ms GPW with Co-injector CS, the pilot pulse burns for ~ 0.07 ms prior to the second injection) and therefore the main fuel pulse is injected into a hot environment which will promote much better combustion. As the pulse width increases, the pilot combustion starts later and later such that the main injection occurs before the initial injection has begun burning. However, it should be noted that it was found while running

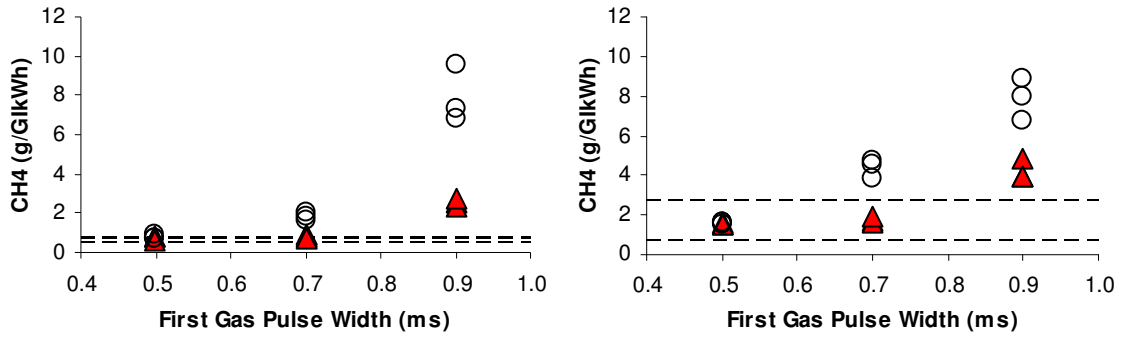
the engine, if the pilot pulse gets too small ($<0.5\text{ms}$), then emissions begin to rise again. This could be due to the fact that at low pulse widths, the injector needle may not be able to open due to the electromechanical properties of the injector.

The 0.7ms GPW pilot event for Co-injector B likely has the most diesel present which can be seen from the IHR curves as well as the knock intensity at 1100 RPM (Figure 5-12). High knock intensity has been found in Chapter 4 to be associated primarily with high diesel/gas ratios. Nonetheless, despite the higher diesel flow used in Co-injector B, the pilot event is weaker than with CS for the 0.7ms GPW, which appears to have the greatest effect at low load, by resulting in increased emissions.

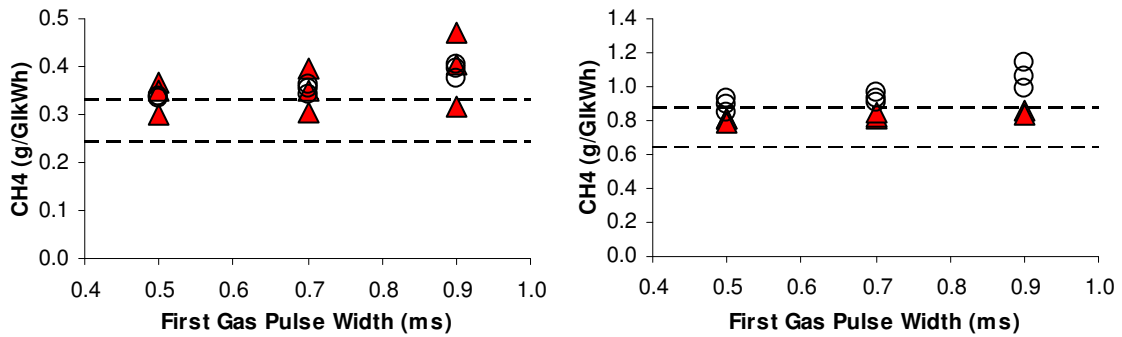
The 0.9 ms GPW cases for Co-injector B follow the same trends as in Co-injector CS, however with a much smaller combustion event and longer ignition delays, evident from the IHR traces. This seems to have the biggest effect at low load, where the emissions are highest.

Figure 5-6 to Figure 5-12 show the gaseous and PM emissions, knock intensity and ignition delay for all the points collected in the GPW tests. The dashed lines show the maximum and minimum values from baseline tests conducted with a CA50 of 10° ATDC with the HPDI (J36) injector (Diesel flow $\sim 10\text{ mg/inj}$).

1100 RPM – Low Load



1100 RPM – High Load



1400 RPM – High Load

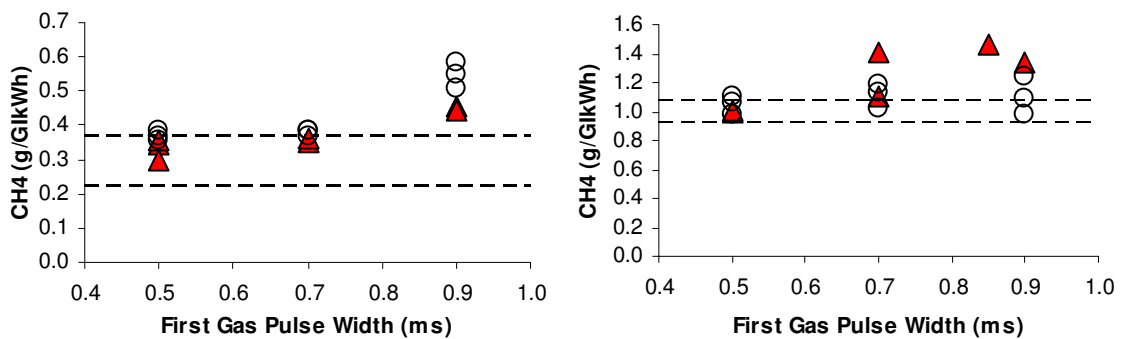
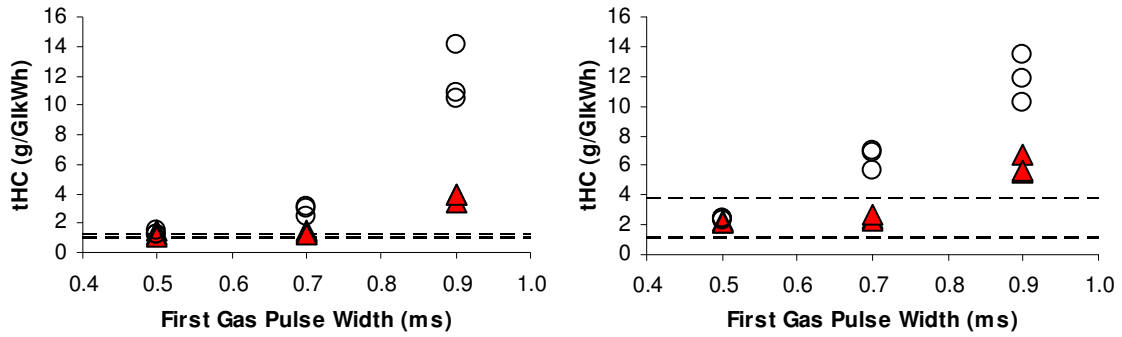
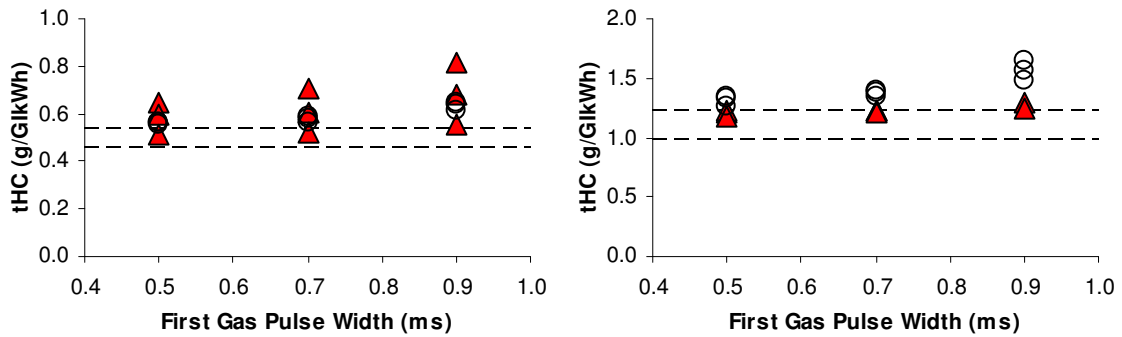


Figure 5-6 – Injector CH₄ Emissions with 0% EGR (Left) and 30% EGR (Right)

1100 RPM – Low Load



1100 RPM – High Load



1400 RPM – High Load

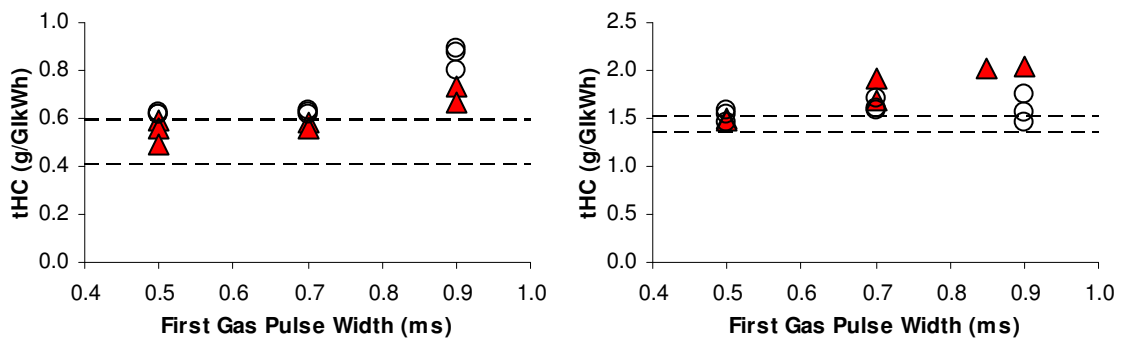
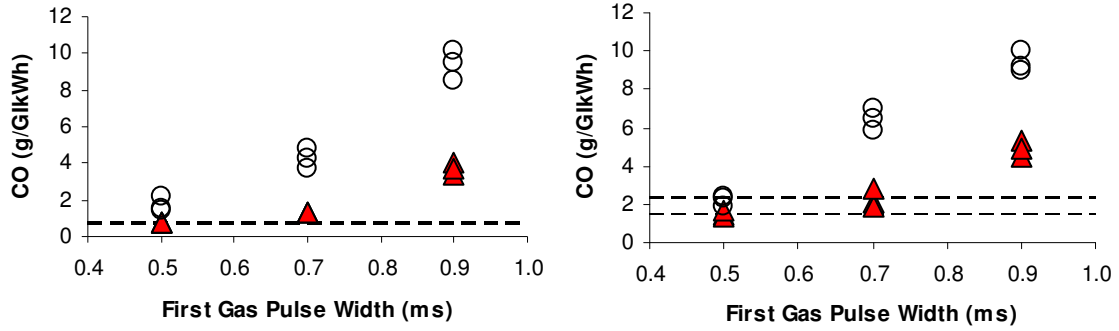
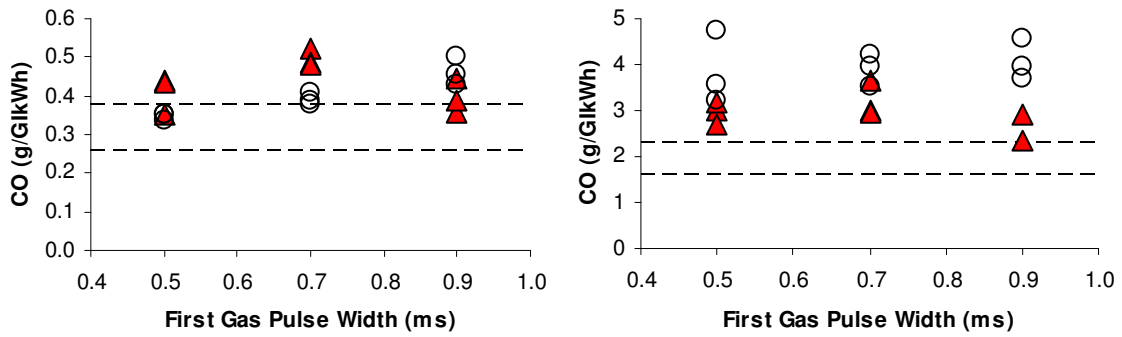


Figure 5-7 – Injector tHC Emissions with 0% EGR (Left) and 30% EGR (Right)

1100 RPM – Low Load



1100 RPM – High Load



1400 RPM – High Load

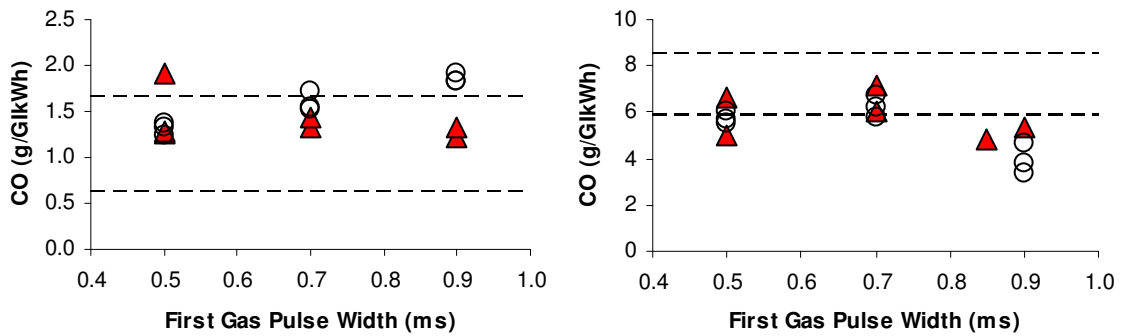
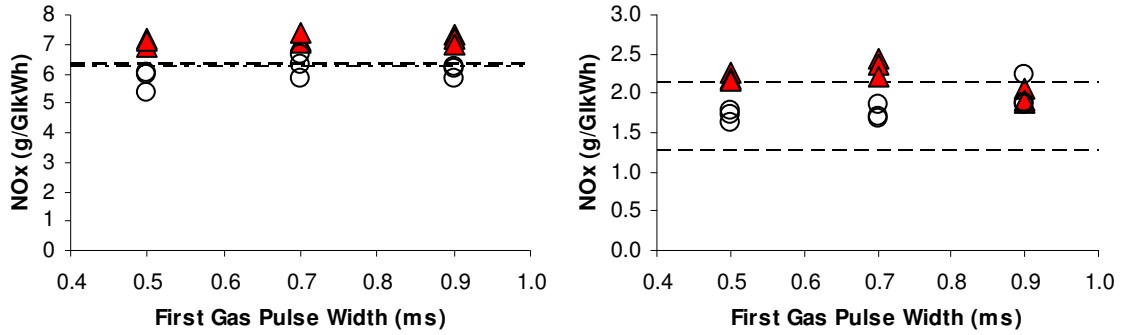
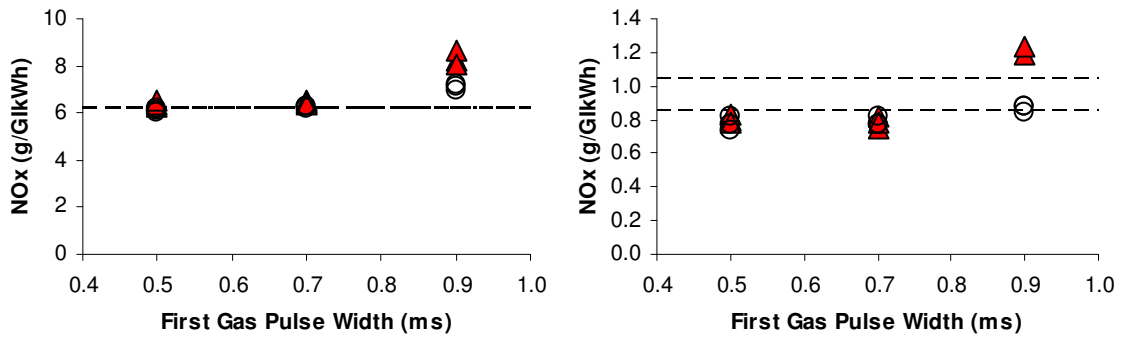


Figure 5-8 – Injector CO Emissions with 0% EGR (Left) and 30% EGR (Right)

1100 RPM – Low Load



1100 RPM – High Load



1400 RPM – High Load

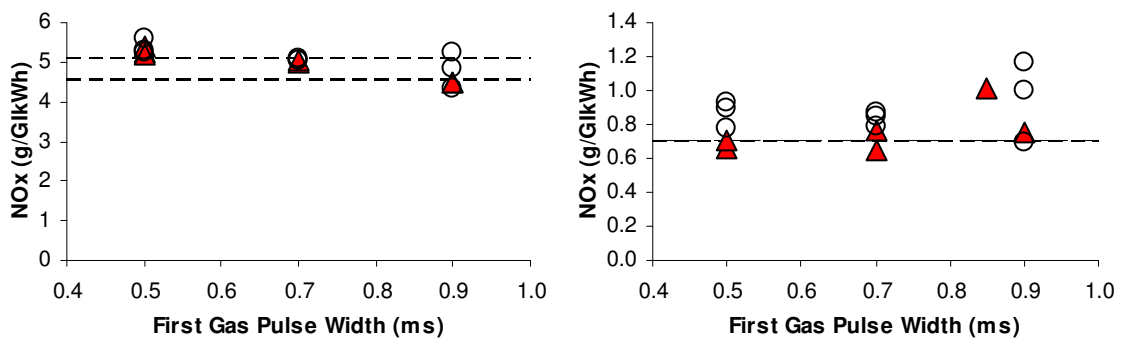
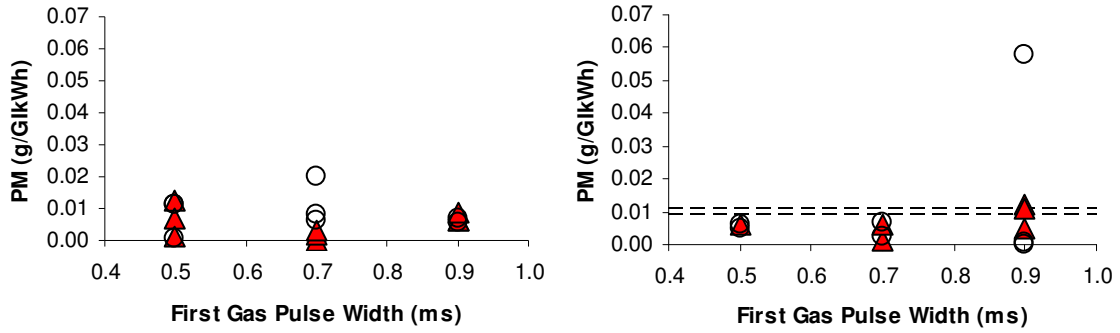
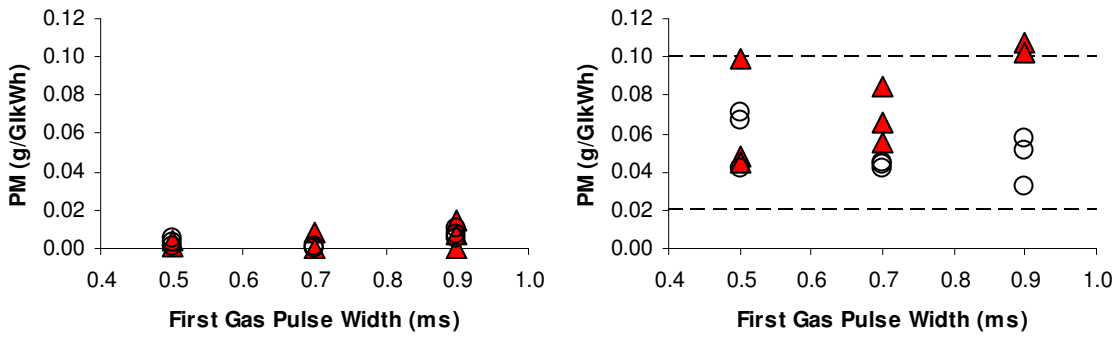


Figure 5-9 – Injector NO_x Emissions with 0% EGR (Left) and 30% EGR (Right)

1100 RPM – Low Load



1100 RPM – High Load



1400 RPM – High Load

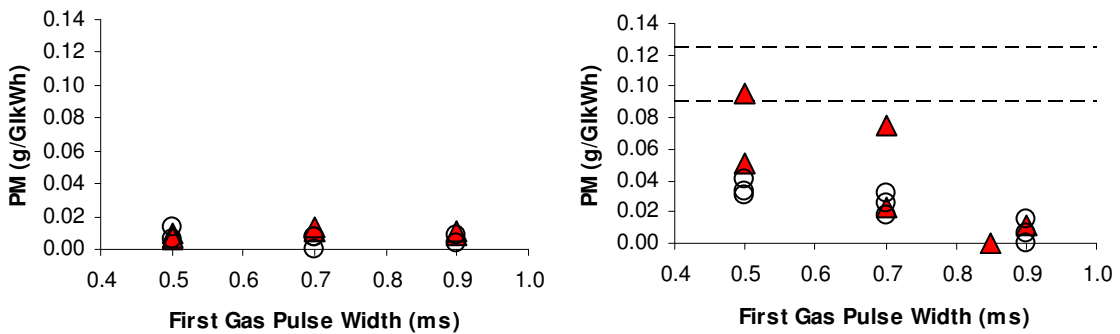
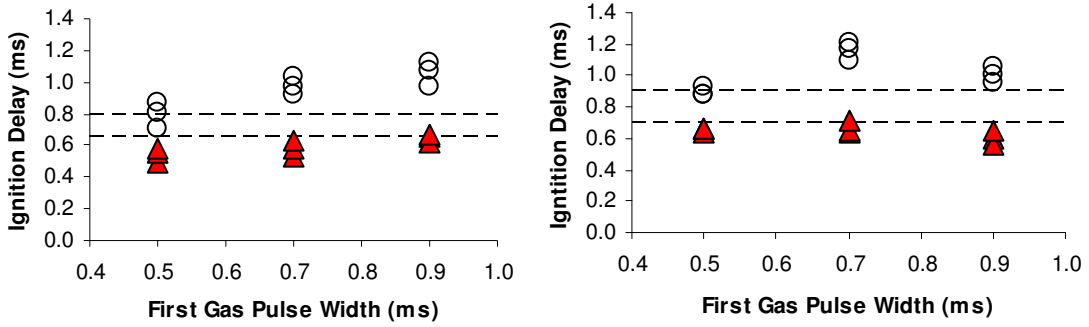
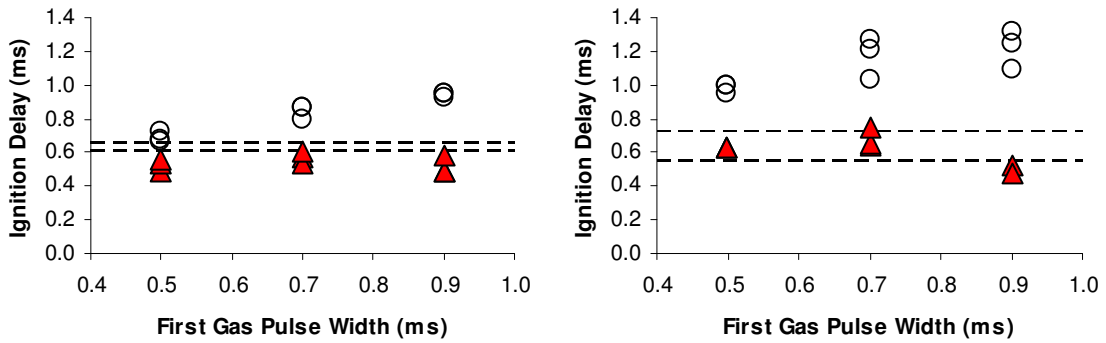


Figure 5-10 – Injector PM Emissions with 0% EGR (Left) and 30% EGR (Right)

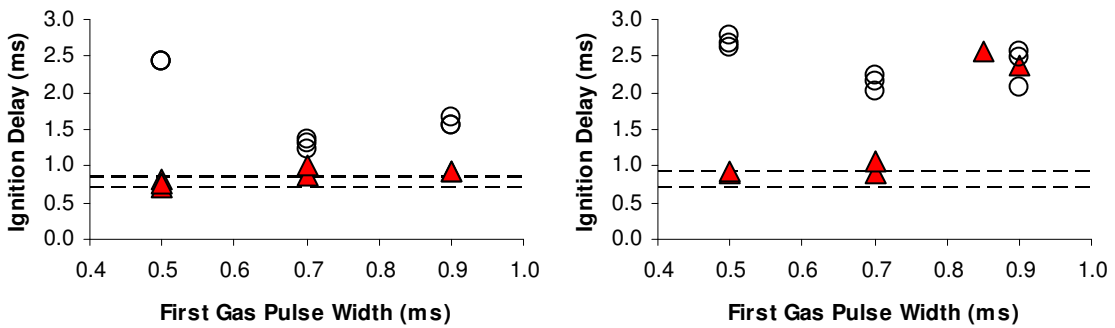
1100 RPM – Low Load



1100 RPM – High Load



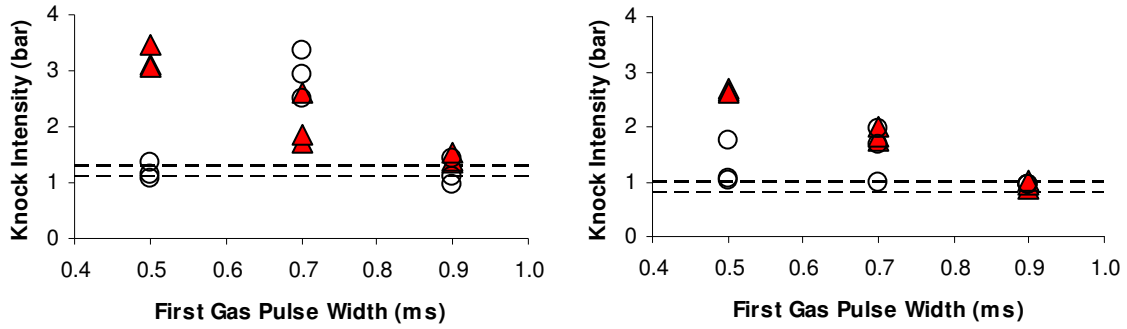
1400 RPM – High Load



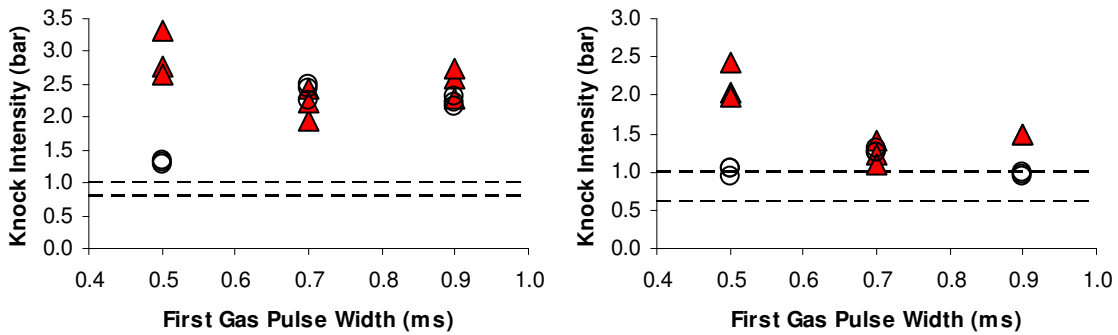
○ B ▲ CS ---- J36

Figure 5-11 – Injector Ignition Delay with 0% EGR (Left) and 30% EGR (Right)

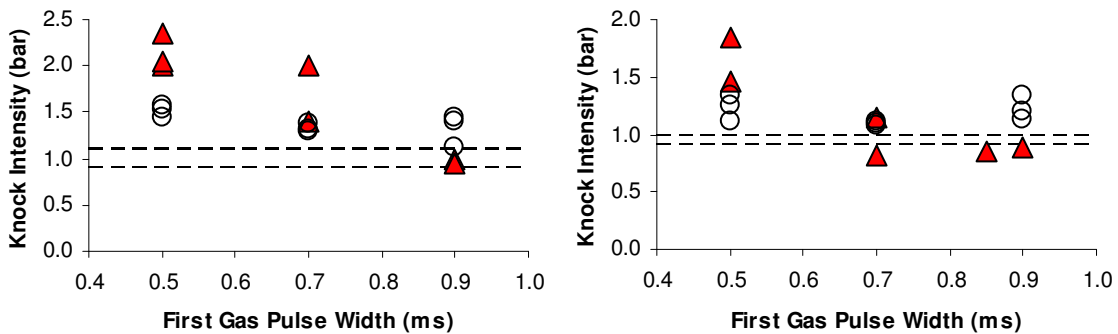
1100 RPM – Low Load



1100 RPM – High Load



1400 RPM – High Load



○ B ▲ CS ---- J36

Figure 5-12 – Injector Knock Intensity with 0% EGR (Left) and 30% EGR (Right)

With the exception of NO_x and CO, emissions are lowest for both co-injectors with the 0.5ms GPW. While in most cases, Co-injector B can match the performance of the J36, it is clear that CS outperforms B at low load, where the CS emissions are lower. At high load, Co-injector B and CS have similar emissions which are comparable to the J36, particularly at low GPWs. The hydrocarbon emissions are lower for CS at 1100 RPM (high load, 30% EGR), but B has lower PM at this condition. The knock intensity, however, is quite high in CS compared to B. It is possible that running CS with a 0.5ms GPW with even less diesel could lower the knock intensity without severely affecting the emissions.

The particulate emissions from the co-injectors typically are lower than for the J36. Ignition delay for CS is in general the lowest of all three injectors at low speed and matches the J36 at high speed with the exception of the 0.9ms GPW case with EGR. This is further evidence that the diesel/gas ratios in the pilot injections of CS are higher than those of B. Note that at low GPWs, the ignition delay is nearly constant for a given speed and EGR level (~0.55ms at 1100 RPM). As load increases with Co-injector B, the ignition delay decreases, which suggests that CS at low pulse widths and low speeds is operating around the minimum ignition delay for co-injection. EGR increases the ignition delay for both co-injectors, but this effect is greater for B than CS. Interestingly, when looking at knock intensity and ignition delay, Co-injector CS shows the trends predicted by the single injection tests carried out in Chapter 4 on Co-injector B. The sharp decrease in knock intensity and only slight increase in ignition delay with increasing GPW suggests that, at least for the 0.5 and 0.7ms GPW cases, the amount of diesel injected in the first pulse is the same, while the amount of gas injected increases. This is not the case for Co-injector B, where knock intensity increases (at low speed) going from 0.5ms to 0.7ms while ignition delay also increases. Clearly the 1st and 2nd pulse interactions [Brown, 2008; Brown, 2009] are much greater in Co-injector B than in CS.

The 0.9ms GPWs appear to only be beneficial at high speed and high load where it tends

to greatly reduce PM emissions with high EGR at the expense of slightly higher gaseous emissions. However, as will be shown below, it is believed that misfiring is occurring at this condition. With such a large GPW, it is possibly better to just run with a single injection.

5.3. FUEL CONSUMPTION AND COMBUSTION STABILITY

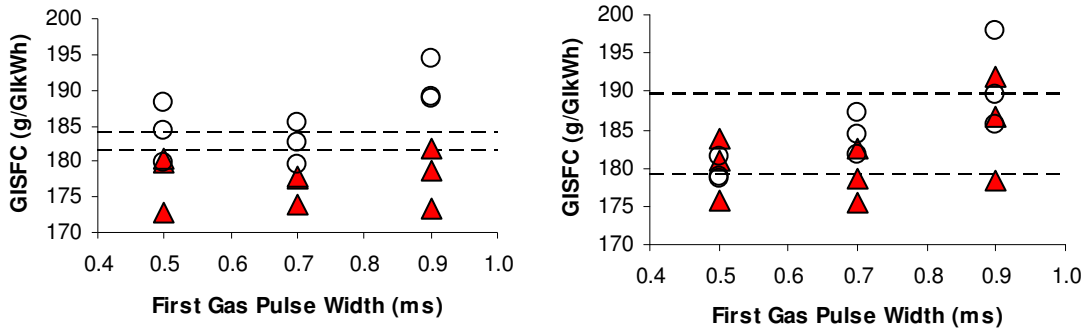
The gross indicated specific fuel consumption (GISFC, Figure 5-13) for both injectors is equal to or less than the J36 fuel consumption for most cases, with CS having a lower GSFC than B, which is in agreement with the lower diesel flow and hydrocarbon emissions. For non-EGR cases, the average GISFC for CS is roughly constant for all GPWs, loads and speeds. High variations in the GISFC measurements for CS were likely the result of a malfunctioning coriolis flowmeter which was used to measure the CNG flow. With EGR, the 0.9ms GPW improved the GISFC at high load and had no effect or raised it slightly at low load (particularly with Co-injector B). The large difference in GISFC between the co-injectors and the J36 for the high speed/ high load case is higher than expected, and further testing in this region is needed to confirm the results.

The coefficients of variation (COV) of GIMEP and maximum cylinder pressure (P_{cyl}) were used to quantify the combustion stability of the co-injectors. Figure 5-14 and Figure 5-15 show that the co-injectors can both match the performance of the J36 in terms of the COV GIMEP for low (0.5 ms) first pulse widths, but they both have higher COV P_{cyl} . The trends in the COV GIMEP and P_{cyl} are similar, except in a couple of cases[†]. The COVs for both B and CS are similar at lower GPWs. P_{cyl} is higher for B at high GPWs while the COV GIMEP is comparable between the two injectors. It was found during testing that misfires which are visible as large pressure fluctuations seen on an oscilloscope, are detected by the COV P_{cyl} and not COV GIMEP (i.e., when misfiring was observed during data collection and compared to collected data where there were no

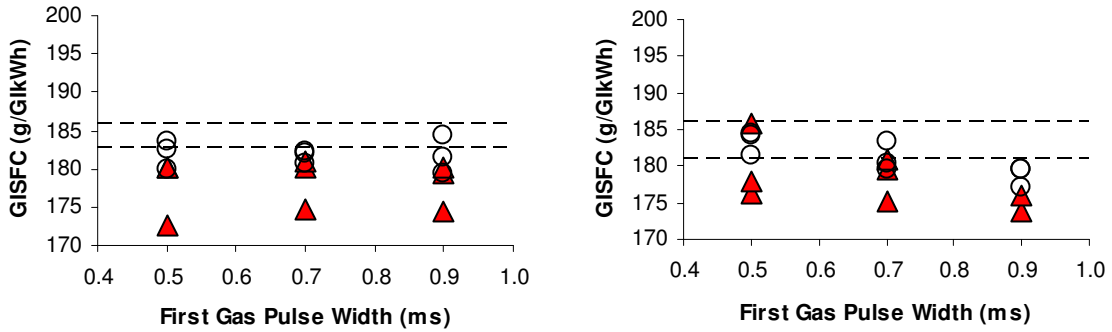
[†] Note that the high COVs of CS for the high load, high speed, non-EGR condition are believed to be caused by drift in the pressure transducer which resulted in high standard deviations of GIMEP and P_{cyl} . The averages are comparable to other repetitions. Thus, the COVs shown for that repetition (which have been circled in Figure 5-14 and Figure 5-15) are believed to be a result of transducer problems, rather than a large variation between repetitions.

misfires, it was found that the COV GIMEPs were not very different while the COV P_{cyl} was 1.5 to 2% higher). Therefore, although the COV GIMEP of CS for the high load, high speed, 30% EGR case with 0.9 and 0.7 ms GPW are comparable to the J36 and 0.5ms case, the fact that COV P_{cyl} is so high at these conditions indicates that some misfiring was likely occurring. This is also seen in Figure 5-6 and Figure 5-7 which show higher hydrocarbon emissions for CS at these conditions. The COV is particularly bad for the 0.9ms pulse width which is possibly the result of the long ignition delay for this point (discussed earlier) leading to overleaning of the mixture, causing the misfires and resulting in the very low PM emissions seen in Figure 5-10.

1100 RPM – Low Load



1100 RPM – High Load



1400 RPM – High Load

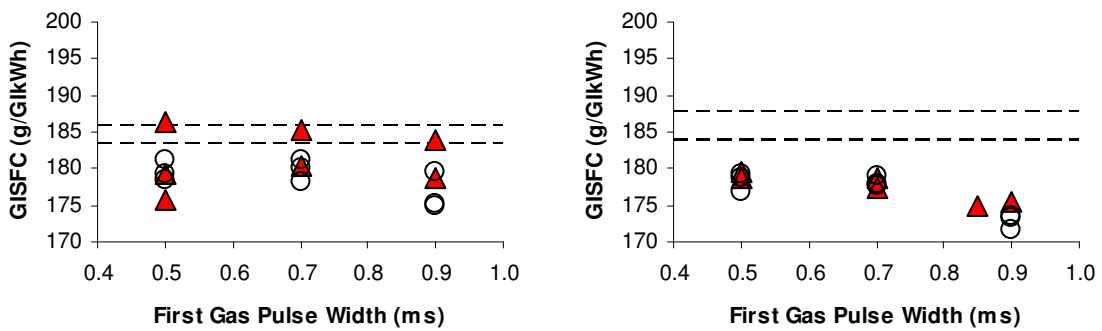
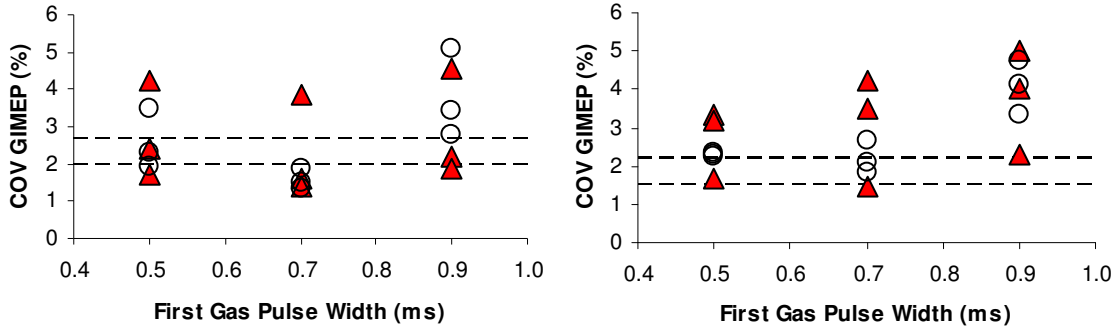
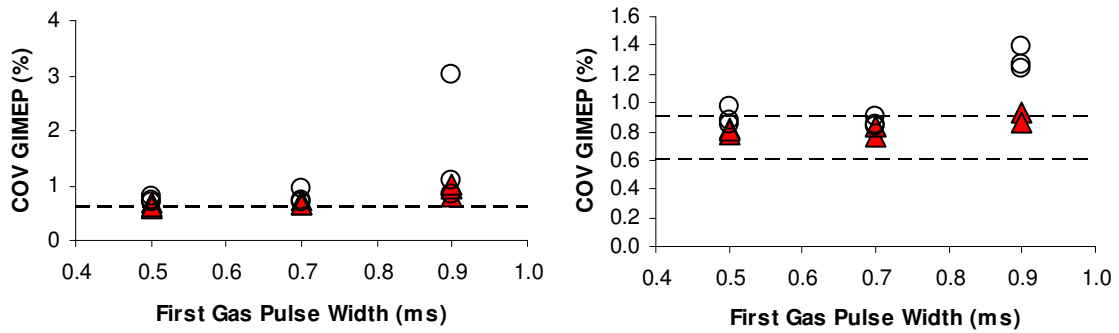


Figure 5-13 – Injector GISFC (Diesel Equivalent) with 0% EGR (Left) and 30% EGR (Right)

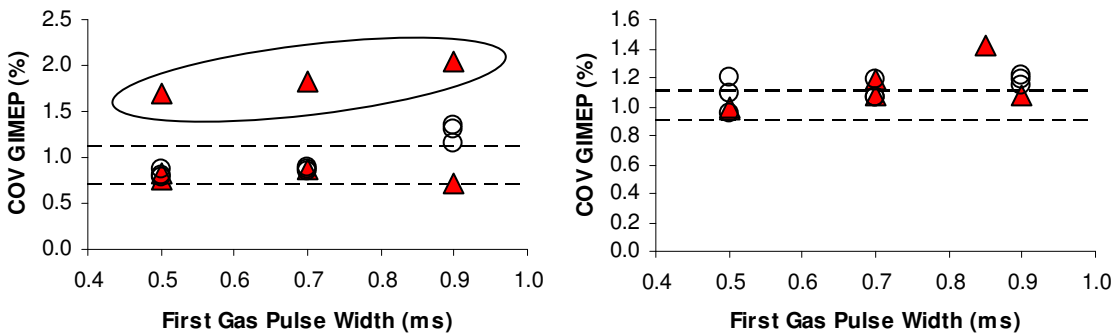
1100 RPM – Low Load



1100 RPM – High Load



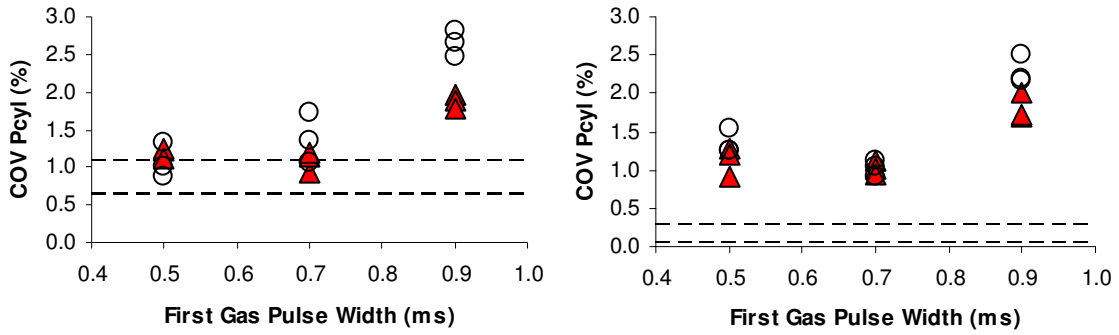
1400 RPM – High Load



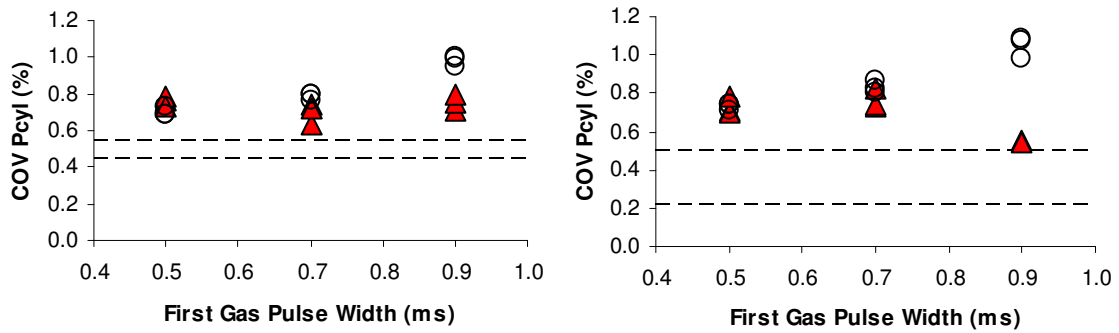
○ B ▲ CS - - - J36

Figure 5-14 – Injector COV GIMEP with 0% EGR (Left) and 30% EGR (Right)

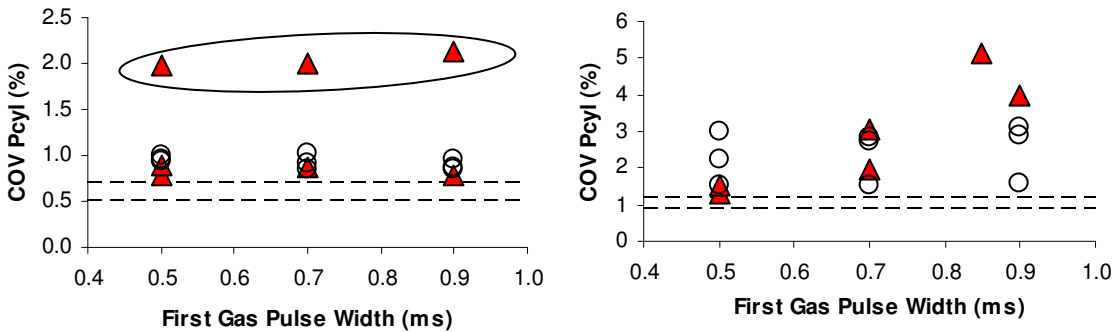
1100 RPM – Low Load



1100 RPM – High Load



1400 RPM – High Load



○ B ▲ CS - - - J36

Figure 5-15 – Injector COV of Max. Cylinder Pressure with 0% EGR (Left) and 30% EGR (Right)

CHAPTER 6 - CONCLUSIONS AND RECOMMENDATIONS

6.1. CONCLUSIONS

Single injection tests of Co-injector B and double injection (two injections per cycle) tests of Co-injectors B and CS have yielded the following results:

It has been found that both Co-injectors B and CS can perform as well (in terms of low hydrocarbon and CO emissions) as the baseline HPDI (J36) injector for the loads and speeds tested (1100 and 1400 RPM with 6 and 13 bar GIMEP). Chapter 5 test results indicate that by using low first gas pulse widths (0.5 ms in these cases), both co-injectors are able to match the hydrocarbon and CO emissions at the load conditions tested. These tests were all done with the CA50 timed at 10° ATDC. With these low first gas pulse widths it was also found that the co-injectors have comparable COV GIMEPs to the J36, but slightly higher COV P_{cyl} for the high load cases. Therefore, combustion stability of the co-injectors are slightly inferior to that of the HPDI at these conditions, but this does not seem to have a negative impact on emissions or fuel consumption (discussed below).

PM emissions of the Co-injectors were equal to or lower than those of the HPDI for 30% EGR cases while the NO_x emissions were comparable to the HPDI for most conditions. At 1100 RPM/6 bar GIMEP and 1400 RPM/13 bar GIMEP, the PM emissions of the co-injectors were lower than those of the HPDI while the co-injectors matched the HPDI emissions at 110 RPM/high load (there is no PM data for the HPDI for the 0% EGR cases). The NO_x emissions from the co-injectors at these conditions were close to the HPDI NO_x for the 30% EGR conditions with the exception being for high loads with high (0.9ms) first GPWs, where CS tended to show higher NO_x. Results were similar for the non-EGR cases, except that CS showed higher NO_x levels at 1100 RPM/6 bar GIMEP.

The fuel consumption for both Co-injectors was lower than the HPDI for most cases tested. The fuel consumption for Co-injector CS was found to be lower than the HPDI

when running with low first gas pulse widths for the engine modes tested, while the fuel consumption for B is slightly higher than CS (and comparable to the HPDI) at low speeds. The combustion in co-injection appears to be more rapid (which correlates with the higher knock intensity seen in co-injection) than the HPDI, resulting in lower fuel consumption.

CS-style co-injection uses the diesel more efficiently such that it can achieve the same emissions as Co-injector B (and the HPDI) while running with at least 23% less diesel.

Integrated heat release (IHR) plots and analysis of gas flow in the second gas injections from the chapter 5 tests indicate that there is more diesel present in the pilot injection of CS than B. The IHR plots show a greater heat release in the pilot combustion events for CS when compared to B for all the conditions tested. This suggests that co-injector CS, despite running with less diesel, is burning more fuel from the pilot injection than B. An estimation of the gas flows from the main injections in the chapter 5 tests give evidence that, even though the total amount of gas injected is roughly the same for both injectors, more gas is being injected in the second pulse for CS relative to B. This suggests that more gas is being displaced by the diesel during the first injection in CS, which supports the claim that more diesel is present in the first injection for CS. The reasons for this are not entirely known. It is thought that in CS, the diesel is able to pool near the bottom of the injector such that it is more easily evacuated in the first injection. In B, the diesel is likely more dispersed throughout the gas in the injector, making it less likely that all the diesel will be injected in the pilot pulse. However, the precise diesel distributions and spray characteristics of the co-injectors are still unknown (i.e. the data cannot be used to check the validity of Figure 1-9).

The high knock intensity present in CS but not B while running with low first gas pulse widths in double injection tests suggests that the diesel flow in CS may be further reduced without resulting in higher hydrocarbon and CO emissions. Results from chapter 4 show strong correlations between knock intensity and diesel flow in co-injection. It was found in chapter 5 that, particularly at low load, the knock intensity of

CS is much higher than B (up to 2 bar higher) with comparable emissions for the 0.5 ms 1st GPW cases. Therefore, it may be possible to reduce the diesel flow in CS further to match the knock intensity of Co-injector B, without sacrificing emissions.

Whereas the pilot combustion event in Co-injector B is weakened by the presence of a second injection, the pilot combustion in CS is independent of the second injection.

Brown (2008) found that the presence of a second injection in Co-injector B reduces the heat released in the pilot injection, which is attributed to diesel being ‘scavenged’ by the second injection. This does not appear to be the case in CS, and the difference is attributed to the way in which the diesel is introduced into the gas plenums within the injectors. As has been discussed above, the IHR plots show greater heat releases in the pilot combustion events for CS, indicating that more diesel is burning in the first injection compared to B, despite running with lower diesel flows.

The co-injectors have the lowest emissions when running with low 1st GPWs (0.5 ms for the current tests). Single injection tests indicate that running Co-injector B with low first pulse widths would give the best combination of low knock intensity and short ignition delay. Double injection tests confirm this in both B and CS, where it was shown that using a 0.5ms GPW for the first injection results in the lowest hydrocarbon and CO emissions. This is valid for the 1100 RPM (6 and 13 bar GIMEP) and 1400 RPM (13 bar GIMEP) conditions tested. The low load, low speed single injection tests suggest the same for Co-injector B, and therefore it is likely that small 1st GPWs are optimal for running the co-injectors over all engine modes, however a wider load/speed test matrix would be needed to confirm this.

Single injection tests show that diesel and the cylinder pressure at the time of injection have the largest effect on knock intensity and ignition delay for Co-injector B.

Increasing the diesel flow or cylinder pressure tends to increase knock intensity and reduce ignition delay. The effect of increased cylinder temperature at injection is the same as increased diesel flow and cylinder pressure, but not as strong. Increasing gas

flow with constant diesel flow tends to reduce knock intensity and increase ignition delay in Co-injector B, but the effect is much weaker than that of the diesel flow. Increasing the injection pressure tends to decrease knock intensity and increase combustion efficiency (for the pilot pulse) of Co-injector B while leaving the ignition delay nearly unchanged. These results build on the initial finding that the emissions and ignition delay are more strongly correlated to the volume ratio, rather than mass ratio of the CNG and diesel. That initial finding was based on an oversimplified calculation of natural gas volume based on peak pressure and ambient temperature. Although the chapter 4 tests only simulate the pilot event, the results confirm that cylinder pressure (at the time of injection for the current tests), which is a component of the volume ratio, is indeed a big factor, particularly in ignition delay where it has been shown that the diesel/CNG effects on ignition delay change with pressure.

The knock intensity/ignition delay relationship in Co-injector B is inverse. This is opposite to the relationship reported for pure diesel and fumigated dual fuel engines, in which knock intensity generally increases with increased ignition delay. In conventional diesel and dual fuel engines, increased ignition delay results in more time for diesel to premix resulting in more rapid combustion and higher knock (typically referred to as combustion noise). It appears that the concentrated amount of CNG surrounding the diesel extends the ignition delay (relative to pure diesel operation) such that the factors which reduce the ignition delay also tend to cause more of the diesel to be ignitable at the start of combustion (see section 4.5), which increases the knock intensity.

Based on the results discussed above as well as past findings, the optimal settings for running the co-injectors are becoming clearer. Firstly, it has been shown that Co-injector CS uses the diesel much more efficiently than Co-injector B (i.e. less diesel is needed to run CS). Also, CS does not require a diesel needle and actuator, making the injector less complex than B. Therefore, the CS-style co-injector appears to be a superior design compared to B (at least for the speed/load range tested). To date, it has been found that B and CS operate best using two injections per cycle using low first gas pulse widths, which

have been found to give the best performance for the conditions tested. CS was run with 11.5mg/inj in the current tests, but high knock intensity at low load indicates that less diesel should be used when running at low load, and perhaps increased as the load and speed increases. For co-injector CS, diesel flow is controlled by the difference of diesel and gas pressures *within the injector*. The bias pressure was measured and controlled using gas and diesel pressures upstream of the engine for the current tests and proved to be adequate for maintaining stable diesel flows.

As will be discussed in section 6.2, further study regarding the effect of the pulse separation as well as the sleeve geometry on Co-injector CS must still be carried out in order to find the best tuning for operation of the co-injectors.

6.2. RECOMMENDATIONS

Co-injection has been shown to be a viable replacement for the J36 under the conditions tested to date. CS, which has no diesel needle, has been able to perform as well and often better than Co-injector B, while running with less diesel. Therefore, future work should focus on single needle co-injection.

Since it has been found that low pulse widths for the pilot injection give the best results, a final co-injector should have better control in the low pulse width range (0.3-0.5ms). CS is currently a modified version of the J36, which has poor control at such low pulse widths.

Further studies involving PSEP (time between the end of the pilot pulse and the beginning of the main pulse) as well as injection pressure are required to ensure that the injector is being run optimally.

Another important variable is the sleeve size inside the co-injector. With Co-injector B, it was found that adding a sleeve which decreases the gas plenum volume and increases

the gas velocity results a stronger pilot event. Since the diesel distribution in CS is likely different to that found in B, the effect of the sleeve on a single-needle co-injector is unclear. A single needle injector with a larger sleeve (called CSX) has already been constructed, but has not yet been fully tested due to equipment malfunctions. Similar double injection tests to the ones in this work should be run on CSX in order to determine the sleeve's effect (different GPWs may be required to optimize this injector). When CSX has been adequately tested, the sleeve should be removed completely and tested in a similar way.

Finally, after all configurations have been tested, it may be wise to take the best injector and change the actuator in order to quantify any performance differences caused by actuator variations. If these tests yield an injector which performs as well as the J36, then a new injector can be built which has the ability to operate reliably at low pulse widths and has the desired gas plenum size. Options for cheaper methods of flow restriction should also be explored to further reduce the cost of the injector.

Further engine testing and modeling is required to gain a deeper understanding of co-injection and how best to design an injector to handle it. Co-injector CS has been shown to outperform previous co-injectors and should be the focus of future research.

Single injection tests similar to the ones performed on Co-injector B should be done with Co-injector CS. This may require using a more restrictive flow restrictor in order to reduce the amount of diesel flow for a given bias. For the current injector, it is not possible to run at 800 RPM with diesel flows lower than 13mg/inj with the current flow restrictor due to the low bias pressure required. Therefore, a smaller restrictor will put the required diesel flows into the bias ranges achievable by the SCRE. Also, a deeper investigation into the role of PSEP is required since Brown (2009) found that although CS was unaffected by the second gas pulse width at the conditions tested, the PSEP did affect it, and the exact reasons and conditions under which that is true are not yet understood.

At this time, there is an enormous amount of double injection data for both CS and B which cover injection timing sweeps and pilot GPW sweeps for six load/speed/EGR conditions. By adding some data points which would account for the interactions between timing and pilot GPW, broad response surfaces could be easily created and used to consolidate the information in the same ways discussed in Chapter 4. Response surface methodology provides techniques (not necessarily used in the current analysis) which can be used to find optimums, something which is crucial for the proper tuning of the co-injectors. With the large number of data points, most repeated in triplicate, a second order response surface over four or five variables should have enough degrees of freedom to provide reliable results.

Currently, some modeling of Co-injector B has begun using AIMSIM. That model should be further developed and coupled with models of spray formation and combustion based on correlations obtained from injector visualizations, as well as the aforementioned response surfaces in a manner similar to what is described in Chiatti *et al.* (2009). Explanations have been put forth to explain the data collected, but a mathematical model which predicts the data would be extremely useful in confirming these explanations and correcting them as needed.

REFERENCES

- AIRNow. 2009. Smog – Who Does it Hurt? Available from <http://www.airnow.gov/index.cfm?action=smog.index>. Accessed October 10, 2009.
- Alla, G., Soliman, H., Badr, O., Rabbo, M. 2000. Effect of Injection Timing on the Performance of a Dual Fuel Engine. *Energy Conversion and Management*. **43**: 269-277.
- Akansu, S., Dulger, Z., Kahraman, N., Veziroglu, T. 2004. Internal Combustion Engines Fueled by Natural Gas-Hydrogen Mixtures. *International Journal of Hydrogen Energy*. 34: 2057-2065
- Birger, N., and Rogak, S. 2009. Flow Characteristics of a Gas-Blast Fuel Injector for Direct-Injection Compression-Ignition Engines. *SAE Technical Paper*. 2009-01-1857.
- Brown, B. S. 2006. *UI-FAC-106-TEST*. Influence of Second Injection on Combustion Associated with the First Injection. SCRE Project Factsheets.
- Brown, B. S. 2008. High-Pressure Direct-Injection of Natural Gas with Entrained Diesel into a Compression-ignition Engine. Master's Thesis, University of British Columbia
- Brown, B. S. 2008b. *UI-FAC-113-TEST*. Performance of the New PM Sampling System. SCRE Project Factsheets.
- Brown, B. S. 2009a. *UI-FAC-115-TEST*. How do the 3 Co-Injectors Compare to the Baseline HPDI Injector? SCRE Project Factsheets.
- Brown, S., Rogak, S., Munshi, S. 2009. Multiple Injection Strategy in a Direct-Injection Natural Gas Engine with Entrained Diesel. *SAE Technical Paper*. 2009-01-1954.
- Bruneaux, G. 2002. A Study of Mixture Formation in Direct Injection Diesel Like Conditions Using Quantitative Fuel Concentration Visualizations in a Gaseous Fuel Jet. *SAE Technical Paper*. 2002-01-1632
- Cathcart, G. and J. Tubb. 2002. Application of Air Assisted Direct Fuel Injection to Pressure Charged Gasoline Engines. *SAE Technical Paper* 2002-01-0705
- Cengel, Y. and Boles, M. 2002. *Thermodynamics: An Engineering Approach*. 4th Ed. New York, NY: McGraw Hill. ISBN: 0072383321

- Chiatti, G., Chiavola, O., and Palmieri, F. Spray Modeling for Diesel Engine Performance Analysis. 2009. *SAE Technical Paper*. 2009-01-0835.
- Chiodi, M., Berner, H., and Bargende, M. Investigation on Different Injection Strategies in a Direct-Injected Turbocharged CNG Engine. 2006. *SAE Technical Paper*. 2006-01-3000.
- Chiriac, R., and Apostolescu, N. Cyclic Variability Patterns in a Spark Ignition Engine Fueled with LPG. 2004. *SAE Technical Paper*. 2004-01-1920.
- Crua, C. 2002. Combustion Process in a Diesel Engine. PhD Thesis, University of Brighton
- Daw, C., Kennel, M., Finney, C., and Connolly, F. 1998. Observing and Modeling Nonlinear Dynamics in an Internal Combustion Engine. *Phys. Rev. E*. 57: 2811-2819.
- Denso Corporation. Gaseous Fuel Injector. US Patent 4,667,088, filed 2005, and issued 04/27/2006.
- Dieselnet. 2009. Emissions Standards: USA Heavy Duty Truck and Bus Engines. Available from <http://www.dieselnet.com/standards/us/hd.php#y2007>. Accessed October 10, 2009.
- Dryer, F. 2007. Spontaneous Ignition of Pressurized Releases of Hydrogen and Natural Gas into Air. *Combustion and Science Technology*. 179: 663-694
- Duc, P., Wattanavichien, K. 2007. Study on Biogas Premixed Charge Diesel Dual Fueled Engine. *Energy Conversion and Management*. 48: 2286-2308
- Dvorak, T. and Hoekstra, R. Optimizing Internal Combustion Engine Performance Through Response Surface Methodology. 1996. *SAE Technical Paper*. 962525.
- Engineering Statistics Handbook. 2009. Normal Probability Plot. Available from <http://www.itl.nist.gov/div898/handbook/eda/section3/normprpl.htm>. Accessed May 18, 2009.
- Engineering Toolbox. 2009. Fuels and Chemicals – Autoignition Temperatures. Available from http://www.engineeringtoolbox.com/fuels-ignition-temperatures-d_171.html. Accessed May 14, 2009.
- Green, J., Daw, C., Armfield J., Finney, C., Wagner, R., Drallmeier, J., Kennel, M., Durbetaki, P. Time Irreversibility and Comparison of Cyclic-Variability Models. 1999. *SAE Technical Paper*. 1999-01-0221.
- Grzegorz, L., Kaminski, T., Czarnigowski, J., Zukowski, D. and Wendeker, M. 2007.

- Cycle-toCycle Oscillations of Heat Release in a Spark Ignition Engine. *Meccanica*. 42: 423-433.
- Harrington, J., Munshi, S., Nedelcu, C., Ouellette, P., Thompson, J., and Whitfield, S. Direct injection of natural gas in a heavy-duty diesel engine. 2002. *SAE Technical Paper*. 2002-01-1630
- Heywood, J. B. 1988. *Internal Combustion Engine Fundamentals*. New York, NY: McGraw Hill. ISBN: 007028637X.
- Hiroyasu, H., and Arai, M. Structure of Fuel Sprays in Diesel Engines. 1990. *SAE Technical Paper*. 900475
- Hodge, B. and Koeing, K. 1995. *Compressible Fluid Dynamics With Personal Computer Applications*. Englewood Cliffs, NJ: Prentice-Hall. ISBN: 013308552X.
- Hodgins, K., Hill, P., Ouellette, P., and Hung., P. Directly injected natural gas fueling of diesel engines. 1996. *SAE Technical Paper*. 961671
- Huang, J., Hill, P., Bushe, K., Munshi, S. 2004. Shock-Tube Study of Methane Ignition Under Engine Relevant Conditions. *Combustion and Flame*, **136**, 25.
- International Association for Natural Gas Vehicles. 2009. Natural Gas Vehicle Statistics. Available from <http://www.iangv.org/tools-resources/statistics.html>. Accessed September 15, 2009.
- Jones, H. L. 2004. Source and Characterization of Particulate Matter from a Pilot-Ignited Natural Gas Fueled Engine. Master's Thesis, University of British Columbia
- Jones, H. L. 2005a. *UI-FAC-091-TEST*. Engine Testing Results from First I2I Coinjector Prototype. SCRE Project Factsheets.
- Jones, H. L. 2005b. *UI-FAC-092-TEST*. Engine Testing Results from First I2I-Coinjector Prototype – 2nd Round of Testing. SCRE Project Factsheets.
- Jones, H. L. 2006. *UI-FAC-093-TEST*. Engine testing results from first I2I-coinjector prototype – 3rd round of testing J36 comparison to I2I injector. SCRE Project Factsheets.
- Karim, G. A. and Zhigang, L. A Predictive Model for Knock in Dual-Fuel Engines. 1992. *SAE Technical Paper*. 921550.
- Kubesh, J. Analysis of Knock in a Dual Fuel Engine. 1992. *SAE Technical Paper*. 922367.

- Lee Company. 2009. Lohm Laws for Liquids – How to Calculate Flow Resistance for Liquids. Available from <http://www.theleeco.com/>. Accessed March 4, 2009.
- Li, S., Williams, F. and Gebert, K. A Reduced Reaction Mechanism for Predicting Knock in Dual-Fuel Engines. 2000. *SAE Technical Paper*. 2000-01-0957.
- Litak, G., Kaminski, T., Czarnigowski, J., Zukowski, D. and Wendeker, M. 2007. Cycle-to-Cycle Oscillations of Heat Release in a Spark Ignition Engine. *Meccanica*. 42: 423-433.
- McTaggart-Cowan, G. 2006. *UI-FAC-098-TEST*. SCRE Project Factsheets.
- McTaggart-Cowan, G., Bushe, K., Hill, P., Munshi, S. 2003. A Supercharged Heavy-Duty Diesel Single Cylinder Research Engine for High Pressure Direct Injection of Natural Gas. *International Journal of Engine Research*. 4: 315-330
- McTaggart-Cowan, G.P., Wu, N., Jin, B., Rogak, S.N., Davy, M.H. and Bushe, W.K. 2009. Effects of Fuel Composition on High-Pressure Non-Premixed Natural Gas Combustion. *Combustion Science and Technology*. 181 (3): 397-416.
- Meyers, R. and Montgomery, D. 2002. *Response Surface Methodology: Process and Product Optimization Using Designed Experiments*. 2nd Ed. New York, NY: Wiley-Interscience. ISBN: 0471412554.
- Miao, H., Milton, B. 2005. Numerical Simulation of the Gas/Diesel Dual Fuel Engine In-Cylinder Combustion Process. *Numerical Heat Transfer, Part A*. 47: 523-547
- Miyake, M., Biwa, T., Endoh, Y., Shimotsu, M., Murakami, S., Komoda, T. 1985. The Development of High Output, Highly Efficient Gas Burning Engines. *International Congress On Combustion Engines*.
- Montgomery, D., Peck, E., Vining, G. 2001. *Introduction to Linear Regression Analysis*. 3rd Ed. John Wiley & Sons. New York, NY. ISBN: 0471315656.
- Munsen, B., Young, D., Okiishi, T. 2002. *Fundamentals of Fluid Mechanics*. 4th Ed. John Wiley & Sons. New York, NY. ISBN: 047144250
- Mustafi, N., Raine, R. A Study of the Emissions of a Dual Fuel Engine Operating with Alternative Gaseous Fuels. 2008. *SAE Technical Paper*. 2008-01-1394
- NETT Technologies. 2009. Emissions FAQ. Available from <http://www.nett.ca/faq/index.html>. Accessed October 10, 2009.
- Nwafor, O. 2002. Knock Characteristics of Dual-Fuel Combustion in Diesel Engines

- Using Natural Gas as Primary Fuel. *Sadhana*. 27: 375-382
- Ouellette, P. 1996. Direct Injection of Natural Gas for Diesel Engine Fueling. PhD Thesis, University of British Columbia
- Ouellette P., Hill, P. 2000. Turbulent Transient Gas Injections. *Journal of Fluids Engineering*. 122: 743-753
- Prakash, G., Ramesh, A. 1999. An Approach for Estimation of Ignition Delay in a Dual Fuel Engine. *SAE Technical Paper*. 1999-01-0232
- Rubas, P., Paul, M., Martin, R., Coverdill, R., Lucht, R., Peters, J. Methane Jet Penetration in a Direct-Injection Natural Gas Engine. 1998. *SAE Technical Paper*. 980143
- Ren, Y., Randall, R., Milton, B. 1999. Influence of the Resonant Frequency on the Control of Knock in Diesel Engines. *Proc Instn Mech Engrs*. 213: 127-133
- Selim, M. 2004. Combustion Noise Measurements and Control from Small Diesel and Dual Fuel Engines. *SAE Technical Paper*. 2004-32-0072
- Song, Y., Acker, G., Schaetzle, W. and Brett, C. Knock Limitations of Methane-Air Mixtures in a Turbocharged Dual-Fuel Engine. 1987. *SAE Technical Paper*. 870794.
- Sovani, S., Sojka, P., Lefebvre, A. 2001. Effervescent Atomization. *Progress in Energy and Combustion Science*. 27: 483-521
- Stone, R. 1999. *Introduction to Internal Combustion Engines*. 3rd Ed. Society of Automotive Engineers. Warrendale, PA. ISBN: 0768004950.
- Tang, X., Tracy, E., Boozer, A., deBrauw, A. and Brown, R. 1995. Symbol Sequence Statistics in Noisy Chaotic Signal Reconstruction. *Phys. Rev. E*. 51: 3871-3889.
- Urano, Y., Nakano, Y., and Takada, H. Optimization Technique for Transient Emission Reduction of Heavy Duty Diesel Engine. 2005. *SAE Technical Paper*. 2005-01-1099.
- US EPA. 2009. Six Common Air Pollutants. Available from <http://www.epa.gov/air/urbanair/>. Accessed October 10, 2009.
- Wagner, R., and Drallmeier, J. Prior-Cycle Effects in Lean Spark Ignition Combustion – Fuel/Air Charge Considerations. 1998. *SAE Technical Paper*. 981047.
- Westport Innovations. 2009a. Westport HD - Specifications. Available from <http://www.westport-hd.com/specifications.php>. Accessed September 14, 2009.

- Westport Innovations. 2009b. Westport HD - Technology. Available from <http://www.westport-hd.com/technology.php>. Accessed May 14, 2009.
- Win, Z., Gakkhar, R., Jain, S., and Bhattacharya, M. 2005. Parameter Optimization of a Diesel Engine to Reduce Noise, Fuel Consumption, and Exhaust Emissions Using Response Surface Methodology. *IMechE*. 219: 1181-1192.
- Yang, J. Dual fuel compression-ignition engine. Patent 6427660, filed 2002, and issued 08/06/2002.

Appendix A - Repeatability Point Gaseous Emissions Plots

The plots below show the CO, O₂, CO₂, CH₄, tHC, and NO_x plots from repeatability points run with Co-injectors B and CS over several days spanning one year.

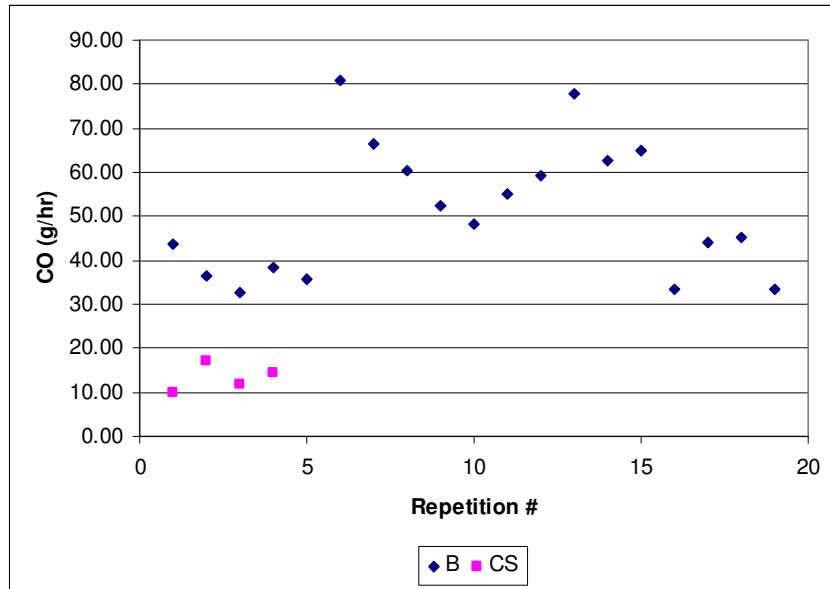


Figure A-1 – Co-Injector CO Emissions from Repeatability Point

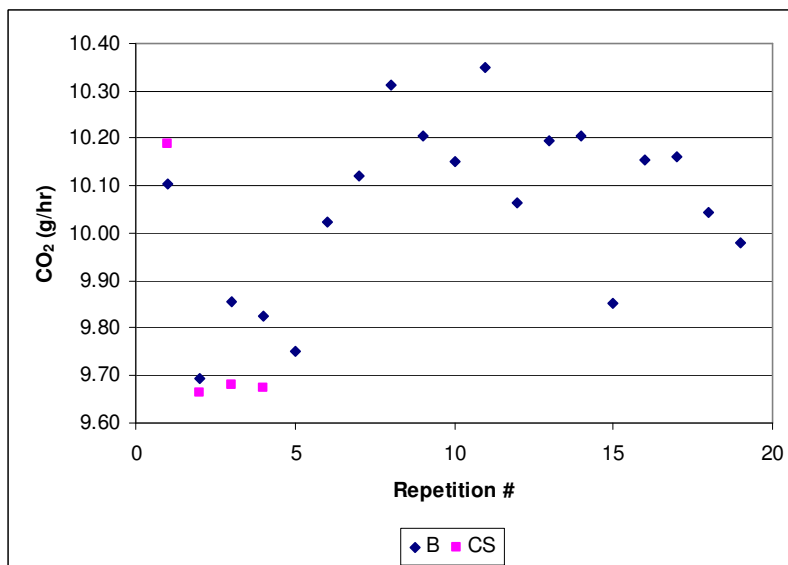


Figure A-2 – Co-Injector CO₂ Emissions from Repeatability Point

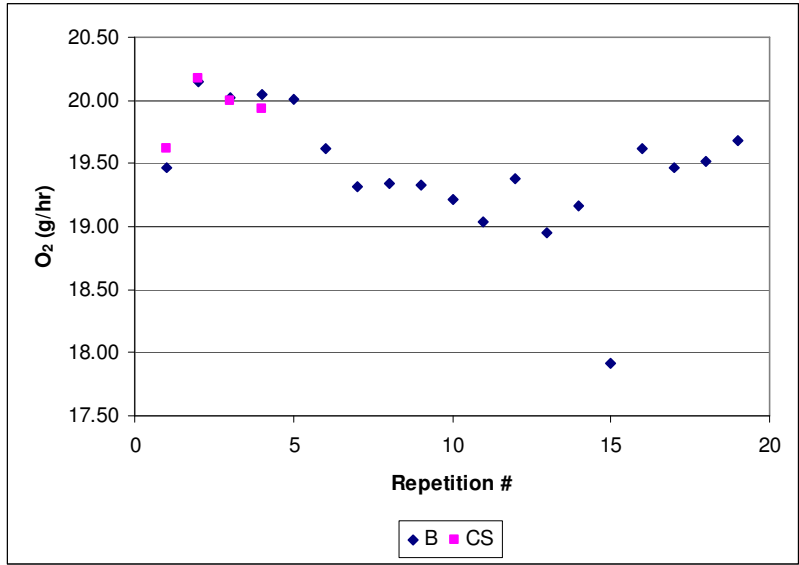


Figure A-3 – Co-Injector O₂ Emissions from Repeatability Point

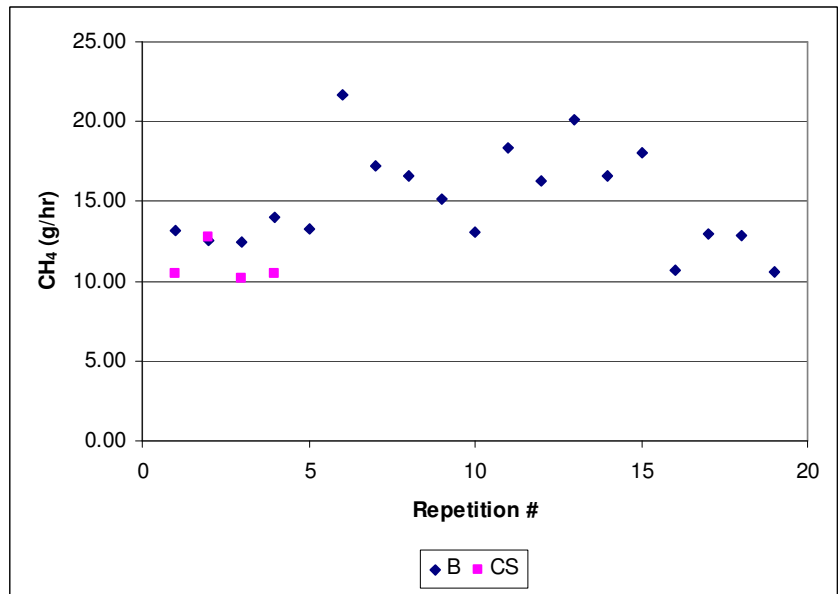


Figure A-4 – Co-Injector CH₄ Emissions from Repeatability Point

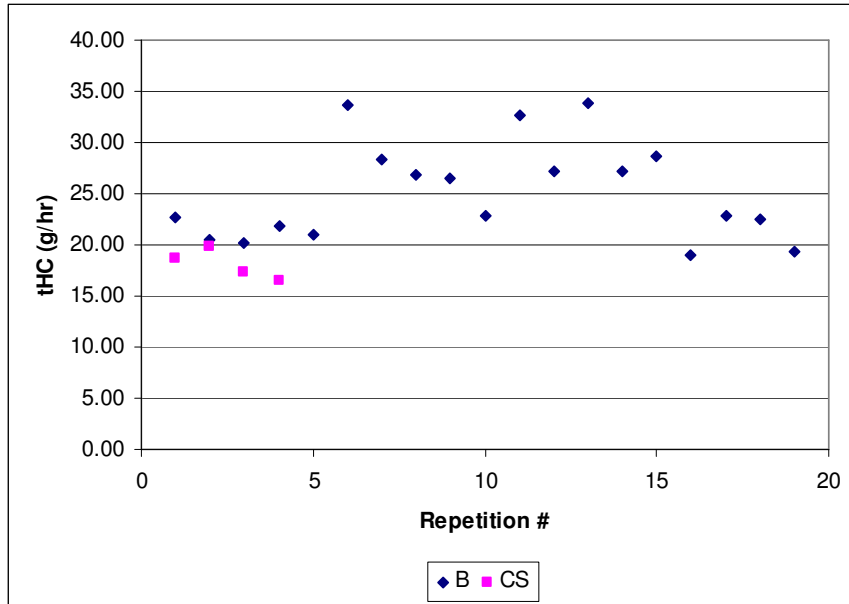


Figure A-5 – Co-Injector tHC Emissions from Repeatability Point

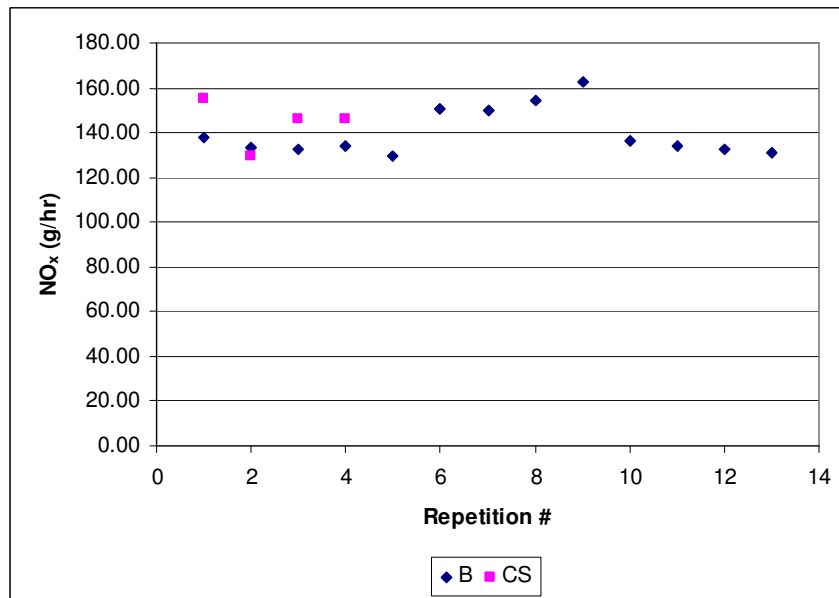


Figure A-6 – Co-Injector NO_x Emissions from Repeatability Point

Appendix B - Bias Control Equations and Flow Restrictor Details

The equation governing the bias is derived below (see Figure 2-7 for the fuel flow schematic). Note the fundamental equation for pressure drop across an ideal needle valve

is given as: $\Delta P = \left(\frac{Q}{k}\right)^2$, where Q is the flow and k represents a loss coefficient which is

proportional to how much the valve is open. When the valve is fully open, k approaches infinity, as it closes, k approaches 0. Losses in the lines are neglected in this analysis. It will be assumed that the flow Q_3 (flow of diesel to the injector) is due only to the bias, and therefore $Q_3 = (k_{inj} + k_{fil})\sqrt{B}$ where k_{inj} is a coefficient meant to account for PPW or flow restriction characteristics within the injector and B is the bias, $P_{DI}-P_{NG}$. To simplify the calculation, only the case in which k_1 is fully open ($k_1 = \infty$) will be derived, which is the typical operating condition.

$$P_{DI} = P_{BP} - \left(\frac{Q_3}{k_{fil}}\right)^2, \quad Q_1 = k_{BP} \sqrt{P_{BP} - P_{CHK-1}}, \quad P_A = P_{BP} + \left(\frac{Q_1 + Q_3}{k_1}\right)^2 = P_{BP}, \quad Q_2 = k_3 \sqrt{P_B - P_{CHK-2}}$$

$$P_B = P_A - \left(\frac{Q_2}{k_2}\right)^2 = P_{BP} - (P_B - P_{CHK-2}) \left(\frac{k_3}{k_2}\right)^2 \Rightarrow P_B = \frac{P_{BP} + P_{CHK-2} \left(\frac{k_3}{k_2}\right)^2}{1 + \left(\frac{k_3}{k_2}\right)^2}$$

$$P_{NG} = P_B - Offset$$

$$P_{DI} - P_{NG} = B = P_{BP} - \left(\frac{Q_3}{k_{fil}}\right)^2 - \frac{P_{BP} + P_{CHK-2} \left(\frac{k_3}{k_2}\right)^2}{1 + \left(\frac{k_3}{k_2}\right)^2} + Offset$$

↓

$$B = P_{BP} \left[1 - \frac{1}{1 + \left(\frac{k_3}{k_2}\right)^2} \right] - B \left(\frac{k_{inj} + k_{fil}}{k_{fil}} \right)^2 - P_{CHK-2} \left[\frac{\left(\frac{k_3}{k_2}\right)^2}{1 + \left(\frac{k_3}{k_2}\right)^2} \right] + Offset$$

$$\therefore B = \frac{1}{1 + \left(1 + \frac{k_{inj}}{k_{fil}}\right)^2} \left[(P_{BP} - P_{CHK-2}) \left(\frac{\left(\frac{k_3}{k_2}\right)^2}{1 + \left(\frac{k_3}{k_2}\right)^2} \right) + Offset \right]$$

Thus, the ratio k_3/k_2 is used to control the bias. Typically, to change the bias, k_3 is kept at a preset position, while k_2 is adjusted. The bias is increased (i.e. the gas pressure drops relative to the diesel pressure) as valve 2 is closed. Figure B-1 shows qualitatively how the valve positions affect the bias pressure.

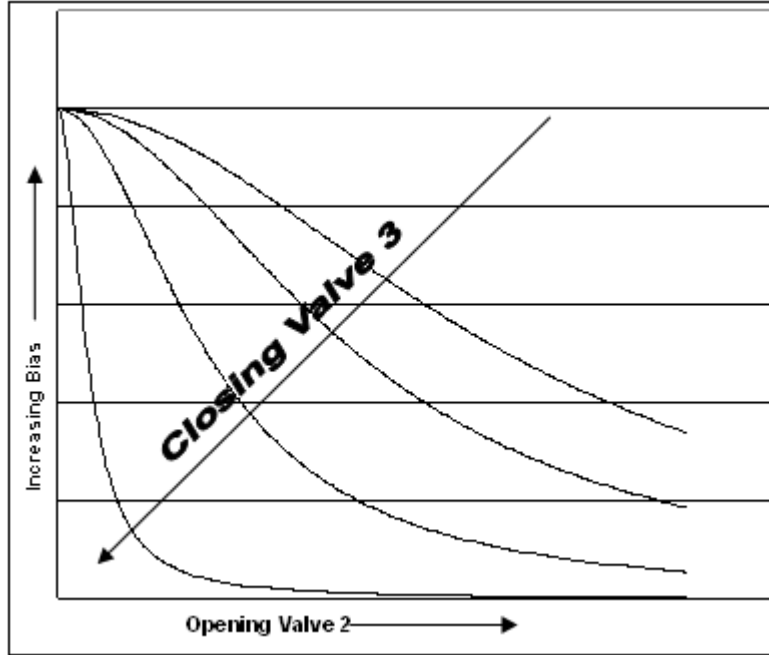


Figure B-1 – Effect of Valve Position on Bias

It should be noted that opening valve 3 too much results in too much diesel flowing out the drain, making it difficult to maintain adequate diesel pressure (i.e. $P_{DI, MAX}$ is limited by the total flow of the system). Since Q_2 is the flow which controls the bias, reducing Q_1 by putting in a higher pressure check valve (P_{CHK-1}) would allow further opening of valve 3 (which would increase Q_2), resulting in a more linear response in the bias control.

Flow Restrictor Calculations

The equation needed to relate the bias pressure to the diesel flow through the flow restrictor was supplied from the LEE Company, namely, their LOHM law [Lee, 2009] which is given below.

$$H = S \left[\frac{F(LOHMS)}{kV} \right]^2$$

Where H is the bias pressure in kPa, S is the specific gravity of the diesel (0.848 [McTaggart-Cowan, 2006]), F is the diesel flowrate in L/min, k is a constant to make the units consistent (28.8 in this case), LOHMS is a measure of the resistance of the restrictor

given by the company as 145000 for this restrictor. V is the viscosity factor which is found in tables from the LEE Company [Lee, 2009]. Based on those tables, and using a viscosity of 4 cSt [Lee, 2009] for the diesel the viscosity effect is negligible at bias pressures above 172 kPa, which is well above the minimum operating bias, and thus the value of V is set to 1.

Appendix C - Cyclic Variation

Analysis of cycle-to cycle variations is a useful tool in combustion analysis. These variations can be used to make comparisons between different combustion conditions by examining not only cyclic variation, but the correlations and patterns which may be present between cycles. Two techniques were used to quantify the correlations between successive cycles for the co-injectors and they are described below.

Return Maps

First return maps are applied to cyclical data to determine the linear correlation (if any) which exists between successive pieces of data. This technique generally involves plotting a variable (GIMEP, IHR, knock, etc.) at cycle X vs. the value at cycle X+L, where L is referred to as the return lag measured in cycles. This gives a scatter plot of points which is used to calculate a Pearson Product-Moment correlation coefficient (R). This coefficient has a value between 1 and -1 and is a measure of the linearity of the relationship between two variables. Thus, a highly positive or negative linear relationship has a coefficient approaching 1 or -1. Examples of strong and weak correlations in IMEP for a return lag of 1 are given in Figure C-1.

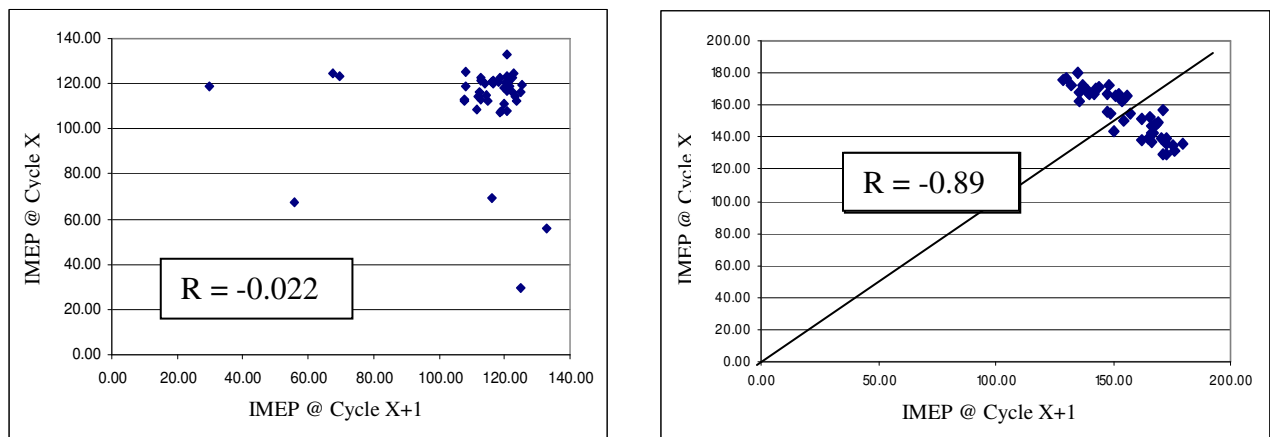


Figure C-1 – Examples of Strong (Right) and Poor (Left) Correlation First Return Maps

The graph on the right has a strong negative correlation, meaning that when one cycle has

a high IMEP, the following cycle typically has a lower one and vice versa. The left graph shows no significant linear correlation between cycles. By calculating the R values for various return lags and then plotting the R value versus return lag, one can see any linear relationships which may exist between non-successive cycles as well. Interpretation of the correlations depends on the variable and the repeatability of the correlations, but it can be a useful tool when comparing the different injectors.

Return maps have been applied in engine research primarily to spark ignition engines. Wagner *et al.* (1998) and Chiriac *et al.* (2004) used return maps for an SI engine running with various equivalence ratios conditions to examine the transition from stochastic to deterministic behaviour in the cyclic variation of the indicated mean effective pressure and heat release. Wagner used a single cylinder CFR engine using iso-octane as the fuel while Chiriac used a 6 cylinder engine running on LPG. The results showed that the cyclic variation became increasingly deterministic as the fuel/air mixture got leaner. Wagner *et al.* (1998) also found that injection timing and swirl had significant effects on the cyclic variation in the engine. Also with the help of return maps, Litak *et al.* (2007) concluded that advancing the spark timing in a spark ignition engine running at stoichiometric conditions changed the distribution of successive heat releases for 1991 consecutive cycles (although in this case, the return maps were used more to support findings from probability distributions). Daw *et al.* (1998) proposed a simple engine model which predicts the stochastic and deterministic cyclic variations in spark ignition engines. The model data was validated with the help of return maps of real engine data. Daw's findings with regards to the effect of equivalence ratio on cyclic variation were the same as above. All the aforementioned analyses used a return lag of 1, which only shows the relationship between immediately successive cycles.

Symbol Sequence Statistics, Shannon Entropy, and Time Irreversibility

The second type of cycle-to-cycle analysis used in this research was symbol sequence statistics. There are different versions of this method which can be used, but for the current work, the binary version is used, which is the most common [Daw *et al.*, 1998;

Tang *et al.* 1995; Chiriac *et al.*, 2004]. This means that the variable in question is given a value of 0 or 1 for each cycle collected. It is a requirement that there are an equal number of 1's and 0's [Tang *et al.* 1995] (i.e. if there are 300 cycles worth of data, there must be 150 ones and 150 zeros). Therefore, the median of the variable for all the cycles is calculated and then for each cycle the variable is assigned a value of 1 if it is above the median and 0 if it is below. Thus, a binary number is created for the variable in question whose number of bits is equal to the number of cycles (called 'word length'). Next, the number of cycles over which to compare the data (byte length) must be chosen. This is chosen based on Shannon Entropy, which will be discussed later. As an example, suppose a comparison will be made using 6 cycles (i.e. byte length = 6) at a time and that 300 cycles were collected. Therefore, over 6 cycles, a six-bit binary number can be formed giving values from 0-64 (i.e 000000, 000010, 000011...111111). For each value of the 6-bit number (called a 'byte') from 0 to 64, the 6 bits are compared to 6 successive bits in the word (see Figure C-2 below). Each byte from 0 to 64 is then given a value based on how many times there was a match between the byte and 6 successive bits of the 300 bit word (i.e. 4 matches gives the byte a frequency of 4) as it slides through all 300 bits. These values are then normalized by the sample size and histograms of Relative Frequency vs. Byte are generated.

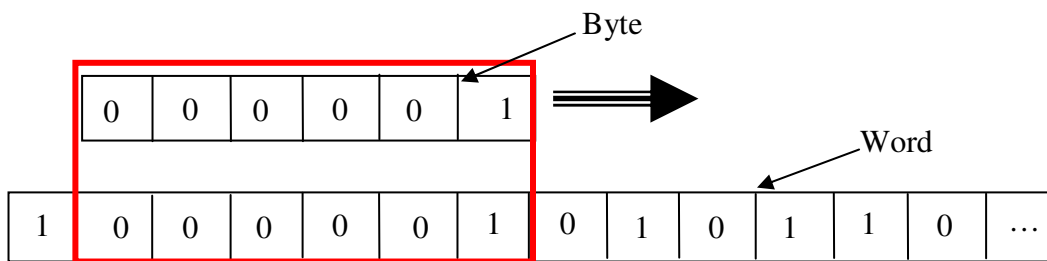


Figure C-2 – Graphical Representation of the Symbol Sequence Statistic Calculation

Any spikes in the aforementioned plots would indicate non-random behaviour in the data (i.e. a Gaussian distribution would have a flat Relative Frequency vs. Byte histogram).

Modified Shannon Entropy [Daw *et al.*, 1998] is used to measure the amount of randomness found in the symbol sequence statistic comparison for a given byte length

used for comparison (in the above example, 6). The Shannon entropy can have a value between 0 and 1. A Shannon Entropy of 1 implies a Gaussian distribution, while a value approaching 0 suggests a non-random result. Shannon Entropy (H) is calculated as follows:

$$H = \frac{1}{\log(n_{seq})} \sum_i p_i \log(p_i)$$

In the above equation, p_i is the probability of byte ‘i’ matching a section of the Word (i.e. the relative frequency of byte ‘i’) and n_{seq} is the number of bytes which have a non-zero relative frequency (Note that it is the fact that only non-zero relative frequencies are counted which makes this ‘Modified’ Shannon Entropy. See Tang *et al.* (1995) as an example of the use of Shannon Entropy for infinite datasets). The Shannon Entropy is calculated for various byte lengths (in the current work byte lengths from 2 to 10 were investigated) and plotted. The byte length with the lowest Shannon Entropy has the least random distribution and is chosen for further analysis. A typical Shannon Entropy plot is shown in Figure C-3 below.

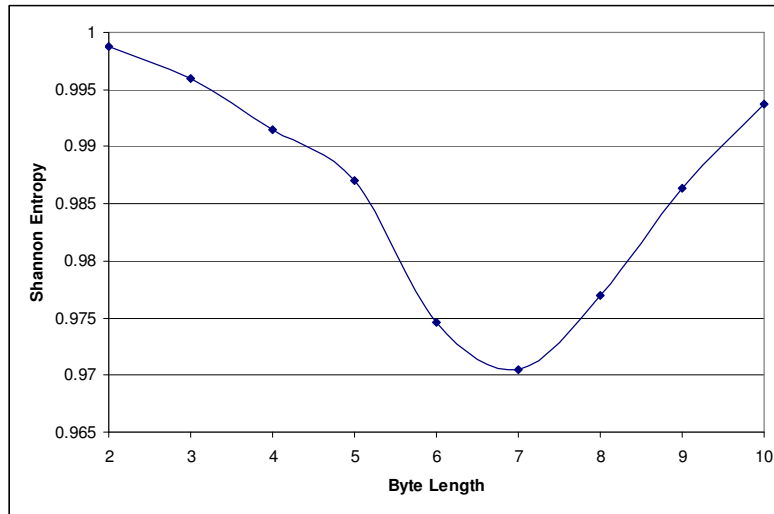


Figure C-3 – Example of a Shannon Entropy Plot

This is a standard Shannon entropy plot shape because when the byte length is too short, it may not hold enough deterministic information, while long byte lengths may contain too much noise (i.e. the amount of data is insufficient for such long sequences) [Daw *et*

al., 1998]. Note that in Figure C-3, a byte length of 7 gives the least random distribution. However, the scale on the y-axis is deceiving and although a byte length of 7 represents the least random distribution in this case, it has a large Shannon Entropy and therefore is still nearly Gaussian. A y-axis scale from 0 to 1 would show a much flatter line near 1, which would be more appropriate, but the purpose of Figure C-3 is to demonstrate the typical shape of the Shannon entropy plot. Modified Shannon entropy is an effective tool for finding temporal patterns in the data because it is sensitive to both linear and non-linear patterns, unlike autocorrelation [Wagner *et al.*, 1998].

The return map studies referenced previously also use symbol sequence statistics to study the cyclic variations of spark ignition engines in the same manner described above. Green *et al.* (1999) used symbol sequence statistics to quantify the time irreversibility of the cyclic variation of combustion (i.e. any patterns seen in the forward time sequence are different in the reversed sequence). While looking for asymmetry in the return maps is a way to qualitatively demonstrate time irreversibility, Green used symbol sequence statistics to quantify it. Essentially, he created symbol sequence histograms as described previously for both the forward and reverse time series. The time irreversibility is then given as [Green *et al.*, 1999]:

$$\tau_{irr} = \sqrt{\sum_i (F_i - R_i)^2}$$

Where $F_i - R_i$ is the difference between the relative frequencies of byte ‘i’ in the forward (F) and reverse (R) time series. If the forward and reverse series are identical, the time irreversibility (τ_{irr}) is zero. Time irreversibility is yet another useful tool to distinguish Gaussian data from deterministic data, since random Gaussian data is time reversible [Green *et al.*, 1999]. However, not all time reversible data is necessarily random (the plot on the right of Figure C- shows symmetry about a 45° line drawn through the origin, which is indicative of time reversibility, but is nonetheless non-random in nature).

These analyses were performed on all the data sets, however no significant patterns were found between cycles.

Appendix D - Modified Knock Intensity Response Surface

As is seen in Figure 4-15, the knock intensity at high cylinder pressure (at 21 MPa injection pressure) for low gas flow seems to become independent of diesel flow with knock intensity ranging between 2 and 3 bar. Because of this, the response surface tries to add curvature in that region in order to fit that low gas flow data. This curvature however, has an effect on the rest of the response surface because to obtain that curvature (which is still insufficient in making the predictions in that region), the rest of the response surface must be distorted. Figure D-1 compares contours of that response surface when the 18 low gas flow points are removed from the calculation.

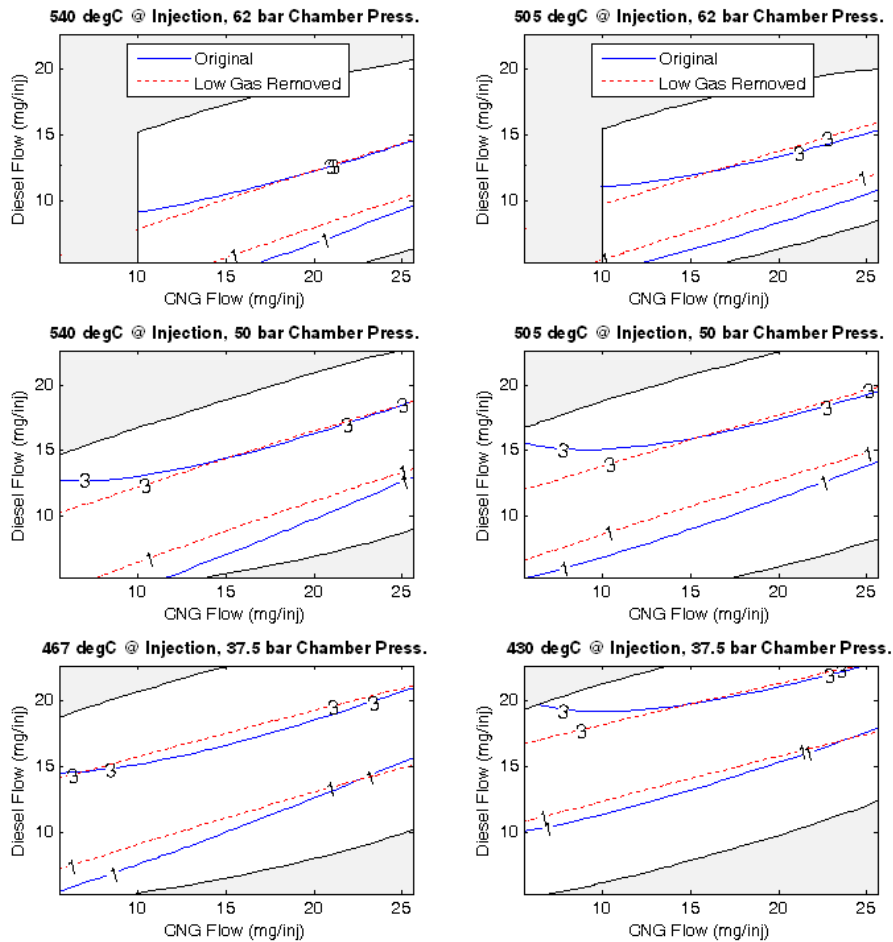


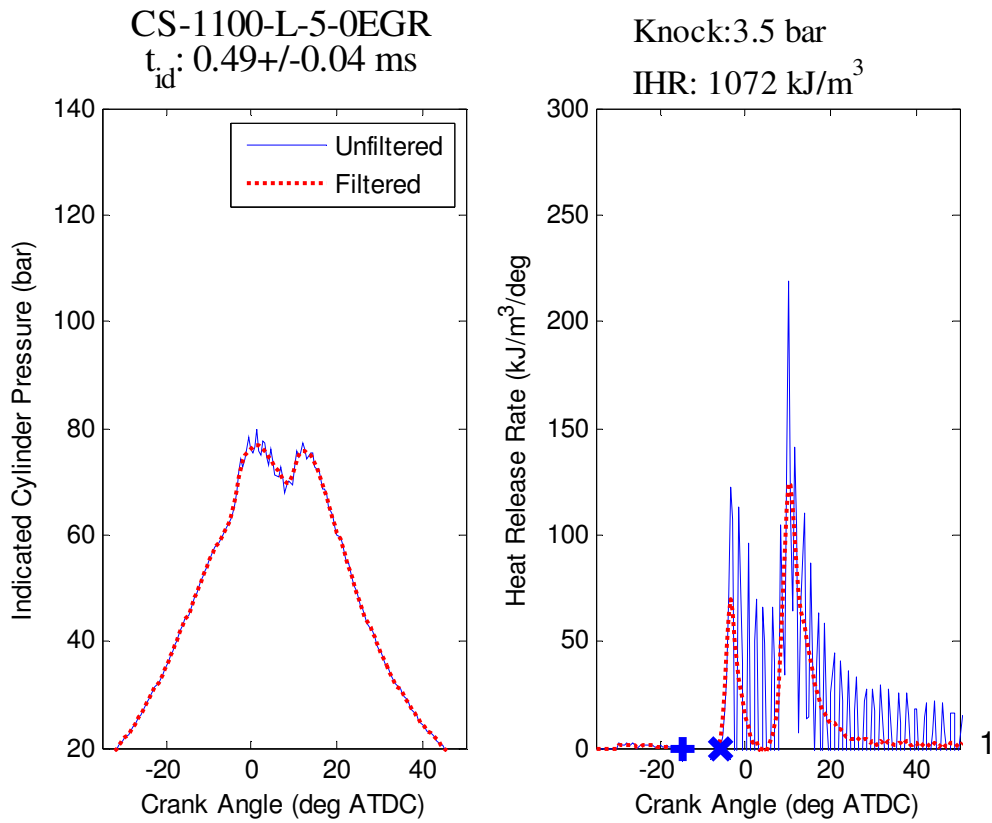
Figure D-1 – Effect of Removing Low Gas Flow/High Cylinder Pressure Points from 21 MPa Knock Intensity Response Surface

As is shown, removing those points causes the contours to become very straight relative to the original. While the high knock intensity prediction is only really different for low gas flows, the lowest knock intensity contours are shifted up for almost every case, indicating that predicted knock intensity was higher than actual for low diesel flows. For high diesel flows at low gas flow, the surface was predicting lower than actual knock intensity.

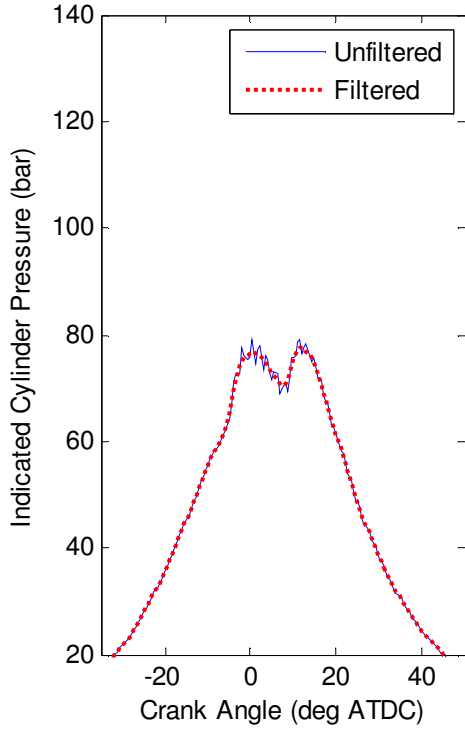
The modified response surface has an R^2 value of 0.86 with a standard error of 0.34 bar (compared to an R^2 of 0.76 and standard error of 0.5 bar for the original surface) with only 18 points removed from the model. That region has been shaded out since the predictions are clearly not meaningful there. Although removal of the low gas flow data makes the response surface fit better, it does not add much to the analysis except that the contours are clearly linear in diesel and CNG mass flow, which may be a useful fact for future modeling of the co-injector.

Appendix E - Double Injection Heat Release Rate Curves

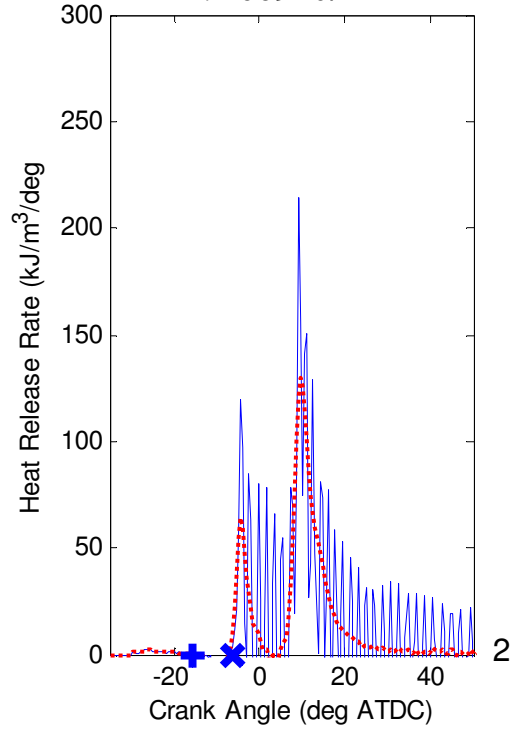
Below are the pressure traces and heat release rate curves for the CS and B double injection tests. Note that the first gas start of injection (GSOI) is marked with a blue cross on the heat release curves and the start of combustion is marked with a blue 'x'. Filtered and unfiltered pressure and heat release rate traces are shown.



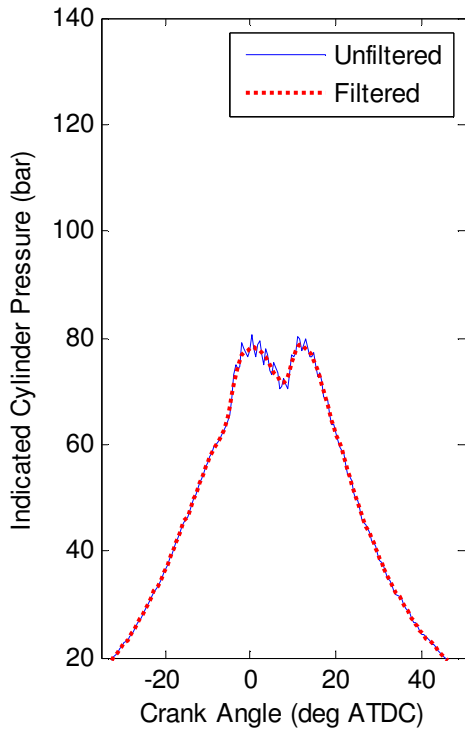
CS-1100-L-5-0EGR-REP1
 t_{id} : 0.56+/-0.04 ms



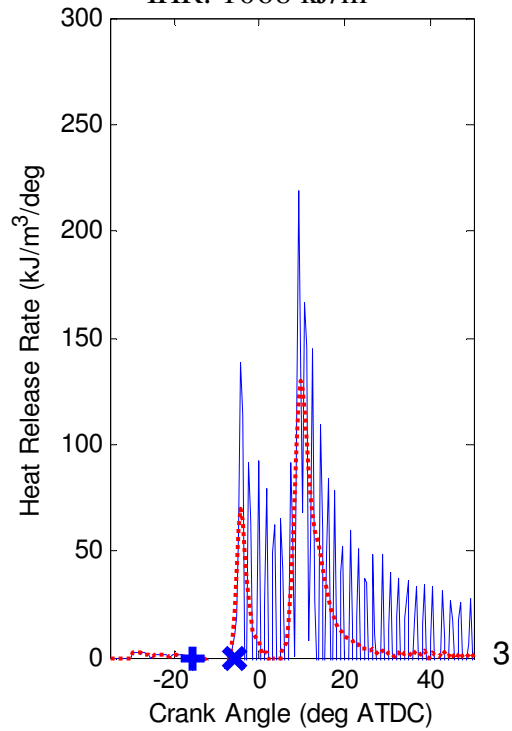
Knock: 3.1 bar
IHR: 1069 kJ/m³



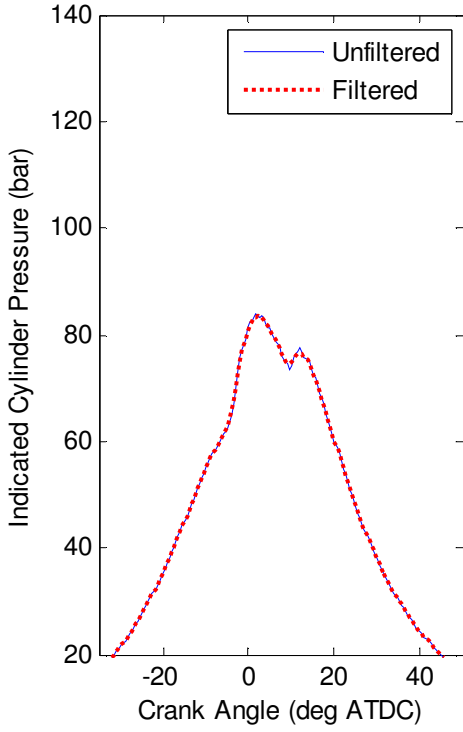
CS-1100-L-5-0EGR-REP2
 t_{id} : 0.55+/-0.04 ms



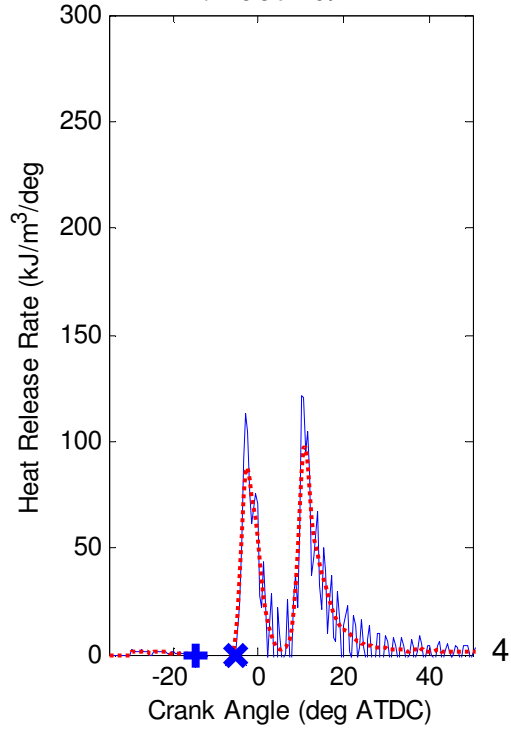
Knock: 3.0 bar
IHR: 1068 kJ/m³



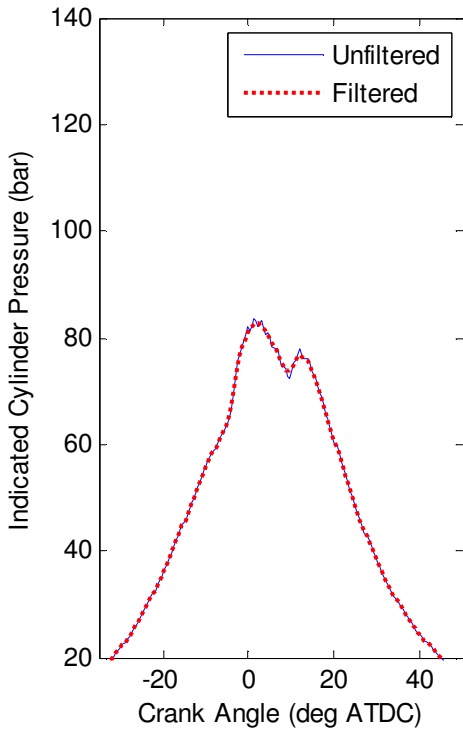
CS-1100-L-7-0EGR
 t_{id} : 0.53+/-0.04 ms



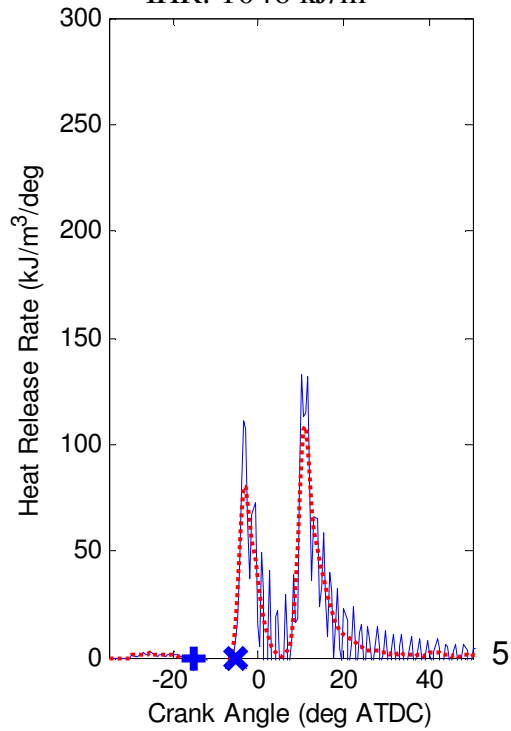
Knock: 1.7 bar
IHR: 1067 kJ/m³



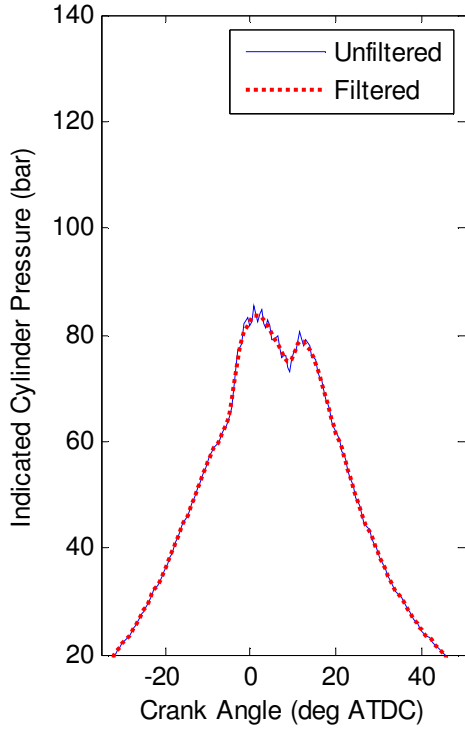
CS-1100-L-7-0EGR-REP1
 t_{id} : 0.58+/-0.04 ms



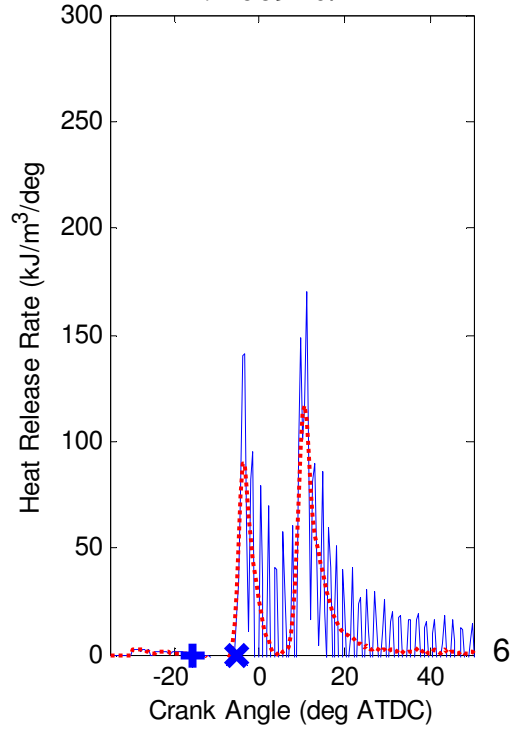
Knock: 1.8 bar
IHR: 1046 kJ/m³



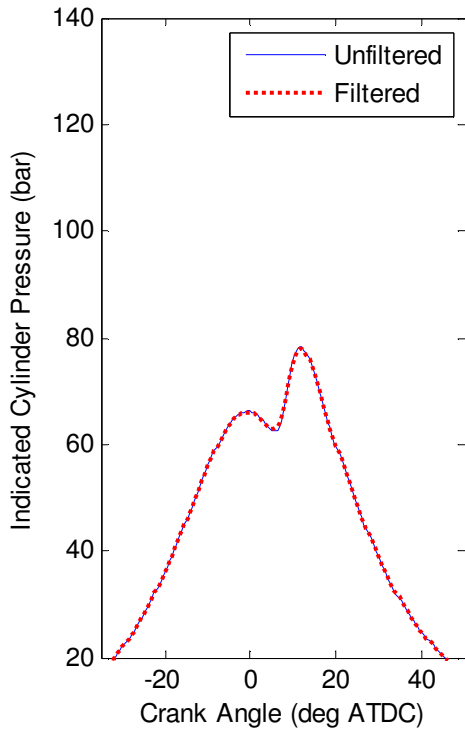
CS-1100-L-7-0EGR-REP2
 t_{id} : 0.61+/-0.04 ms



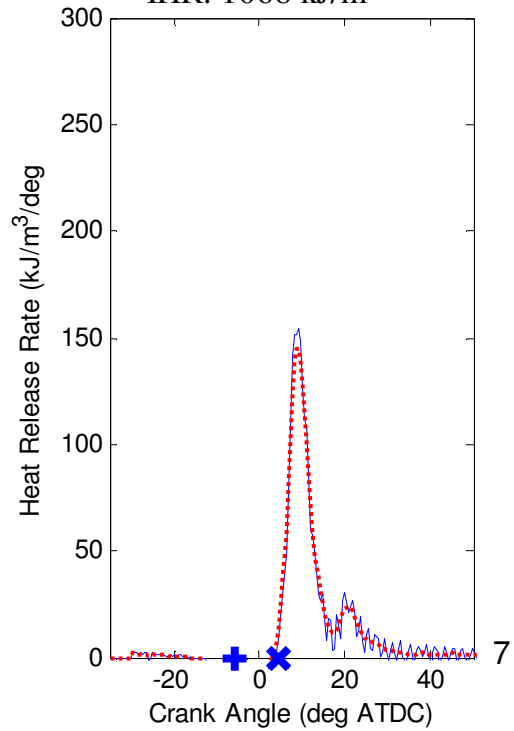
Knock: 2.6 bar
IHR: 1069 kJ/m³



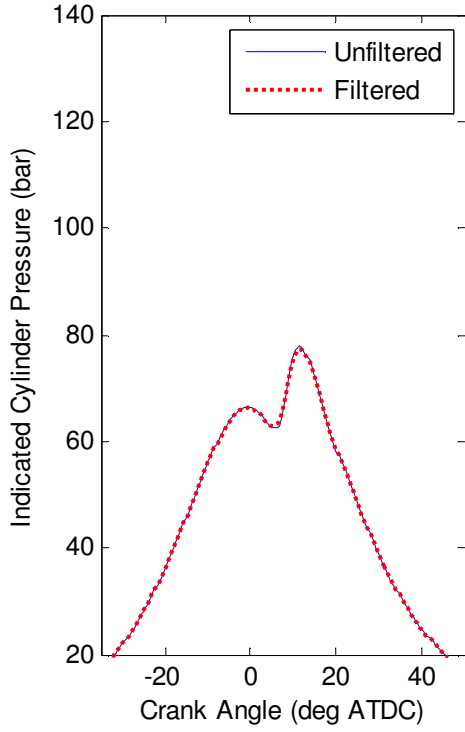
CS-1100-L-9-0EGR
 t_{id} : 0.66+/-0.04 ms



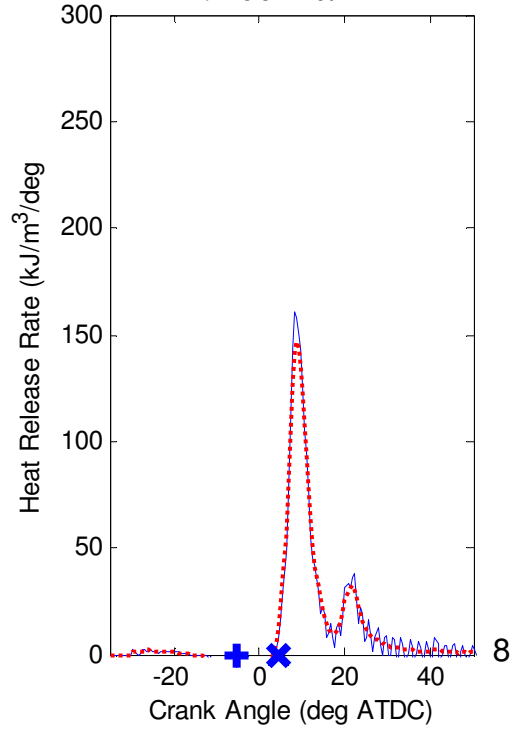
Knock: 1.4 bar
IHR: 1068 kJ/m³



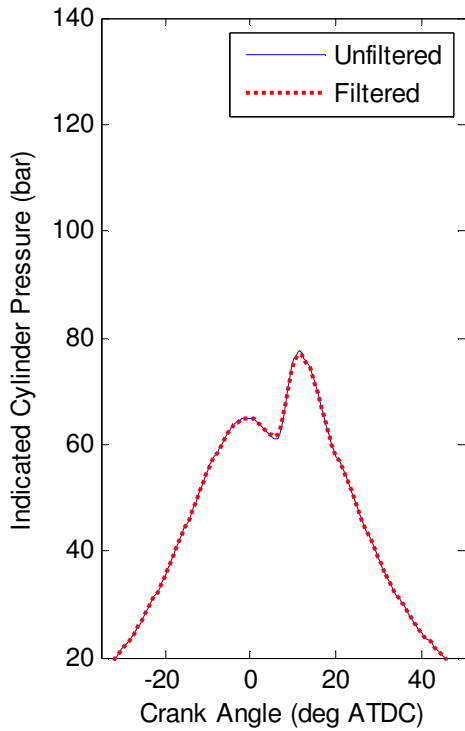
CS-1100-L-9-0EGR-REP1
 t_{id} : 0.62 \pm 0.04 ms



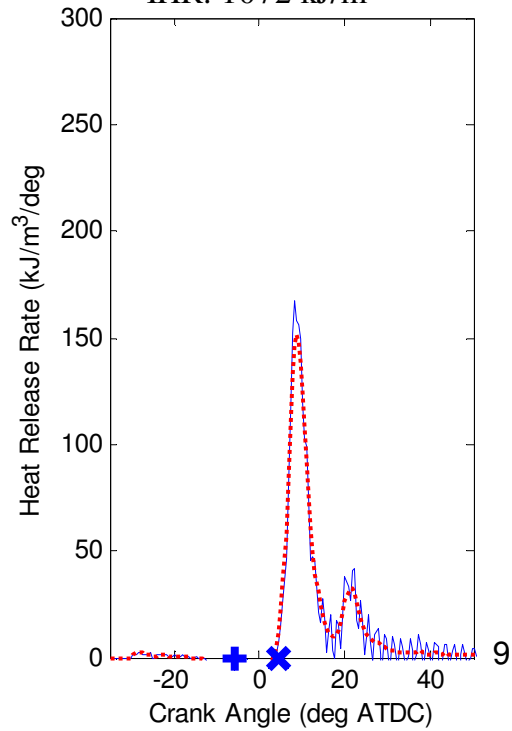
Knock: 1.4 bar
IHR: 1061 kJ/m³



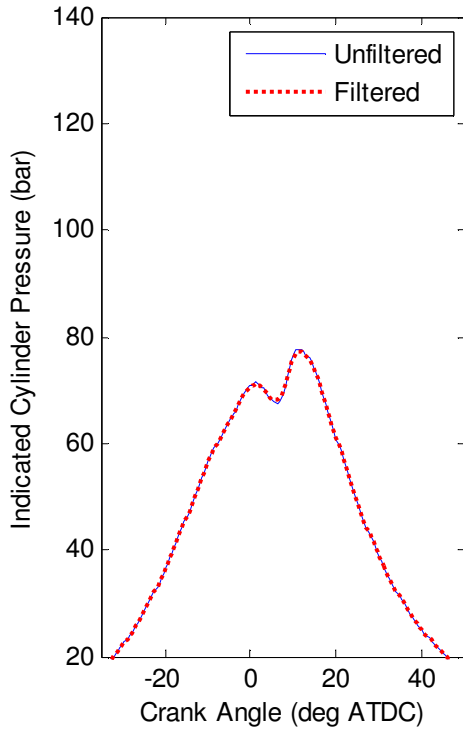
CS-1100-L-9-0EGR-REP2
 t_{id} : 0.67 \pm 0.04 ms



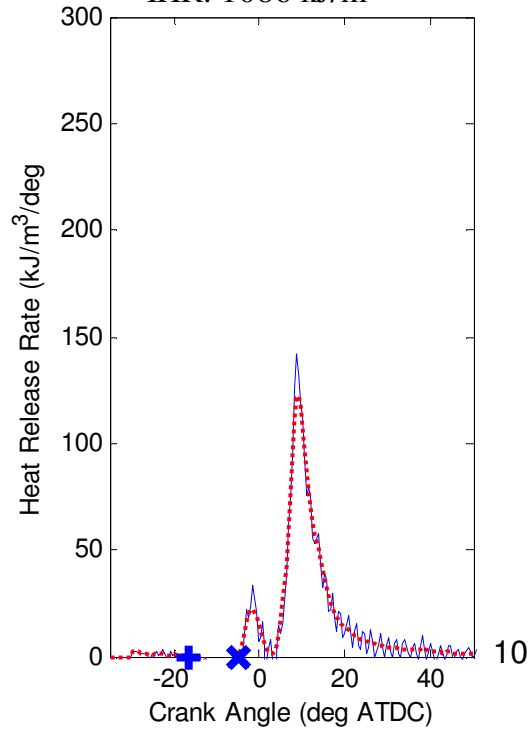
Knock: 1.5 bar
IHR: 1072 kJ/m³



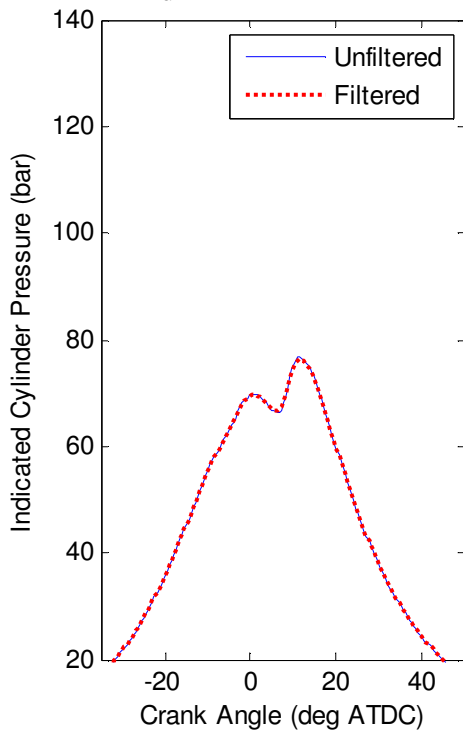
B-1100-L-5-0EGR
 t_{id} : 0.87 \pm 0.11 ms



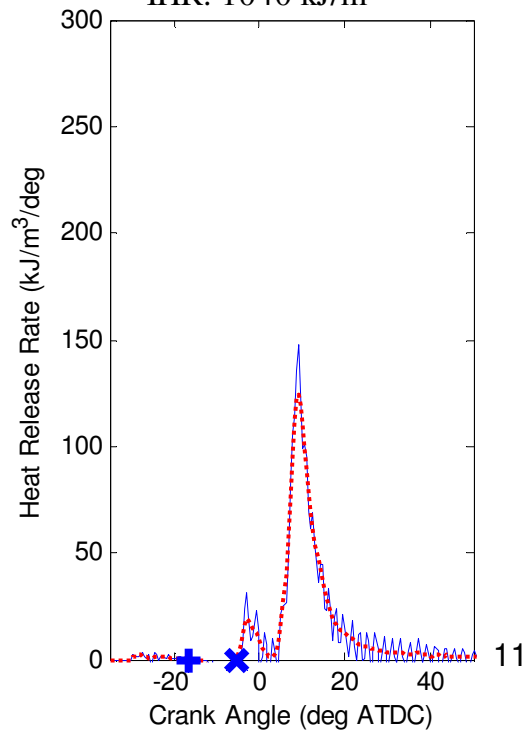
Knock: 1.1 bar
IHR: 1086 kJ/m³



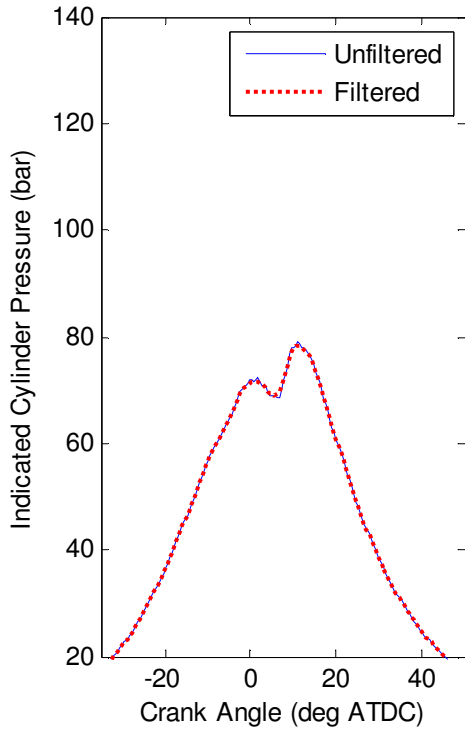
B-1100-L-5-0EGR-REP1
 t_{id} : 0.81 \pm 0.09 ms



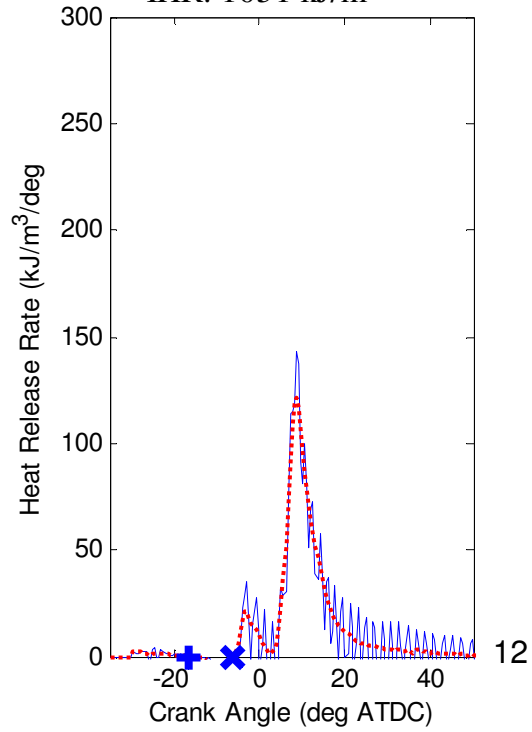
Knock: 1.2 bar
IHR: 1040 kJ/m³



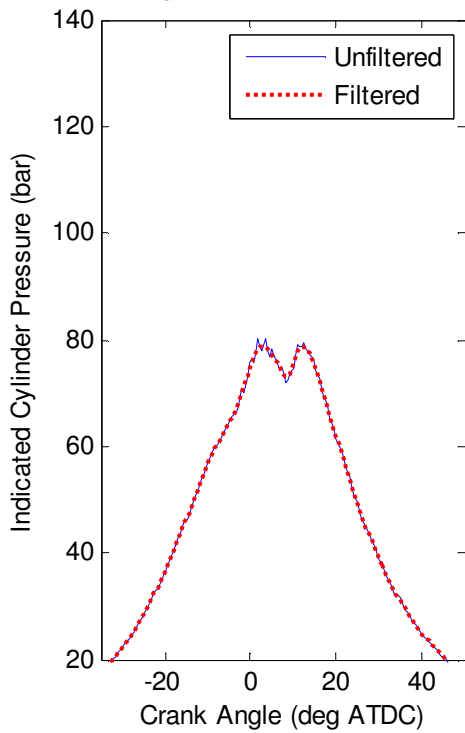
B-1100-L-5-0EGR-REP2
 t_{id} : 0.71+/-0.11 ms



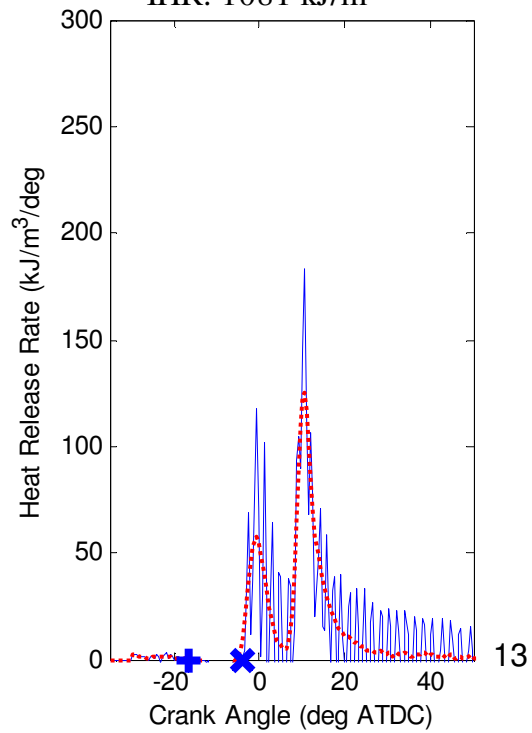
Knock: 1.3 bar
IHR: 1051 kJ/m³



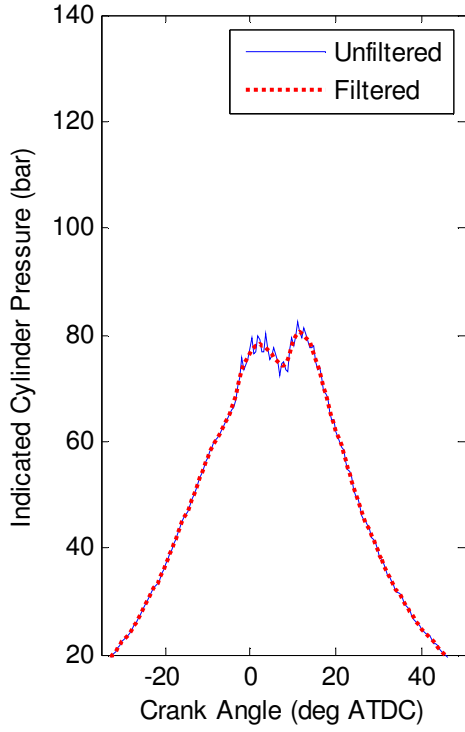
B-1100-L-7-0EGR
 t_{id} : 1.04+/-0.04 ms



Knock: 2.5 bar
IHR: 1081 kJ/m³

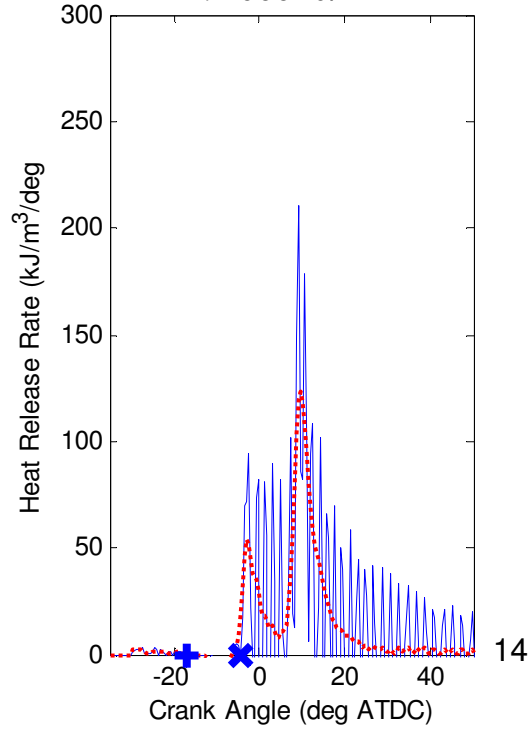


B-1100-L-7-0EGR-REP1
 t_{id} : 0.96 \pm 0.04 ms

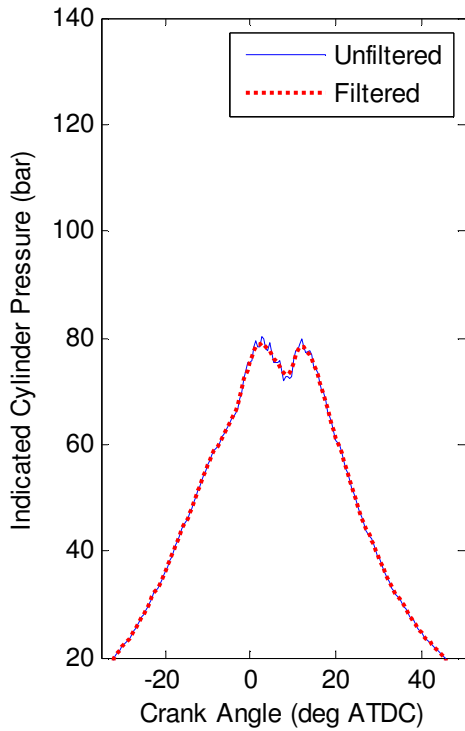


Knock: 3.4 bar

IHR: 1066 kJ/m³

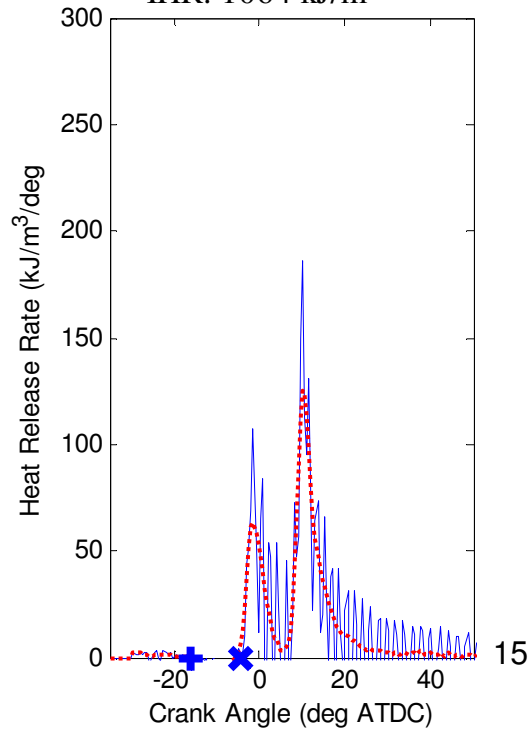


B-1100-L-7-0EGR-REP2
 t_{id} : 0.93 \pm 0.04 ms

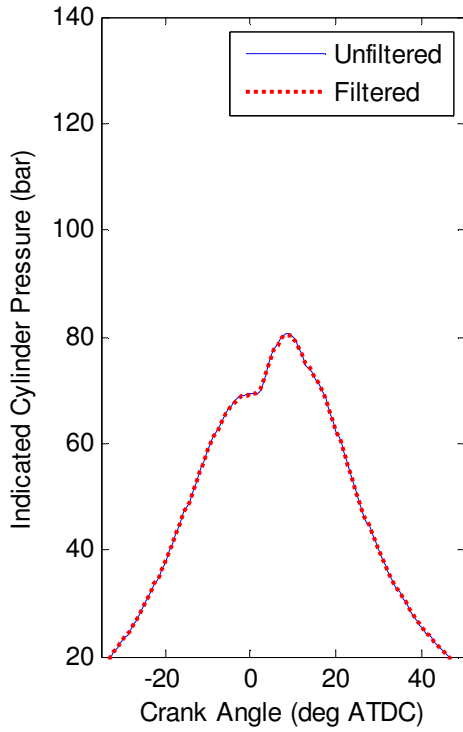


Knock: 2.9 bar

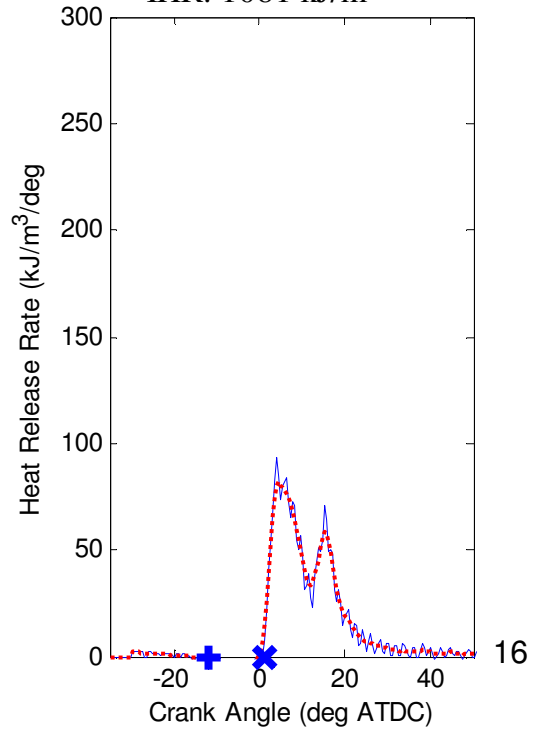
IHR: 1064 kJ/m³



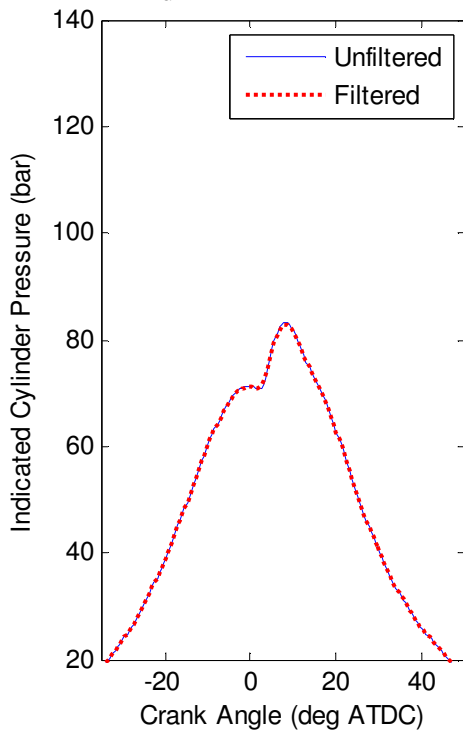
B-1100-L-9-0EGR
 t_{id} : 1.07+/-0.04 ms



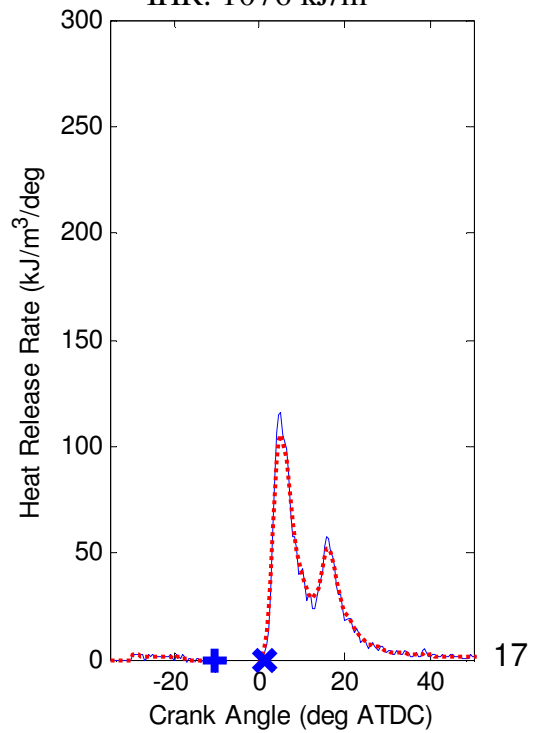
Knock: 1.0 bar
IHR: 1081 kJ/m³



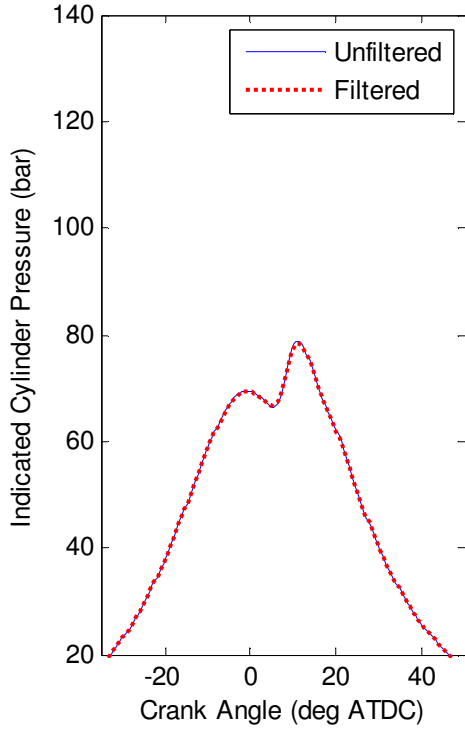
B-1100-L-9-0EGR-REP1
 t_{id} : 0.88+/-0.04 ms



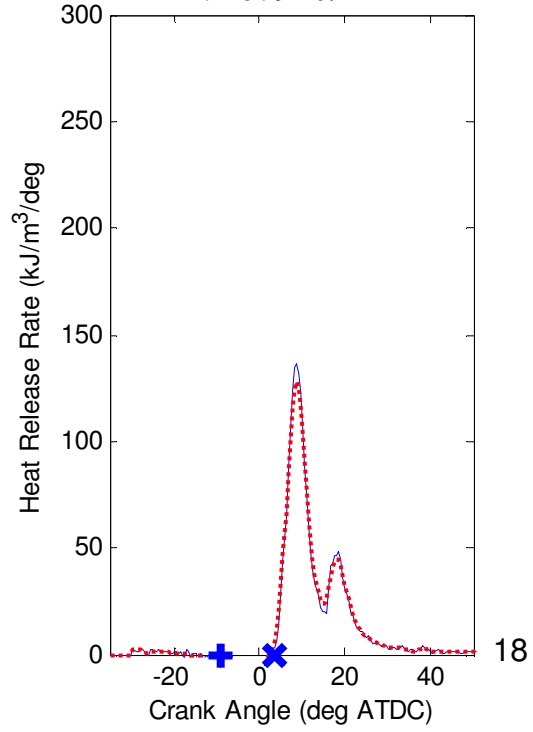
Knock: 1.4 bar
IHR: 1076 kJ/m³



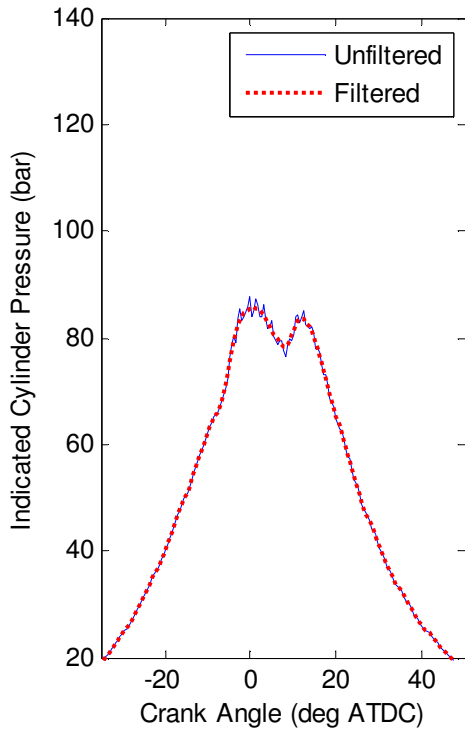
B-1100-L-9-0EGR-REP2
 t_{id} : 1.00+/-0.04 ms



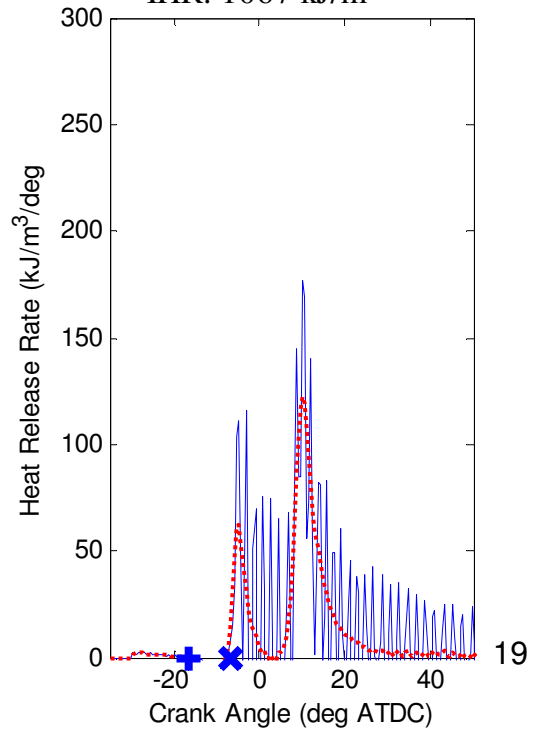
Knock: 1.1 bar
IHR: 1079 kJ/m³



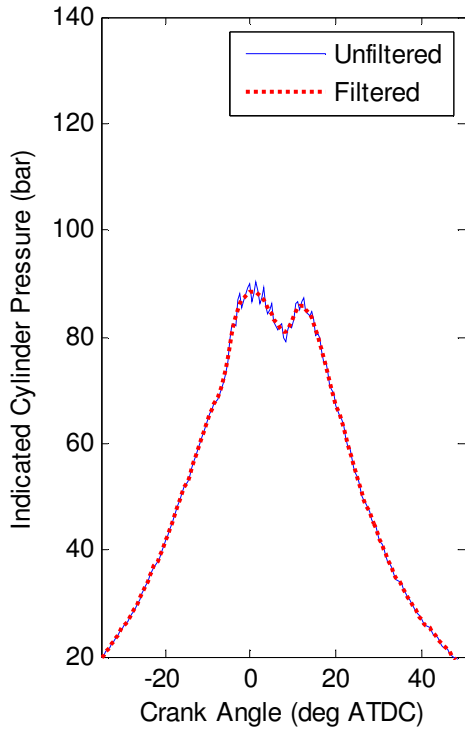
CS-1100-L-5-30EGR
 t_{id} : 0.62+/-0.04 ms



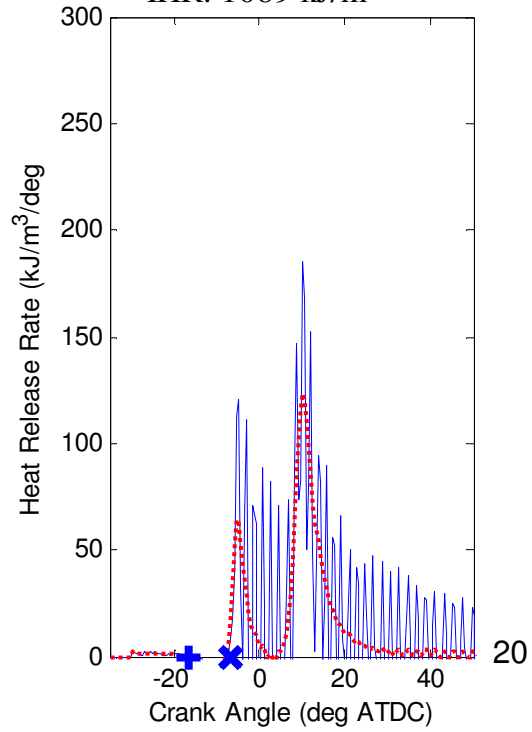
Knock: 2.6 bar
IHR: 1067 kJ/m³



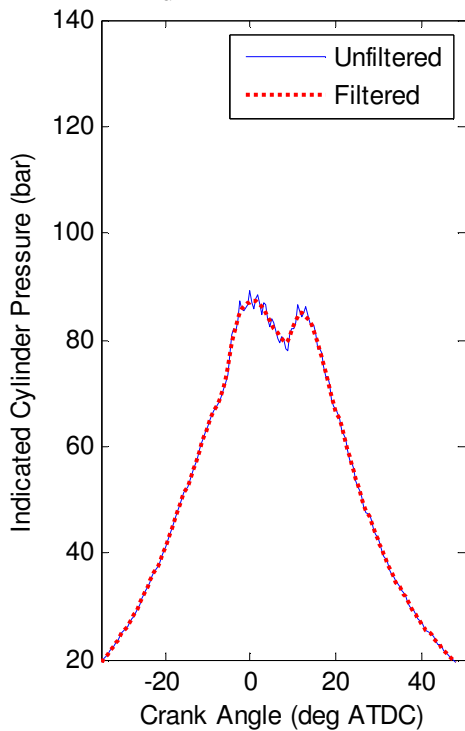
CS-1100-L-5-30EGR-REP1
 t_{id} : 0.63+/-0.04 ms



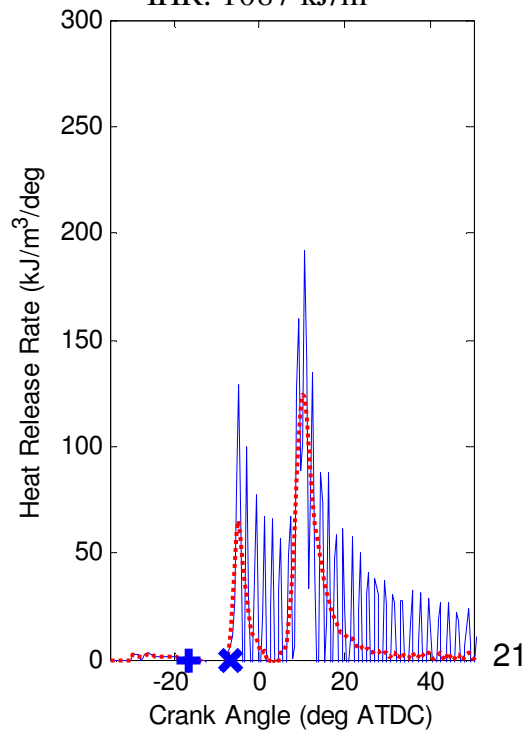
Knock: 2.7 bar
IHR: 1089 kJ/m³



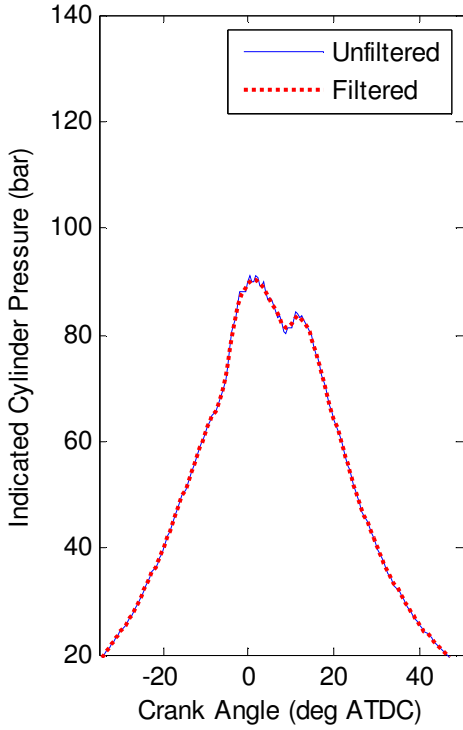
CS-1100-L-5-30EGR-REP2
 t_{id} : 0.66+/-0.04 ms



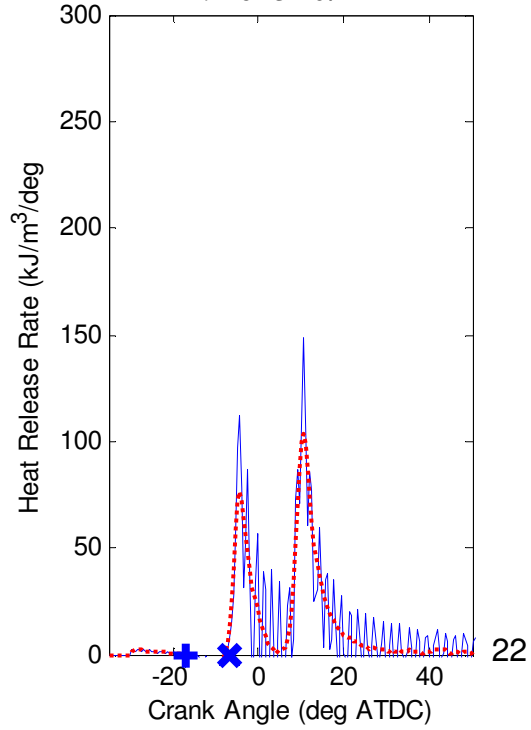
Knock: 2.6 bar
IHR: 1087 kJ/m³



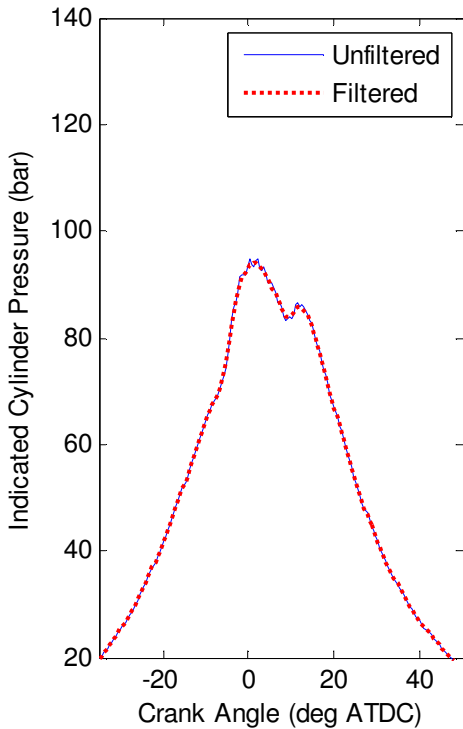
CS-1100-L-7-30EGR
 t_{id} : 0.64+/-0.04 ms



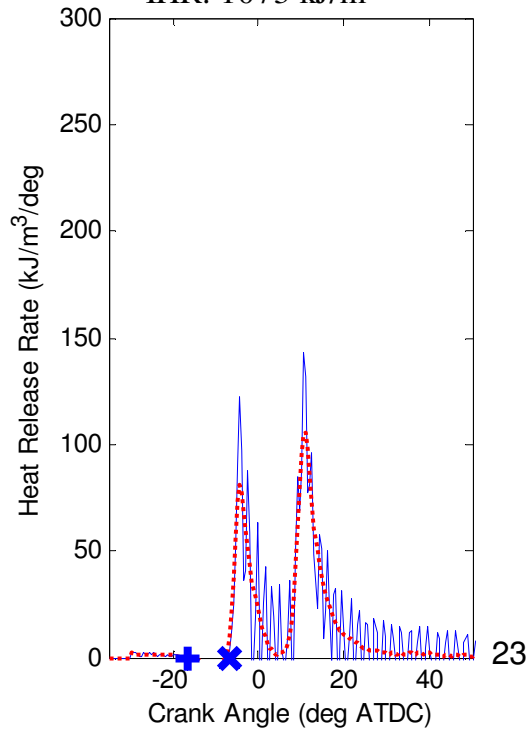
Knock: 1.7 bar
IHR: 1023 kJ/m³



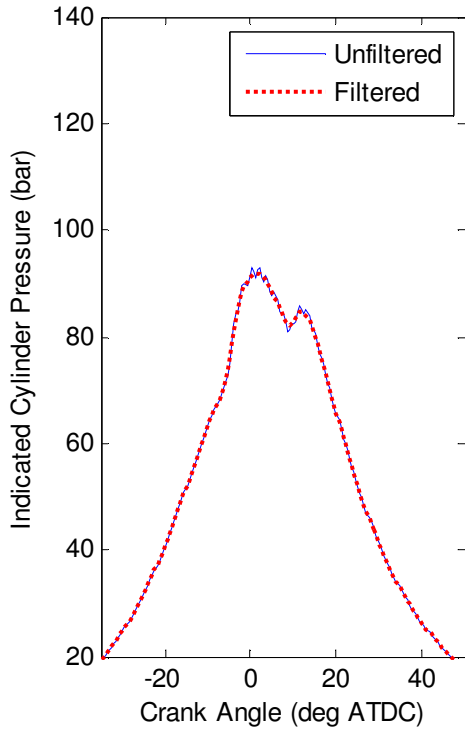
CS-1100-L-7-30EGR-REP1
 t_{id} : 0.64+/-0.04 ms



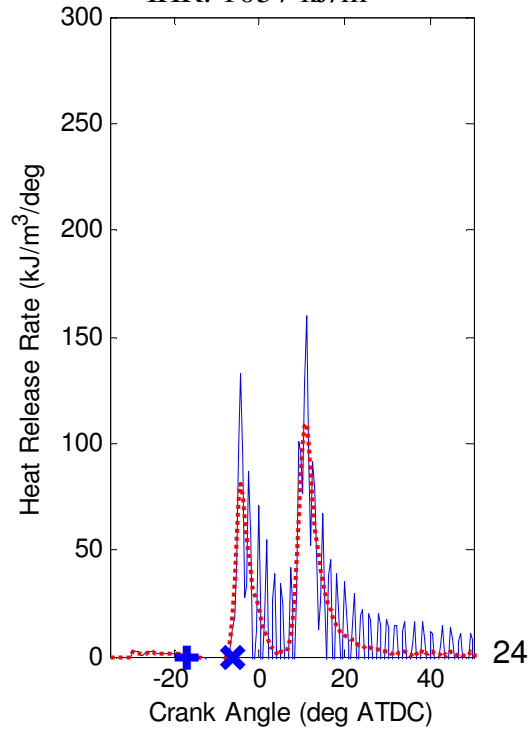
Knock: 1.8 bar
IHR: 1073 kJ/m³



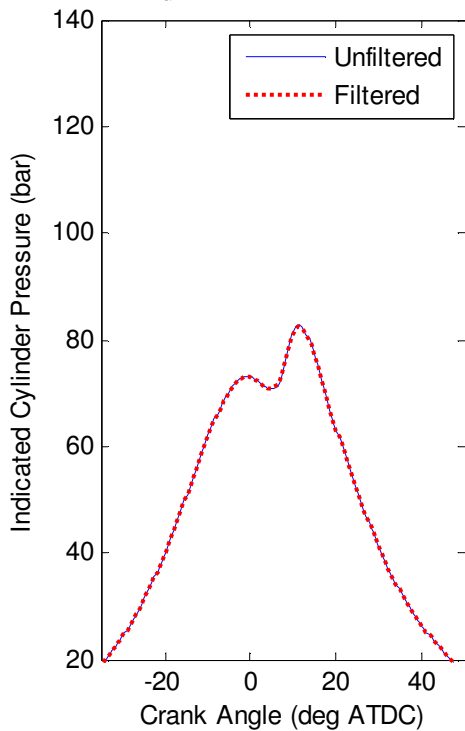
CS-1100-L-7-30EGR-REP2
 t_{id} : 0.70+/-0.04 ms



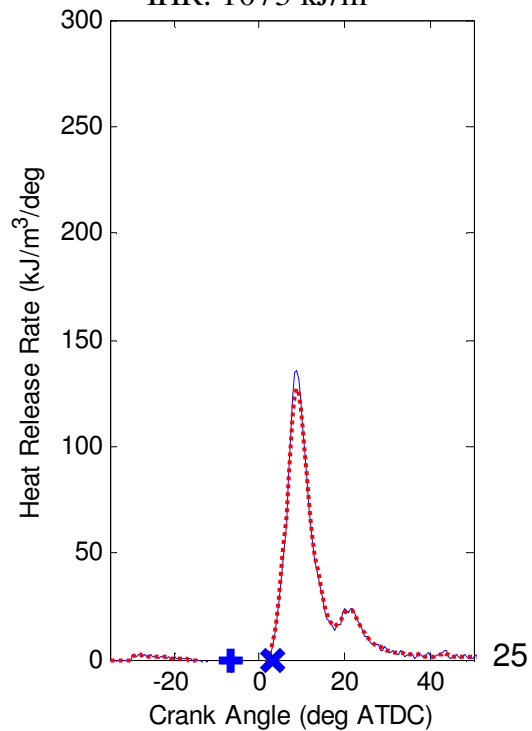
Knock: 2.0 bar
IHR: 1057 kJ/m³



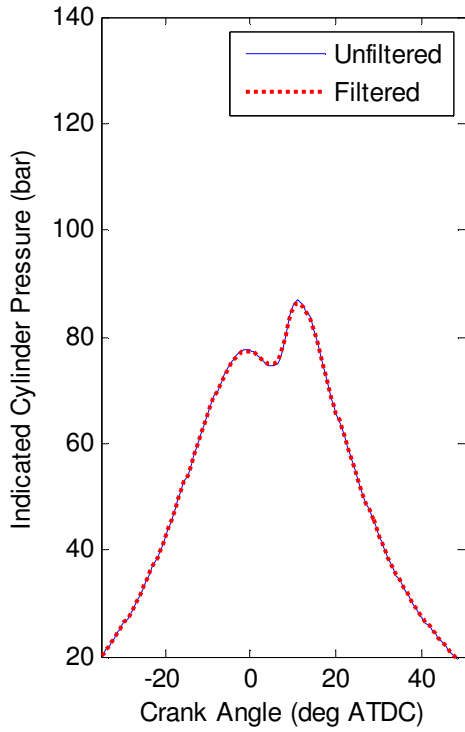
CS-1100-L-9-30EGR
 t_{id} : 0.60+/-0.04 ms



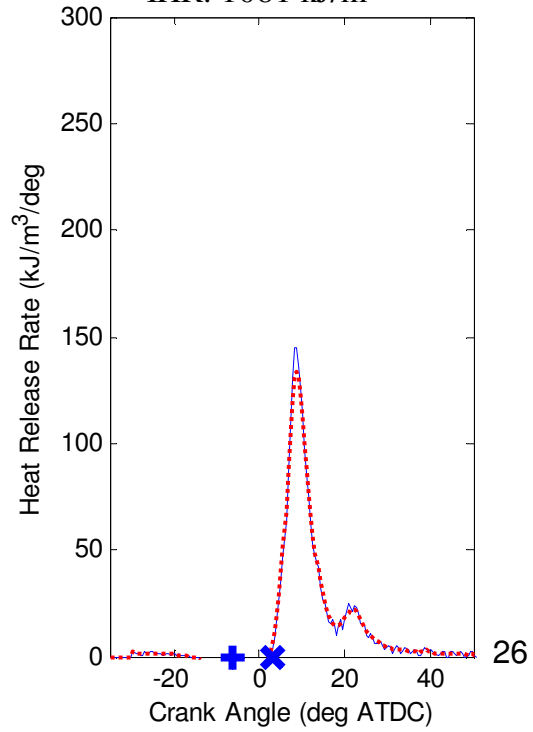
Knock: 0.9 bar
IHR: 1073 kJ/m³



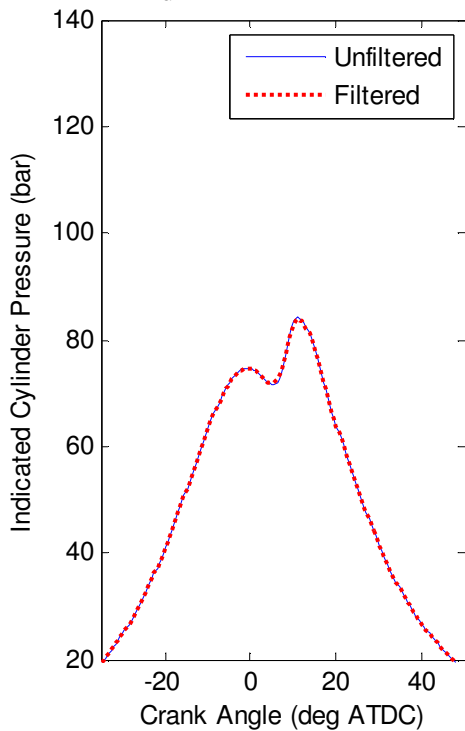
CS-1100-L-9-30EGR-REP1
 t_{id} : 0.56+/-0.04 ms



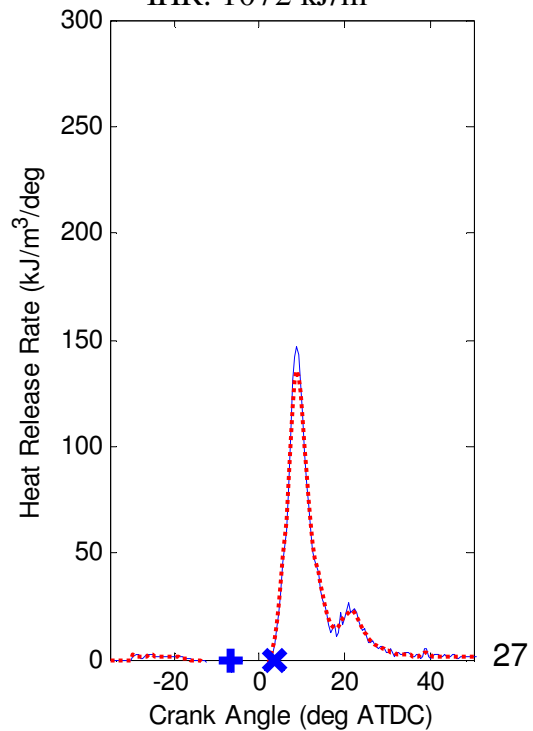
Knock: 0.9 bar
IHR: 1081 kJ/m³



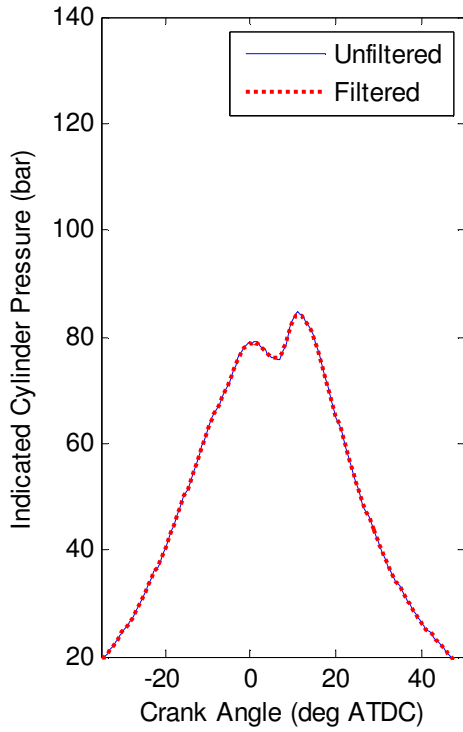
CS-1100-L-9-30EGR-REP2
 t_{id} : 0.65+/-0.04 ms



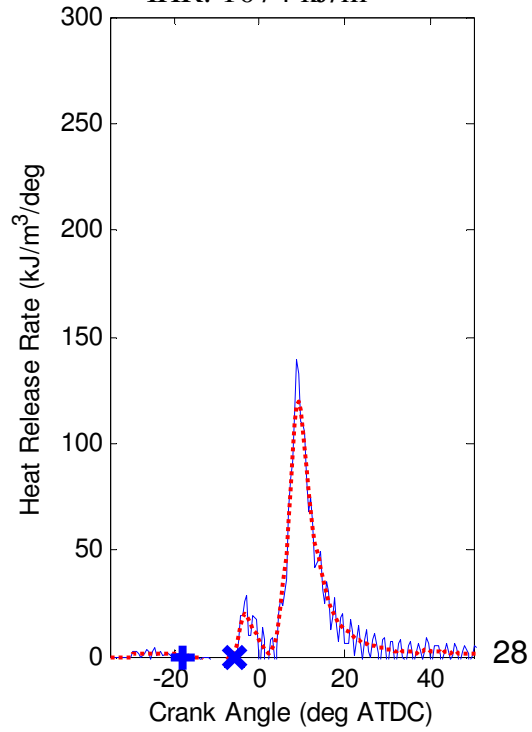
Knock: 1.0 bar
IHR: 1072 kJ/m³



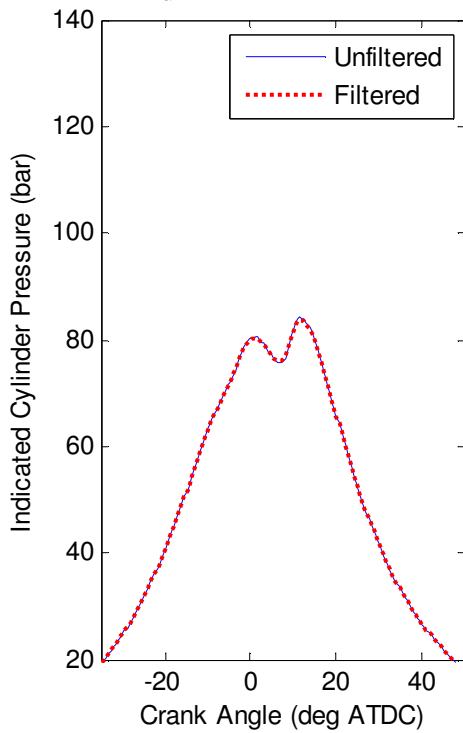
B-1100-L-5-30EGR
 t_{id} : 0.93+/-0.10 ms



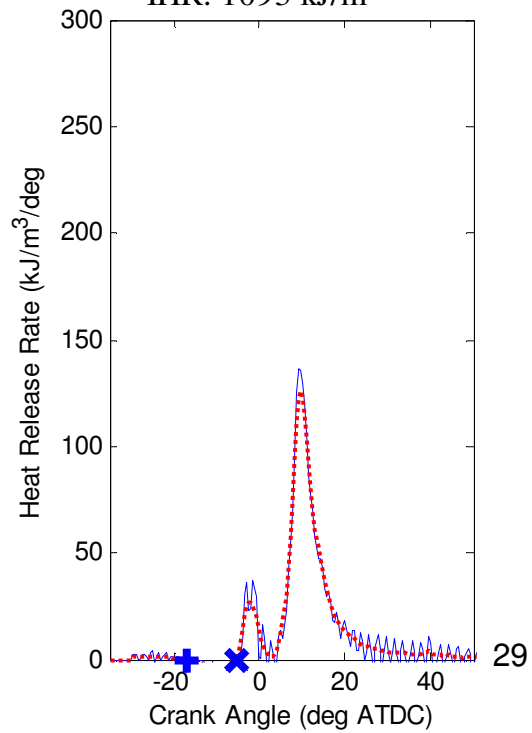
Knock: 1.0 bar
IHR: 1074 kJ/m³



B-1100-L-5-30EGR-REP1
 t_{id} : 0.88+/-0.12 ms

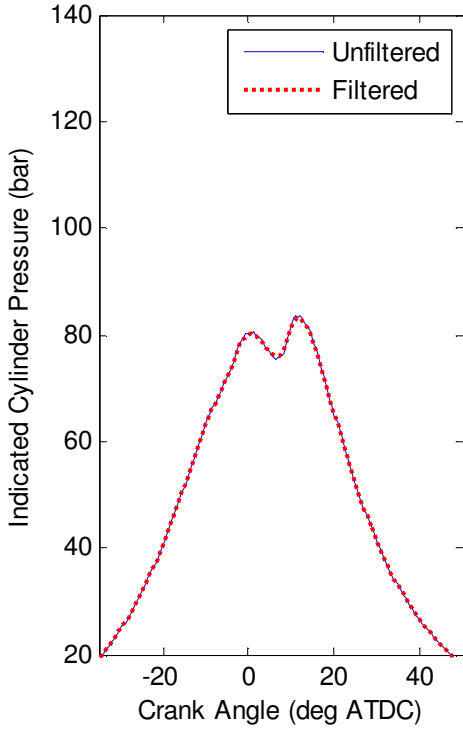


Knock: 1.1 bar
IHR: 1093 kJ/m³



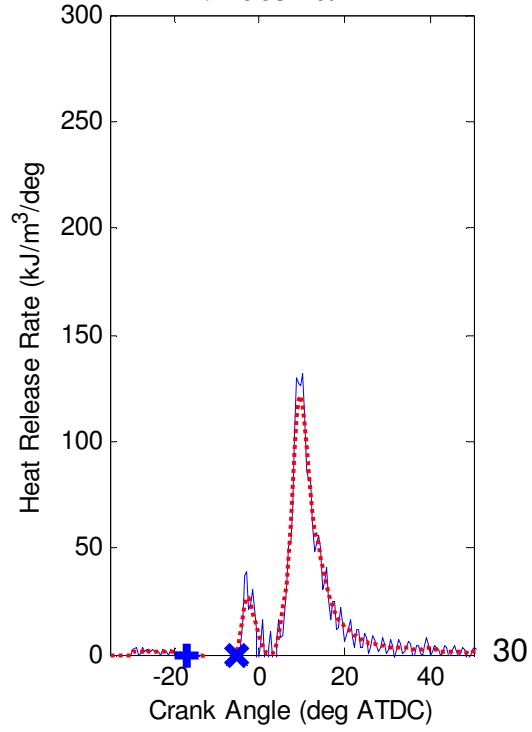
B-1100-L-5-30EGR-REP2

t_{id} : 0.88 \pm 0.12 ms



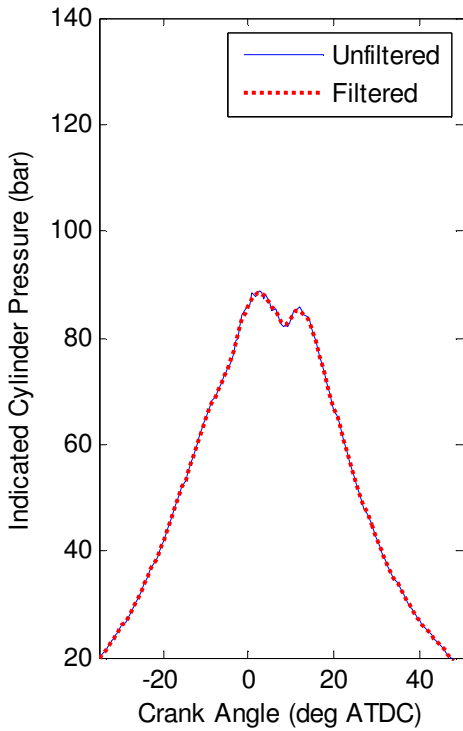
Knock: 1.0 bar

IHR: 1063 kJ/m³



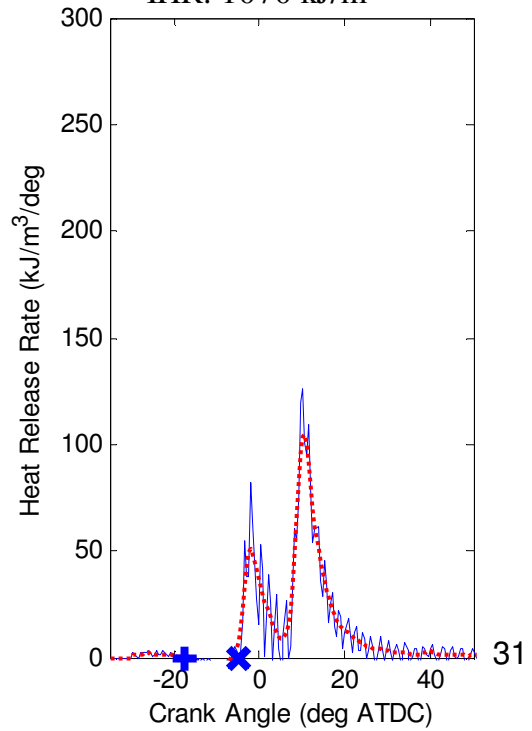
B-1100-L-7-30EGR

t_{id} : 1.08 \pm 0.04 ms

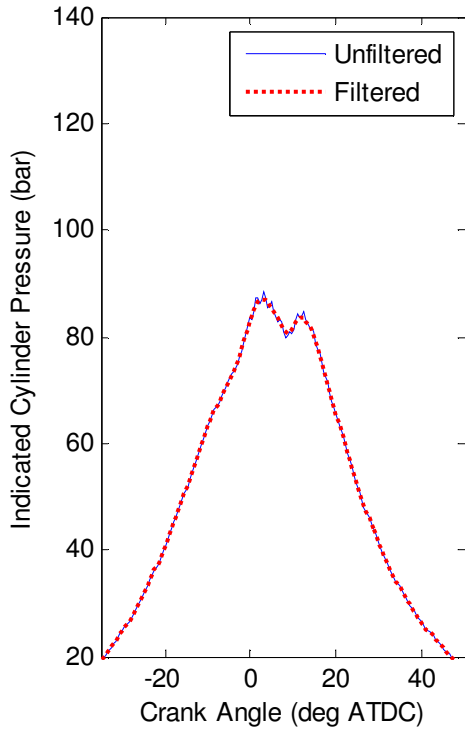


Knock: 1.8 bar

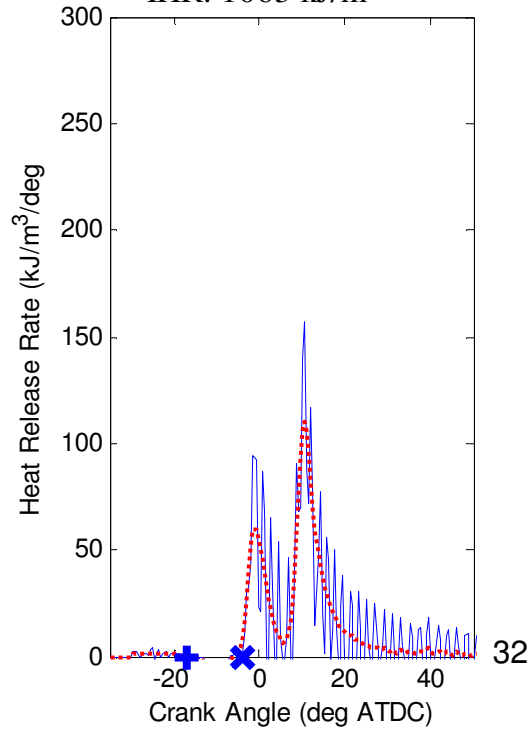
IHR: 1070 kJ/m³



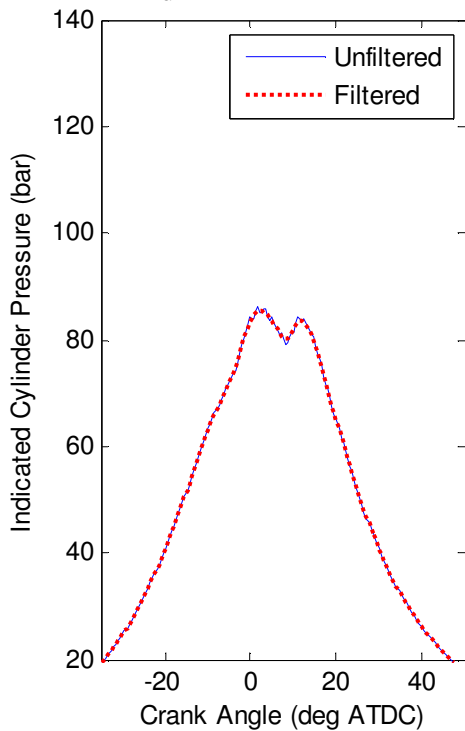
B-1100-L-7-30EGR-REP1
 t_{id} : 1.14+/-0.04 ms



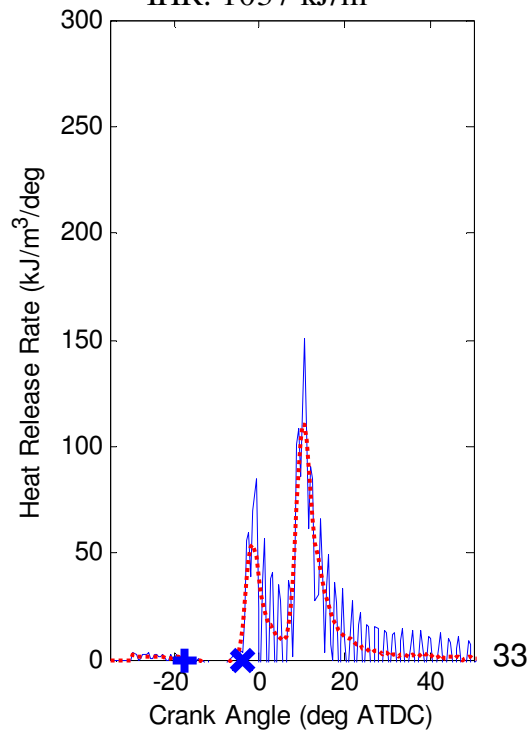
Knock: 2.0 bar
IHR: 1063 kJ/m³



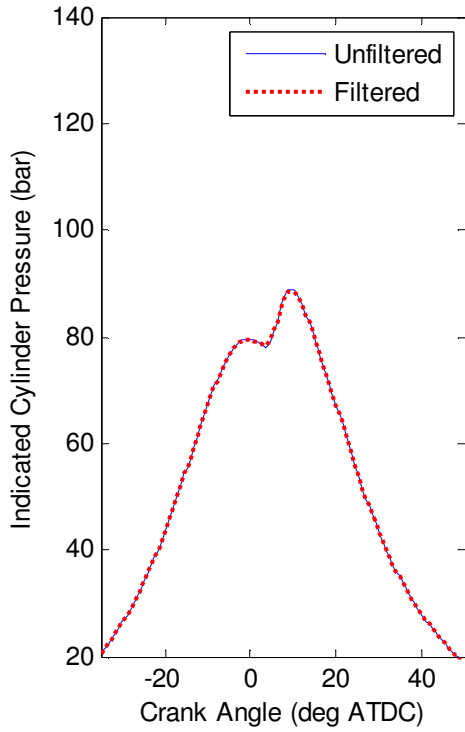
B-1100-L-7-30EGR-REP2
 t_{id} : 1.18+/-0.04 ms



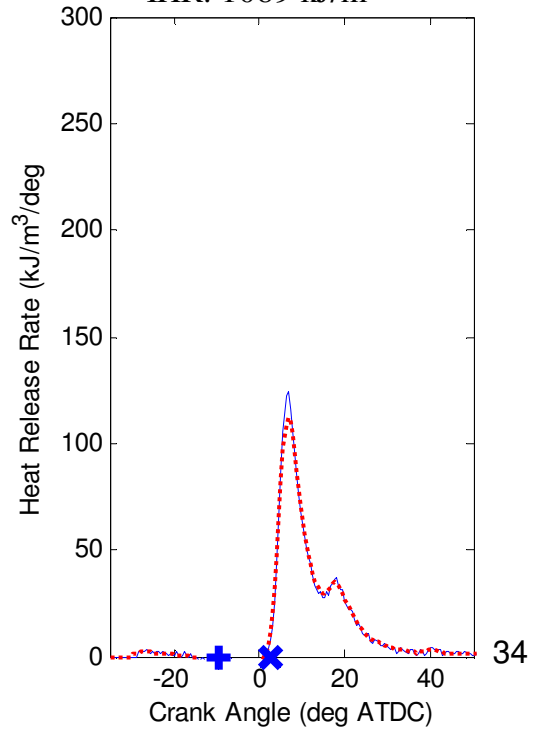
Knock: 1.7 bar
IHR: 1037 kJ/m³



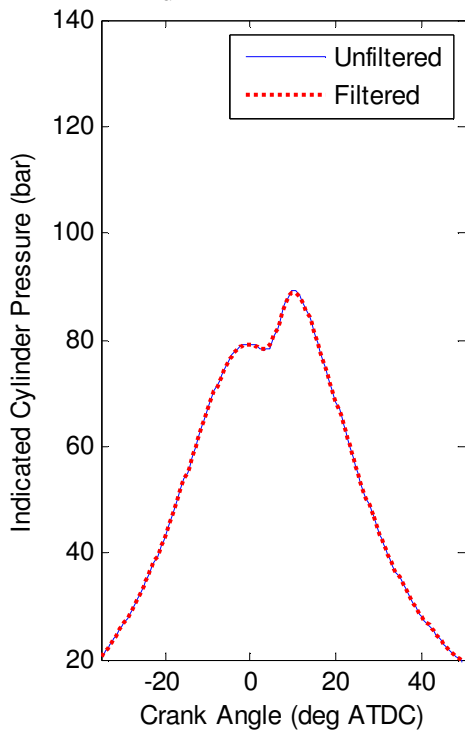
B-1100-L-9-30EGR
 t_{id} : 0.96+/-0.04 ms



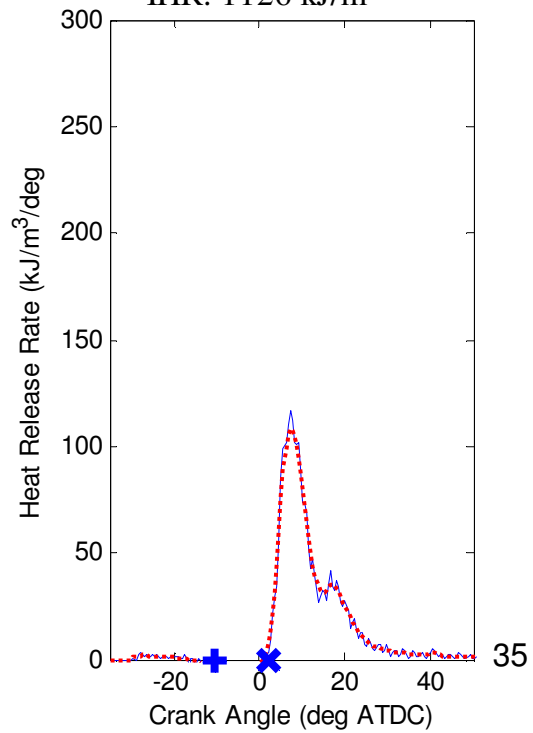
Knock: 1.0 bar
IHR: 1089 kJ/m³



B-1100-L-9-30EGR-REP1
 t_{id} : 1.01+/-0.04 ms

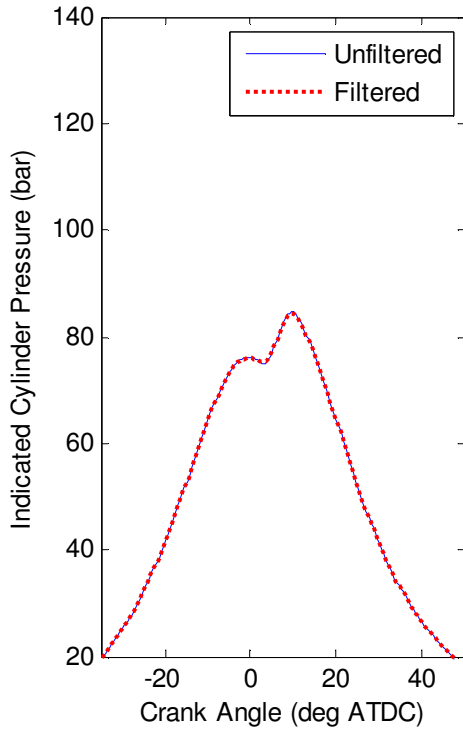


Knock: 0.9 bar
IHR: 1126 kJ/m³



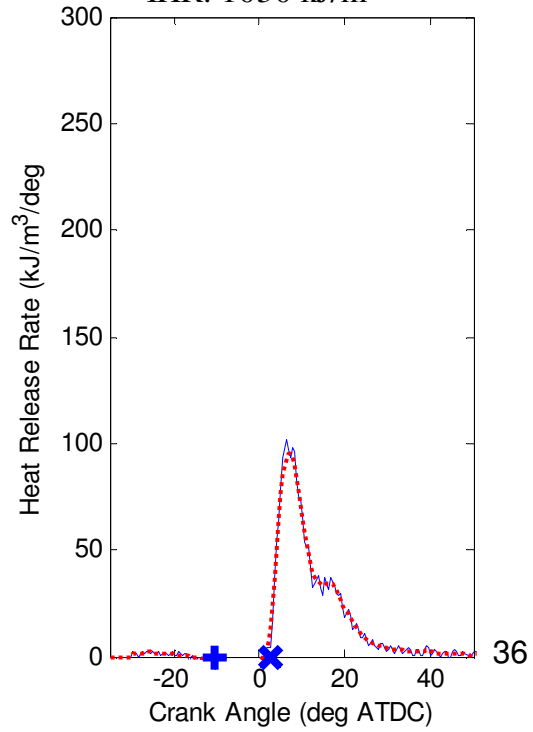
B-1100-L-9-30EGR-REP2

t_{id} : 1.06+/-0.04 ms



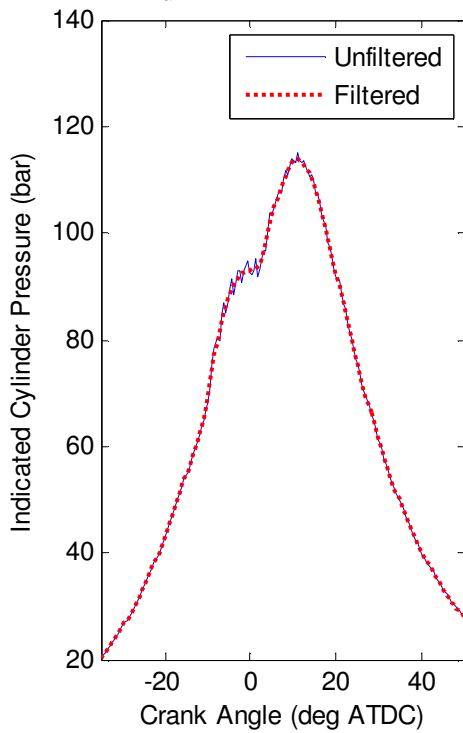
Knock: 1.0 bar

IHR: 1030 kJ/m³



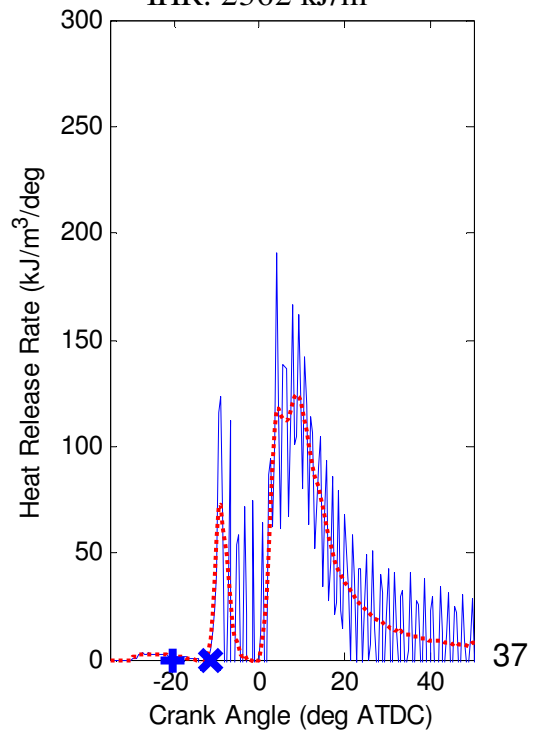
CS-1100-H-5-0EGR

t_{id} : 0.49+/-0.04 ms

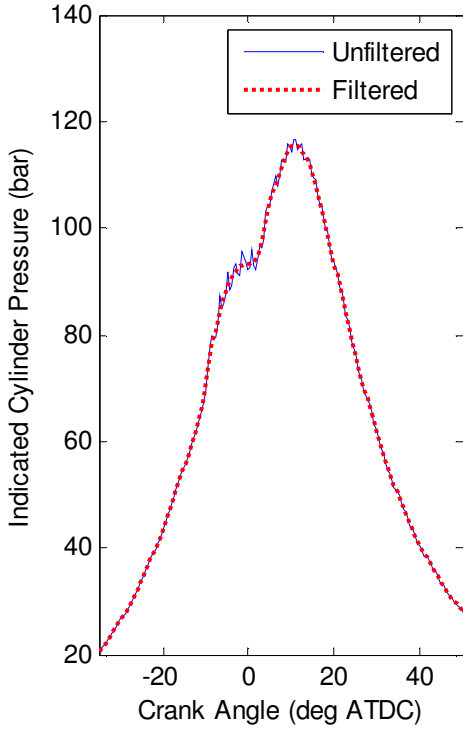


Knock: 2.6 bar

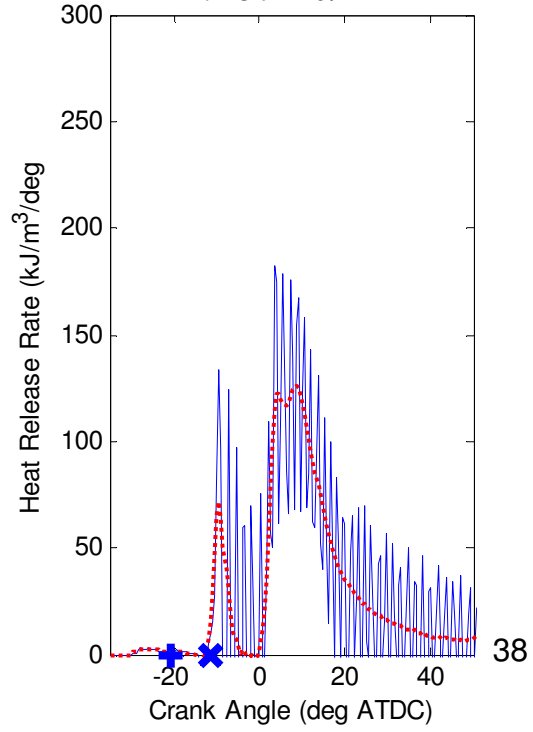
IHR: 2362 kJ/m³



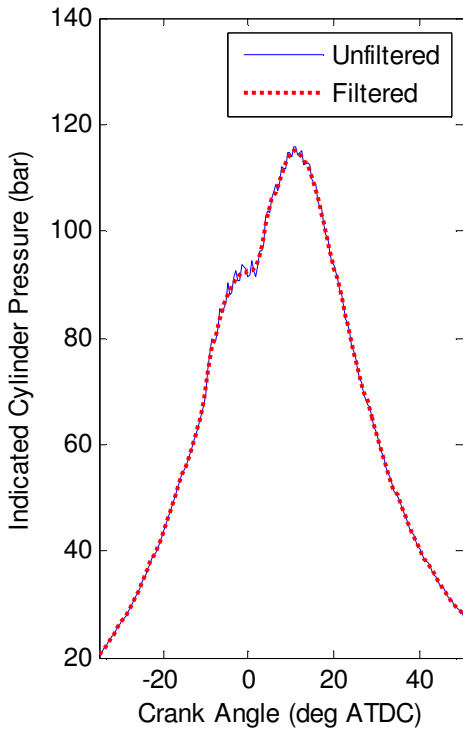
CS-1100-H-5-0EGR-REP1
 t_{id} : 0.51+/-0.04 ms



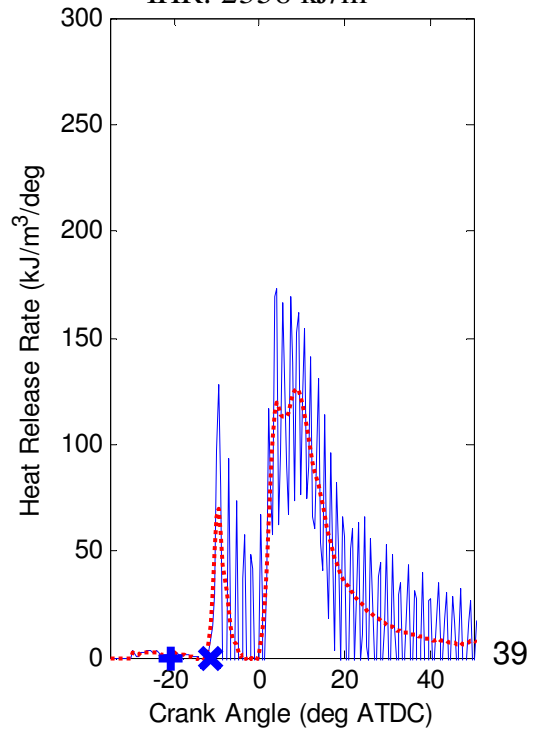
Knock: 3.3 bar
IHR: 2371 kJ/m³



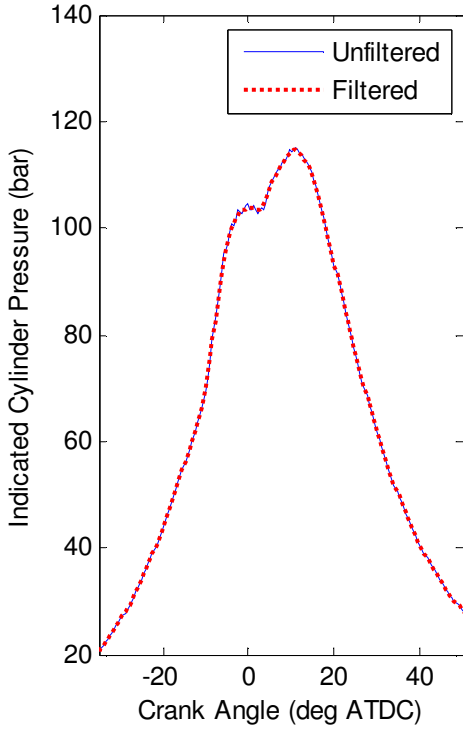
CS-1100-H-5-0EGR-REP2
 t_{id} : 0.54+/-0.04 ms



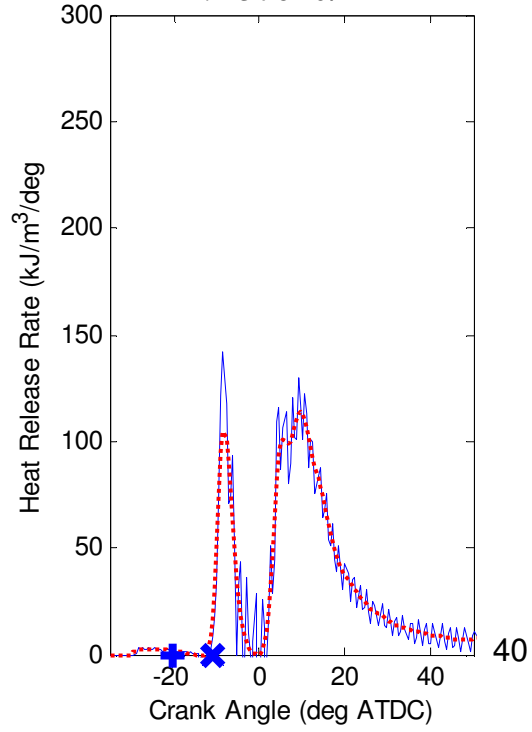
Knock: 2.6 bar
IHR: 2358 kJ/m³



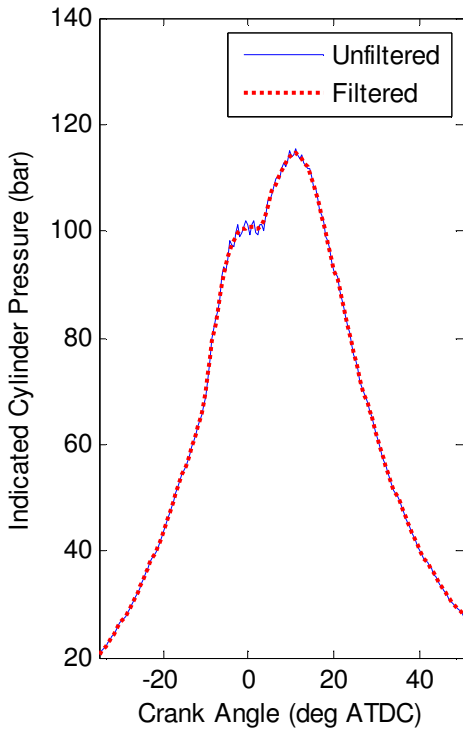
CS-1100-H-7-0EGR
 t_{id} : 0.53 \pm 0.04 ms



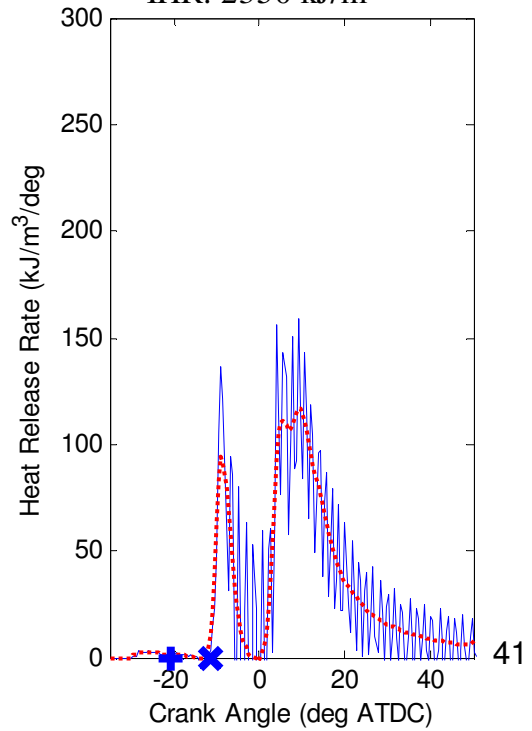
Knock: 1.9 bar
IHR: 2376 kJ/m³



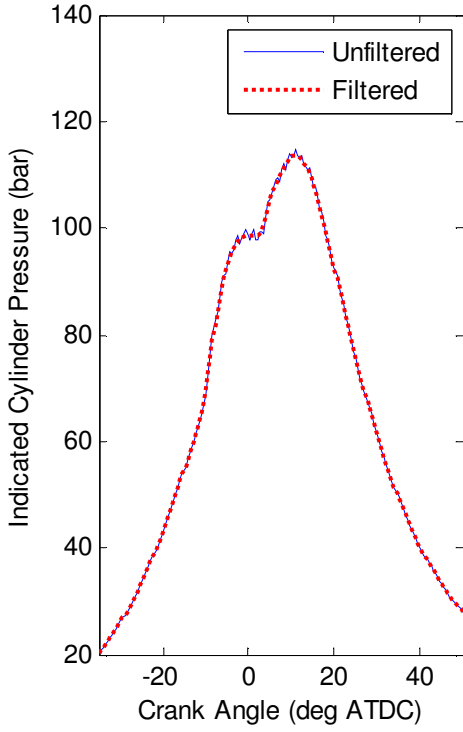
CS-1100-H-7-0EGR-REP1
 t_{id} : 0.53 \pm 0.04 ms



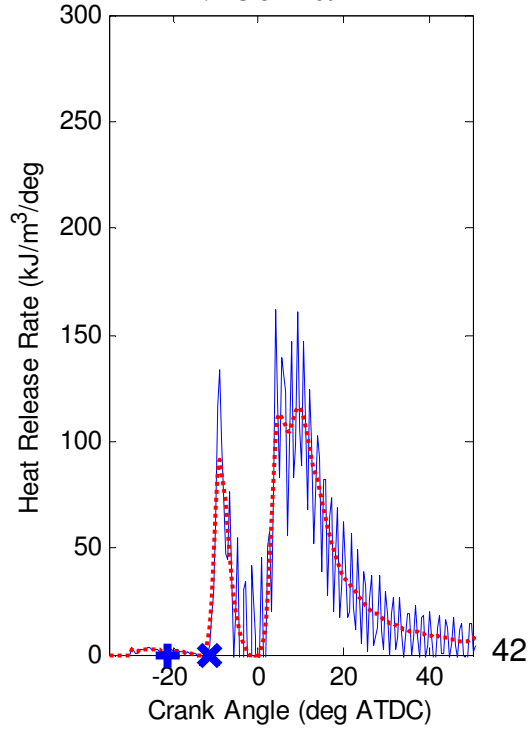
Knock: 2.4 bar
IHR: 2350 kJ/m³



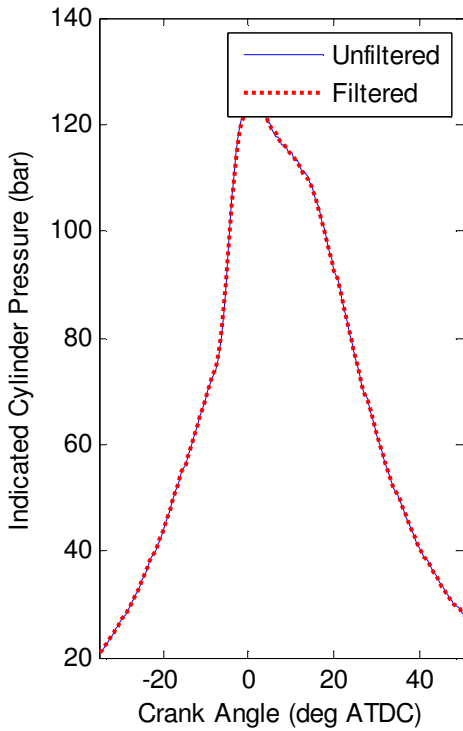
CS-1100-H-7-0EGR-REP2
 t_{id} : 0.56 \pm 0.04 ms



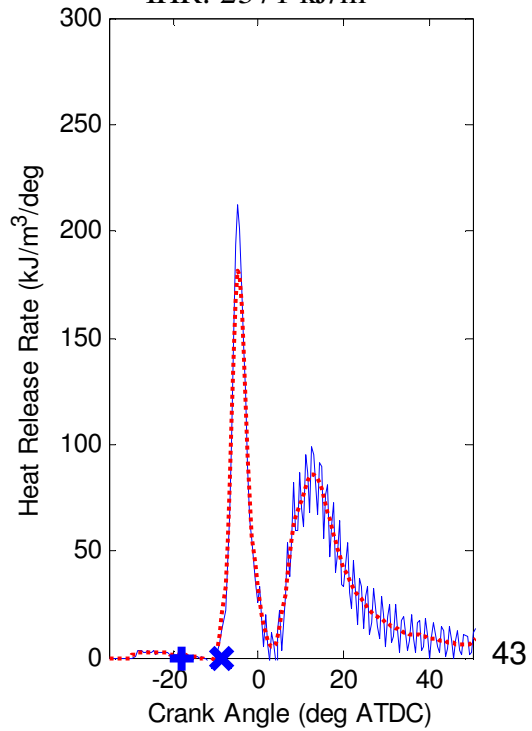
Knock: 2.1 bar
IHR: 2362 kJ/m³



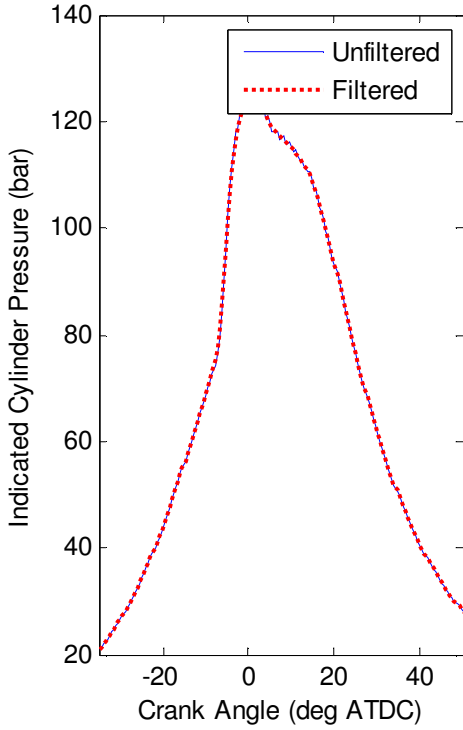
CS-1100-H-9-0EGR
 t_{id} : 0.48 \pm 0.04 ms



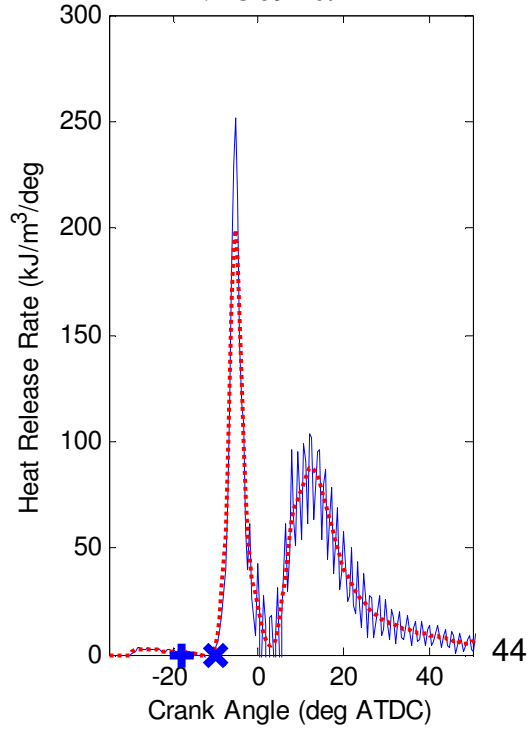
Knock: 2.2 bar
IHR: 2371 kJ/m³



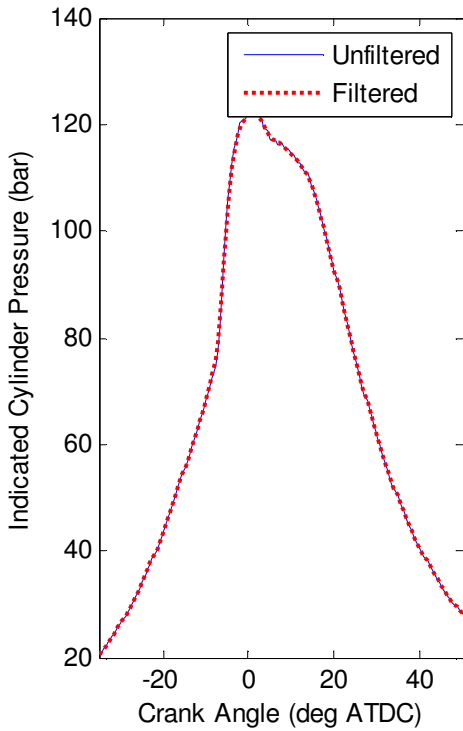
CS-1100-H-9-0EGR-REP1
 t_{id} : 0.33+/-0.04 ms



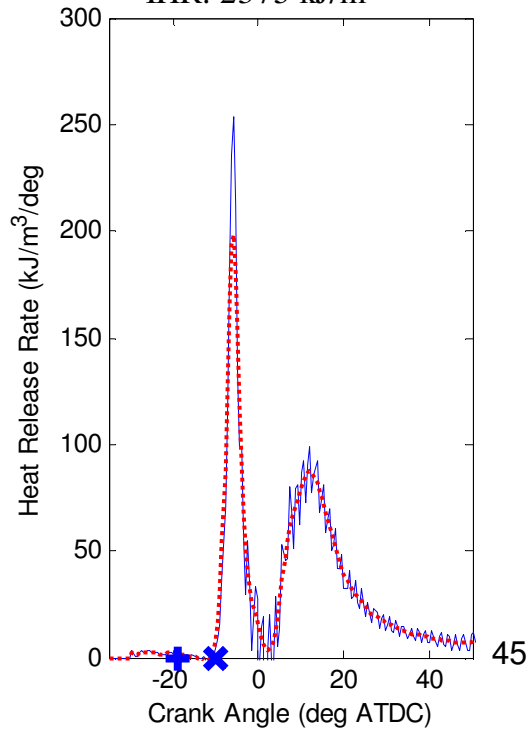
Knock: 2.5 bar
IHR: 2369 kJ/m³



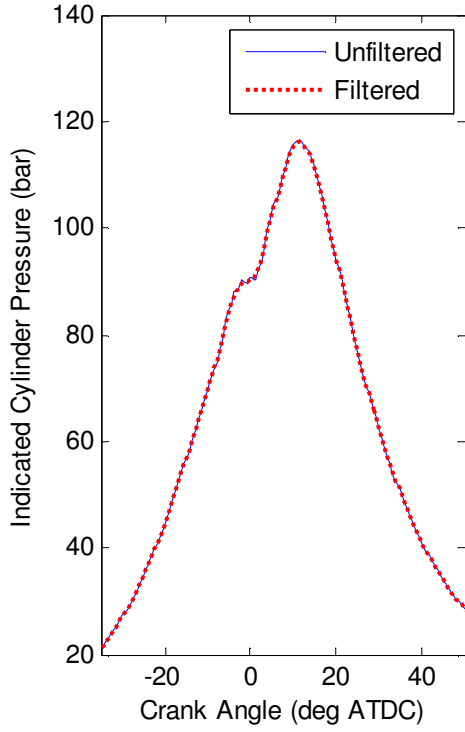
CS-1100-H-9-0EGR-REP2
 t_{id} : 0.43+/-0.04 ms



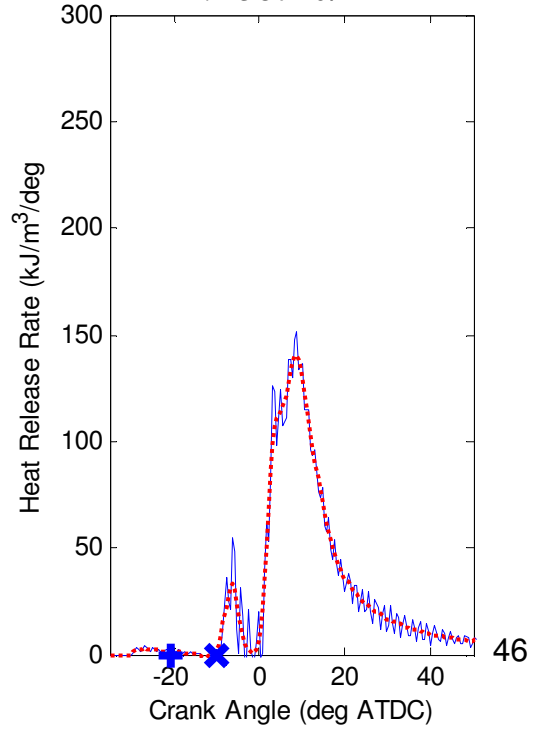
Knock: 2.7 bar
IHR: 2375 kJ/m³



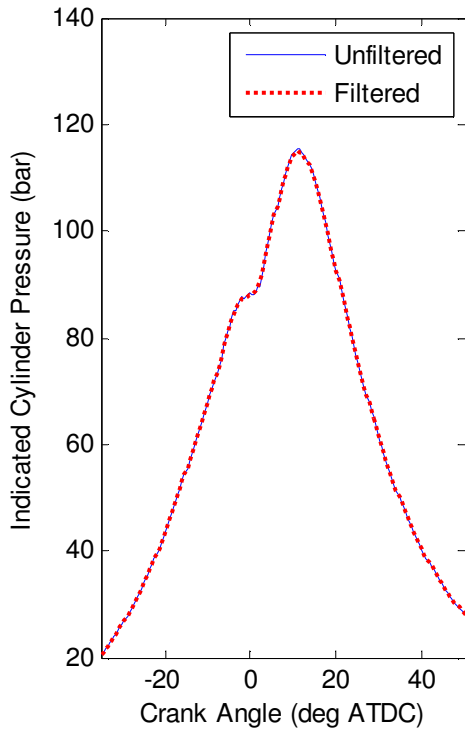
B-1100-H-5-0EGR
 t_{id} : 0.73+/-0.06 ms



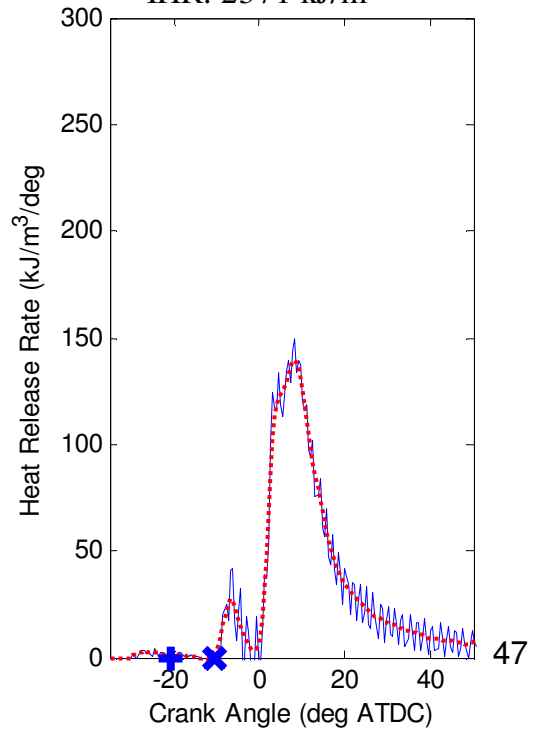
Knock: 1.3 bar
IHR: 2387 kJ/m³



B-1100-H-5-0EGR-REP1
 t_{id} : 0.66+/-0.08 ms

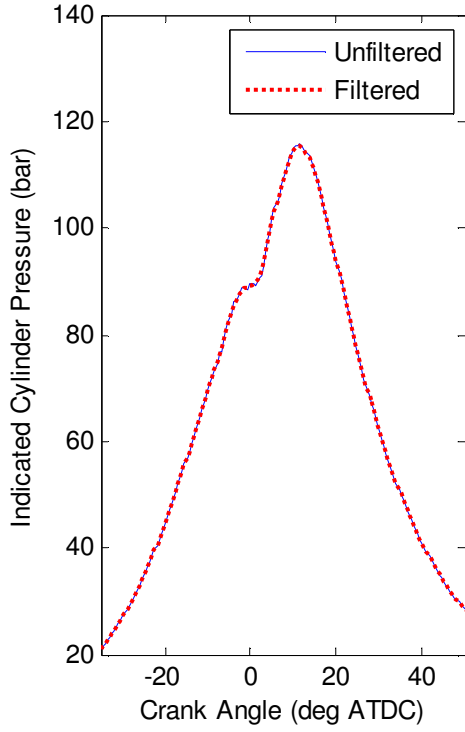


Knock: 1.3 bar
IHR: 2371 kJ/m³



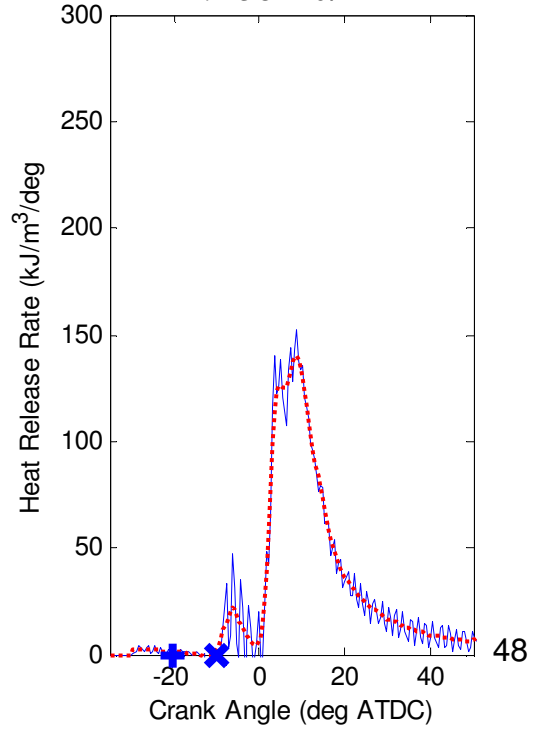
B-1100-H-5-0EGR-REP2

t_{id} : 0.67+/-0.10 ms



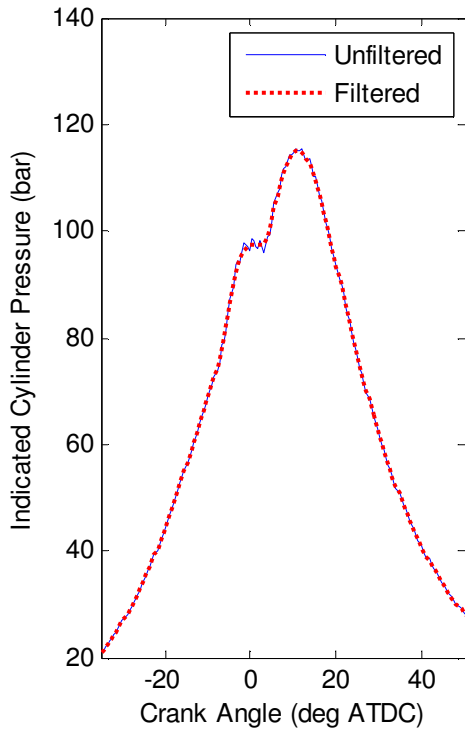
Knock: 1.3 bar

IHR: 2381 kJ/m³



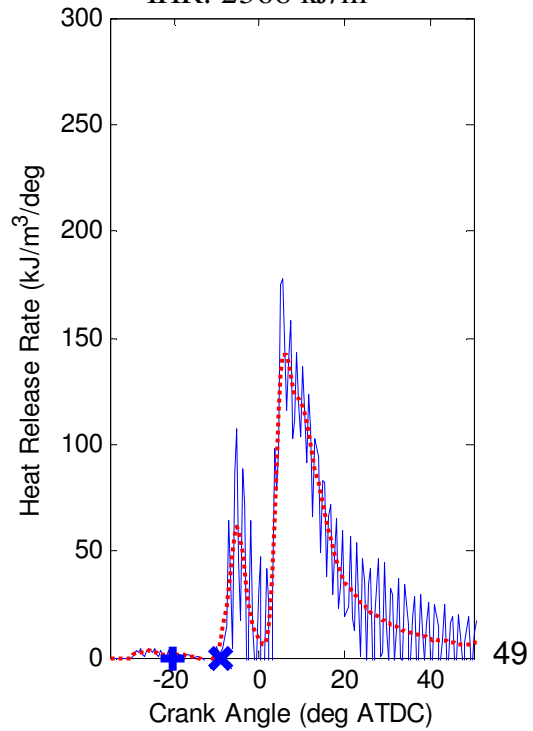
B-1100-H-7-0EGR

t_{id} : 0.87+/-0.04 ms

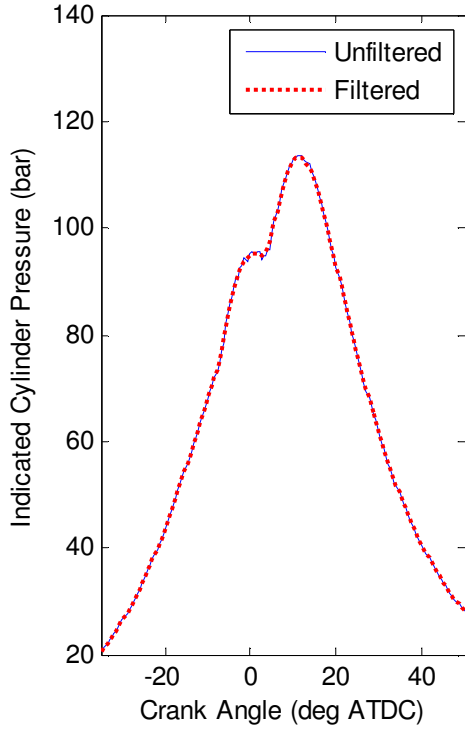


Knock: 2.5 bar

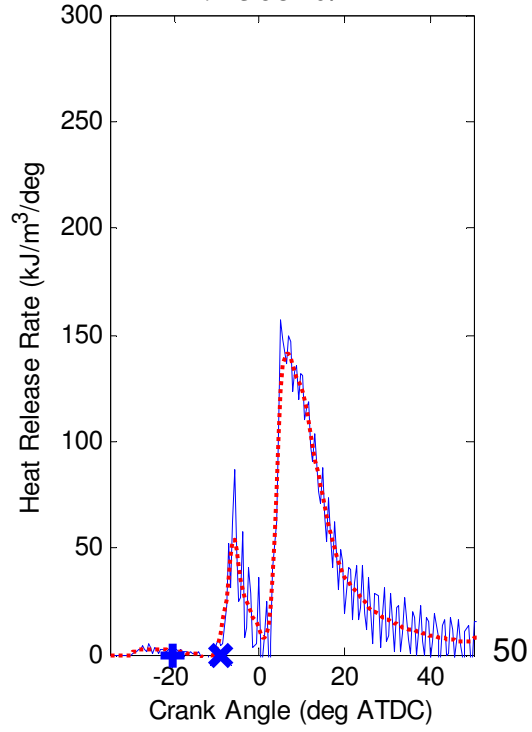
IHR: 2368 kJ/m³



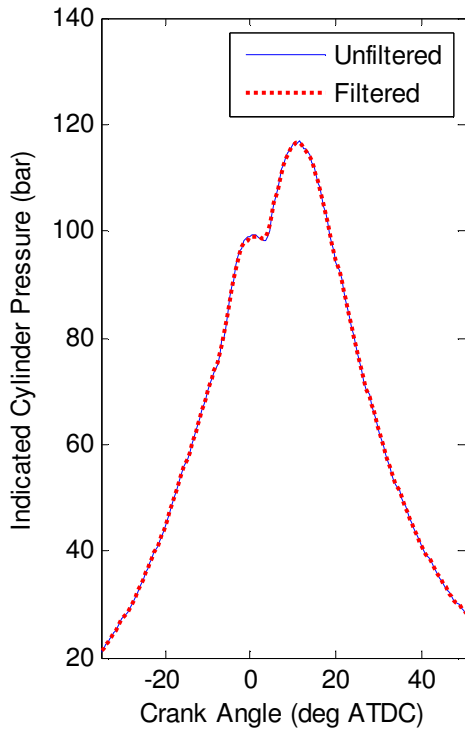
B-1100-H-7-0EGR-REP1
 t_{id} : 0.87 \pm 0.04 ms



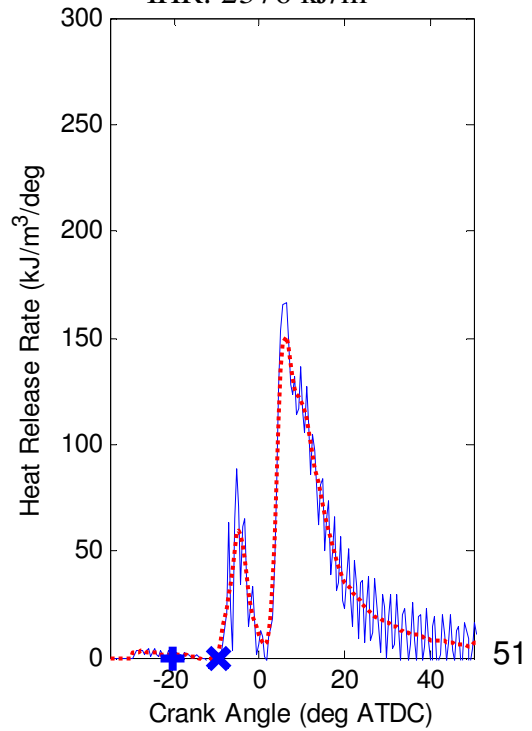
Knock: 2.4 bar
IHR: 2368 kJ/m³



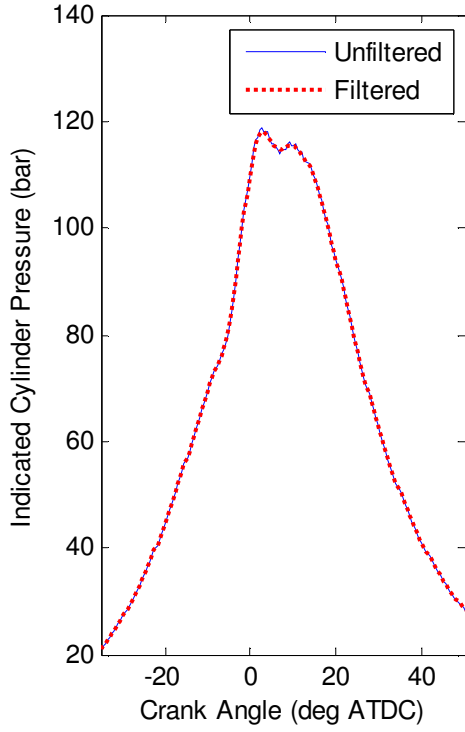
B-1100-H-7-0EGR-REP2
 t_{id} : 0.79 \pm 0.04 ms



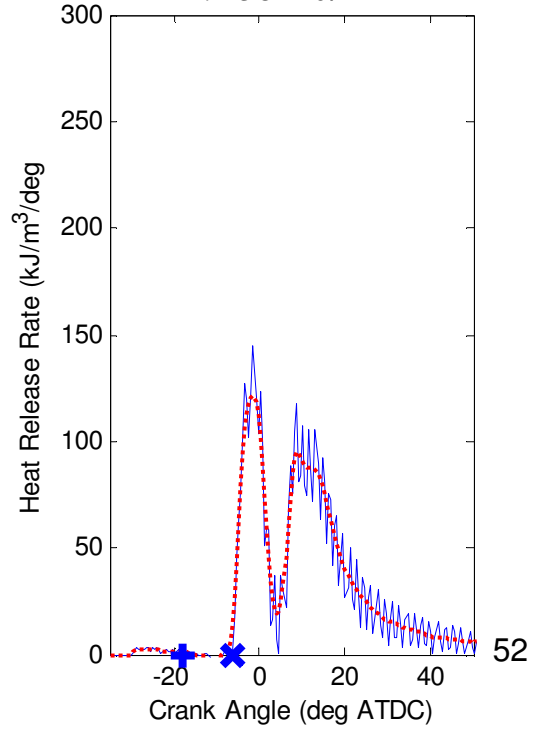
Knock: 2.3 bar
IHR: 2376 kJ/m³



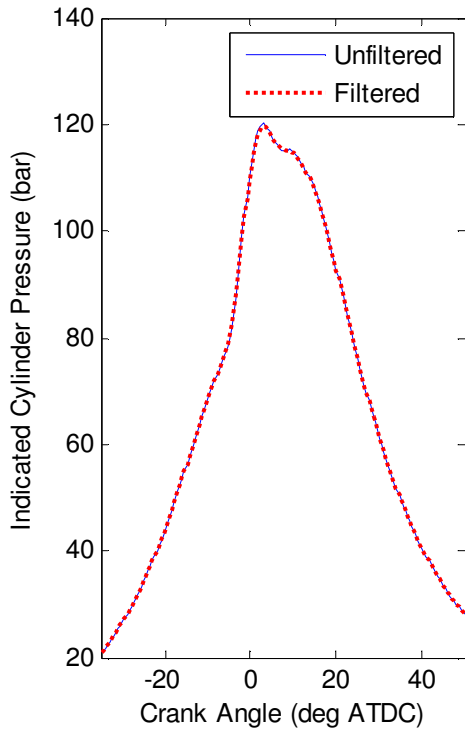
B-1100-H-9-0EGR
 t_{id} : 0.95 \pm 0.04 ms



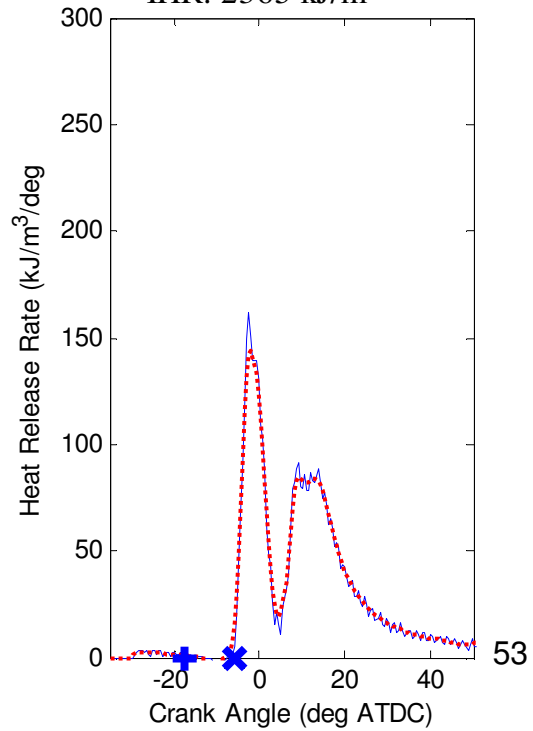
Knock: 2.3 bar
IHR: 2381 kJ/m³



B-1100-H-9-0EGR-REP1
 t_{id} : 0.93 \pm 0.04 ms

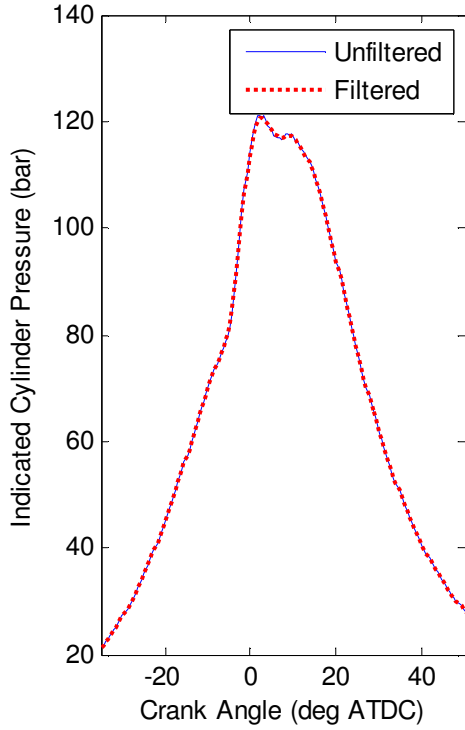


Knock: 2.2 bar
IHR: 2365 kJ/m³



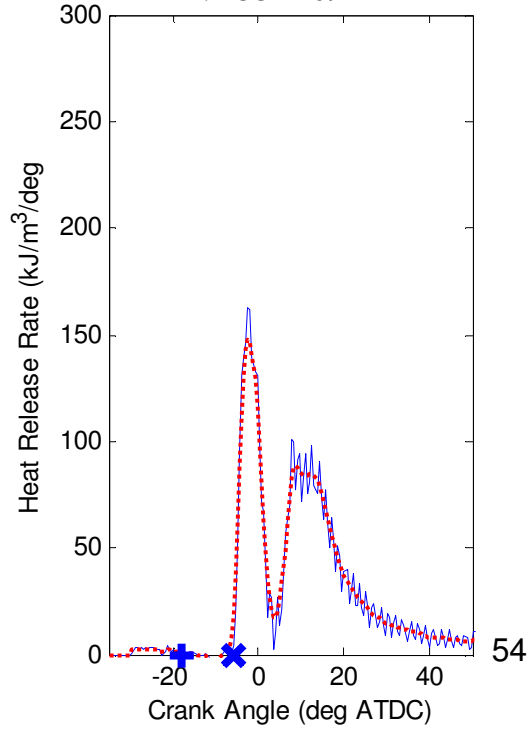
B-1100-H-9-0EGR-REP2

t_{id} : 0.95 \pm 0.04 ms



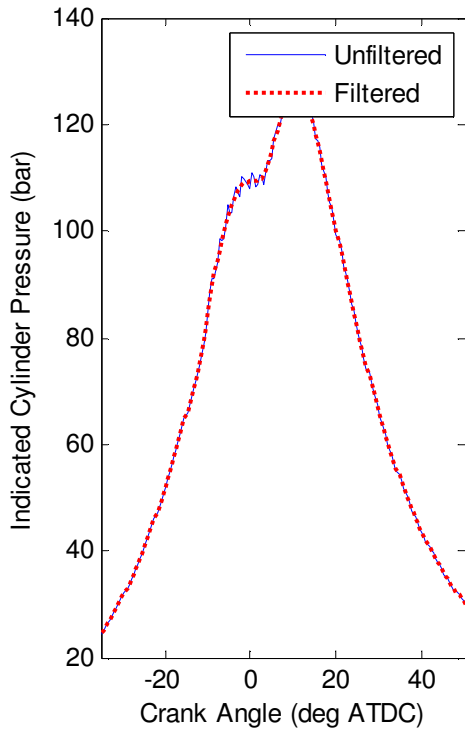
Knock: 2.2 bar

IHR: 2351 kJ/m³



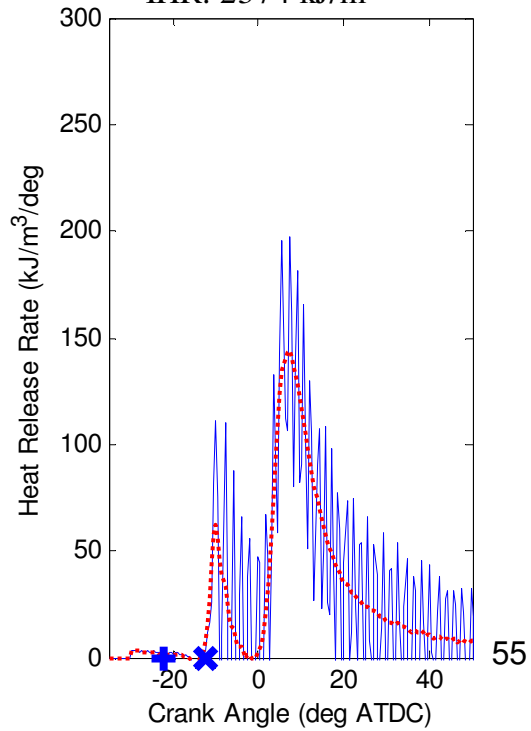
CS-1100-H-5-30EGR

t_{id} : 0.55 \pm 0.04 ms

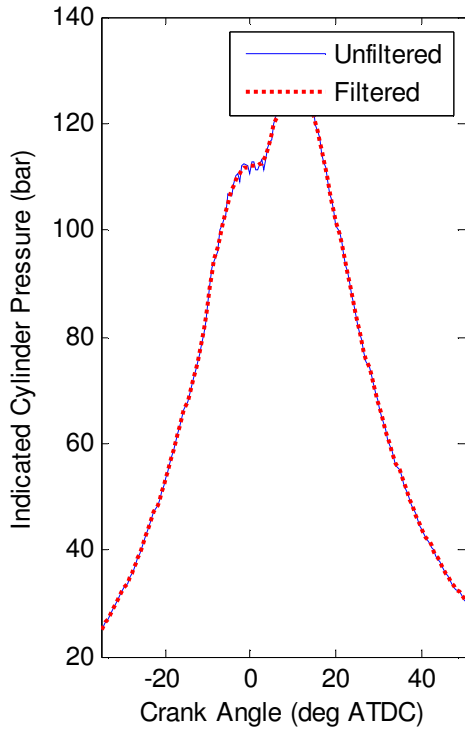


Knock: 2.4 bar

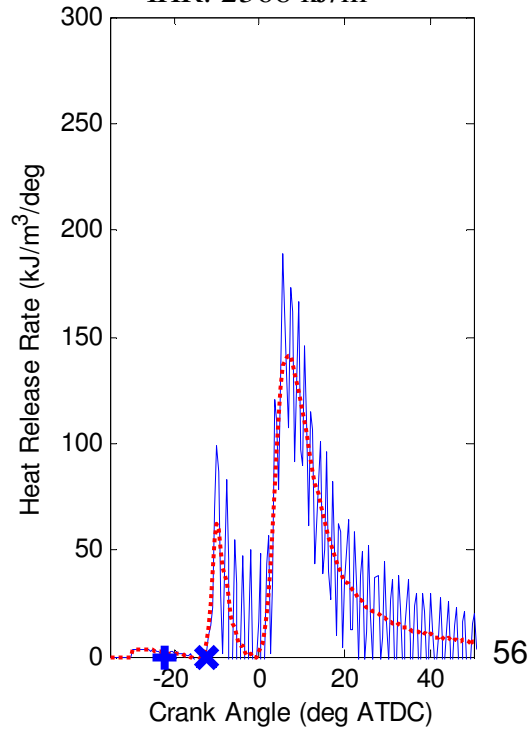
IHR: 2374 kJ/m³



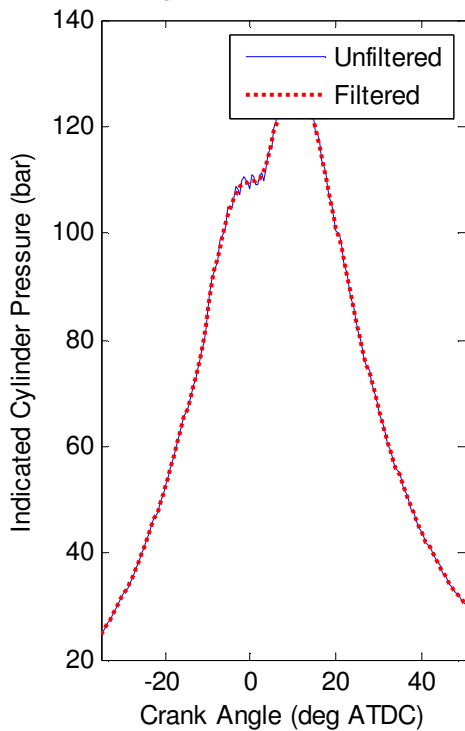
CS-1100-H-5-30EGR-REP1
 t_{id} : 0.59 \pm 0.04 ms



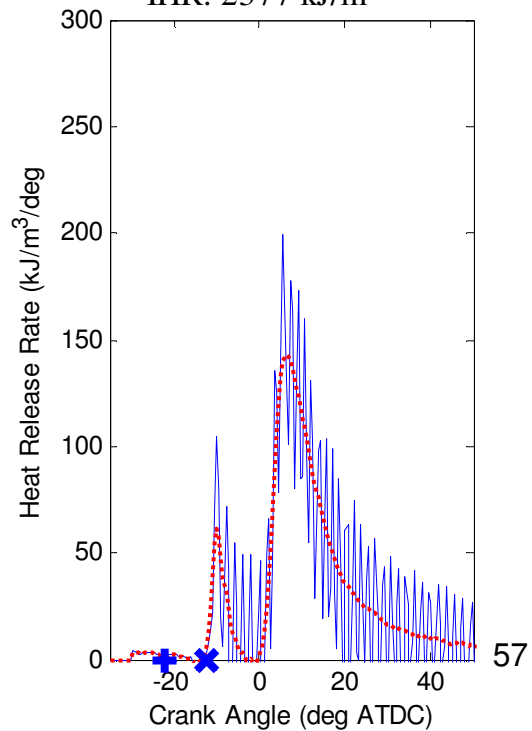
Knock: 2.0 bar
IHR: 2368 kJ/m³



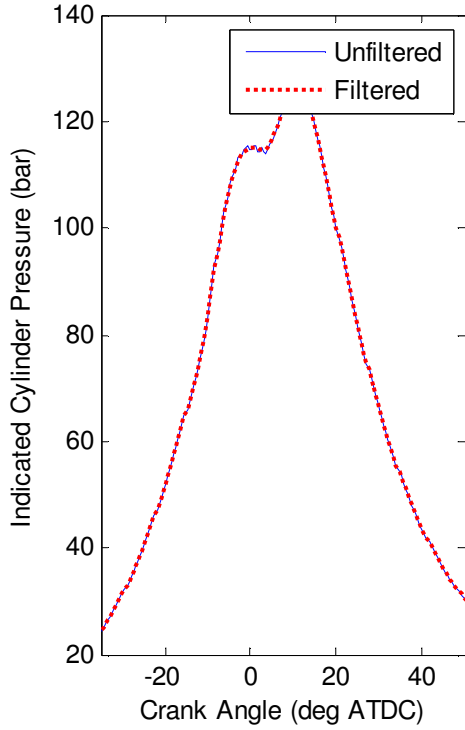
CS-1100-H-5-30EGR-REP2
 t_{id} : 0.59 \pm 0.04 ms



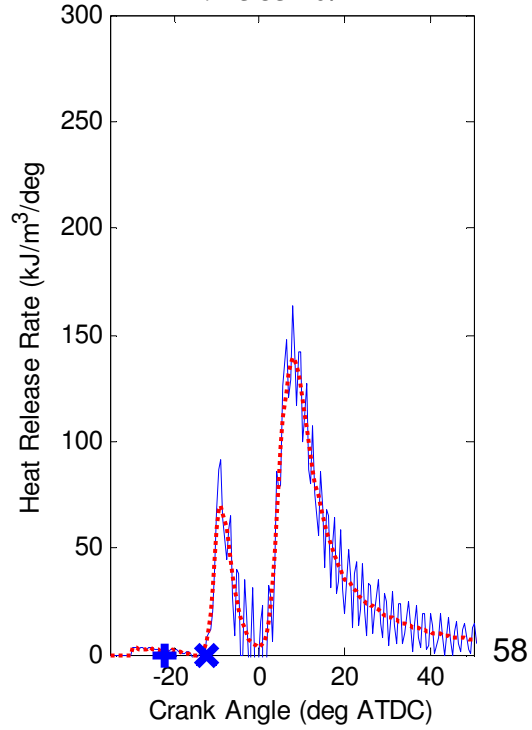
Knock: 1.9 bar
IHR: 2377 kJ/m³



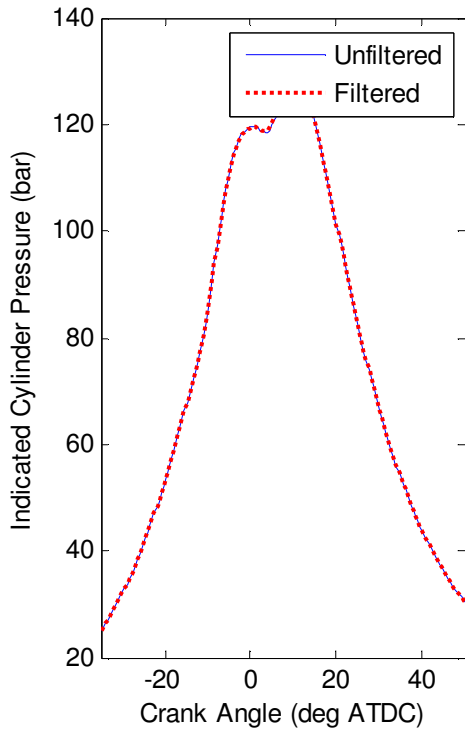
CS-1100-H-7-30EGR
 t_{id} : 0.64+/-0.04 ms



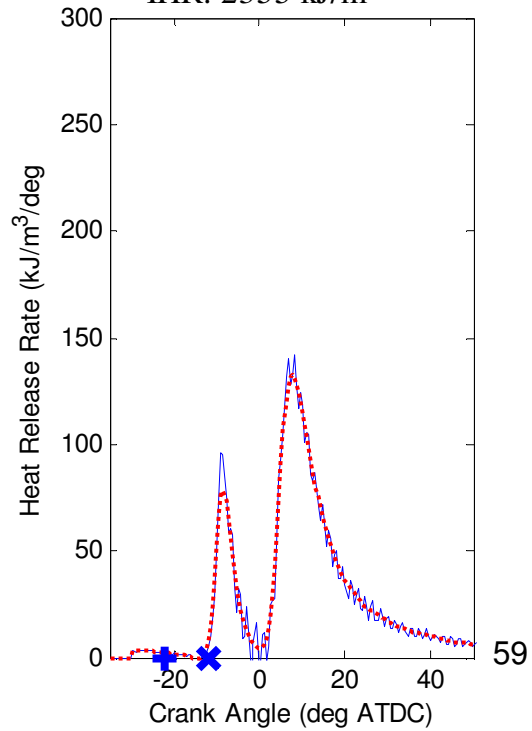
Knock: 1.4 bar
IHR: 2385 kJ/m³



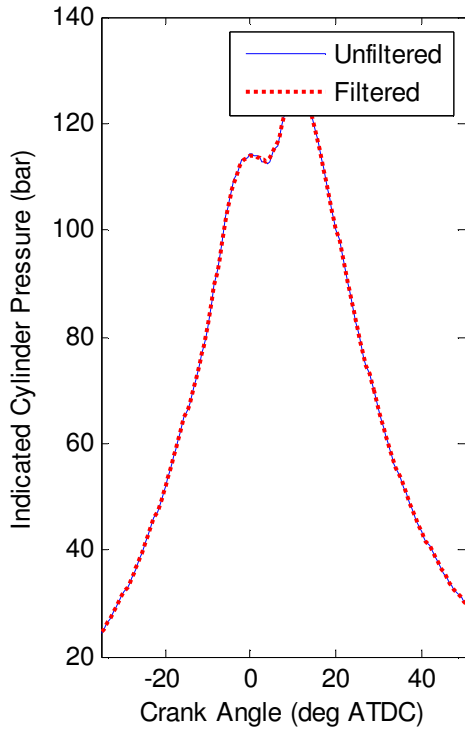
CS-1100-H-7-30EGR-REP1
 t_{id} : 0.66+/-0.04 ms



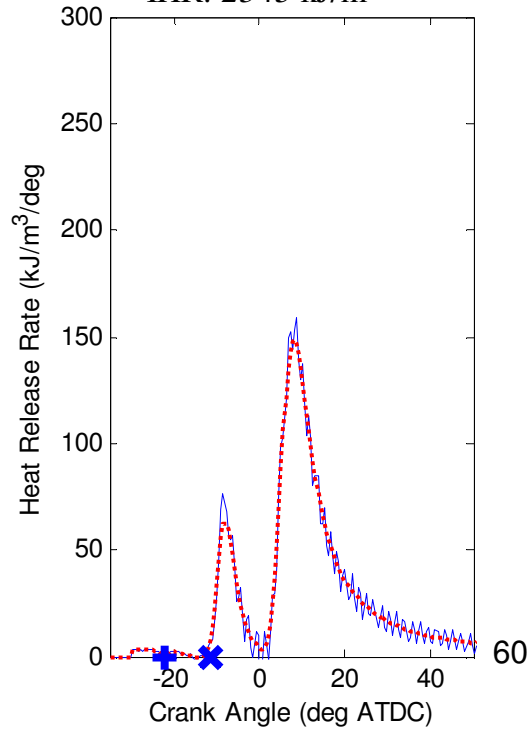
Knock: 1.2 bar
IHR: 2355 kJ/m³



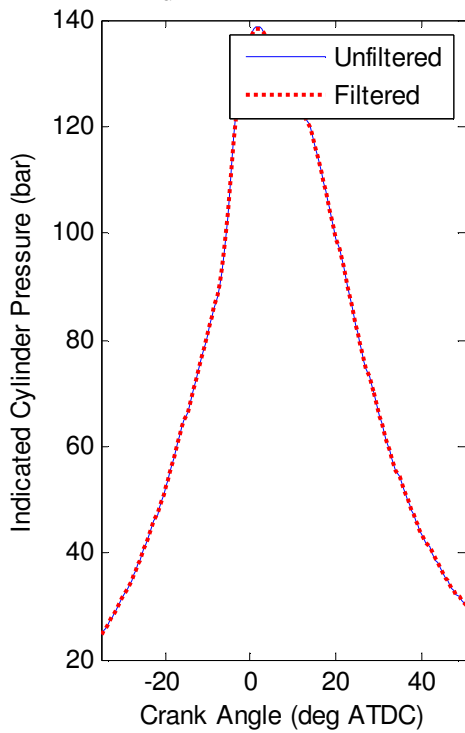
CS-1100-H-7-30EGR-REP2
 t_{id} : 0.75 \pm 0.04 ms



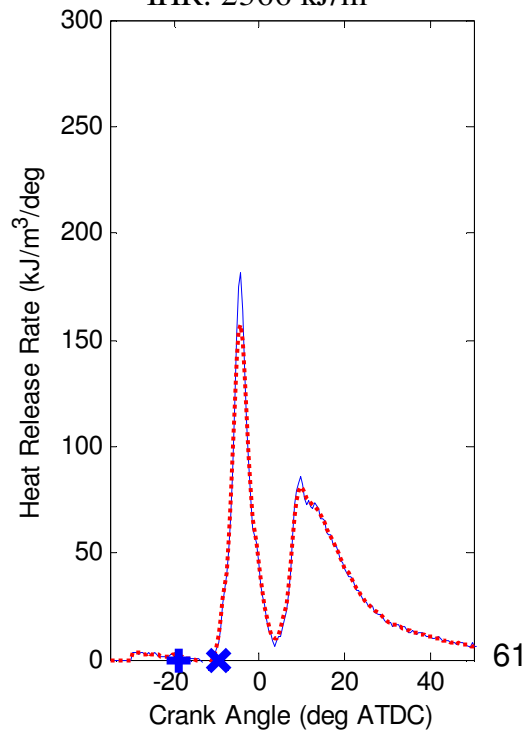
Knock: 1.1 bar
IHR: 2345 kJ/m³



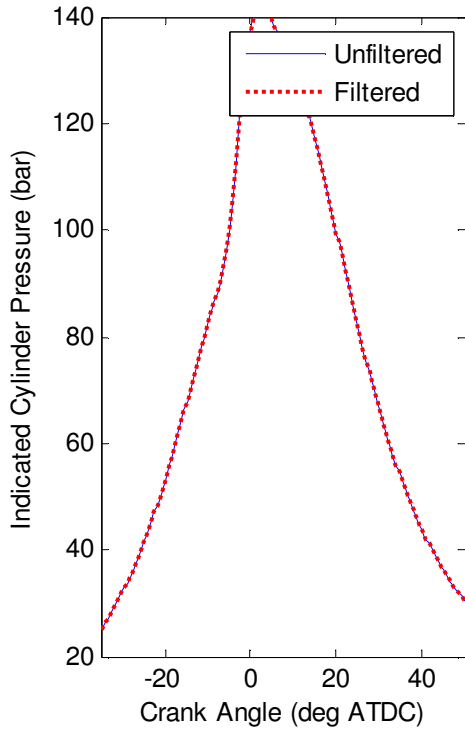
CS-1100-H-9-30EGR
 t_{id} : 0.53 \pm 0.04 ms



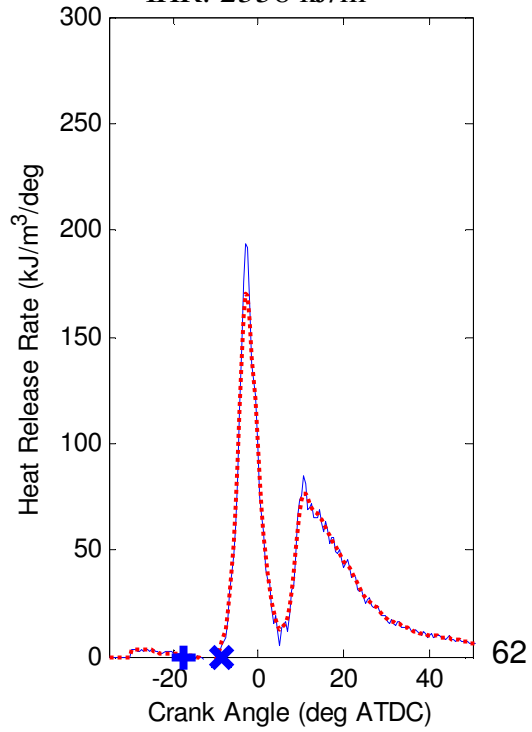
Knock: 1.5 bar
IHR: 2366 kJ/m³



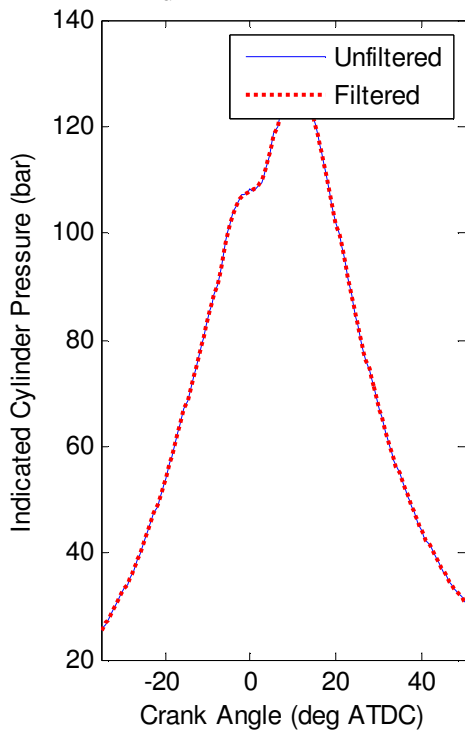
CS-1100-H-9-30EGR-REP1
 t_{id} : 0.48 \pm 0.04 ms



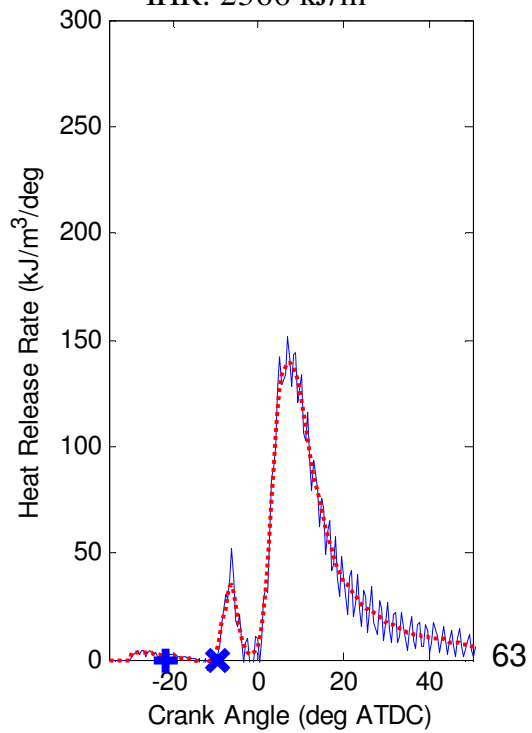
Knock: 1.5 bar
IHR: 2358 kJ/m³



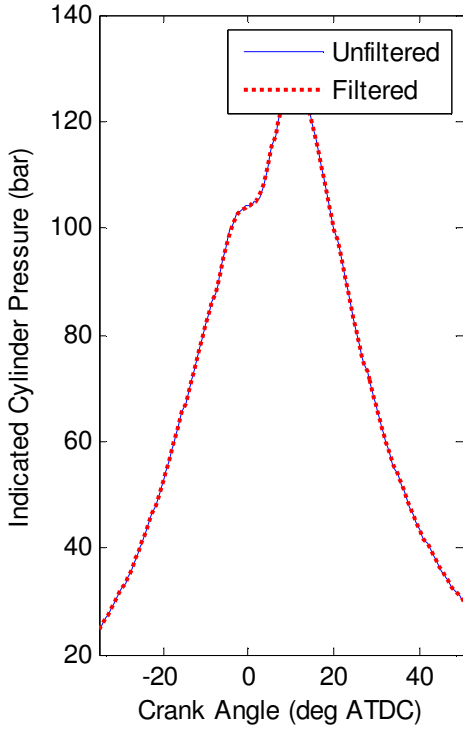
B-1100-H-5-30EGR
 t_{id} : 0.94 \pm 0.05 ms



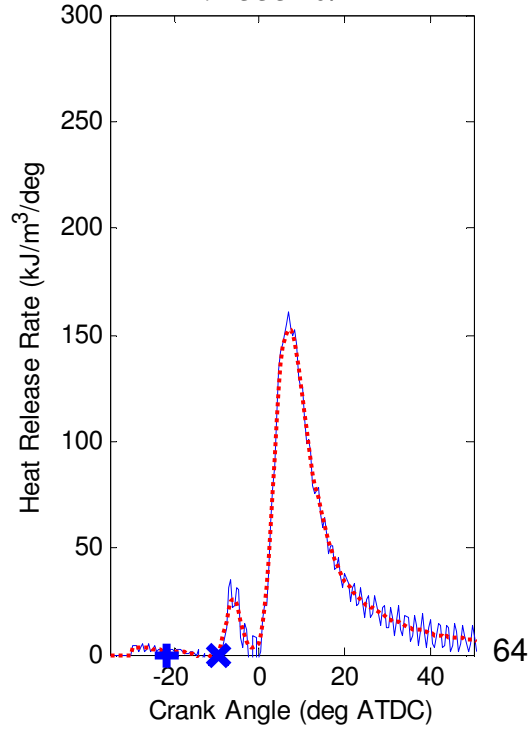
Knock: 1.0 bar
IHR: 2366 kJ/m³



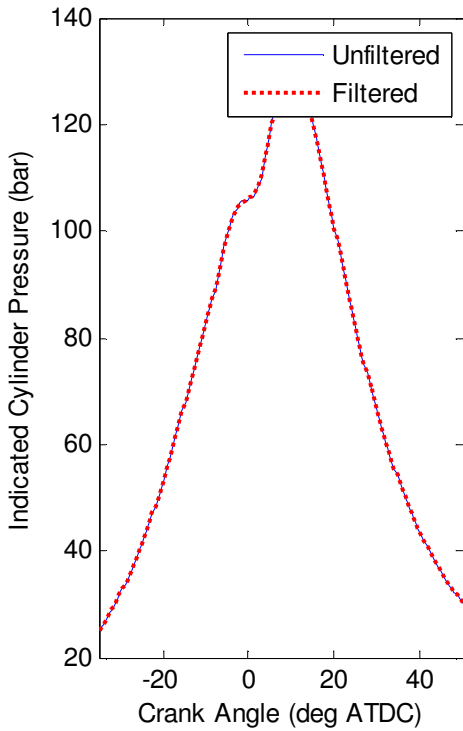
B-1100-H-5-30EGR-REP1
 t_{id} : 0.99 \pm 0.11 ms



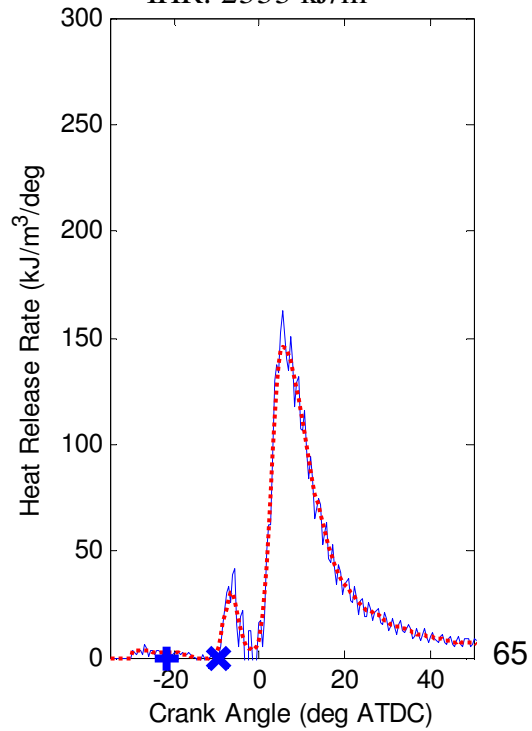
Knock: 0.9 bar
IHR: 2333 kJ/m³



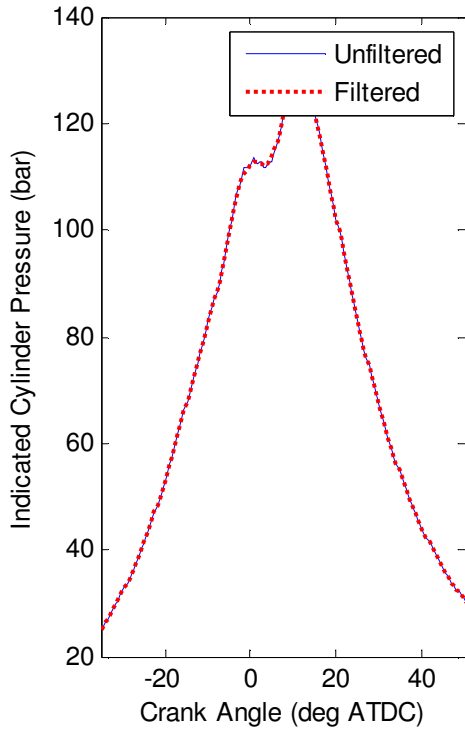
B-1100-H-5-30EGR-REP2
 t_{id} : 0.99 \pm 0.07 ms



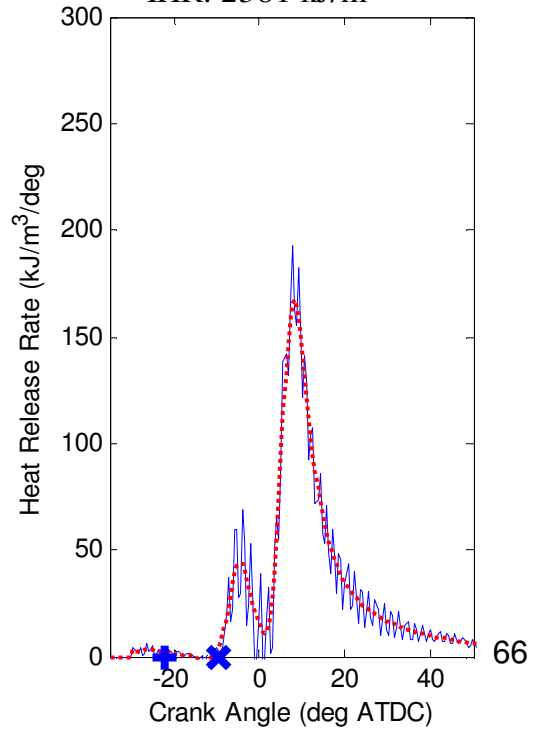
Knock: 1.0 bar
IHR: 2333 kJ/m³



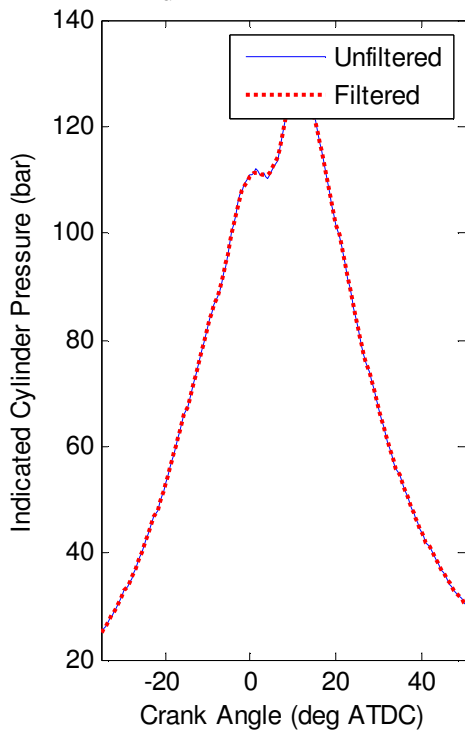
B-1100-H-7-30EGR
 t_{id} : 1.04+/-0.04 ms



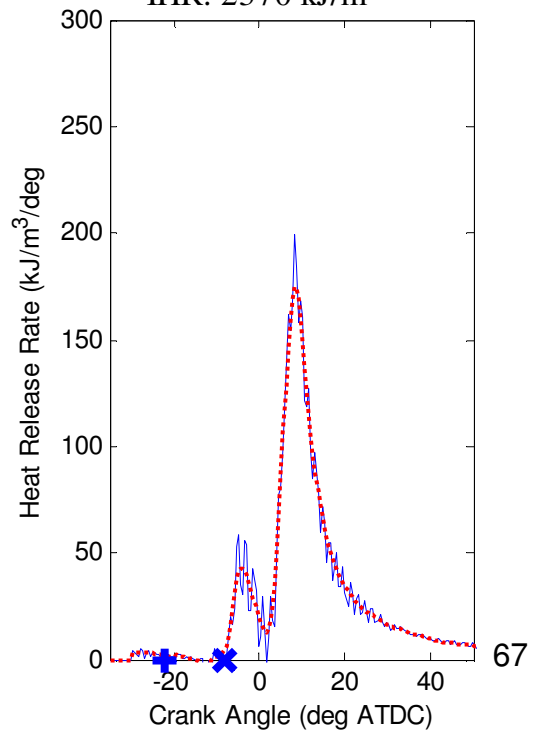
Knock: 1.3 bar
IHR: 2381 kJ/m³



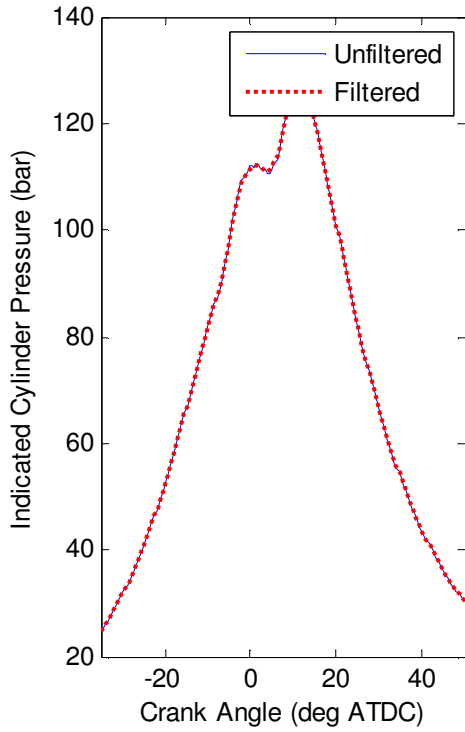
B-1100-H-7-30EGR-REP1
 t_{id} : 1.27+/-0.04 ms



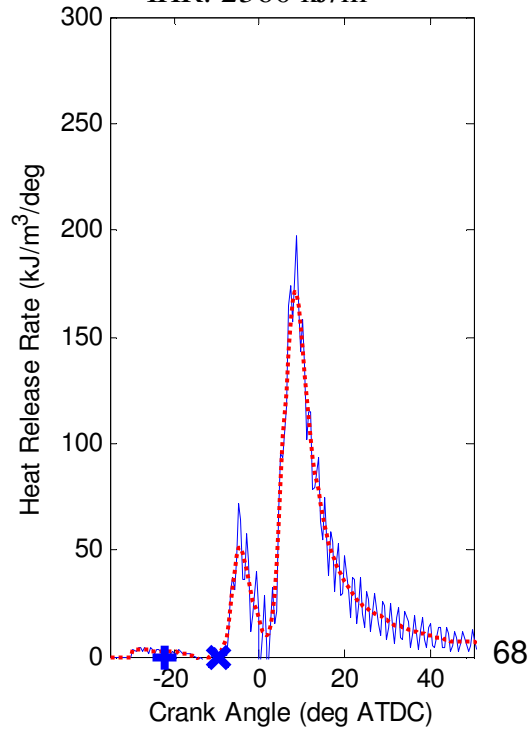
Knock: 1.2 bar
IHR: 2370 kJ/m³



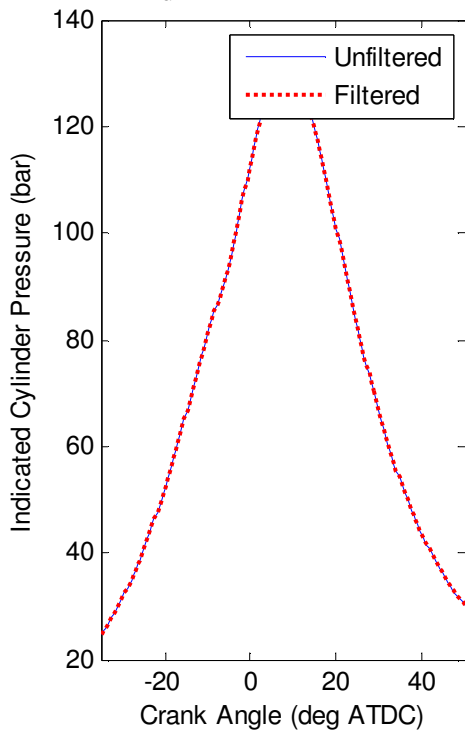
B-1100-H-7-30EGR-REP2
 t_{id} : 1.01+/-0.04 ms



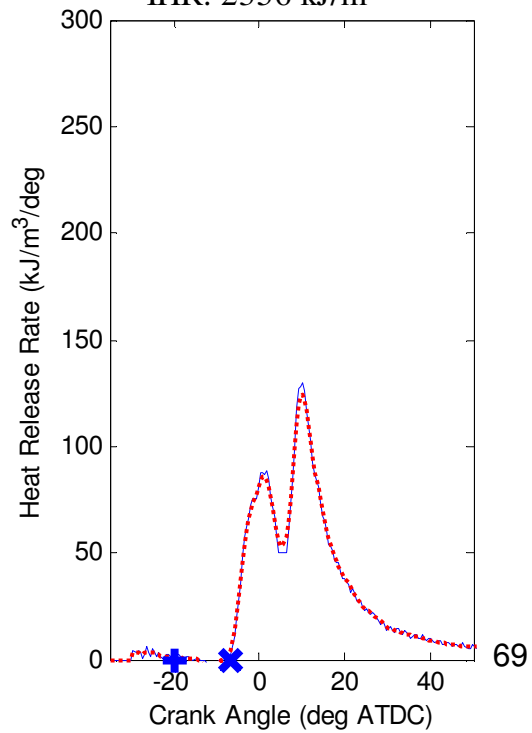
Knock: 1.2 bar
IHR: 2360 kJ/m³



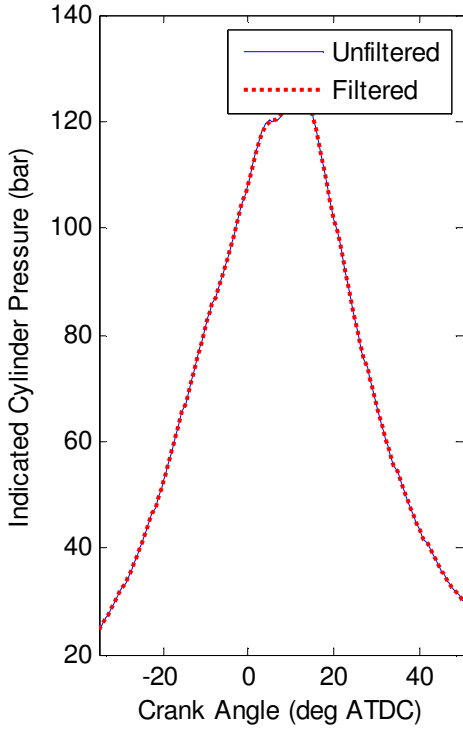
B-1100-H-9-30EGR
 t_{id} : 1.09+/-0.04 ms



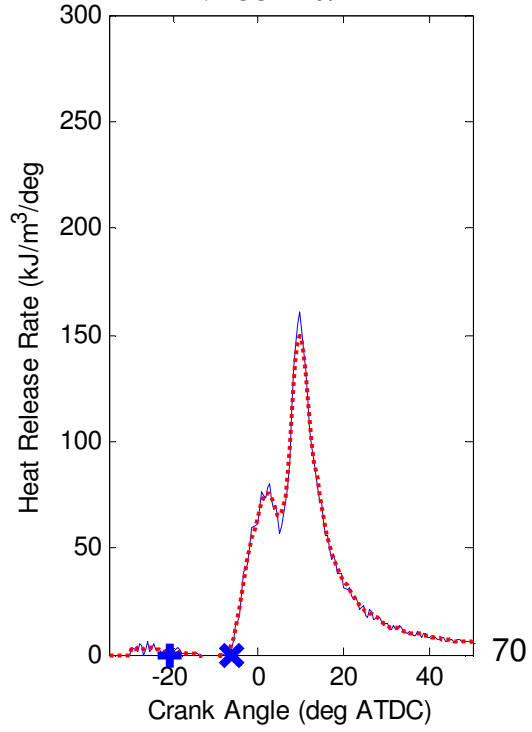
Knock: 1.0 bar
IHR: 2356 kJ/m³



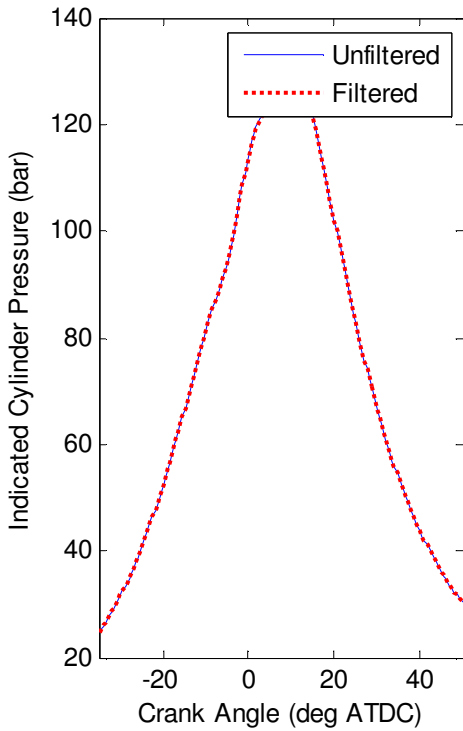
B-1100-H-9-30EGR-REP1
 t_{id} : 1.25+/-0.04 ms



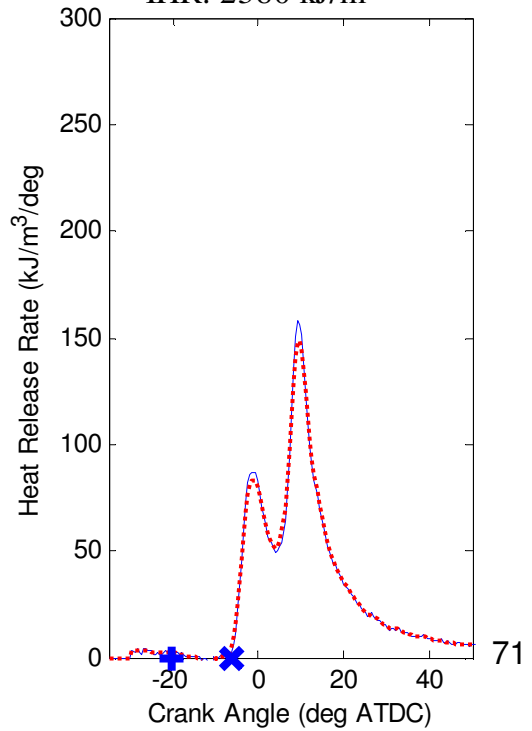
Knock: 1.0 bar
IHR: 2332 kJ/m³



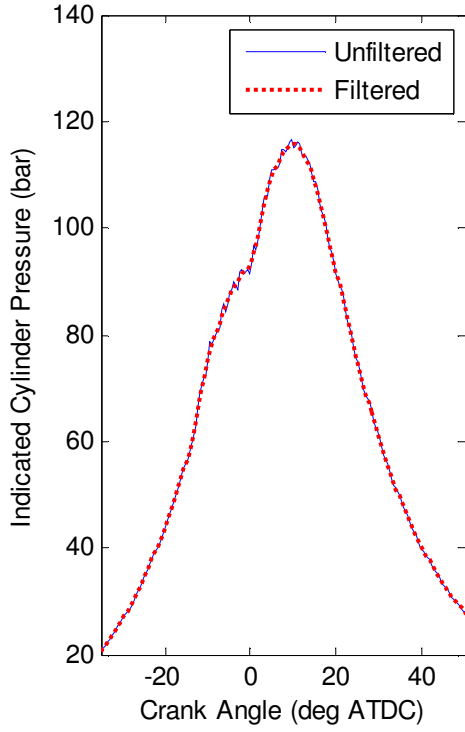
B-1100-H-9-30EGR-REP2
 t_{id} : 1.26+/-0.04 ms



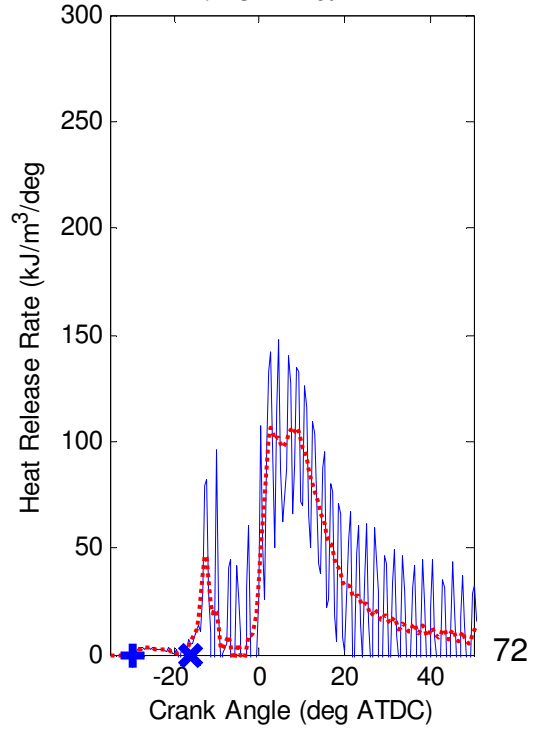
Knock: 0.9 bar
IHR: 2380 kJ/m³



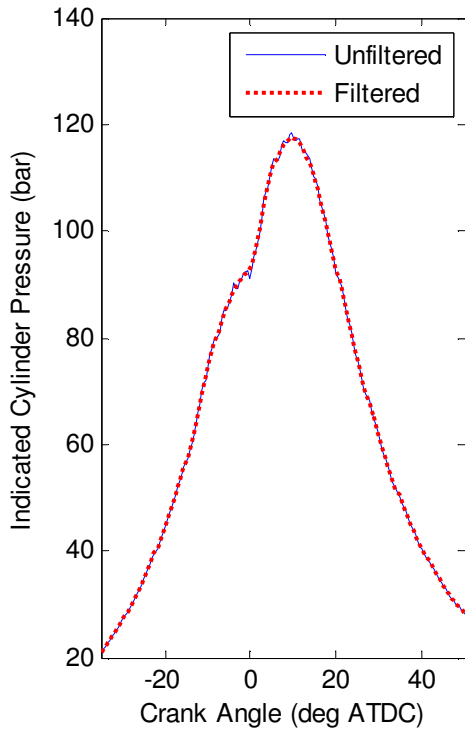
CS-1400-H-5-0EGR
 t_{id} : 0.69+/-0.03 ms



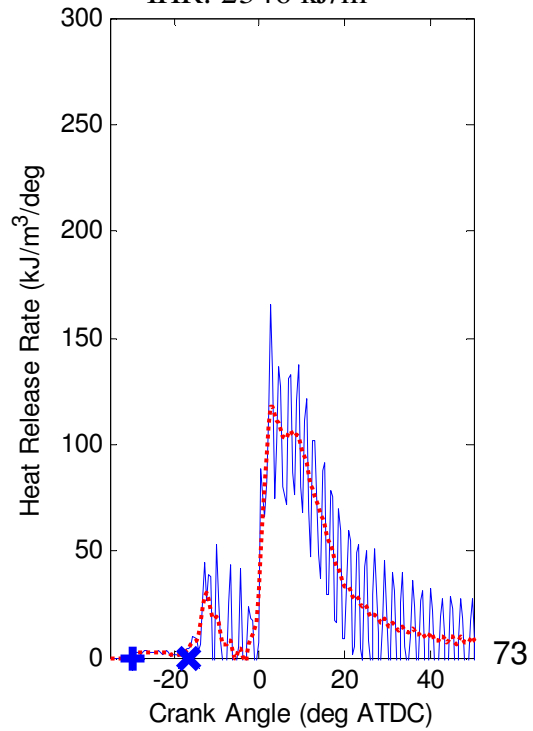
Knock: 2.3 bar
IHR: 2342 kJ/m³



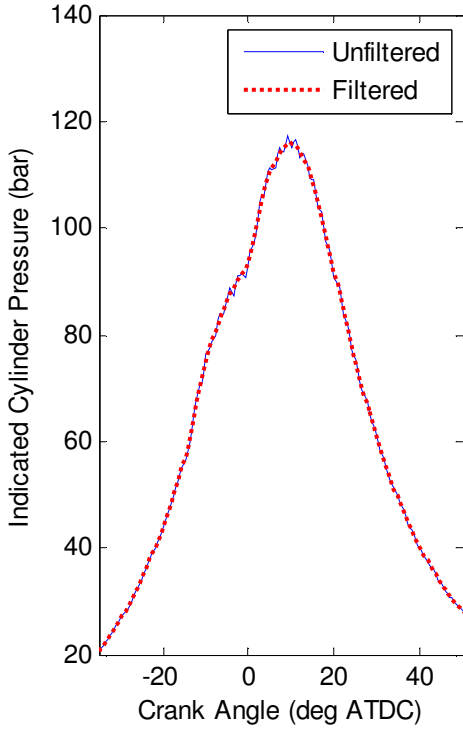
CS-1400-H-5-0EGR-REP1
 t_{id} : 0.70+/-0.06 ms



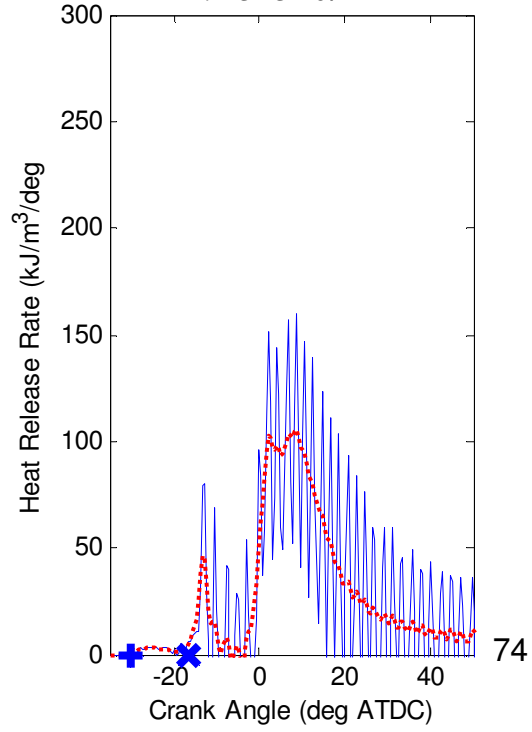
Knock: 1.9 bar
IHR: 2346 kJ/m³



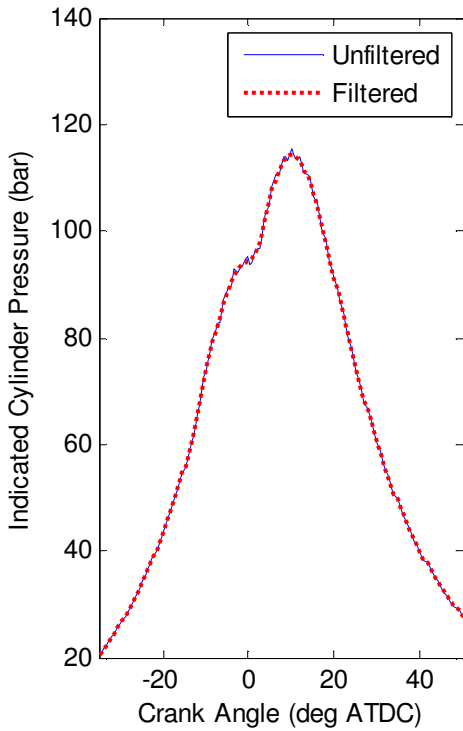
CS-1400-H-5-0EGR-REP2
 t_{id} : 0.73+/-0.03 ms



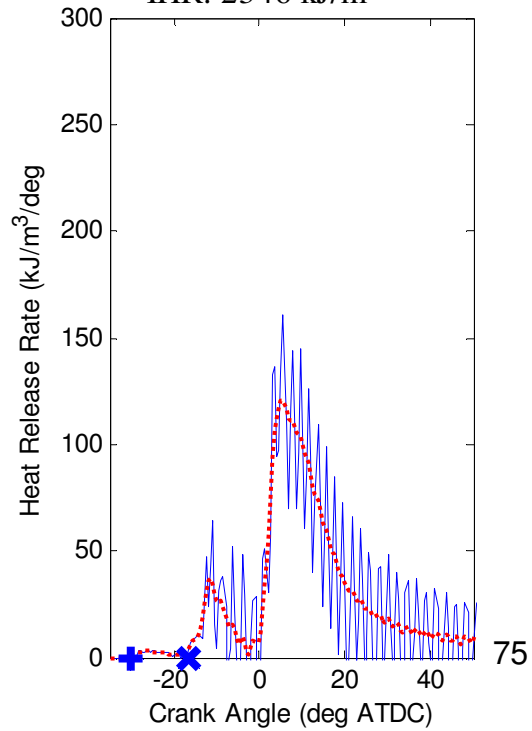
Knock: 2.0 bar
IHR: 2345 kJ/m³



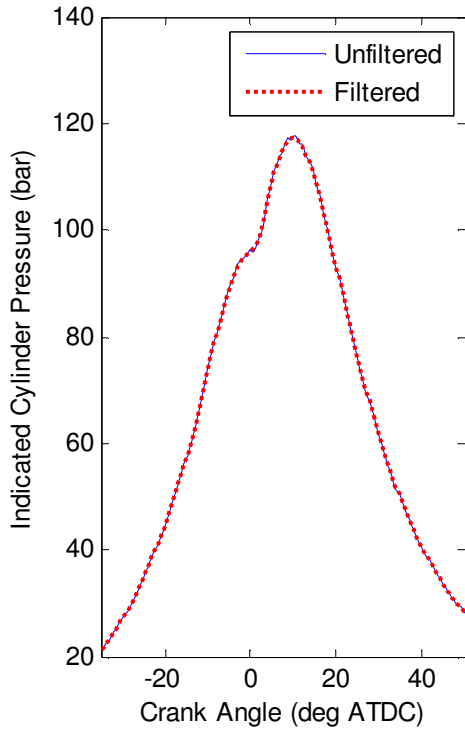
CS-1400-H-7-0EGR
 t_{id} : 0.72+/-0.03 ms



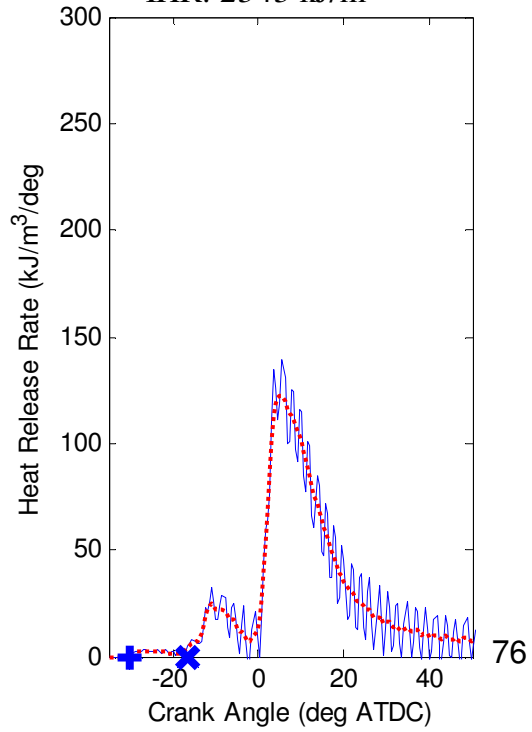
Knock: 2.0 bar
IHR: 2346 kJ/m³



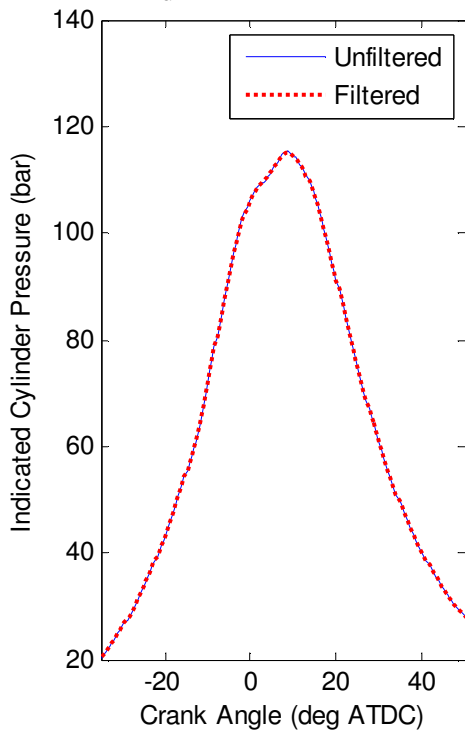
CS-1400-H-7-0EGR-REP1
 t_{id} : 0.73+/-0.10 ms



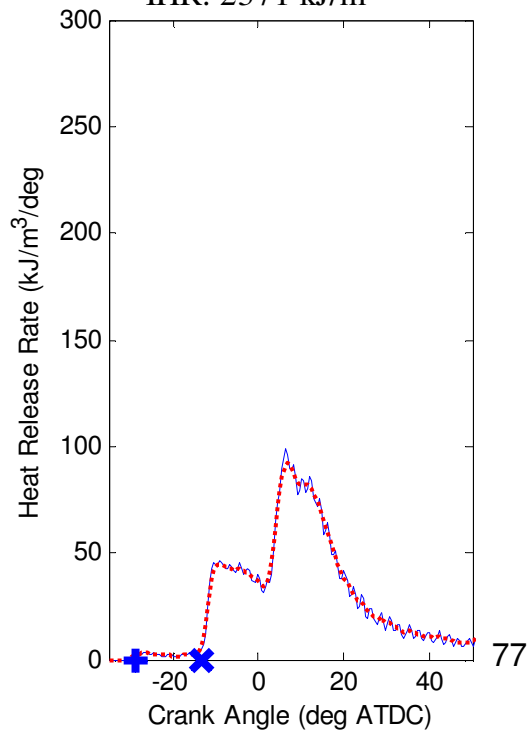
Knock: 1.4 bar
IHR: 2343 kJ/m³



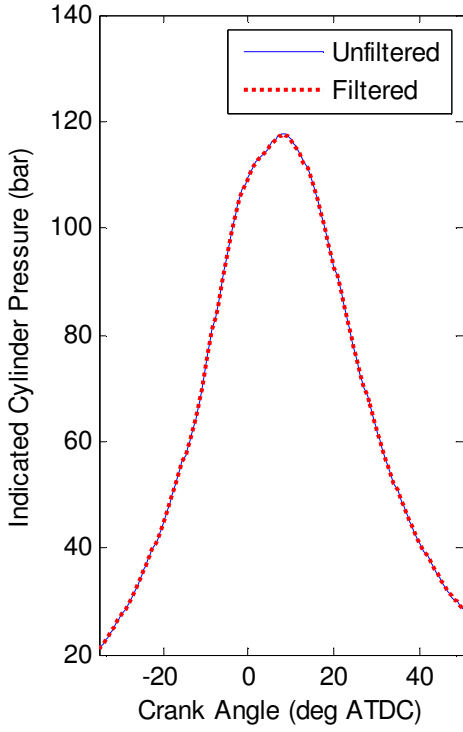
CS-1400-H-9-0EGR
 t_{id} : 0.92+/-0.03 ms



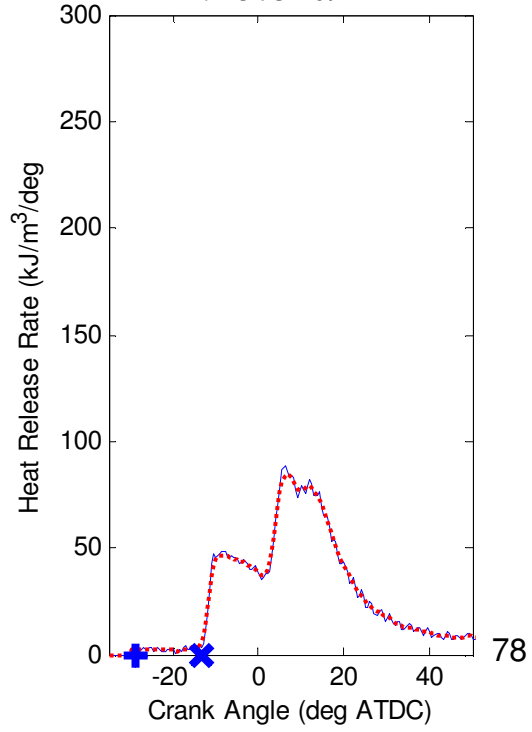
Knock: 1.0 bar
IHR: 2371 kJ/m³



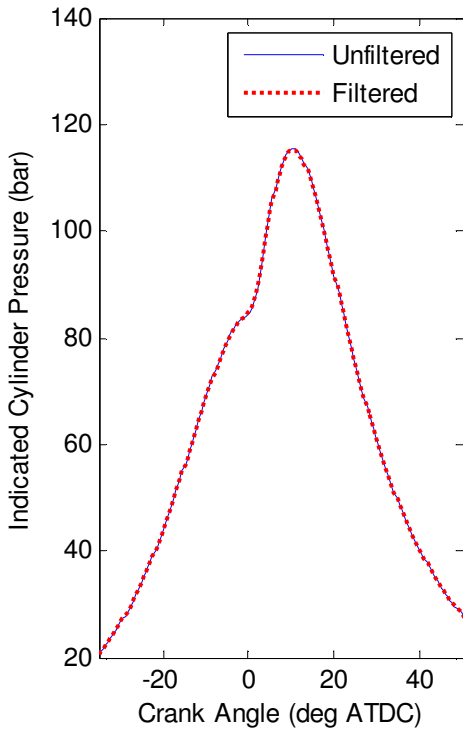
CS-1400-H-9-0EGR-REP1
 t_{id} : 0.92 \pm 0.03 ms



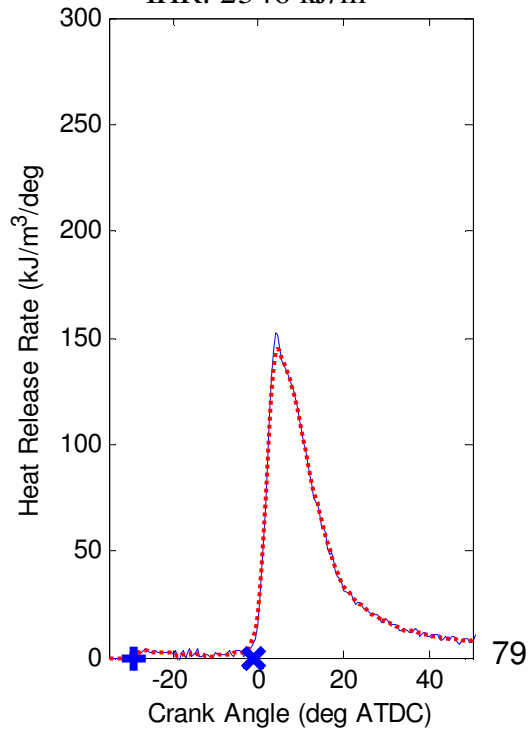
Knock: 1.0 bar
IHR: 2375 kJ/m³



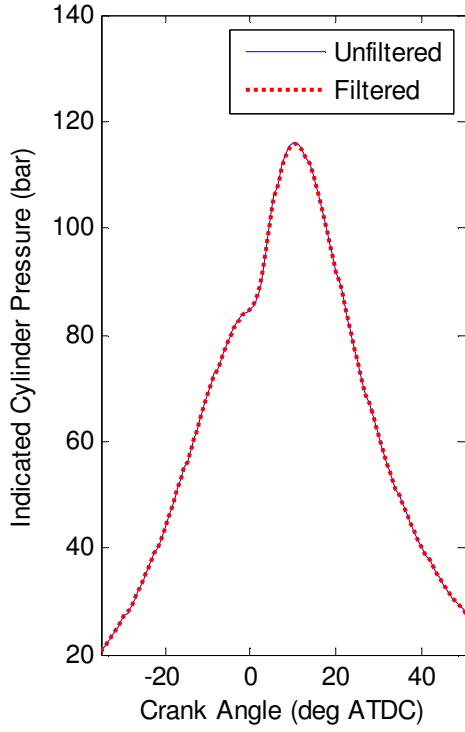
B-1400-H-5-0EGR
 t_{id} : 2.42 \pm 0.03 ms



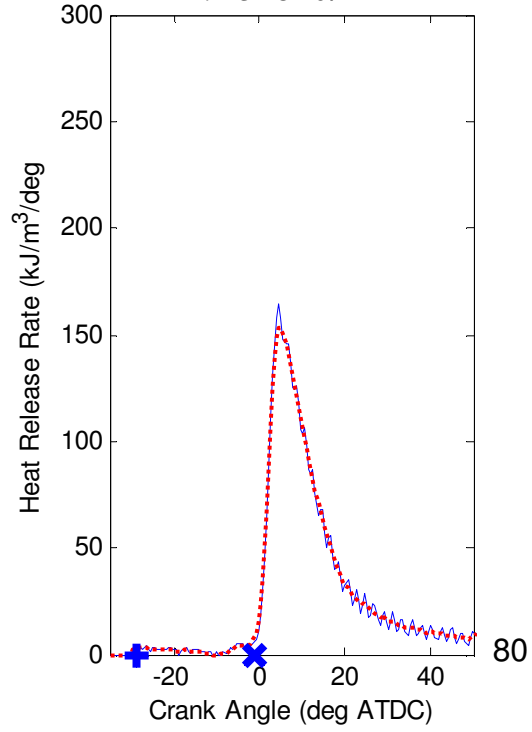
Knock: 1.5 bar
IHR: 2346 kJ/m³



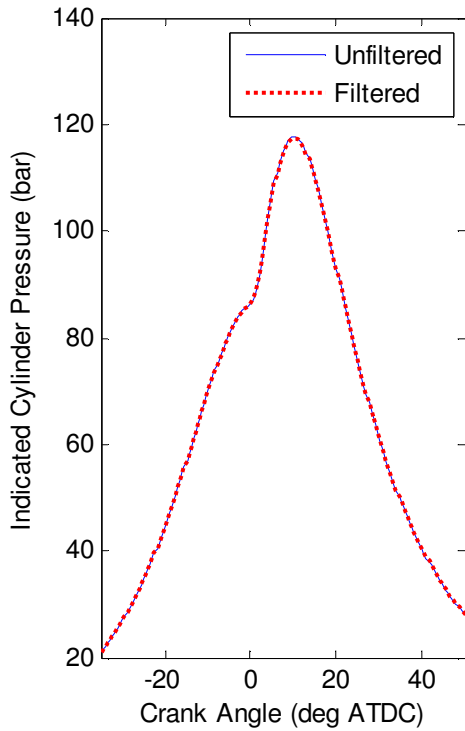
B-1400-H-5-0EGR-REP1
 t_{id} : 2.42 \pm 0.03 ms



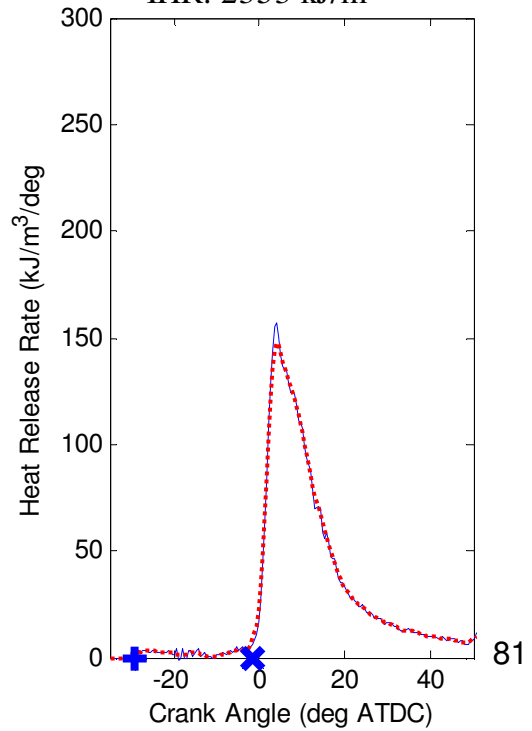
Knock: 1.4 bar
IHR: 2348 kJ/m³



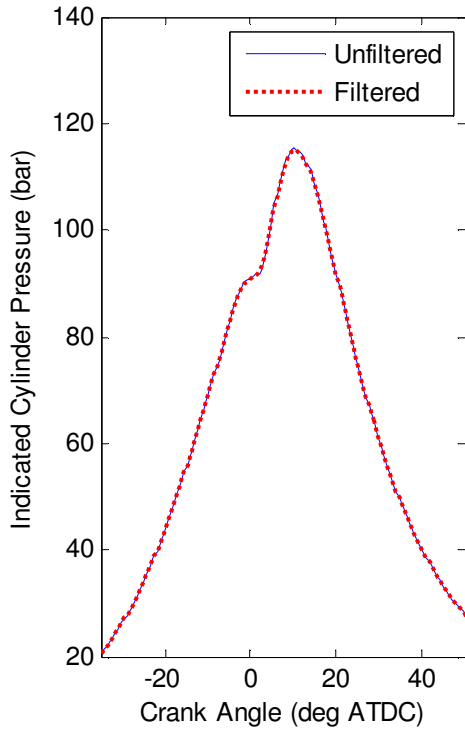
B-1400-H-5-0EGR-REP2
 t_{id} : 2.42 \pm 0.03 ms



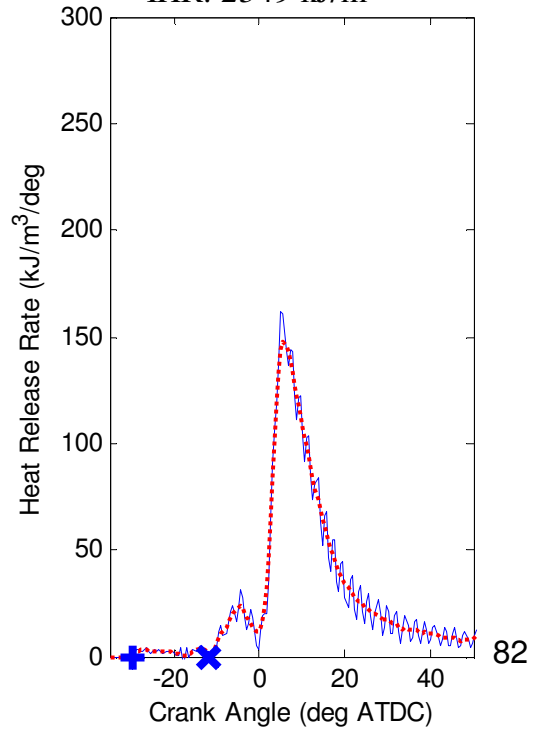
Knock: 1.6 bar
IHR: 2353 kJ/m³



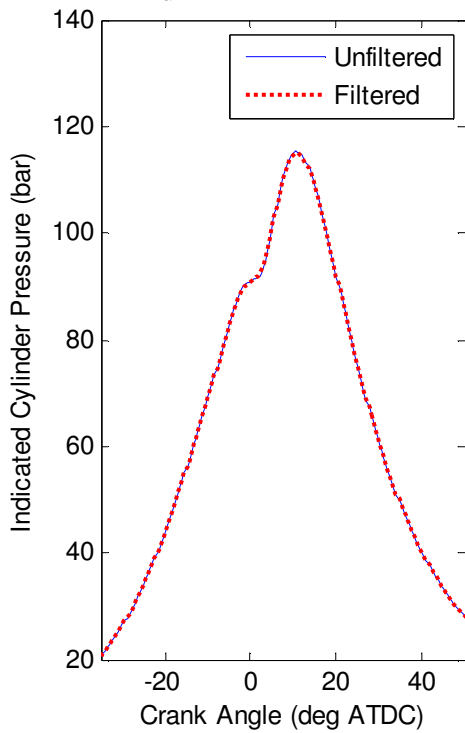
B-1400-H-7-0EGR
 t_{id} : 1.22+/-0.10 ms



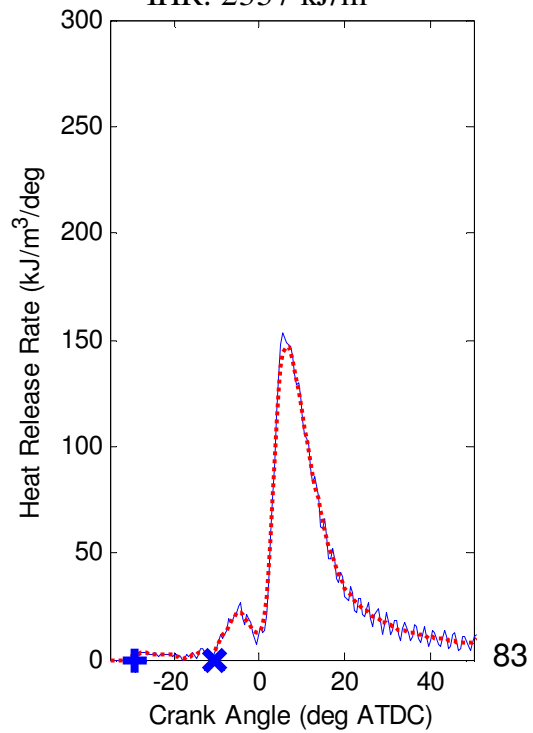
Knock: 1.4 bar
IHR: 2349 kJ/m³



B-1400-H-7-0EGR-REP1
 t_{id} : 1.32+/-0.08 ms

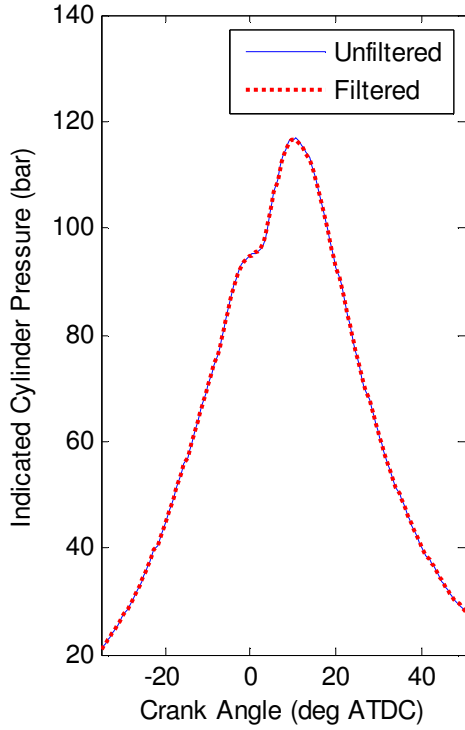


Knock: 1.3 bar
IHR: 2357 kJ/m³



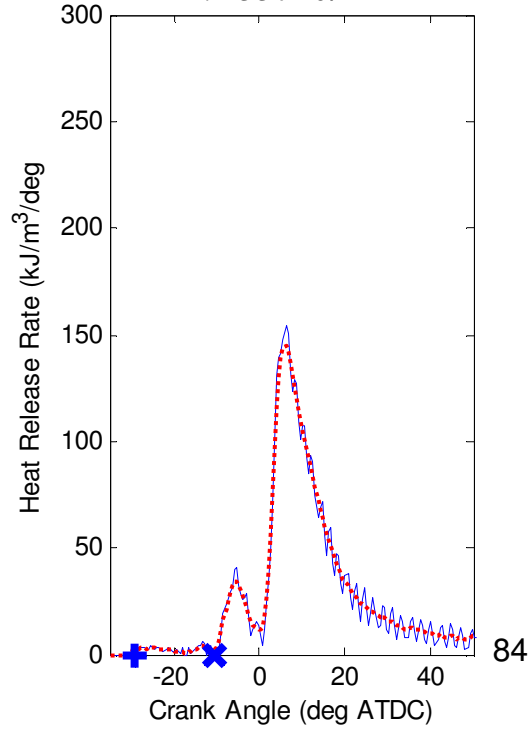
B-1400-H-7-0EGR-REP2

t_{id} : 1.36+/-0.04 ms



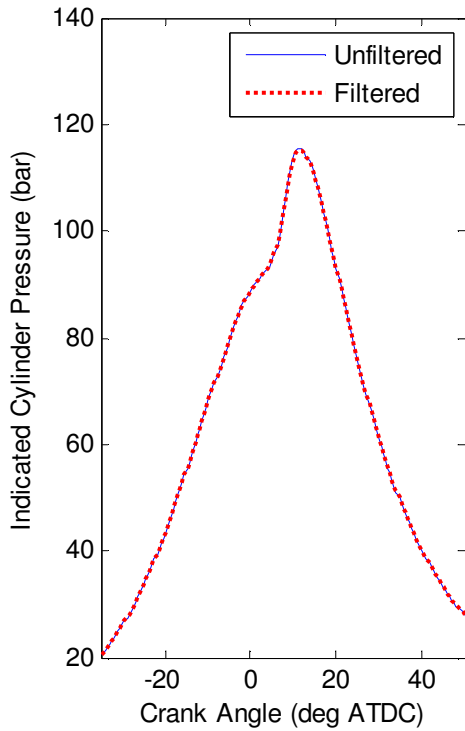
Knock: 1.3 bar

IHR: 2337 kJ/m³



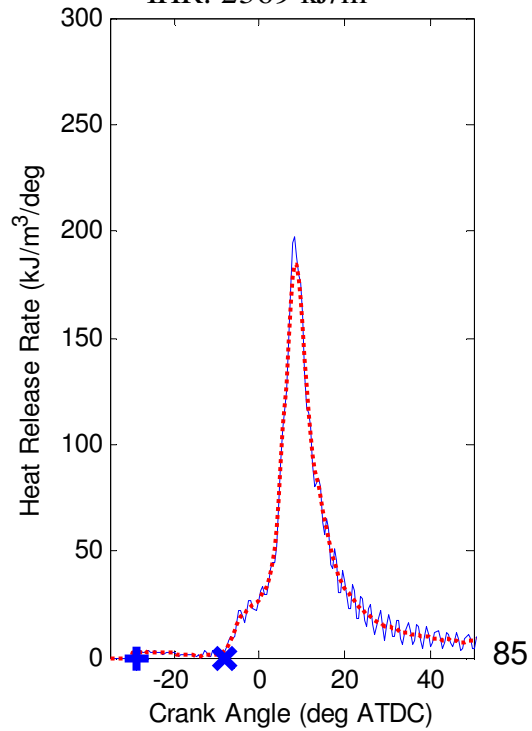
B-1400-H-9-0EGR

t_{id} : 1.56+/-0.14 ms

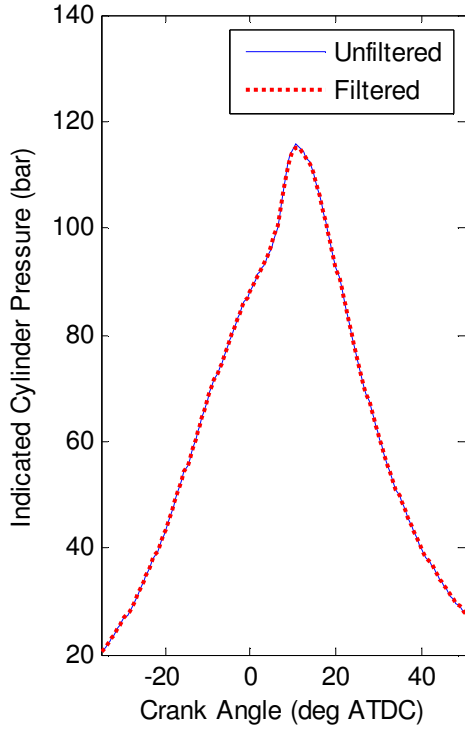


Knock: 1.5 bar

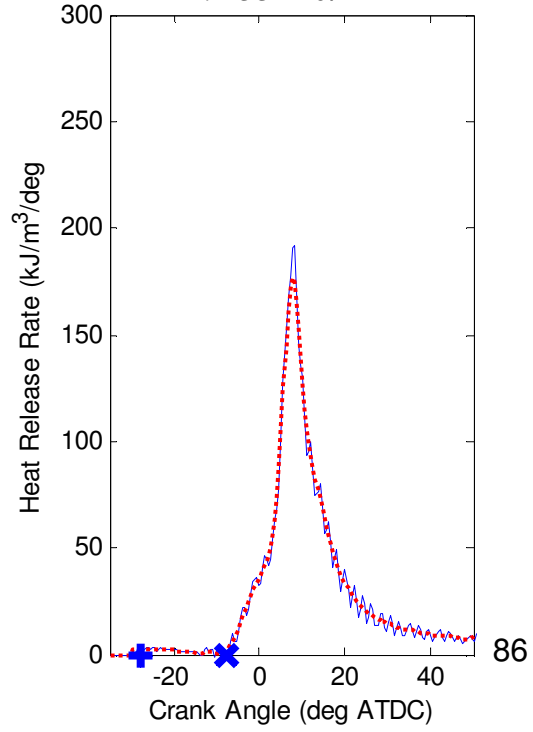
IHR: 2369 kJ/m³



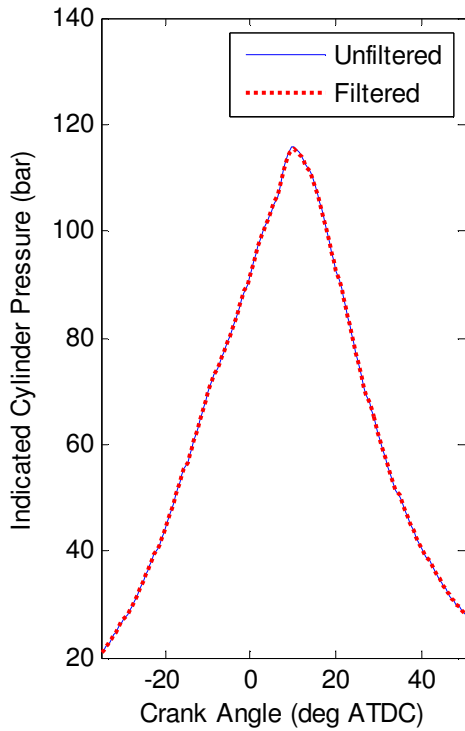
B-1400-H-9-0EGR-REP1
 t_{id} : 1.55+/-0.04 ms



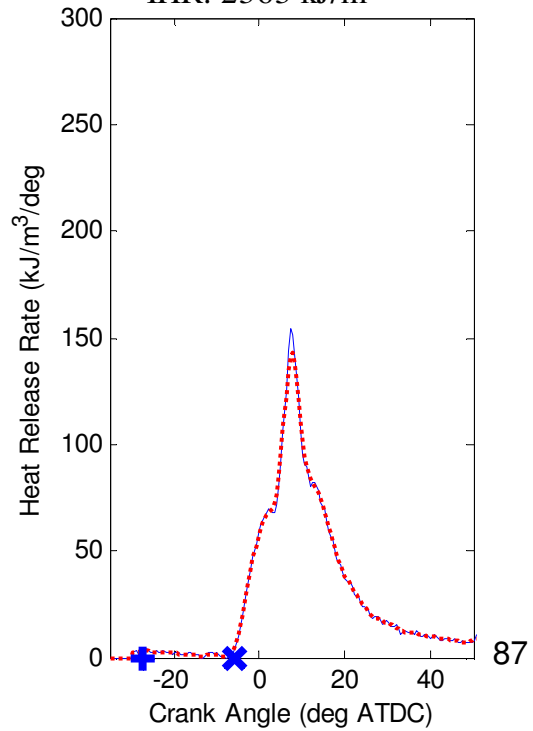
Knock: 1.4 bar
IHR: 2354 kJ/m³



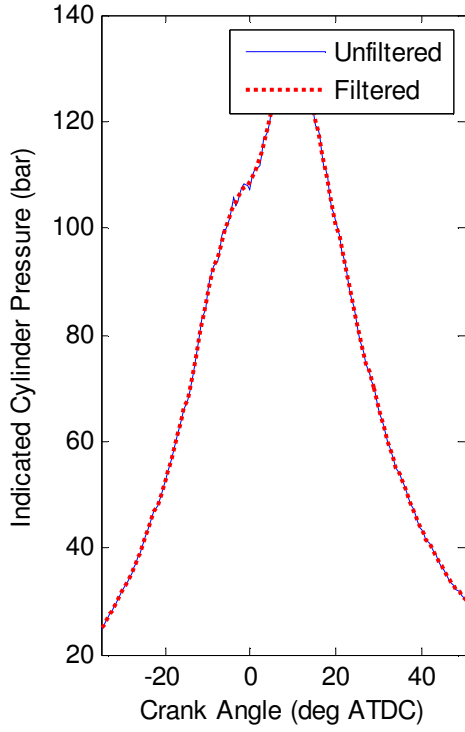
B-1400-H-9-0EGR-REP2
 t_{id} : 1.67+/-0.03 ms



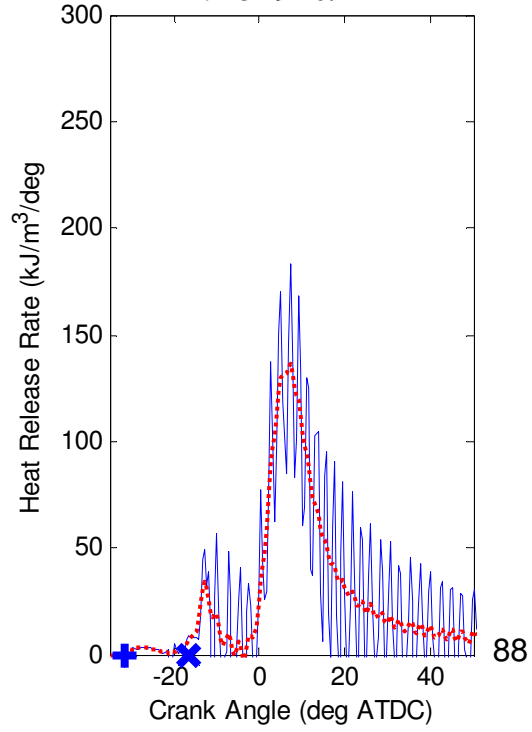
Knock: 1.1 bar
IHR: 2363 kJ/m³



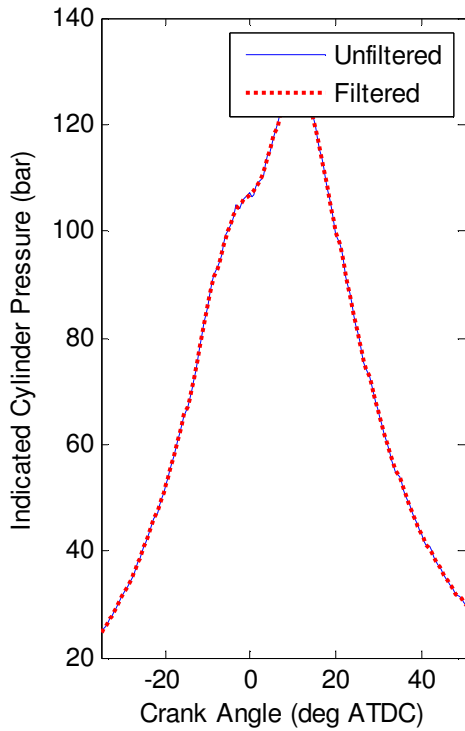
CS-1400-H-5-30EGR
 t_{id} : 0.90 \pm 0.03 ms



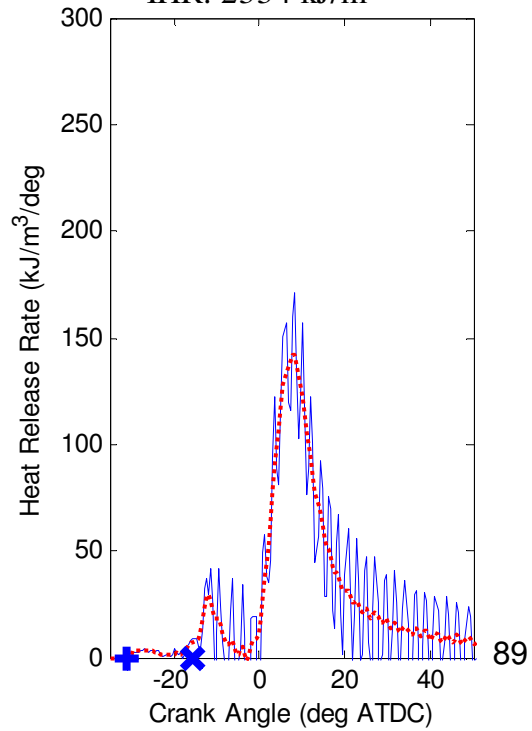
Knock: 1.8 bar
IHR: 2349 kJ/m³



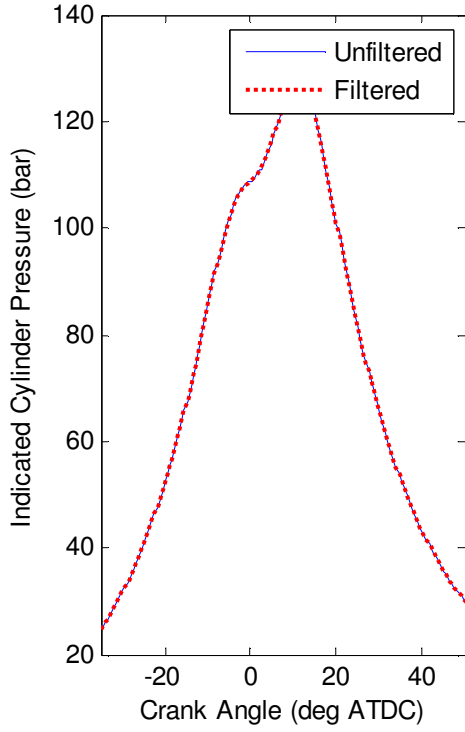
CS-1400-H-5-30EGR-REP1
 t_{id} : 0.94 \pm 0.05 ms



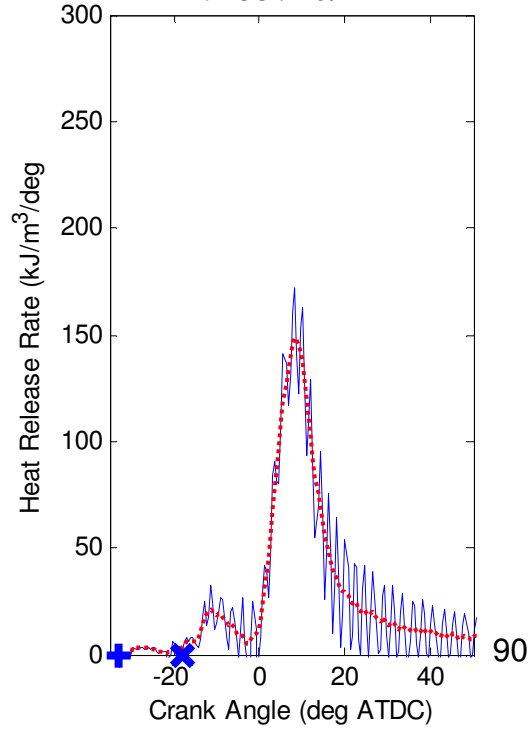
Knock: 1.4 bar
IHR: 2334 kJ/m³



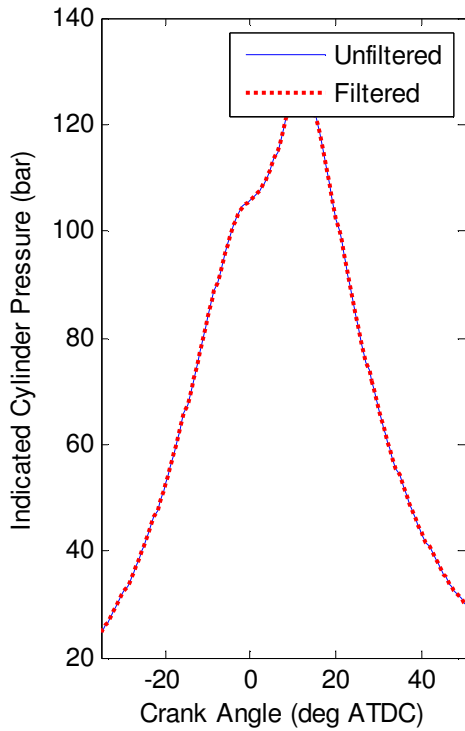
CS-1400-H-7-30EGR
 t_{id} : 0.90+/-0.09 ms



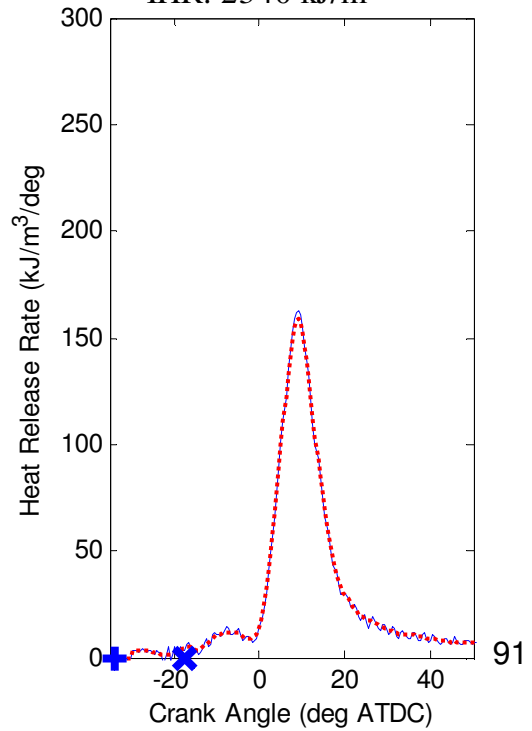
Knock: 1.1 bar
IHR: 2337 kJ/m³



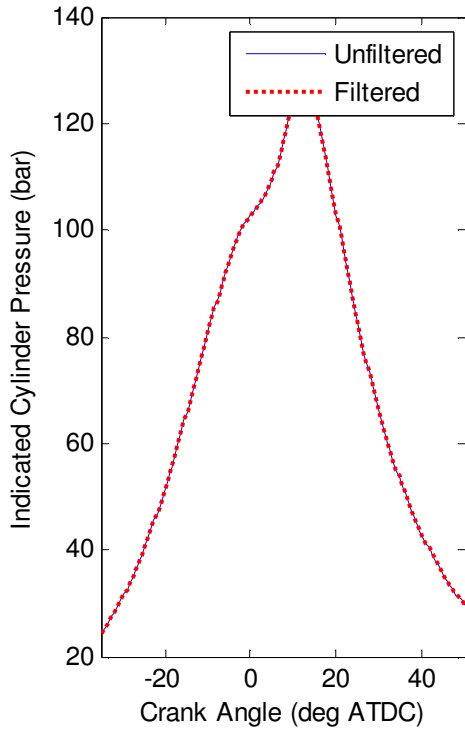
CS-1400-H-7-30EGR-REP1
 t_{id} : 1.07+/-0.05 ms



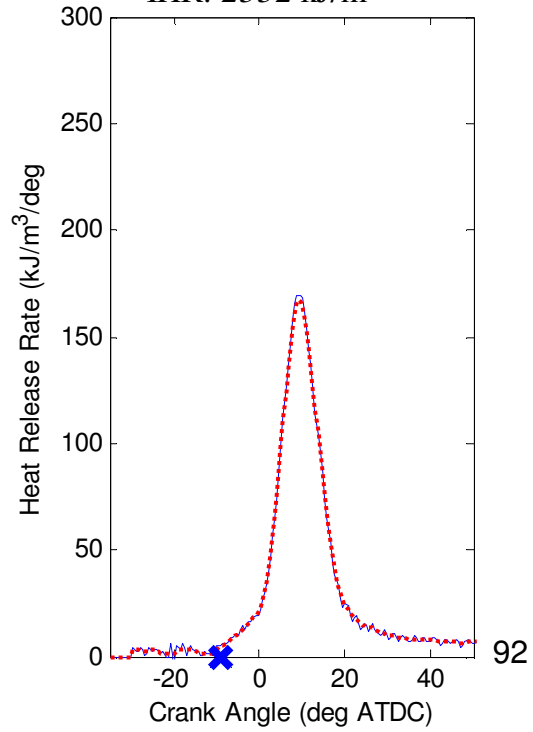
Knock: 0.8 bar
IHR: 2340 kJ/m³



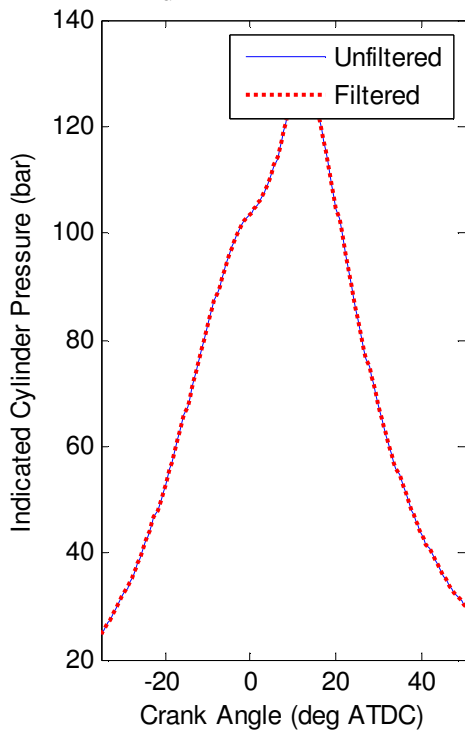
CS-1400-H-9-30EGR
 t_{id} : 2.38 \pm 0.04 ms



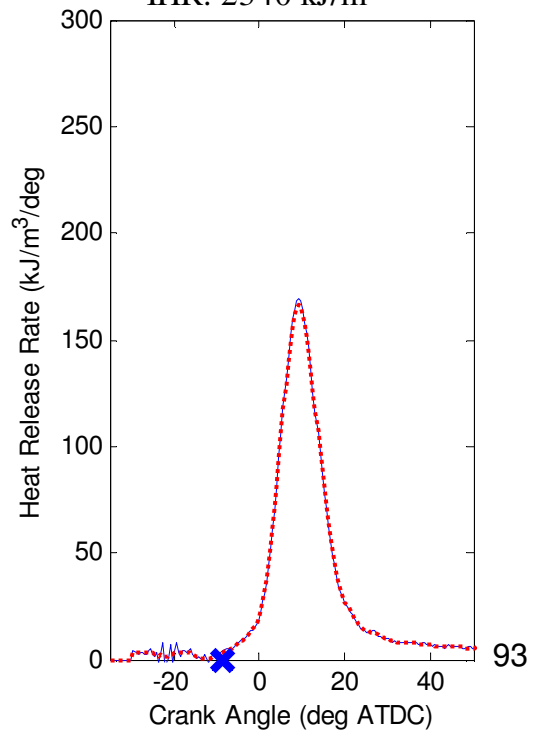
Knock: 0.9 bar
IHR: 2332 kJ/m³



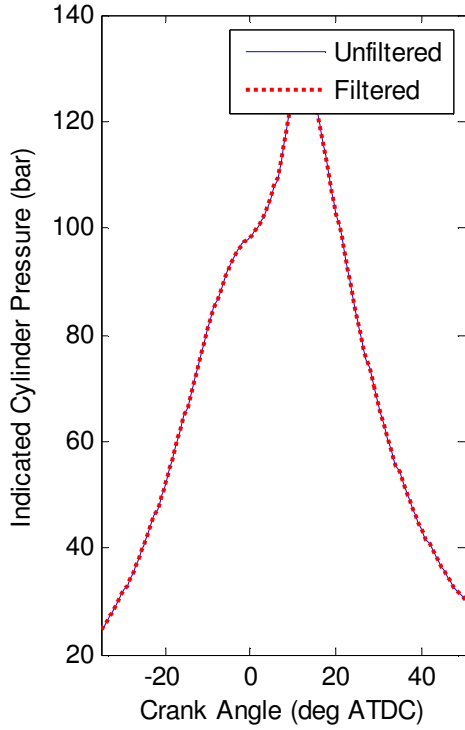
CS-1400-H-9-30EGR-REP1
 t_{id} : 2.56 \pm 0.04 ms



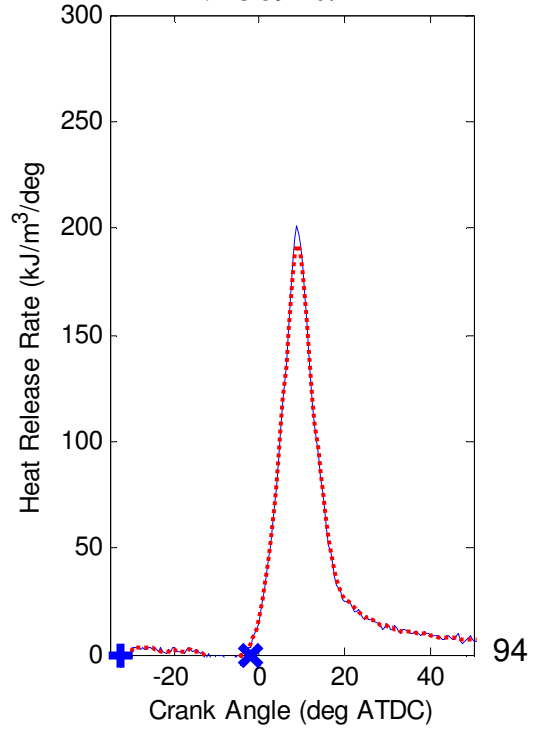
Knock: 0.9 bar
IHR: 2340 kJ/m³



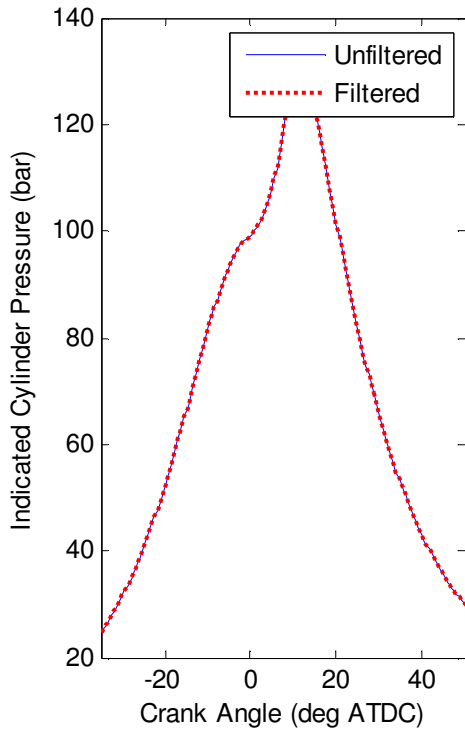
B-1400-H-5-30EGR
 t_{id} : 2.78+/-0.03 ms



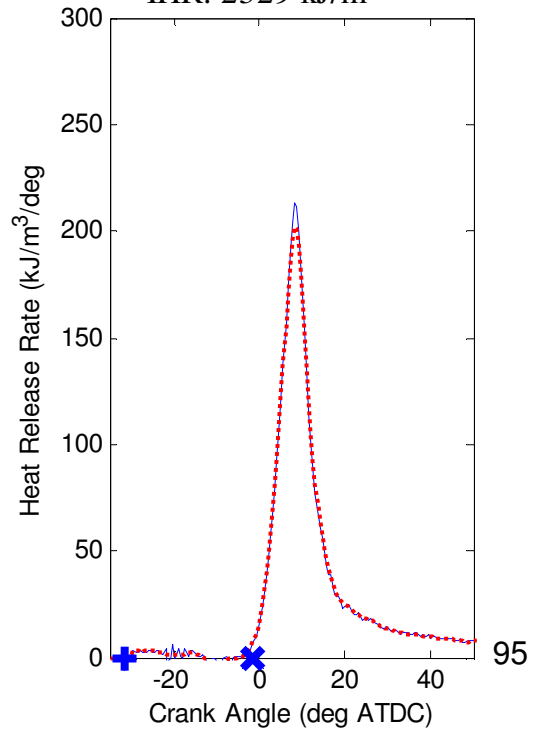
Knock: 1.1 bar
IHR: 2369 kJ/m³



B-1400-H-5-30EGR-REP1
 t_{id} : 2.68+/-0.03 ms

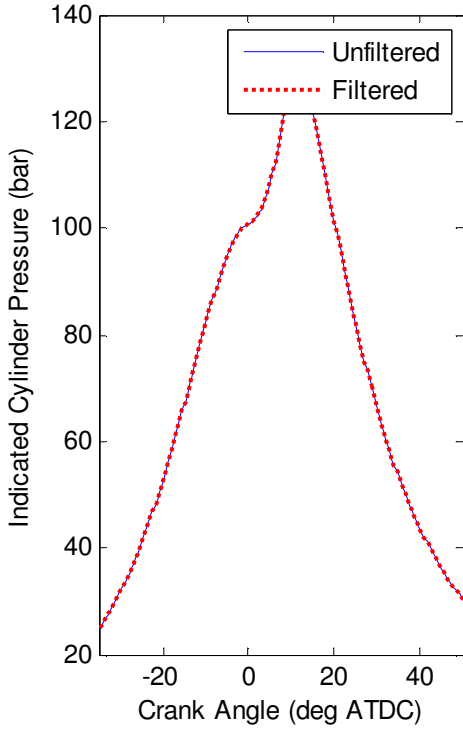


Knock: 1.3 bar
IHR: 2329 kJ/m³



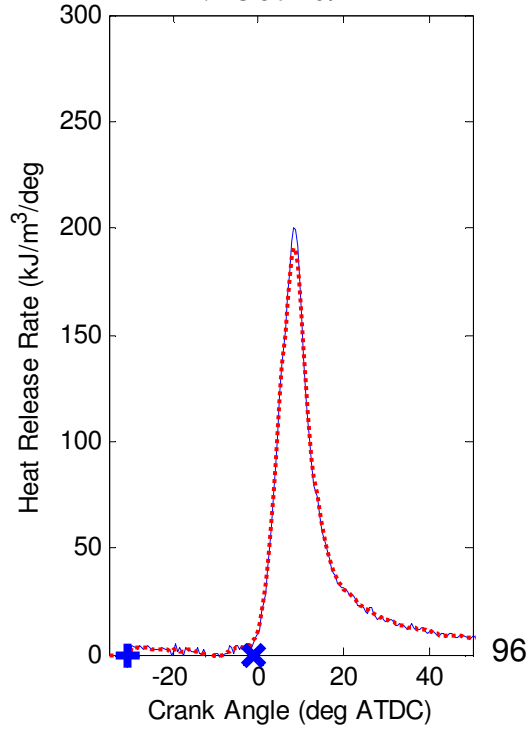
B-1400-H-5-30EGR-REP2

t_{id} : 2.63+/-0.03 ms



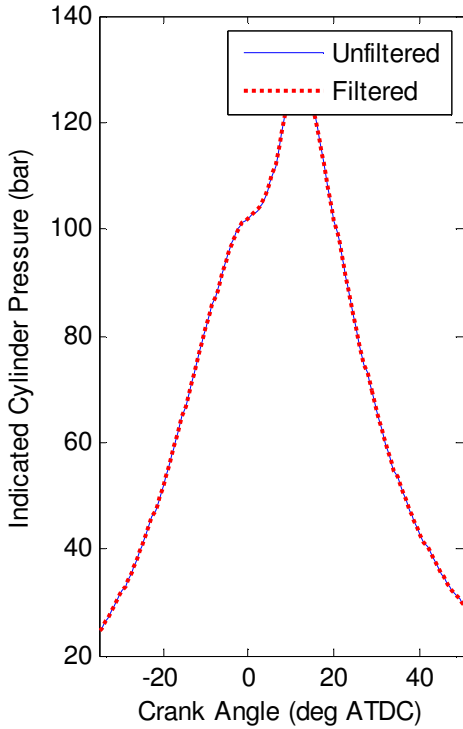
Knock: 1.2 bar

IHR: 2367 kJ/m³



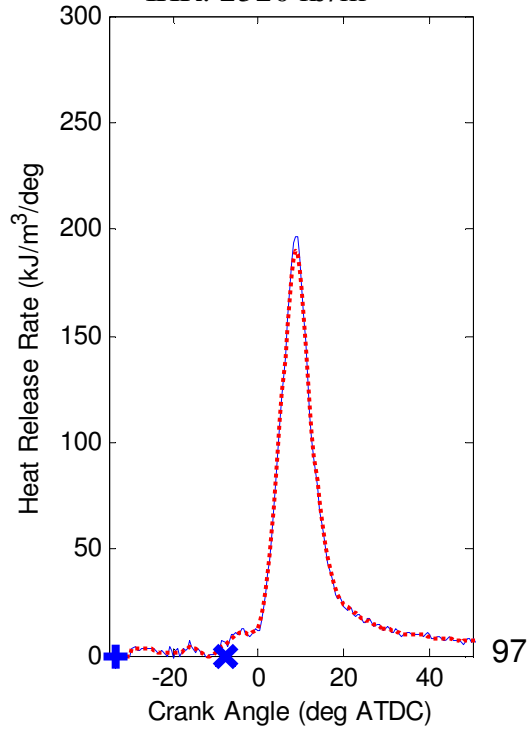
B-1400-H-7-30EGR

t_{id} : 2.19+/-0.05 ms

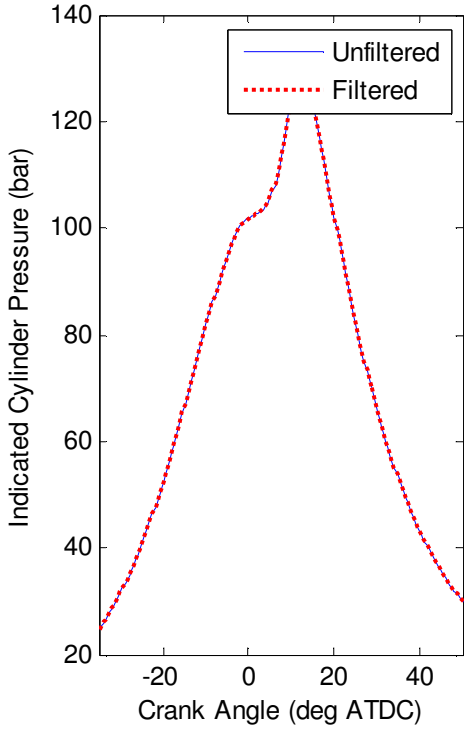


Knock: 1.1 bar

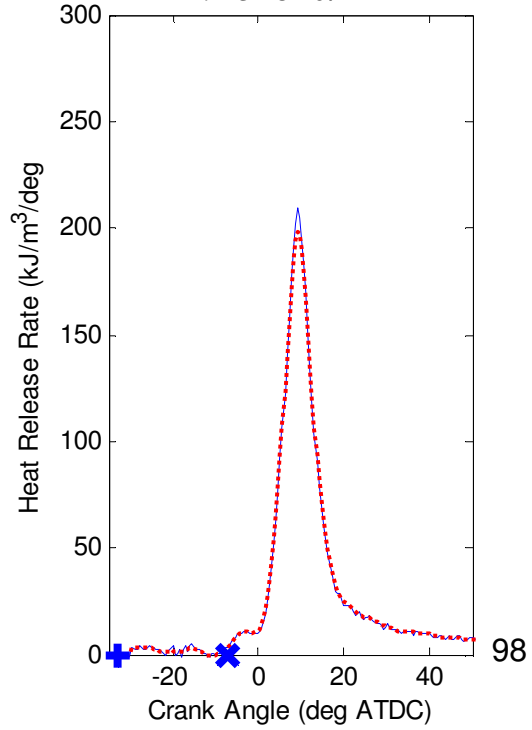
IHR: 2320 kJ/m³



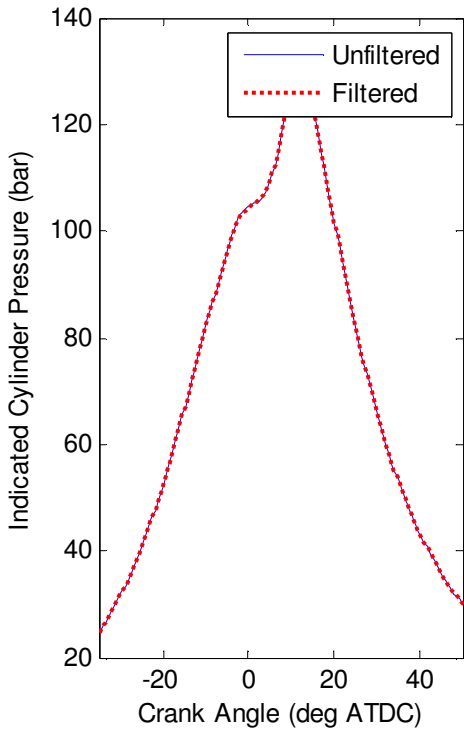
B-1400-H-7-30EGR-REP1
 t_{id} : 2.14+/-0.05 ms



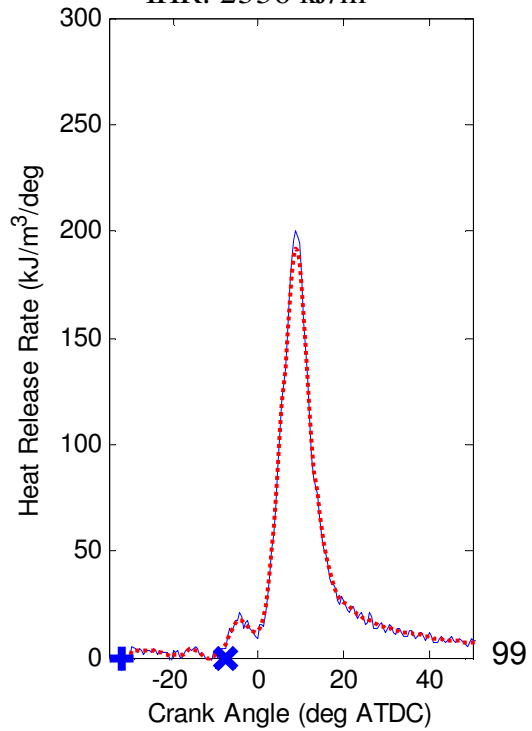
Knock: 1.1 bar
IHR: 2328 kJ/m³



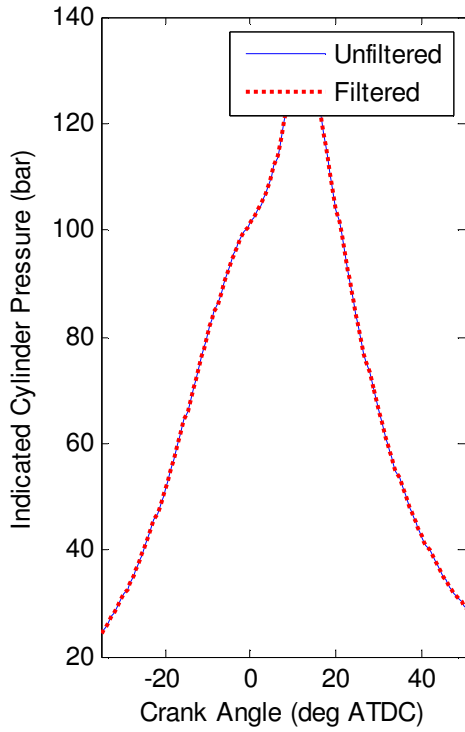
B-1400-H-7-30EGR-REP2
 t_{id} : 2.01+/-0.06 ms



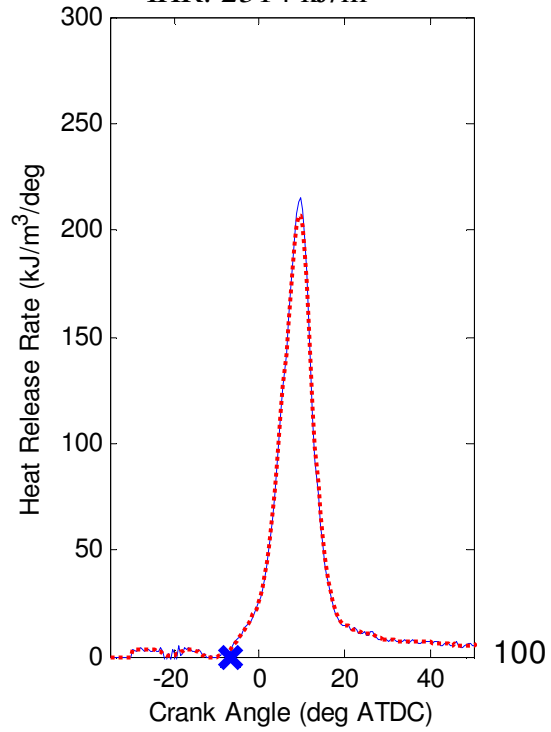
Knock: 1.1 bar
IHR: 2336 kJ/m³



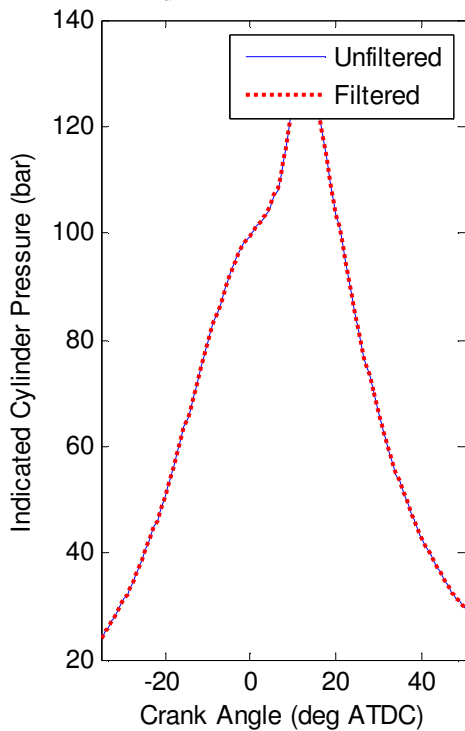
B-1400-H-9-30EGR
 t_{id} : 2.58+/-0.04 ms



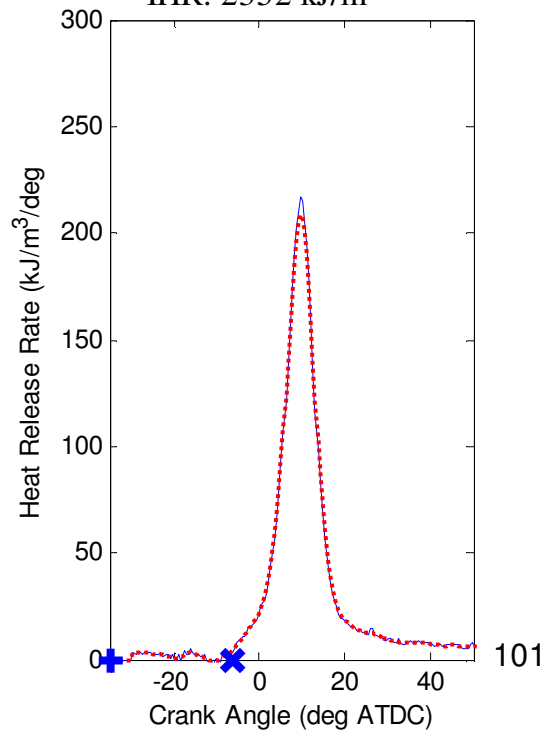
Knock: 1.3 bar
IHR: 2314 kJ/m³



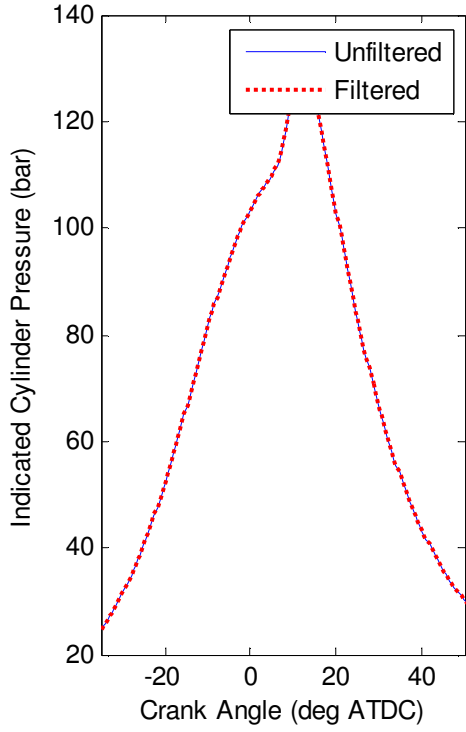
B-1400-H-9-30EGR-REP1
 t_{id} : 2.47+/-0.04 ms



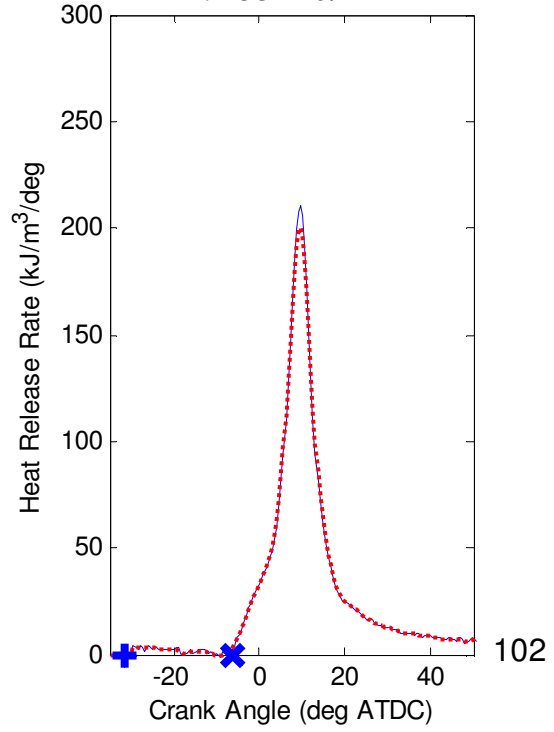
Knock: 1.2 bar
IHR: 2352 kJ/m³



B-1400-H-9-30EGR-REP2
 t_{id} : 2.08+/-0.03 ms



Knock: 1.1 bar
IHR: 2354 kJ/m³



Appendix F - Gas Flows from IVC Experiments

In order to help clarify some of the gas pulse width data, tests were done by Nick Birger in the injector visualization chamber (IVC) to find the effect of chamber pressure on gas flow. The figures below show plots of gas flow vs. cylinder pressure for Co-injectors B and CS (equations from least squares fit to the data are shown on the plots) for 0.8 and 1.4ms GPW.

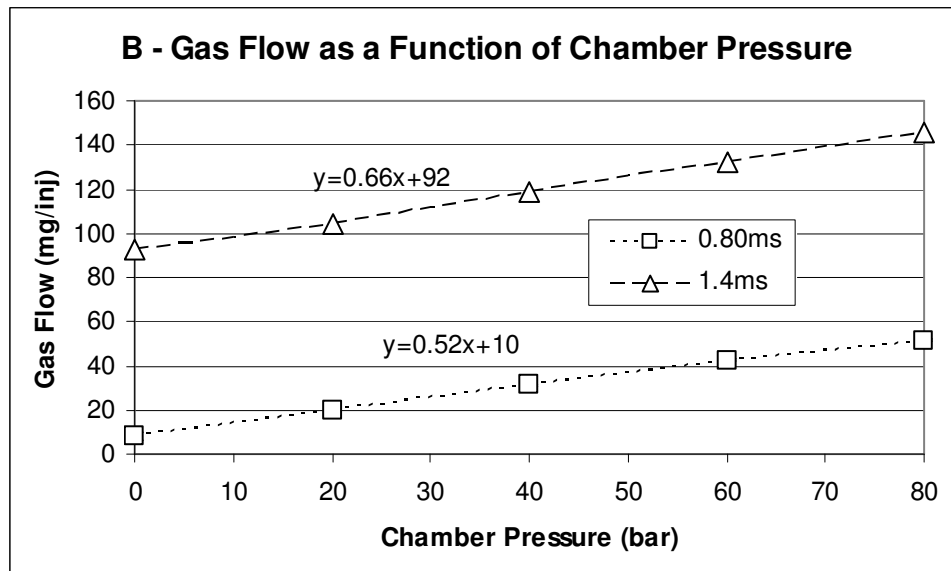


Figure F-1 – Gas Flow vs. Cylinder Pressure for Co-Injector B

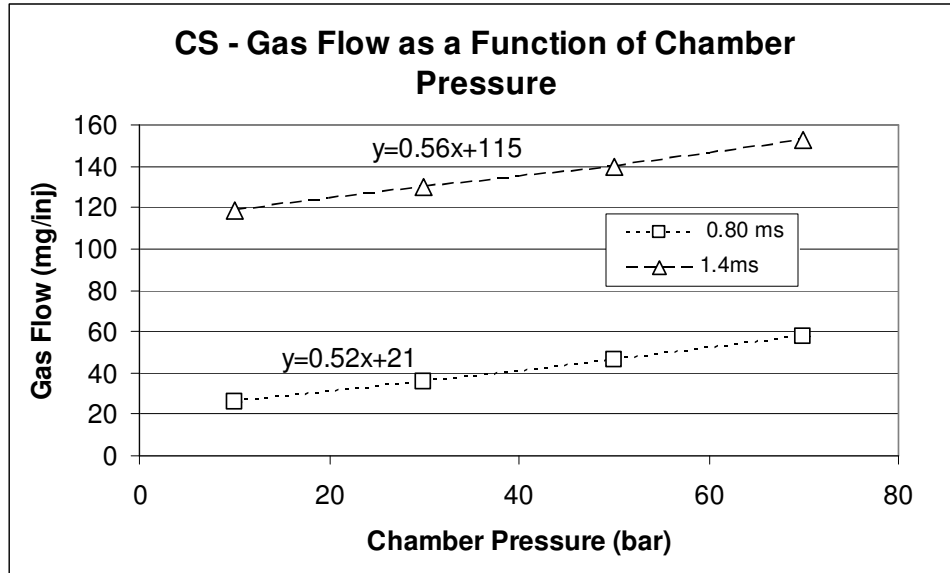


Figure F-2 – Gas Flow vs. Cylinder Pressure for Co-Injector CS

Co-injector B was tested with ~11mg/inj of diesel and CS had ~13mg/inj. Due to test rig limitations, the chamber pressure could not be increased beyond 80 bar. Therefore, it was assumed that the relationship remained linear and the data was extrapolated to higher cylinder pressures according to the equations given on the plots. Tests were conducted with 21 MPa gas injection pressure.

Appendix G - Raw Data Information

The raw data used in the experiments is stored on a UBC network drive. It is accessible through the use of an SSH client and is stored on the host: “origin.mech.ubc.ca”. Contact Dr. Steven Rogak at UBC for access to the drive. The directory containing the files is: “[/home/netapp2/rogak/claforet/](http://home/netapp2/rogak/claforet/)”.

The data for the single injection tests are located in the subdirectory: “[/Thesis/Data/Ch4/](http://Thesis/Data/Ch4/)”. In this directory, the raw data has been further separated into groups of injection pressure, then intake temperature and pressure, and finally repetitions as shown in the figure below.

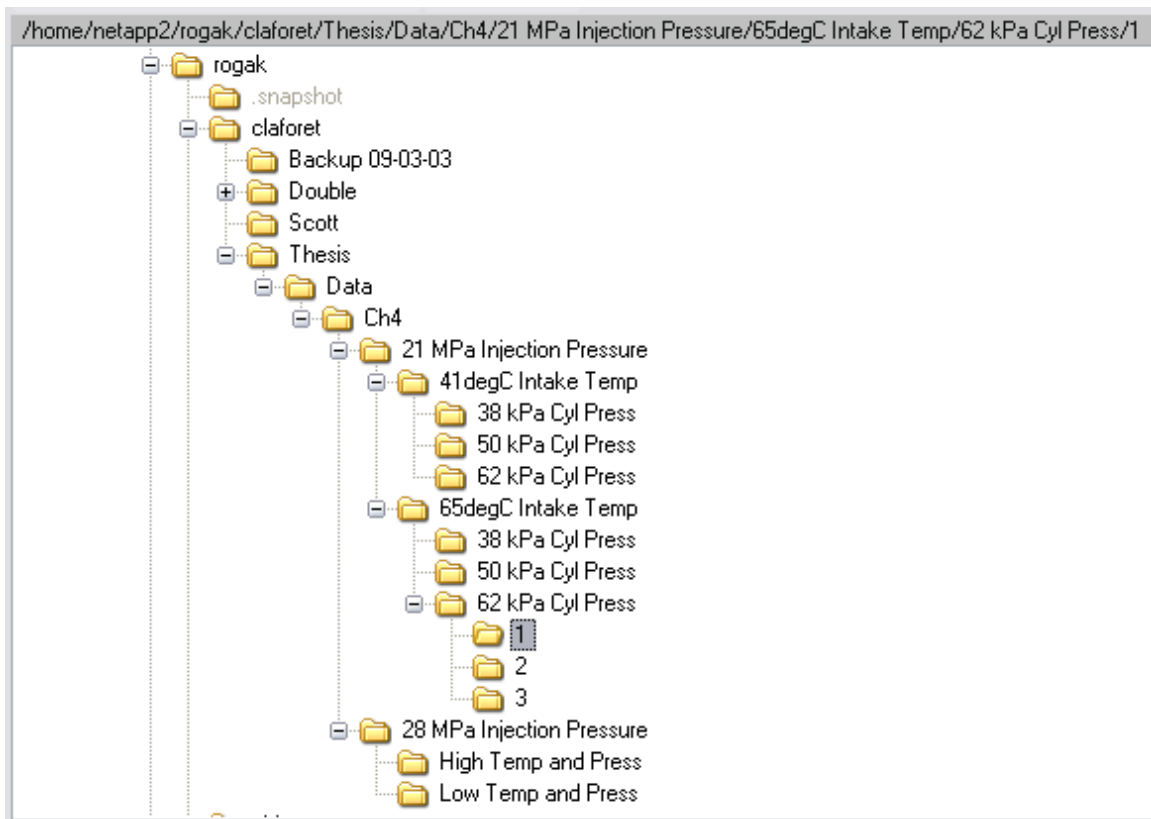


Figure G-1 – Chapter 4 Data Storage Structure

Each repetition directory contain the fast and slow files for each test, as well as a file called 'Data Summary.xls' and the 'SCRE Emissions Spreadsheet', which contain all the processed data. An example test name is:

B-800-20-50-60-H

Where 'B-800' is the same for all tests indicating that Co-injector B was tested at 800 RPM. The '20' represents the intake temperature (value can be 20 which represents 41°C or 75 which is 65°C). The value '50' represents the intake pressure (values can be 65 for the 62 kPa cylinder pressure tests, 30 for the 50 kPa cylinder pressure tests, and 50 for the 38 kPa Cylinder pressure tests). The '60' represents the gas flow rate (values can be 60 for the 25 mg/inj flow, 45 for the 18.8 mg/inj flow, 30 for the 12.5 mg/inj flow, or 15 for the 6.3 mg/inj flow). The 'H' represents the diesel flow which is H for high, M for medium or L for low. Note that the naming convention was originally based on different temperatures, pressures and flow rates which is why the numbers don't match the values used in this thesis.

The chapter 5 data is in the subdirectory "/Data/Ch5/". The raw data is split into B and CS directories and then into repetitions. Again, each directory has a 'Data Summary' and 'SCRE Emissions Spreadsheet' along with the raw data. There is also a spreadsheet in the "/Data/Ch5/" directory called 'Combined Data.xls', which contains all the relevant B and CS data and GPW plots from chapter 5, as well as the J36 data used. An example test name for this data is:

CS-1100-L-5-0EGR

In this case, 'CS' is either CS or B, indicating the injector. The '1100' is the speed being 1100 or 1400 RPM. 'L' represents the load, having L for low load or H for high load. And finally, '0EGR' means 0% EGR, where 30EGR represents 30% EGR.

All the Matlab code used is in the *“/Thesis/Code/”* subdirectory. The code used to generate the response surface coefficients is called ‘Response Surface Coeffs.m’ located in the *“/Thesis/Code/Response Surface/”* subdirectory. This file takes in data from a file named ‘XXY.xls’ in order to generate response surface coefficients. An example XXY.xls file has been included in the folder as well. The format is set up such that the first four columns should have all the raw input data from the 4 input variables. All subsequent columns should have the response data (i.e.: Knock intensity, ignition delay, etc.). The first row should have the variable names and the second row should have their units. Note that the code is written to accept 4 input variables with a maximum second order response surface. The code would need to be modified for any other conditions. The ‘Response Surface Coeffs.m’ file is a stripped down form of the code used in this thesis. The code used in the current work is in the files ‘Resp_Surf_Post_Prc.m’ and ‘resp_surf.m’, which have the code which plots the contours. However, the code will not be explained here as it was made very specific for certain plots and would likely be difficult to use easily for anyone other than the author.

The code used to process the fast data and generate the ‘Data Summary.xls’ files is called ‘Process_Fast_Data.m’ and is located in the *“/Thesis/Code/Raw Data Processing/”* subdirectory, along with the files needed to run it. This program processes all the high-speed data from the cylinder pressure transducer and also uses the ‘SCRE Emissions Spreadsheet’ (which must be created before running the fast data processor) to calculate knock, ignition delay, pressure and heat release curves, as well as cycle-to-cycle variation statistics discussed in Appendix C.